OBSERVATIONS OF SUPERNOVAE AND THEIR ENVIRONMENTS

GEORGIOS LELOUDAS

Dissertation

Submitted for the Degree of

PHILOSOPHIÆ DOCTOR

Dark Cosmology Centre

Niels Bohr Institut

Det Naturvidenskabelige Fakultet
Københavns Universitet

Submitted: *May 6th, 2010*

Supervisor: *Assoc. Prof. Jesper Sollerman*
Co–Supervisor: *Assoc. Prof. Johan P. U. Fynbo*

Στην Εμιλία και το Γιάννη

All other creatures look down toward the earth, but man was given a face so that he might turn his eyes toward the stars and gaze upon the sky.

Ovid
Metamorphoses

ABSTRACT

Supernovae are the explosions of stars. They are fascinating phenomena because in a period of only a few days they release an extremely large amount of energy, comparable to what an ordinary star, like our sun, will produce in its entire lifetime of a few billion years. Supernovae occur on average once every hundred years in every galaxy and the last events in our Milky Way were experienced on Earth as the appearance (and disappearance) of a new bright star in the sky. Supernovae are extremely important for the evolution of the universe because only in the extreme conditions that develop during the explosion, the elements heavier than iron can form efficiently. They are thus responsible for the chemical enrichment of the universe and for this reason it is often stated that we are all made of material that was formed long ago during a supernova explosion. Supernovae have attracted great attention worldwide during the recent years due to the observation that a class of distant supernovae appear fainter than they would if the universe was decelerating. This has led to the exciting discovery that our universe is dominated by a mysterious component that forces it to accelerate and that we call 'Dark Energy'. At the same time we have witnessed the proof that another class of supernovae is closely linked to the mysterious cosmic explosions that are observed at very high energies: gamma-ray bursts. For all the reasons above it is vital that supernovae are studied in great detail and this is the area that the present PhD thesis aims in contributing a small, tiny, brick.

Although thermonuclear supernovae are used as 'standard candles' to derive distances in an empirical way, it is actually embarrassing that we know neither the exact progenitor of these explosions nor their detailed physics. With our study of the thermonuclear SN 2003hv, we wished to address the following questions: supernovae are known to produce lots of positrons. Can these positrons escape the ejecta or do they remain trapped in it due, e.g., to a strong magnetic field? At the same time we wanted to probe the existence of the so-called 'infrared catastrophe', a phenomenon that has been predicted but never observed in thermonuclear supernovae. We provide an extensive dataset for this supernova that has been collected from many different telescopes. Our study features the longest monitor period ($>$700 days) of such a supernova in multiple wavelengths, including near-infrared, and the farthest in time near-infrared detection of a thermonuclear supernova with the Hubble Space Telescope. By constructing a bolometric light curve we conclude that positrons most likely do not escape the ejecta, while it is apparent that there is no prevalent infrared catastrophe. By inspecting our late time photometry and spectra and by comparing with a simple model we propose that the ejecta might be clumpy and that a mild infrared catastrophe only in the highest density regions might be able to explain the data. We also confirm that the explosion was probably asymmetric and briefly describe the implications of this hypothesis.

Stripped-envelope core-collapse supernovae result from the gravitational collapse of massive stars that have lost their outer hydrogen envelope. A sub-class of these explosions is also linked to gamma-ray bursts. Theory predicts that the most viable progenitors of these explosions are Wolf-Rayet stars, which have also expelled their hydrogen envelope, although this has never been directly confirmed. In this thesis I have tried to attack the problem indirectly, through the environments of these explosions. By studying the locations of the Wolf-Rayet stars within their galaxies I show that they are indeed compatible with those of stripped-envelope core-collapse supernovae and even of gamma-ray bursts. Agreement is also found between specific star and explosion sub-classes. In addition, I have led a project to study spectroscopi-

cally the locations of normal stripped-envelope core-collapse supernovae with the purpose of deriving the chemical properties (metallicity) and the age of the stellar population in the explosion environment. These observations can help distinguish between different scenaria leading to these hydrogen deficient explosions. Preliminary results indicate that there is no statistically significant difference between the metallicities of Types Ib and Ic supernovae, at least within the precision we can reach.

ACKNOWLEDGEMENTS

Three years is a short time for a PhD, especially for somebody that had never before worked with real astronomical data. I would have never managed to succeed without the help of several people. It is appropriate to thank them here.

The most important is of course my supervisor, Jesper Sollerman. Despite the fact that he got a permanent position in Stockholm shortly after I started my PhD, he continued visiting Denmark and we always stayed in a close contact. Of course, coordination was not always easy but we managed, and I know that Jesper tried a lot to make it work. Many times I could not help thinking that if it hadn't been for me, Jesper would have stayed with his family instead of getting in a flight to Copenhagen. But I am glad that he did and, like this, I also got my free trips in Stockholm! Jesper was a good and fair advisor: he was always very thorough when correcting my work, his critique was very valuable and we have had many stimulating discussions. I think that we ended up developing a good collaboration and a good relation. I am indebted to him.

Anyway, being in the same physical location implies a constant annoyance and nobody felt this more than my co-supervisor, Johan Fynbo. Unable to say 'no', he must have suffered so much (ok, it wasn't only me) that at some point he tried to create a 'safe haven' for people to stop bothering him! Despite this, I do not remember him ever throwing me out. Instead he would always spend the time to discuss with me and even to play the occasional game of squash. I am mostly grateful to him for his always positive attitude and his good ideas.

I, of course, do not forget that during my first months, my co-supervisor was Max Stritzinger. A unique personality among astronomers (and not only), Max was not exactly the kind of person I expected to meet when I travelled down to La Palma for my first observing trip! During these years Max offered me his help and his friendship and I am very happy to have met him.

While all the people above were more or less obliged to help me, special credit should be given to those that spent their time on their own free will. In that sense, the biggest thanks goes to Daniele Malesani. Always available, he covered for me many gaps from my lack of astronomy background: from 'basic' issues (that can however confuse experienced researchers) to practical matters and to his field of expertise (GRBs), I learned a lot from Daniele. And I am not the only one: I think that the people acknowledging Daniele's help constitute a small club!

I also profited a lot from the interaction with Justyn Maund. Luckily for me, his arrival was coincident with the break-up of the supernova group at DARK and like this I was never left without a supernova scientist to talk to. Justyn was a wealth of information and it was always a pleasure discussing with him.

DARK has in general been a very inspiring environment to work in. I have big respect for all the people, especially Jens Hjorth, that have contributed in creating such an environment. I am grateful for all the opportunities to travel, all the visitors, and all the motivating coffee time discussions (plus cookies) on a daily basis. But, like everybody that has been around knows, DARK has been more than just a workplace: it is a fun place to be. With lots of activities, parties, friday bars, 'fun days', 'julefrokosts' and lots of interesting people around, it is difficult to get bored here. I will just mention here my friends Danka, Paul and Peter, but I have enjoyed meeting everyone, really *everyone*. Summarizing, the only disadvantage with DARK is that it will be very difficult for many of us to find a comparable work place in the future!

Except from all the people already mentioned, I wish to thank Jakob Nordin and Linda Östman for letting me use in this thesis their reductions of the spectra we obtained for the SDSS and Mat Smith for observing with me at the NTT. Bo Milvang-Jensen gave valuable practical advice for the reduction of the data presented in Chapter 6. For the UltraVISTA related study I acknowledge discussions with Kevin Krisciunas, Chris Burns, Jens Melinder and, especially, Ariel Goobar, to whom I am grateful for helping out with the numerical calculations. I thank Keiichi Maeda for a collaboration done exclusively by email, without ever meeting, and that I enjoyed a lot.

During these 3 years, I spent around 30 nights observing at telescopes in Spain and Chile. I feel privileged that I was given this chance.

I dedicate this thesis to my wonderful children in the hope that, one day, they will be for this a little proud of me. I dare not say ‘as proud as I am of them’ because this is impossible!

CONTENTS

LIST OF FIGURES

LIST OF TABLES

PREFACE

This thesis is the result of my PhD studies at the Dark Cosmology Centre, Copenhagen University, between December 2006 and May 2010. My work concentrated on the field of cosmic explosions, mainly supernovae (SNe) but also gamma-ray bursts (GRBs), and the places they occur. The results presented here consist of two published first-author papers, a few contributions to other publications and some work in progress.

The first chapter is a short introduction to SNe focusing mostly on historical aspects. The first observations of SNe are mentioned and their modern classification scheme is explained. The distinction is made between thermonuclear and core-collapse (CC) SNe and the importance of these phenomena for the evolution of the universe is outlined. The chapter is closed by an analogous brief introduction to GRBs.

The next two introductory chapters make a more detailed approach to thermonuclear and stripped-envelope CC SNe that is necessary for the understanding of the rest of the thesis. Chapter 2 is dedicated to thermonuclear (i.e. Type Ia) SNe: their observational properties, as they have been recorded in the literature, and their use as distance indicators that has revolutionized cosmology through the discovery of the acceleration of the universe are discussed. The recent progress in this field is examined as are the scientific questions that still remain unanswered. Some of these are related to the progenitors and the mechanisms of these explosions. I explain why it is believed today that SNe Ia result from the delayed detonation of a white dwarf (WD) star and I conclude by arguing why late-time observations can offer a wealth of information about the physics of these explosions. Chapter 3 contains an introduction to stripped-enveloppe core-collapse SNe (SNe Ib/c). Emphasis is given on the connection of this class of explosions to GRBs as well as on the study of their birthplaces. It is reviewed how the study of environmental properties can be used to deduce conclusions on the nature of SNe Ib/c. A case study of SN 2008D is presented as an example of a stripped-envelope CC SN. This was a very interesting event and during my PhD I have contributed in two studies concerning both the SN itself and its host galaxy. It is also worth mentioning that I have enriched these chapters with some illustrative spectra of SNe that I obtained during my participation in the SDSS-II SN Survey, an aspect of my PhD that is not highlighted elsewhere in this thesis.

The following chapters contain the main work conducted during my PhD: Chapter 4 presents a detailed study of the thermonuclear SN 2003hv from the time of discovery out to very late phases. Data was collected from many different ground-based telescopes and the Hubble space telescope (HST). For the first time was a SN Ia followed in multiple filters, including near-infrared (NIR), to phases $>$700 days past maximum light. By examining the late-time light curves and spectra of the SN, we study the issues of the infrared catastrophe and positron escape in SNe Ia. The study features also the longest (in wavelength coverage) nebular spectrum of a SN Ia, extending from the optical to mid-infrared when combined with other published data, and a comparison with a synthetic model spectrum. Sections 4.1 to 4.6 are presented as they were published with only very minor modifications. SN 2003hv triggered also some follow-up work in the field of SN Ia explosion asymmetry. This resulted to two more relevant publications in which I participated and that are briefly presented in the final section of this chapter.

Chapter 5 presents my work in comparing the locations of SNe Ib/c and (long) GRBs to those of Wolf-Rayet (WR) stars, which are the favored progenitors of these explosions according to theory. This study is possible for two nearby galaxies and care is taken to make the comparison viable with more

distant galaxies. Uncertainty factors are treated with the help of Monte Carlo simulations. It is concluded that the locations of WR stars within their galaxies are indeed compatible with those of these cosmic explosions. Furthermore, the WC sub-class stars seem to be distributed in brighter locations than WN stars, in accordance to what is observed for SNe Ic and Ib respectively.

Chapter 6 presents a spectroscopic survey of host galaxies of SNe Ib/c, a program of which I was the principal investigator (PI) and that was awarded telescope time at the European Southern Observatory (ESO). I describe the motivation behind this effort, namely to obtain metallicities and stellar population ages at the SN explosion locations and use this information to constrain the SN Ib/c explosion mechanism. I describe how the observing run was executed and the data reductions. The spectra are presented and line fluxes are measured. In contrast to the previous chapters, this is work in progress and only preliminary results are presented. These seem to indicate that there is no significant difference between the environmental metallicities of SNe Ib and Ic.

Finally, the last chapter contains a science case investigation I have conducted on the feasibility and impact of using the UltraVISTA survey for discovering SNe at NIR wavelengths. It is shown that this distant galaxy survey has also a great potential for SN science.

1

A SHORT HISTORICAL OVERVIEW OF COSMIC EXPLOSIONS

The skies above us are not static but filled with periodic and transient phenomena. It is indeed these phenomena that have most intrigued the curiosity, interest and phantasy of our ancestors, perhaps even more than the marvelous, but static, constellations. Throughout human history, the wandering planets, mysterious variable stars, shining comets or the brief appearance of meteors have had a deep impact on the culture of people that were observing them, sometimes affecting their beliefs and religion. While these are the most accessible examples of the restless sky, there have also been recordings of more rare, really exceptional events, such as the sudden appearance of new bright stars, shining intensively before disappearing again for ever. Today we know that some of these were due to cosmic explosions that marked the end state of a stellar configuration.

In this thesis I examine only the most violent and spectacular, in my opinion at least, of these explosions: supernovae (SNe) and gamma-ray bursts (GRBs). A short historical introduction to both phenomena is given below.

1.1 SUPERNOVAE

The history of supernova observations, in the sense of the existence of written records, begins with the Chinese. Believing astronomy was important, chinese had a positioned court astronomer and kept records of all astronomical events for over 2000 years. It is there that the first official observations of a SN were recorded in 185 AD (e.g. Clark & Stephenson, 1977; Stephenson & Green, 2005). Supernovae are today named with the prefix SN, followed by their year of discovery, so this SN is referred to as SN 185. The next convincing SN found in chinese records took place in 393 AD, while a number of other associations are less certain.

SN 1006 must have been the brightest historical SN and was observed simultaneously by many people around the world. It was brighter than Venus and reached one quarter of the brightness of the moon, being clearly visible during daylight, according to the arab scholar Ali ibn Ridwan. Only 48 years later, SN 1054 was another explosion, noticed by chinese, arabs and japanese, which is mostly famous for leaving behind the Crab nebula and the Crab pulsar.

About half a millennium later, another supernova exploded in the constellation Cassiopeia. SN 1572 was extensively observed by the Danish astronomer Tycho Brahe. The observations were published in his study *De stella nova* (on the new star), from which the term *nova* was pulled out. Just three decades later, SN 1604 was the last SN recorded to explode in the Milky Way and was observed extensively by Johannes Kepler (it is still not clear why the explosion that created the *Cas A* SN remnant, believed to occur the same century, has not been documented). These last two observed SNe were important for another reason as well: they contributed to the fall of the Aristotelian idea that the universe beyond the moon and the planets

was constant and unchangeable. But the parallax of these events was measured to be zero by Tycho Brahe and Galileo respectively, indicating that they were not located in the immediate environment of the Earth but much further away. They thus coincided with and marked the end of the european middle-age thinking.

The study of *S Andromedae*, i.e. SN 1885 in the neighbor Andromeda galaxy, combined with the newly computed distances to the extragalactic 'nebulae', led the Swedish astronomer Knut Lundmark to suggest this might be a very luminous event, distinct from regular Novae and similar to Tycho's Nova, although 'one may hesitate to accept such a luminosity' (Lundmark, 1925). The term super-nova was first introduced by Walter Baade and Fritz Zwicky, probably during their lectures at Caltech. In a remarkably insightful way, they proposed that SNe 'represent the transition of an ordinary star into a body of considerably smaller mass' (Baade & Zwicky, 1934b), which they identified as a neutron star (Baade & Zwicky, 1934a)! Probably nobody has been so influential in the history of SN science as Fritz Zwicky. He later initiated observational campaigns to discover SNe by regularly monitoring nearby galaxies (Zwicky, 1938) and until the early sixties he had himself discovered more than half of the SNe in the literature. Nowadays, hundreds of SNe are discovered every year and they are announced through the Central Bureau of Astronomical Telegrams (CBAT) of the International Astronomical Union (IAU). Letters of the latin alphabet have been added to the SN names, to indicate the row of discovery within the year (e.g. SN 1987A, SN 2003hv). A fairly complete list of SNe is maintained in the Asiago SN catalogue (Barbon et al., 1989).

The first classification scheme dates back to Minkowski (1941, 1964) who separated SNe in Types I & II, based on their observational properties. The addition, by Zwicky, of Types III, IV and V did not last long, and Minkowski's classification has not changed a lot since. A major modification was made to this scheme in the early 80s, when it was realized that Type I SNe was not such a homogeneous class. Observations of SNe 1983N and 1984L, together with a re-evaluation of previous observations, clearly demanded the introduction of SNe Ib as a separate class (Wheeler & Levreault, 1985; Uomoto & Kirshner, 1985; Panagia et al., 1986). SNe Ic were introduced shortly after (see Wheeler & Harkness, 1990).

Today, SNe are classified based on their optical spectra at maximum light (Filippenko, 1997). This classification is illustrated in Fig. 1.1. The main distinction is made by the presence or absence of hydrogen, where Type II SNe display hydrogen in their spectra, while Type I are hydrogen deficient and contain more sub-classes. SNe Ia are distinguished by the presence of a moderately strong Si II absorption line observed at $\sim$6150 Å. The other Type I SNe (collectively SNe Ib/c) lack this feature, although they possess silicon, and are further divided to SNe Ib and Ic based on the presence or absence of strong helium lines, the most notable of which is He I λ5876. This classification scheme is supplemented by the use of light curves, which enable further subdivisions, and by spectra obtained at later phases, that help better differentiate between the classes. In particular, SNe II are further divided to SNe IIL ('linear') and SNe IIP ('plateau') depending on whether their light curve declines linearly or displays an almost constant luminosity after maximum. To these sub-divisions, we add the SNe IIn ('narrow') that display narrow hydrogen lines in their spectra and the hybrid class of SNe IIb that start as a Type II but metamorphose later to Ib.

This phenomenological classification, however, does not directly reflect real physical differences in the SN explosions. Today we know that SNe fall in two broad categories: thermonuclear and core-collapse. Type Ia SNe are believed to be the nuclear fusion burning of a hydrogen deficient compact object (a white dwarf). Type II SNe are the result of the gravitational collapse of a stellar core after it has exhausted its nuclear fuel. It is very important to stress that SNe Ib/c are *not* of thermonuclear but of core-collapse nature and are thus closely linked to SNe II. Their main difference is that SNe Ib/c result from the collapse of a star that has stripped away its hydrogen envelope. For this reason they are also known as *stripped-envelope* core-collapse SNe. All explosions are accompanied by a shock wave that ejects the material into the interstellar medium at velocities that reach tens of thousands km/sec. However, while thermonuclear explosions are believed to completely destroy their progenitor star, core-collapse SNe are believed to leave behind them a compact object, such as a neutron star or a black hole. It is an interesting historical irony to point out that the suggestion by Baade & Zwicky that SNe are the result of gravitational collapse to neutron stars, was entirely based on SNe of thermonuclear nature (i.e. SNe Ia; Kirshner, 2009).

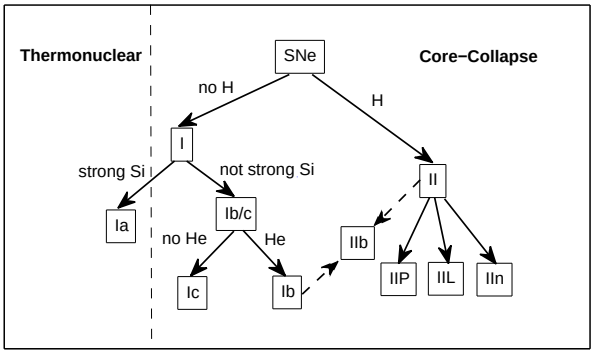

Figure 1.1: *The classification scheme of supernovae.*

During my PhD I have not worked with Type II SNe and these are mentioned very little throughout this thesis. With a sense of humour, one could say that this is a 'Type I SN thesis', although this lacks a clear physical connection, besides the hydrogen deficiency that characterizes them.

The hypothesis of stellar gravitational collapse was spectacularly confirmed in the explosion of SN 1987A in the Large Magellanic Cloud, a satellite galaxy of the Milky Way. Except from being extremely nearby and extensively observed, the most important events related to this was the unambiguous detection of neutrinos that escaped the collapsing star and the identification of the progenitor star of this explosion, the first of its kind. More than 1000 publications exist on the topic of SN 1987A (for reviews see e.g Arnett et al., 1989; McCray, 1993).

Supernovae, except from being just very luminous and spectacular events, are essentially linked to the evolution of our universe and to several important astrophysical processes. They represent the only effective way of producing, through explosive nucleosynthesis, all the elements that are heavier than iron. Furthermore, they are distributing them into space, enriching the interstellar medium with metals, elements other than hydrogen and helium, from which the newer generation of stars is formed. The released energy is an important factor in the energy balance affecting galaxy and structure formation. The remnants of the explosions are one of the main candidates for the origin of cosmic rays, an idea that dates back to Baade & Zwicky (1934a). Finally, as discussed later throughout this thesis, due to their high luminosities, they can be seen from extreme distances and used as distance indicators.

This section mostly meant to cover historical aspects. A more thorough introduction on the physics of thermonuclear and (stripped-envelope) core-collapse SNe is given in Chapters 2 & 3 respectively.

1.2 GAMMA-RAY BURSTS

As implied by its name, a GRB is a burst observed in high energies (gamma-rays). The history of GRBs is much younger than the one of SNe, as are the satellites that can detect them above the atmosphere, which is opaque to gamma-rays. The last years, however, have experienced some intense progress and exciting discoveries. This section is not meant to be a complete introduction to GRBs but is written in analogy to the previous section on SNe and highlights just few of the main milestones in the history of GRB research. For the purposes of this thesis, it is only the relation of GRBs to SNe that is really relevant and is further discussed in Sect. 3.2. Broader reviews on the topic of GRBs can be found in e.g. van Paradijs et al. (2000); Mészáros (2002); Gehrels et al. (2009).

The first GRB was discovered in 1967 by the american *Vela* satellite, whose purpose was to look for

(gamma-ray) signs of nuclear bomb tests by the Soviet Union. Since GRBs are named after the date they are discovered, this first explosion is known as GRB 670702. Although it was quickly realized that the Soviets were not attacking, the nature of these explosions remained a mystery for a long time.

Important progress in the GRB field came with the observations of BATSE onboard the CGRO satellite: the discovery that the distribution of GRBs was isotropic in the sky led to the reasonable conclusion that they are extragalactic. In addition, based on the duration and spectral ratio distribution of the bursts that proved bimodal, Kouveliotou et al. (1993) established the main classification scheme for GRBs that holds until today, despite many alternative suggestions. According to this, GRBs can be divided into *short* and *long*, where the dividing limit is 2 seconds. Since this thesis does not deal with short GRBs at all, it should be understood that, unless otherwise specified, the term GRB will from now on mean a long GRB.

Despite many earlier efforts to detect the GRBs at longer wavelengths, the first localization of X-ray emission from a GRB was achieved by the Beppo-SAX satellite in 1997 (Costa et al., 1997). Together with the discovery of the optical afterglow (van Paradijs et al., 1997) this opened a whole new way of studying GRBs: the first spectroscopic *redshift* (a measure of distance in the universe) by Metzger et al. (1997) established the fact that GRBs came from cosmological distances, while it also became possible to detect and study their host galaxies (Sahu et al., 1997; Bloom et al., 2002). It was quickly realized that the emission from GRBs must be collimated, i.e in the form of a relativistic jet, else the energy released would be too hard to explain ($> 10^{53-54}$ ergs). See e.g. Mészáros (2002) for a description of the physical procedures governing the prompt and the afterglow emission of a GRB, focusing on the fireball model.

A breakthrough in our understanding of the nature of GRBs came when Galama et al. (1998) found a peculiar, very energetic SN Ic coincident with the location of GRB 980425. This was the first observational hint that long GRBs were connected to the core-collapse of massive stars. The SN-GRB connection was unambiguously proved by observations of GRB 030329/SN 2003dh (Hjorth et al., 2003; Stanek et al., 2003). It is therefore believed that long GRBs mark the core-collapse of massive stars (Woosley & Bloom, 2006), although some complications have been induced to this simple picture by the discovery of two nearby SN-less events (Fynbo et al., 2006; Della Valle et al., 2006).

On the other hand, short GRBs remain more of a mystery. The first short GRB was accurately localized in 2005 (Hjorth et al., 2005) while no convincing spectrum of a short GRB has been published to date. The current consensus is that they originate in the collision of compact objects, such as neutron stars or black holes (e.g. Eichler et al., 1989). This is supported by the fact that they seem to occur in different, typically older, environments than long GRBs (Berger, 2009).

The specifically designed *Swift* satellite, launched in 2004, has detected numerous GRBs and several have been localized at a mean redshift of $z = 2.3$ (Fynbo et al., 2009). Nevertheless, the majority of GRBs remain *dark*, i.e. without a detected afterglow. This might be due to a selection bias, i.e. dust extinction.

GRBs are very luminous events: GRB 080319B reached an optical magnitude of 5 (Racusin et al., 2008), becoming briefly visible to the naked eye, although it is unlikely that it was noticed by somebody. The discovery of this event, viewed probably directly through the jet, proves that more GRBs must have been visible during the course of history and that some of these might even have been noticed, or even recorded, as unexplainable curiosities. Due to their extreme luminosities, GRBs can be detected at very high redshifts, even beyond 6 (e.g Kawai et al., 2006; Greiner et al., 2009). Recently, a GRB became the furthest detected object at $z \sim 8.2$, further than any spectroscopically confirmed galaxy or quasar (Tanvir et al., 2009; Salvaterra et al., 2009). Furthermore, according to the predictions, there is no reason why GRBs should not be detectable at even higher redshifts (Bromm & Loeb, 2006). GRBs are thus lighthouses of the early universe and can be used to directly probe the epochs of first star-formation.

GRB astronomy is an active field of research and is expected to continue yielding exciting results in the future. The latest tool for the study of GRBs, together with *Swift*, is the FERMI satellite, which has detected emission from a few GRBs at very high energies ($>$100 MeV) opening a new wavelength window.

2

THERMONUCLEAR SUPERNOVAE

This chapter contains a more detailed introduction on thermonuclear supernovae (SNe Ia). As such, it sets the context for the work presented in Chapter 4, but it is also necessary for the understanding of Chapter 7. A short review of the observational properties of SNe Ia is given and their importance as cosmological distance indicators is highlighted. I also briefly discuss our current understanding and open questions related to the physics of these explosions, such as the progenitor system and the explosion mechanism. Particular focus is given on the role of late-time observations and what can be gained through these.

2.1 OBSERVATIONAL PROPERTIES

There exists a vast literature on SN Ia observations. Leibundgut (2000) provides a good summary at least until 2000. Most available data have been obtained at the optical wavelengths, followed by the NIR, and the main observables remain the evolution of luminosity with time (i.e. the *light curves*) in different filters, as well as spectroscopy.

The optical light curves have a characteristic bell-shape with a rise-time of approximately 18 days. They are powered by the radioactive decay of ^{56}Ni to ^{56}Co and finally to ^{56}Fe. In the NIR, maximum luminosity is typically reached a few days before the optical and there is a secondary maximum a couple of weeks after the primary. Due to the importance of SNe Ia for cosmology (see Sect. 2.2), there has been an increased interest in these explosions and we are witnessing now the releases of excellent datasets resulting from large observational campaigns, such as the ones by the CfA (185 SNe; Hicken et al., 2009a) and the first Carnegie Supernova Project release (35 LCs, including NIR; Contreras et al., 2010).

As discussed previously, the defining feature of SNe Ia is the appearance of Si II $\lambda\lambda$6347, 6371 (blue-shifted to $\sim$6150 Å) in their maximum light spectrum. Other strong features are Ca II H & K $\lambda\lambda$3934, 3968 and the W-shaped S II $\lambda\lambda$5454, 5460, while there are also prominent lines by other intermediate mass elements (IMEs), such as O and Mg. At later times, however, as the photosphere recedes deeper into the ejecta, heavier, iron-family elements start dominating the spectrum (e.g. Filippenko, 1997). The spectral evolution of SNe Ia is illustrated in Fig. 2.1. It is pointed out that this sequence is, unconventionally, constructed by the montage of *many different* SNe.

Spectropolarimetry of SNe Ia (see Wang & Wheeler, 2008, for a review) shows that their continuum polarization is low, indicating a nearly spherical explosion. Individual strong lines, however, demonstrate significant polarization, indicating that there might be asymmetries in the way different elements are distributed at different depths.

Few observations in the ultraviolet exist, with HST (see Foley et al., 2008, and references therein) or *Swift* (Brown et al., 2009; Bufano et al., 2009) while there is only one successful detection in the X-rays (Immler et al., 2006). Only two SNe Ia have been observed in the mid-infrared (MIR) by *Spitzer* (one of them being SN 2003hv; Gerardy et al., 2007), while all efforts to detect SNe Ia in the radio have proven fruitless (Panagia et al., 2006).

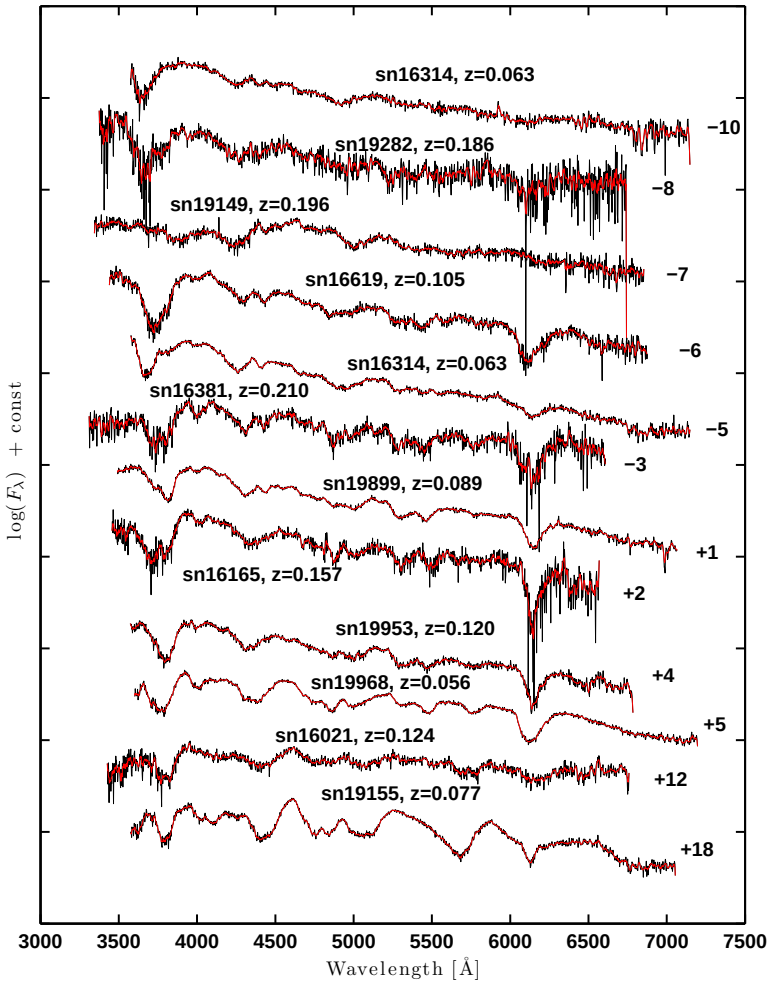

Figure 2.1: *A spectral sequence of SNe Ia, observed by GL at the NOT and NTT telescopes, in a series of runs for the SDSS-II SN Survey, together with co-observers Max Stritzinger, Mat Smith and Jesper Sollerman. The present reductions are made by Linda Östman and Jakob Nordin in the consistent manner described by Östman et al. (in prep.). These spectra, as part of a larger sample, have been used by Nordin et al. (in prep.) to investigate spectroscopic evolution in SNe Ia. Although these spectra belong to different objects, this figure illustrates well the main temporal evolution characteristics of SNe Ia: pre-max spectra are more featureless while around maximum the IMEs prevail. Two weeks later, the spectrum is dominated by iron-family elements. At the same time, the figure illustrates the degree of spectroscopic diversity between SNe Ia: the depth of the* Si II *λ6150 line is clearly different between some objects. The SNe are displayed here with their SDSS ID name, instead of their IAU designation, together with their redshift z. All spectra have been converted to the rest frame and have a super-imposed (red) smoothed version (moving average filter of 5). The number on the right of the spectra is their phase (days) with respect to maximum light, as derived from their light curves.*

Although SNe Ia form a relatively homogeneous class, there exist objects that show obvious deviations from this general picture. Except really peculiar SNe (mentioned in Sects. 2.3 and 2.4), there exist at least

two established sub-groups of thermonuclear SNe, often represented by their prototype objects SNe 1991T (Filippenko et al., 1992b) and 1991bg (Filippenko et al., 1992a). The first class contains over-luminous SNe ($M_V < -19.6$), while the second sub-luminous ($M_V > -17.5$), compared to the normal SNe that have luminosities between $-18.5 > M_V > -19.5$. Their spectral appearance is also different: 1991T-like objects demonstrate strong Fe II and Fe III absorption and weaker Si II than normal events at maximum light, while the spectra of 1991bg-like objects show smaller expansion velocities indicating smaller explosion energies and a strong Si II λ5970 feature combined with Ti II absorption lines near 4200 Å. In addition, 1991bg-like objects lack the secondary maximum in NIR bands. These two classes together are believed to constitute a fair fraction of the total number of SN Ia explosions (39%; Li et al., 2001). Even, however, among normal SNe Ia, there is an observed spectral diversity, often parametrized by the velocity evolution of the Si II λ6150 line, apparently not related to their photometric properties (Benetti et al., 2005; Branch et al., 2009).

Supernovae Ia, unlike core-collapse SNe, are discovered in all kinds of environments, including early-type galaxies that are dominated by old stellar populations. As a matter of fact, it is sub-luminous SNe that have a larger tendency of appearing in early-type galaxies, and this is a statistically significant result (Hamuy et al., 2000; Howell, 2001; van den Bergh et al., 2005). It is also interesting to point out the enhanced rate of SN Ia explosions in radio-loud galaxies (Della Valle et al., 2005).

2.2 COSMOLOGICAL IMPLICATIONS

One of the largest revolutions in modern cosmology was the discovery of the acceleration of the universe and the inference of the existence of Dark Energy (Riess et al., 1998; Perlmutter et al., 1999). The related history of the discovery, as well as the follow-up developments are reviewed in e.g. Leibundgut (2001, 2008) and Kirshner (2009) and the reader is referred there for more details.

The key fact is that distant SNe Ia appear fainter than they would if the universe was decelerating. The idea to use SNe Ia as distance indicators is almost as old as the realization that SNe are extragalactic objects (Wilson, 1939) and the first local Hubble diagram based on SNe was made by Kowal (1968). The first systematic effort to detect SNe at higher redshift was attempted by a Danish group, although the relevant technology had not matured yet, leading to very few discoveries (Hansen et al., 1987; Nørgaard-Nielsen et al., 1989).

Contrary to a usual misconception, SNe Ia are not 'standard candles', i.e. they do not have a constant luminosity, but present a scatter of the order of 50%. An important step forward came when Phillips (1993) realized that there is a relation between the SN Ia luminosity and their light curve width: namely brighter SNe have also broader LCs. After correcting for this empirical correlation, which has been parametrized under many different names, SNe Ia become decent standard candles and their scatter is reduced significantly, allowing to distinguish between (some) cosmological models.

Making use of this, two different teams, the Supernova Cosmology Project and the High-z SN Search Team, searched for and discovered distant SNe ($0.2 < z < 1$) and independently announced the acceleration of the universe. The initial skepticism around this surprising result has now been lifted since the proposed alternative explanations (such as strange dust properties or a cosmic evolution in the SN luminosity) have been dismissed and the need for an extra energy component has been confirmed by different methods, such as Baryonic Acoustic Oscillations (BAO; Eisenstein et al., 2005) and observations of the Cosmic Microwave Background (CMB; Komatsu et al., 2009).

The last years have seen an intense activity in SN cosmology: the first generation surveys have been followed by more systematic and sophisticated approaches, such as SNLS (Astier et al., 2006) and ESSENCE (Wood-Vasey et al., 2007). These surveys are complemented at higher redshift ($z < 1.7$) by SNe discovered by HST (Riess et al., 2004a, 2007), reaching back to the epoch when the universe was decelerating, and at lower-intermediate redshift ($0.15 < z < 0.35$) by the SDSS-II SN Survey (Kessler et al., 2009). At the same time, large excellent data-sets of nearby SNe are being released, addressing what had, surpris-

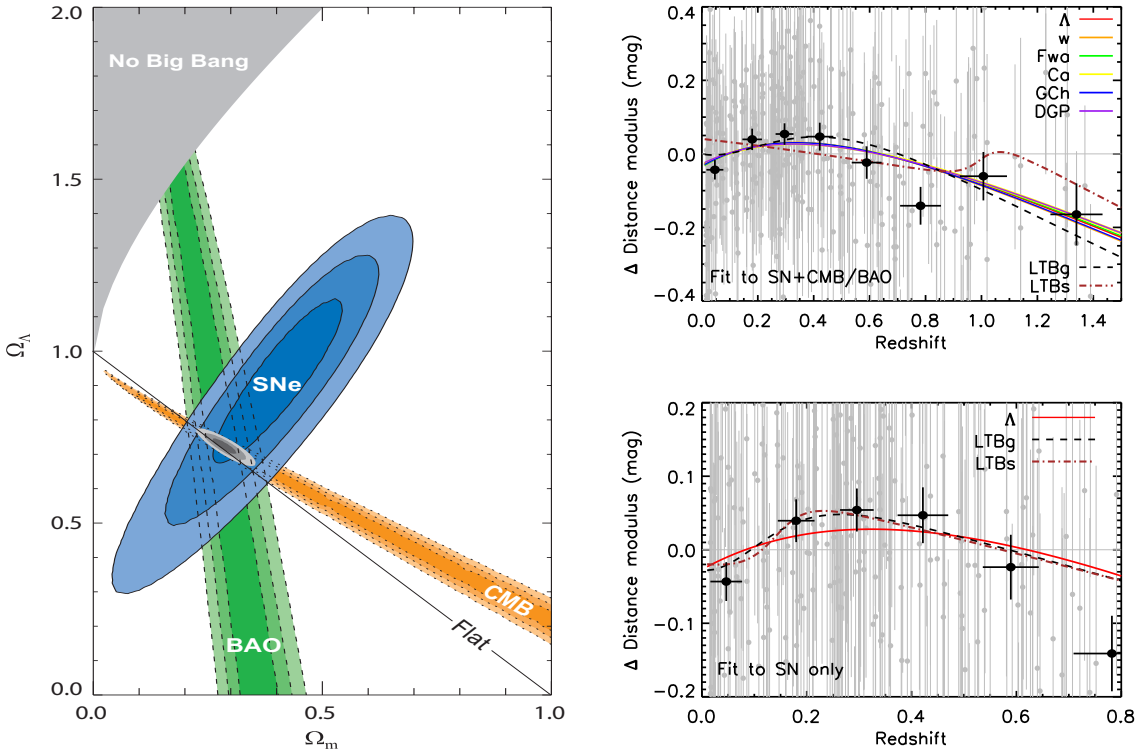

Figure 2.2: ***Left:*** *From Kowalski et al. (2008). Confidence level contours on Ω_Λ and Ω_M obtained from the 'Union' SN data-set, from BAO, from the CMB and from their combination (assuming $w = -1$).* ***Right:*** *From Sollerman et al. (2009). Hubble diagrams for a sample of SNe, including the intermediate-redshift ones discovered by SDSS (Kessler et al., 2009), alone (lower panel) and including CMB and BAO data (upper panel). Differences in magnitudes with respect to an empty universe are shown. The black crosses represent binned SN data (in grey) and the different curves are fits to different cosmological models.*

ingly, become one of the dominating uncertainties, i.e. the lack of a good local comparison sample (Hicken et al., 2009b; Folatelli et al., 2010). The goal has been shifted to distinguishing between a cosmological constant Λ and a dark energy with a variable equation of state, or even more exotic cosmological models (Fig. 2.2).

The number of discovered SNe is now so large that SN cosmology has reached a critical point where the systematic errors dominate over the statistical. It is therefore impossible to achieve further progress before the related systematic errors are better understood and solved. It is also embarrassing that the cosmological results seem to depend on the tools we use to (empirically) fit the SN light curves (Kessler et al., 2009). It is therefore of vital importance to better master the physics of the SN explosions and the knowledge of their progenitor system. Are we looking at more than one family of explosions and are there systematics related to their environment, as many of the recent studies suggest? Finally one of the largest systematic uncertainties is the issue of extinction in the SN host galaxies that seems to follow a law different than in the average Milky Way. A promising tool is to move towards the NIR wavelengths where SNe Ia are better standard candles and where the effect of dust is suppressed (Kirshner, 2009).

2.3 THE POSSIBLE PROGENITOR SYSTEMS

Livio (2000) and Hillebrandt & Niemeyer (2000) give comprehensive reviews on the issue of the progenitors of SNe Ia. They summarize work mainly done in the 80s and 90s, with contributions by Branch, Nomoto and Woosley, among others, and phrase, what is considered today to be common knowledge, i.e.

that the relative homogeneity of SNe Ia and absence of hydrogen in their spectra strongly suggest that the exploding star is a C-O WD. However it must also accrete mass from somewhere. Two scenaria are in play: the single-degenerate scenario, where the WD accretes mass from a companion star (Whelan & Iben, 1973) and the double-degenerate scenario, where the companion star is also a WD (Iben & Tutukov, 1984; Webbink, 1984)

The single-degenerate scenario is clearly the most favored today, although both face individual problems (Livio, 2000; Hillebrandt & Niemeyer, 2000, and refs. therein). Nevertheless, efforts to detect the secondary star signatures have until now proven fruitless. Pakmor et al. (2008), however, shows that this failure is still compatible with observational constraints. There has been a claimed progenitor system detection in archival X-ray images (Voss & Nelemans, 2008), which would be consistent with the accretion scenario, that has however been retracted (Roelofs et al., 2008). More importantly, hydrogen has been detected in the spectra of SN 2002ic (Hamuy et al., 2003; Kotak et al., 2004) and SN 2005gj (Aldering et al., 2006), but the thermonuclear nature of these explosions has been questioned (Benetti et al., 2006). Finally, recently, there have been 3 cases, the most notable being SN 2006X (Patat et al., 2007), where circumstellar material was detected through its variable ionization state. This explanation is, however, as well not unambiguous (Chugai, 2008).

The possibility should be stressed that not all SNe Ia need come from one single channel. For instance, there have also been some SNe that challenge the single-degenerate scenario: SN 2003fg (Howell et al., 2006), SN 2006gz (Hicken et al., 2007), SN 2007if (Scalzo et al., 2010) and SN 2009dc (Yamanaka et al., 2009) are simply too luminous to be explained by this picture and super-Chandrasekhar models or double-degenerate mergers have been invoked to explain them. In addition, recently, Pakmor et al. (2010) managed to successfully model a SN Ia explosion by the merger of 2 WDs and produce a sub-luminous, 1991bg-like SN. Although considerable tuning in their masses was needed, this demonstrates that such an explosion is in principle possible. Finally, studies of SN rates and host galaxies indicate that the population of SNe Ia might be bimodal, consisting of one prompt and one delayed component (see e.g. Scannapieco & Bildsten, 2005; Sullivan et al., 2006b; Brandt et al., 2010). In this picture, the brightest SNe Ia tend to be found in younger environments, while the dimmest among older stellar populations.

2.4 THE EXPLOSION MECHANISM

Irrespective of the nature of the companion star, another hot topic of debate has always been the way the explosion proceeds, after ignition. All proposed mechanisms can ultimately be divided into two categories: *deflagrations*, where the nuclear burning front moves at subsonic velocities, and *detonations*, i.e. supersonic blast waves.

An extensive review on SN explosion models is again given by Hillebrandt & Niemeyer (2000). Since then, however, significant progress has taken place, especially in multidimensional simulations, that is worth mentioning. Models are becoming increasingly sophisticated and the increase in computing power has allowed them to be conducted in 3D. Most importantly, it seems now that a consensus is being reached that the favored model is a Delayed Detonation (DDT), i.e. an explosion that starts as a deflagration but transitions to a supersonic detonation.

It was recognized early on that a pure detonation burns the whole WD to heavy iron-group elements, leaving too few IMEs behind, while a pure deflagration produces explosions too weak compared to SNe Ia (Hillebrandt & Niemeyer, 2000). A delayed detonation (Khokhlov, 1991) was proposed to better match the observations (Hoeflich & Khokhlov, 1996). The problem has always been that the physics of this transition is unknown and it has been initiated largely arbitrarily (e.g. Gamezo et al., 2005), making many people feel uncomfortable with the concept. Although many ways to start a detonation have been proposed (see e.g. Plewa et al., 2004; Röpke & Niemeyer, 2007), it is still uncertain whether any of them are sensible. Nevertheless, it is now widely agreed that a pure deflagration can perhaps only explain the least energetic SNe Ia and that invoking a DDT is mandatory (Gamezo et al., 2003; Röpke et al., 2007).

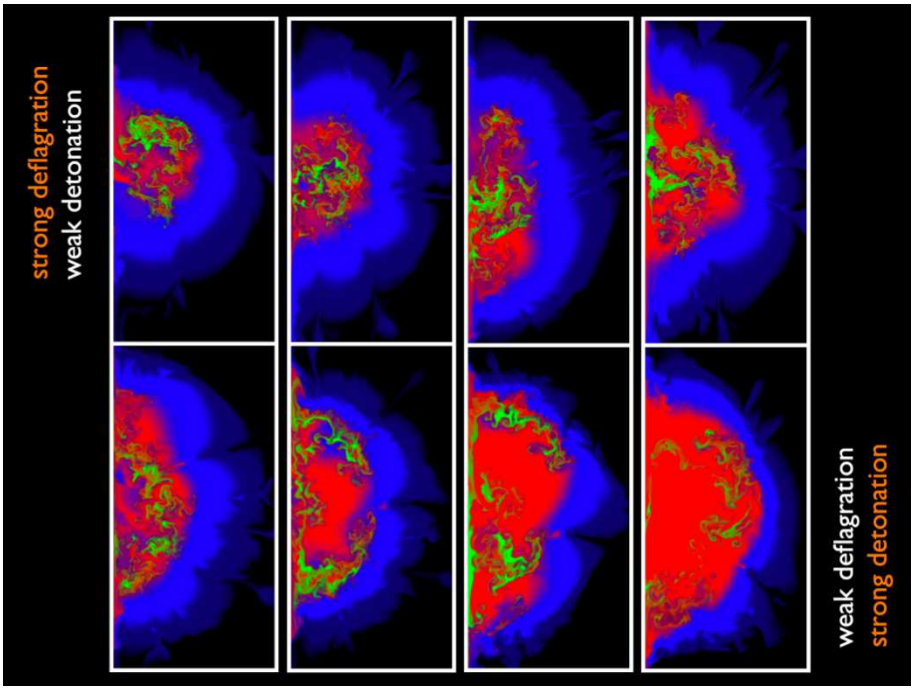

Figure 2.3: *From Kasen et al. (2009). A simulation of a SN Ia explosion. This is a delayed detonation model showing different relative strengths of the deflagration and detonation components in the upper and lower panel. The chemical structure as the burning proceeds (from left to right) is color-coded: blue represents IMEs, green stable iron group elements produced by electron capture and red* ^{56}Ni*. As expected, a strong detonation burns a larger fraction of the progenitor to* ^{56}Ni*, leaving behind less IMEs and will thus be observed as a brighter SN Ia. We also observe that, due to Rayleigh-Taylor instabilities, the inner regions are turbulently mixed rather than radially stratified.*

The goals of the models today have been shifted towards explaining the observational diversity of SNe Ia. In Figs. 2.3 & 2.4 we show the latest simulations and results by Kasen et al. (2009), which are able to explain the diversity in the properties of normal SNe Ia, by varying the relative strength of the two explosion phases and by inducing different degrees of asymmetry in the explosion. The importance of asymmetry as a parameter of diversity has been realized recently and some progress in this field will be presented in Sect. 4.7. Nevertheless, there have been some peculiar under-luminous events, such as SN 2005hk (Phillips et al., 2007) and SN 2008ha (Foley et al., 2009) for which a pure deflagration represents a viable model, although SN 2008ha has been proposed to actually be a core-collapse event (Valenti et al., 2009).

So it might be that we are looking at a whole family of progenitors and explosion mechanisms. Today many observational goals remain. The question, especially for cosmology, is to realize if at least all normal SNe Ia are products of the same mechanism and how to exclude the peculiar events. It remains to be confirmed observationally that a DDT explosion can at least describe the normal SNe and to figure out how the explosion proceeds (e.g. is the initial deflagration ignited off-centre?). But also observations of peculiar events are needed if we want to understand exactly where they fit in this picture. Except from the most traditional methods, such as early photometry and spectroscopy, other promising tools, more expensive observationally, have to be exploited, such as late-time observations, the importance of which is outlined in the next section, or spectropolarimetry (Wang & Wheeler, 2008; Patat et al., 2009).

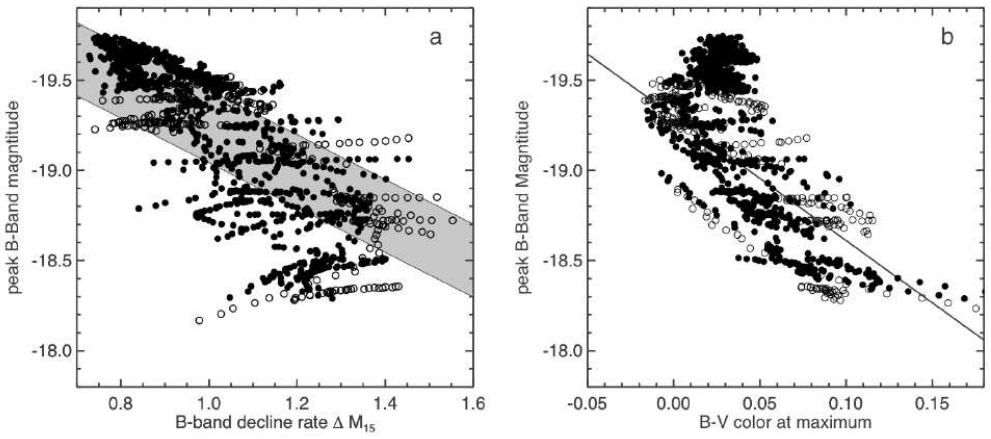

Figure 2.4: *From Kasen et al. (2009). Peak B-band luminosity versus Δm_{15} and $B-V$ color for a family of 44 models like the ones in Fig. 2.3 observed from 30 different viewing angles. It is shown that varying the model parameters (and the observing angle) creates a dispersion in the observed properties of the SN, which is similar, although not identical, to the dispersion that is actually observed (indicated by the grey zone and the solid line). This 'unified' explosion model can still, however, not explain the sub-luminous or the extremely over-luminous (e.g. Howell et al., 2006) SNe.*

2.5 WHAT CAN LATE-TIME OBSERVATIONS TELL US?

With time, the SN ejecta become more and more optically thin and we can look deeper and deeper, towards the centre of the explosion. This is called the *nebular* phase of the SN (as compared to the early *photospheric* phase). Some authors use the term *nebular* to describe SNe Ia already at phases $\sim$60 days past maximum, when the optical depth is reduced sufficiently and the spectrum is dominated by Fe lines. Iron-family elements are synthesized deeper in the explosion but are hidden at earlier phases by IMEs that are produced in the outer layers (e.g. Fig. 2.3). As a convention, in this thesis, *nebular* will only be used for even later phases, in any case not before 200 days, when the outer ejecta are really transparent to photons.

A wealth of information can be deduced from studying the nebular phases. Nebular spectroscopy, combined with modeling, allows the estimate of the total mass of Fe-group elements (stable and radioactive) generated at the explosion. This has been used to demonstrate that most SNe Ia, including sub-luminous, originate from progenitors of similar masses (Mazzali et al., 2007). Nebular spectroscopy can also be used to test explosion models of SNe Ia such as the pure deflagration by Röpke (2005). Kozma et al. (2005), by synthesizing a nebular spectrum for this model, was able to show that the increased mass of produced IMEs, should be demonstrated by a non-observed prominent O line, thus ruling it out. The explosion mechanism can also be probed by studying the line-widths of lines and thereby the degree of ejecta stratification. Gerardy et al. (2007) argue that the ejecta of SNe appear stratified, contrary to deflagration models that predict a considerable amount of mixing. The line-profiles can further be used to test the existence and extent of a central region of stable, as opposed to radioactive, elements created by electron-capture (Höflich et al., 2004; Motohara et al., 2006). The velocity shift of lines can be studied to probe potential asymmetries of the explosion (Motohara et al., 2006; Gerardy et al., 2007). Until recently, it was thought that this was only possible with isolated lines at IR wavelengths, but in Sect. 4.7 we show that this is also possible with optical spectra.

The late-time light curves of SNe Ia can be used to test whether the positrons produced at the radioactive decays escape the ejecta or remain confined in it. The idea behind this test is the following: the SN light curves are powered by energy deposited by gamma-rays and positrons produced in the decays $^{56}\mathrm{Co} \rightarrow {}^{56}\mathrm{Fe}$ (with a half-life of $\sim$77 days; the preceding $^{56}\mathrm{Ni} \rightarrow {}^{56}\mathrm{Co}$ decay has a half-life of only 6 days and is thus irrelevant at late phases). The bulk of the energy ($\sim 97\%$) is carried by the photons and this is why the

contribution of the positrons at early phases is negligible. At nebular phases, however, the ejecta is optically thin and thus all gamma-rays are able to escape and the light curve is only powered by the thermalization of the positrons. By comparing the rate of decline of the bolometric LC with that of ^{56}Co, we can conclude if positrons escape the ejecta or not (Cappellaro et al., 1997; Milne et al., 1999, 2001; Lair et al., 2006). This has at least two important implications: positrons are charged particles and are therefore subject to the magnetic field of the SN ejecta, and therefore of the WD (Colgate et al., 1980). If positrons escape the ejecta it means that the magnetic field is weak and/or radial, while if they don't, it is strong and/or tangled (Ruiz-Lapuente & Spruit, 1998). In addition, positrons escaping from SNe Ia are suspected to contribute to the galactic 511 keV annihilation line, whose origin is yet unknown (Chan & Lingenfelter, 1993; Prantzos, 2008).

At late times it is also possible to study the presence of the Infrared Catastrophe (IRC). The IRC is a thermal instability, which occurs when the ejecta temperature falls below a critical limit. The emission is then predicted to shift from the optical and NIR wavelengths to the mid- and far-infrared fine-structure lines (Axelrod, 1980). The IRC has been proposed to explain the line evolution of SN 1987A (Spyromilio & Graham, 1992; Kozma & Fransson, 1998a), but it has never been observed for a thermonuclear SN. The IRC should manifest itself as a sudden drop in the optical and NIR light curves at times $>$500 days for SNe Ia.

All the above tests pre-suppose the construction of an accurate bolometric LC based on the observed data at late times. Previous studies, using optical data alone, were based on an assumption that the bolometric LC followed the optical bands at late times (e.g. Cappellaro et al., 1997; Milne et al., 1999). Important observations of SN 2000cx, however, showed that there is a significant color evolution at late times, towards the NIR that demonstrates almost constant emission between 300-500 days (Sollerman et al., 2004). Hints for this behavior were also seen by Spyromilio et al. (2004), based on only two data points, and were later confirmed by Stritzinger & Sollerman (2007). It becomes therefore obvious that the correct answer to all the questions above cannot ignore NIR observations.

In individual cases, late time observations can also reveal the presence of echoes, which are useful in studying the nature and geometry of intervening material to the SN. Such echoes for thermonuclear SNe have been examined by Schmidt et al. (1994); Cappellaro et al. (2001); Wang et al. (2008); Crotts & Yourdon (2008).

Finally, late time observations are also essential for the study of peculiar SNe. For instance, despite the evidence for SN 2006gz being a super-Chandrasekhar explosion (Hicken et al., 2007), observations by Maeda et al. (2009) suggest, surprisingly, rather the opposite behavior at nebular phases.

Section 3.4.1 is based on: Malesani, D.; Fynbo, J. P. U.; Hjorth, J.; Leloudas, G.; Sollerman, J.; Stritzinger, M. D.; Vreeswijk, P. M.; Watson, D. J.; Gorosabel, J.; Michałowski, M. J.; Thöne, C. C.; Augusteijn, T.; Bersier, D.; Jakobsson, P.; Jaunsen, A. O.; Ledoux, C.; Levan, A. J.; Milvang-Jensen, B.; Rol, E.; Tanvir, N. R.; Wiersema, K.; Xu, D.; Albert, L.; Bayliss, M.; Gall, C.; Grove, L. F.; Koester, B. P.; Leitet, E.; Pursimo, T.; Skillen, I. – *Early Spectroscopic Identification of SN 2008D*. Astrophysical Journal Letters, vol. 692, pp. 84-87, February 2009.
Section 3.4.2 is based on: Thöne, C. C.; Michałowski, M. J.; Leloudas, G.; Cox, N. L. J.; Fynbo, J. P. U.; Sollerman, J.; Hjorth, J.; Vreeswijk, P. M. – *NGC 2770: A Supernova Ib Factory?* Astrophysical Journal, vol. 698, pp. 1307-1320, June 2009.

3

STRIPPED-ENVELOPE CORE-COLLAPSE SUPERNOVAE

This chapter offers an introduction to stripped-envelope core-collapse SNe, the explosions of stars that have lost their outer layers. After a general literature review on their observational properties, key points and big question-marks, I focus on their relation to GRBs and on their corresponding environments, aspects that are necessary for the understanding of Chapters 5 and 6. The chapter concludes with a relevant example case study, in which I have participated, of a stripped-envelope CC event, SN 2008D, and its host galaxy.

3.1 OVERVIEW

As discussed in Sect. 1.1, the history of SNe Ib/c started in the mid-80s (see e.g. Wheeler & Harkness, 1990). Today, it is widely accepted that these explosions represent the core-collapse of stars that have lost their hydrogen envelope, due to strong winds or binary interaction, while in the case of SNe Ic the mass loss is so extreme that even (most of) the helium envelope is also expelled. This picture is supported by their optical spectra at maximum light that lack hydrogen and are characterized by the presence, or not, of He lines (see Fig. 3.1). They are however more clearly distinguished from SNe Ia with the help of late-time spectra that present emission lines from IMEs, such as O and Ca (while SNe Ia show Fe lines).

Due to the fact that they have expelled their outer envelope, they are also collectively known under the name 'stripped-envelope' CC SNe. This class formally also contains SNe IIb, which are an intermediate class between Type II and Ib. These objects display hydrogen in their initial phase spectra, but they later evolve similar to SNe Ib, demonstrating that they were stripped from all but a little part of their hydrogen envelope. The prototype of this family is the very nearby SN 1993J (e.g. Nomoto et al., 1993; Woosley et al., 1994; Filippenko et al., 1993). Their existence is important in proving the continuity in the scheme of SNe II, IIb, Ib and Ic being all of core-collapse nature with a gradual degree of mass loss.

Despite the fact that SNe Ib/c constitute about 30% of all core-collapse SNe (Cappellaro et al., 1999), until recently only a small fraction of the stripped-envelope CC SNe from the ones discovered and reported in the IAU circulars were well-observed. For many years, the prototype SN Ib was SN 1983N (Wheeler & Levreault, 1985; Uomoto & Kirshner, 1985), while SN 1994I (Filippenko et al., 1995; Richmond et al., 1996) was considered the prototype SN Ic, although we now know that it might not be that representative. Richardson et al. (2006) collected and studied the LCs of 20 stripped-envelope CC SNe (in the V-band where most data was available). The LCs show considerable diversity in peak brightness, the width of the peak, and the slope of the late-time tail. Richardson et al. (2006) conclude that the probability of having only one, or even two, families of explosions is very low. The situation, concerning lack of data, has radically changed in the last years with the extensive observations of events, such as SN 2005bf (Folatelli et al., 2006), SN 2007Y (Stritzinger et al., 2009), SN 2007gr (Valenti et al., 2008a), SN 2008ax (Pastorello et al., 2008), SN 2008D (Sect. 3.4) and the SNe observationally connected to GRBs (Sect. 3.2). In addition,

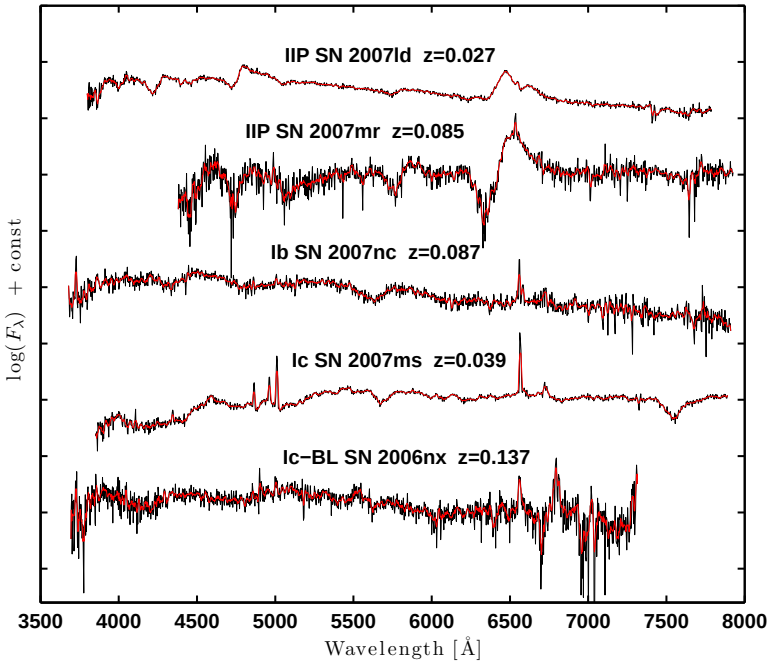

Figure 3.1: *Example spectra of CC SNe observed by GL for the SDSS-II SN survey (see caption, Fig. 2.1). Since the SDSS was targeting mainly SNe Ia, the selection of CC SNe from our database was limited with respect to S/N or phase. Nevertheless, some representative examples have been displayed to illustrate the observational diversity of explosions due to the same cause (i.e. core-collapse of a massive star) but with different degrees of mass loss prior to explosion. SN 2007ld is a Type II SN, demonstrating broad H lines (H_α, H_β, H_γ) revealing the presence of a massive H envelope. It belongs to the IIP sub-class, the most common type of SNe observed. SN 2007mr is a similar explosion. Despite having lower S/N it has been displayed here to illustrate the prominent P-Cygni profile of the H_α line, a feature very characteristic of SN explosions (and outflows in general). The next SN (2007nc) has clearly no signs of H in its spectrum and is classified as a Ib, as it displays He (e.g. λ5876). SN 2007ms is a more difficult case as it gave fits to both SNe Ic and peculiar SNe II such as SNe 1987A and 1993J (using the SNID code; Blondin & Tonry, 2007) and this is why it was classified as a Type II in the IAU circular (Bassett et al., 2007). A more careful look shows, however, that it is a SN Ic, most similar to SN 2004aw (also reclassified as such in Östman et al.). Finally the last (noisy) spectrum belongs to the rare class of broad-lined Ic, sometimes related to GRBs, (SN 2006nx; see also Modjaz et al., 2008b). All spectra demonstrate super-imposed narrow nebular lines from their host galaxy that are very useful for determining the exact redshift.*

a number of events have been closely monitored by programs such as the CSP and the SDSS-II SN Survey, but await publication.

Stripped-envelope CC SNe are often radio emitters (see Weiler et al., 2002, for a review). This emission is attributed to the strong interaction of the ejecta with the circumstellar medium and is very useful for studying the mass-loss properties of the progenitor (e.g. Chevalier & Fransson, 2006). Stripped-envelope CC SNe are therefore today the targets of large radio surveys with more than 140 objects targeted to date (e.g. Soderberg et al., 2006, 2010).

Stripped-envelope CC SNe are believed to be aspherical explosions. This is based both on spectropolarimetric observations (e.g. Maund et al., 2007; Wang & Wheeler, 2008; Maund et al., 2009) but also on observations of nebular spectra. This is in particular based on analysis of the [O I] $\lambda\lambda$6300, 6364 line that

is found to display various profiles interpreted as a torus-jet explosion viewed from different angles (Maeda et al., 2008; Modjaz et al., 2008c; Taubenberger et al., 2009). However the unambiguity of this technique has been questioned (Milisavljevic et al., 2010).

One of the key questions related to stripped-envelope CC SNe is whether they come from the evolution of single or binary stars. Based on the observed ratio of SNe Ib/c to II, combined with the IMF, Smartt (2009) argues that there are not enough massive stars to explain all the SNe Ib/c as coming from single massive stars. A similar reasoning is given by Fryer et al. (2007) based on the Ic/Ib ratio but this is dismissed by Boissier & Prantzos (2009). In addition, pre-explosion images put strict upper limits on the progenitors' luminosities that, combined with the current models, are inconsistent with those of single massive stars (Maund et al., 2005; Crockett et al., 2007, 2008b,a). The progenitor system of the Type IIb SN 1993J was also proposed to be a binary star (Podsiadlowski et al., 1993) and the companion of the exploding star has been identified (Maund et al., 2004). Combining these facts with the demonstration by Podsiadlowski et al. (1992) that a significant fraction of stars (15-30%) loose their hydrogen envelope due to binary evolution, has shaped the favored belief in the astrophysical community that, at least a fraction of SNe Ib/c must originate from the binary evolution channel. In any case, the progenitor star prior to explosion should be (or have characteristics similar to) a Wolf-Rayet (WR) star, stars that have also expelled their hydrogen mantle.

3.2 THE RELATION TO GRBS

The possibility that the gravitational collapse of massive stars might result in relativistic polar jets was proposed by Woosley (1993). Although the original collapsar model spoke about 'failed supernovae' (MacFadyen & Woosley, 1999), the discovery of SN 1998bw coincident with the location of the under-energetic GRB 980425 gave the first observational evidence that GRBs were related to the collapse of massive stars accompanied by SNe (Galama et al., 1998). The unambiguous association of GRB 030329 to SN 2003dh (Fig. 3.2) erased all doubts and confirmed this picture (Hjorth et al., 2003; Stanek et al., 2003). Previously, many bumps in GRB afterglow light curves were interpreted as SNe peaking a couple of weeks after explosion (Woosley & Bloom, 2006), while there had also been a more uncertain (noisy) spectroscopic association (Della Valle et al., 2003).

Since then, there have been two more unambiguous associations, those of SN 2003lw with GRB 031203 (Malesani et al., 2004) and of SN 2006aj with XRF 060218 (Pian et al., 2006; Campana et al., 2006; Sollerman et al., 2006), the last one being actually an X-ray flash.[1]

It is remarkable that all the confirmed GRB-SNe are of a peculiar Type Ic class, demonstrating very broad lines in their spectra and unusually high luminosities. The width of the lines imply very high expansion velocities ($\sim$30000 km/s) and this is why these energetic explosions have also been known as 'hypernovae'. However, the term 'broad-lined' SNe is often preferred to describe a broader class with similar spectra (also containing objects not connected to a GRB), since not all these events are super-energetic (Richardson et al., 2006). It is also worth mentioning that most of the confirmed SN-GRBs (with the exception of GRB 030329) are sub-energetic, compared to the global GRB population, indicating a probable local selection bias.

A shadow on our understanding of these explosions, as established by the observations of the 4 objects above, was cast by the observations of the nearby long GRBs 060505 (Fynbo et al., 2006) and 060614 (Fynbo et al., 2006; Della Valle et al., 2006; Gal-Yam et al., 2006; Gehrels et al., 2006) that were not accompanied by a SN to limits many magnitudes fainter than SN 1998bw or even fainter SNe Ic ($M_R > -13.5$). The most obvious interpretation is that, as in the original collapsar model, all (or most of) the ejected material fell back in the forming black hole, not producing a SN (or a very faint one) (Fynbo et al., 2006) . The possible interpretation of the faint SN 2008ha as a CC SN (Valenti et al., 2009) might

[1] The very same days this section was written, *Swift* discovered another unambiguous case: SN 2010bh associated with the nearby ($z = 0.059$) GRB 100316D (Bufano et al., 2010; Chornock et al., 2010)!

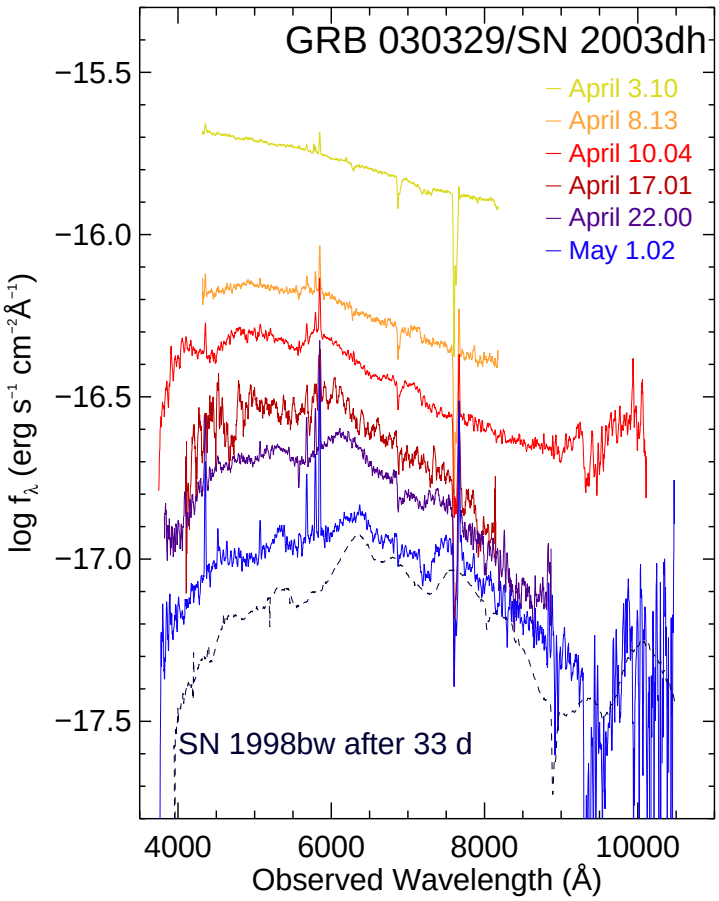

Figure 3.2: *From Hjorth et al. (2003). The gradual emergence of a broad-lined SN spectrum, similar to SN 1998bw, is demonstrated in observations of the GRB 030329 afterglow.*

constitute a possible discovery of such a stripped-envelope SN, at limits almost consistent with the non-detections above ($M_R = -14.5$). However, more speculative interpretations have also been given, such as that these two long GRBs are not related to the collapse of a massive star. In any case, there are still many open questions in the SN-GRB connection that remain to be answered.

The serendipitous discovery of SN 2008D through transient X-ray emission has also been interpreted by some groups as a signature of a GRB jet, although this is controversial. This is further discussed in Sect. 3.4.3. Certainly, however, except from giving us insight to the nature of GRBs, the discovery of SNe through their high energy emission, unlike traditional discovery methods, permits to strictly constrain the time of explosion and allows detailed studies of the early explosion physics such as the shock-breakout phase.

Since the GRB emission is collimated, it is very probable that some jets 'miss us', while we only detect the SN emission. Such a scenario has been proposed for individual broad-lined SNe Ic, such as SN 2003jd (Mazzali et al., 2005), but this has been questioned (Soderberg et al., 2006). What is definitely certain is that not all SNe Ib/c have an associated GRB. Arguments related both to radio emission (Soderberg et al., 2006) and rates (Guetta & Della Valle, 2007), place an upper limit not higher than 10% in the fraction of SNe Ib/c (even broad-lined) that contain GRBs. It is therefore natural to ask: what are the conditions that will produce a GRB and what makes the difference between a GRB-SN and 'ordinary' SN Ib/c?

In the collapsar model (Woosley, 1993; MacFadyen & Woosley, 1999), three key ingredients are necessary to form a GRB jet: (i) the formation of a black hole from a collapsing massive star, (ii) fast rotation, so that the infalling matter will form an accretion disc around the black hole, and (iii) the loss of the hydrogen envelope, for the jet to escape the collapsing star. It has been proposed that in order to satisfy the above criteria (especially the last two simultaneously), the collapsing star should be metal-poor (Yoon & Langer, 2005; Woosley & Heger, 2006). Lots of effort has therefore been concentrated in studying the environments of these explosions, especially in relation to this picture. These efforts are reviewed in the next section.

3.3 THE BIRTHPLACES OF SNE IB/C AND GRBS

Concerning the global properties of SN host galaxies, van den Bergh et al. (2005) have shown that the SNe Ib/c hosts are morphologically indistinguishable from the ones of SNe II. Prantzos & Boissier (2003), however, showed that the ratio of SNe Ib/c to SNe II increases as one moves towards brighter and therefore, on average, more metal-rich galaxies. This was confirmed by Prieto et al. (2008), in a more direct way, i.e. by using metallicities computed from host galaxy spectra from the SDSS.

But what about the local environments of the SN explosions? van Dyk et al. (1996) argued that the association degree of SNe Ib/c and SNe II with H II regions are not different. This is in contrast to the result by Anderson & James (2009) who show that there is an observed increasing trend in the distances of SNe II, Ib and Ic respectively, from actively star forming regions (measured by H_α emission). But also Kelly et al. (2008) show that SNe Ic have a tendency of occurring in the brightest pixels of their galaxies, in contrast to SNe II that follow their host galaxy light distribution. These results are in agreement with SNe II, Ib and Ic having increasingly more massive progenitors, at least in the single evolutionary channel scenario (see also the models by Raskin et al., 2008). Boissier & Prantzos (2009), taking this time into account the offset distance of the SN to the galaxy centre and a metallicity gradient, show that their result on the ratio of Ib/c to II, holds as well for the local explosion sites. For normal SNe, this is the expected trend since Vink & de Koter (2005) have shown that the strength of stellar winds, and thus the ability to expel the outer envelope, increases with metallicity.

As far as GRB host galaxies are concerned, they are globally different from the SN hosts (Fruchter et al., 2006): instead of spirals, they tend to be less massive, more actively star-forming, dwarf irregulars. This view is supported by many investigations (e.g. Michałowski et al., 2008; Castro Cerón et al., 2008; Savaglio et al., 2009). The suspicion that they are also metal-poor, based on their luminosities, is also confirmed directly spectroscopically (Levesque et al., 2010a).

Few studies of the local environments of GRBs have been conducted. Based on the higher resolution of the HST, Fruchter et al. (2006) demonstrated that GRBs tend to occur in the brightest pixels of their hosts, a distribution not very different than the one of SNe Ic (Kelly et al., 2008). These authors use a method to compare locations of regions within galaxies, irrespective of the galaxy size and brightness. This method is also used in the work presented in Chapter 5 and uses the concept of the pixel 'fractional flux'. This is defined as the fraction of light (i.e. counts) contained in all pixels with flux less than the pixel in question (e.g. i-th pixel) over the light contained in all pixels belonging to the galaxy:

$$FF_{\text{i-th pixel}} = \frac{\sum_{\text{pixels with counts} < \text{i-th pixel}} \text{counts}}{\sum_{\text{all galaxy pixels}} \text{counts}} \tag{3.1}$$

Otherwise, resolved GRB host studies are by necessity restricted to the nearby universe. The host of GRB 980425 has been studied in detail by many authors (e.g. Christensen et al., 2008) that note the presence of a very bright highly star-forming region containing WR stars not far, but not coincident with, the explosion. Thöne et al. (2008) studied the resolved host of the SN-less GRB 060505 and showed that the explosion location had a younger age and lower metallicity than the average host.

Sollerman et al. (2005) obtained spectra at the locations of nearby GRB-SNe and showed that they were located at metallicities below solar. Modjaz et al. (2008b) compared these metallicities with those obtained at the locations of other broad-lined SNe Ic, not related to GRBs, and showed that they are systematically lower. This is consistent with the requirement suggested for the formation of a GRB jet (Yoon & Langer, 2005; Woosley & Heger, 2006). Although this paradigm seems to be supported by observations, it is not clear how much it is affected by biases: we measure metallicities for the GRBs we see, while *dark* GRBs can be hidden by dust in likely more metal-rich environments (Fynbo et al., 2009; Svensson et al., 2010; Hashimoto et al., 2010). The discovery of a dark GRB (Levesque et al., 2010b) and a relativistic SN at supersolar metallicities (Soderberg et al., 2010) seems to put this general picture at least under some questioning.

Much of the discussion on explosion host sites has been centered around metallicity. There are however other important diagnostics that can constrain the progenitor system. One of these is constraining the age of the stellar population and thereby the masses of the progenitors. This can be especially useful in differentiating the single from the binary channel scenario for the stripped envelope CC SNe. Since single massive stars live fast and die young, demonstrating a large age could be in favor of the binary evolution. This is a difficult task however, since there exist many uncertainties, especially related to the star formation history (i.e. continuous or instantaneous; see e.g. Östlin et al., 2008).

3.4 A CASE STUDY: THE TYPE IB SN 2008D

In the last part of this Chapter dedicated to stripped-envelope CC SNe, I will present SN 2008D as an example. This SN Ib and its birthplace was studied by our group and using it as a case study serves as an excellent transition between the introduction above and my work presented in Chapters 5 & 6. The observations of the SN itself (Malesani et al., 2009) are presented in Sect. 3.4.1, while its birthplace and host (Thöne et al., 2009) are discussed in Sect. 3.4.2. This SN was definitely the 'supernova of the year' for 2008, and has attracted a lot of attention. For this reason, in Sect. 3.4.3, I reproduce parts of the discussions and opinions expressed about this object.

3.4.1 OBSERVATIONS OF THE SUPERNOVA

SN 2008D was discovered serendipitously through X-ray transient emission, while the XRT instrument onboard *Swift* was observing SN 2007uy in NGC 2770 (Berger & Soderberg, 2008). An optical counterpart was identified by Deng & Zhu (2008) and was given a SN designation by Li & Filippenko (2008). Based on an optical spectrum obtained just 1.7 days after the X-ray outburst, Malesani et al. (2008a) were the first to suggest that it was of Type Ib/c. Valenti et al. (2008b) and Blondin et al. (2008) also classified it as a SN Ic, while it still appeared as such 6 days after explosion (Malesani et al., 2008b). One week later, however, it developed clear He lines and was given its final classification as a SN Ib (Modjaz et al., 2008a).

Immediately after the X-ray outburst we started an observational campaign and collected photometry and spectra of the SN. Most of the data were obtained at the NOT, but we also obtained data with the VLT, WHT, LT and UKIRT telescopes. The light curves are shown in Fig. 3.3. In the bluest bands (but even in the R-band) we observe an initial fading followed by a re-brightening. This was also observed in SNe 1993J, 1999ex (Stritzinger et al., 2002) and 2006aj (Sollerman et al., 2006), which were also stripped-envelope CC SNe caught shortly after explosion. The fading is attributed to the initial cooling of the stellar envelope after the shock breakout. Subsequently, the SN LC rises again as it is powered by the radioactive decays of material nucleosynthesized during the explosion. By using Arnett's rule (Arnett, 1982), we estimated that the explosion generated $\sim$0.09 $M_{\odot}$ of ^{56}Ni. The SN seems significantly reddened and we determined an $A_V \sim 0.8$ mag using different methods, including the comparison of the colors at maximum light with the ones of other stripped envelope core-collapse SNe.

The first spectrum of SN 2008D is comparable in age only with the first spectrum of SN 1987A. An

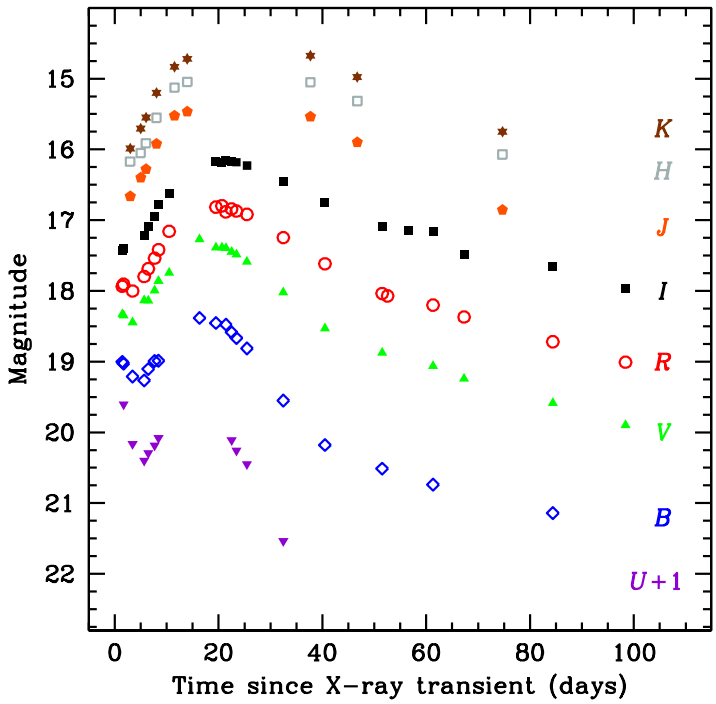

Figure 3.3: *From Malesani et al. (2009). $UBVRIJHK$ light curves of SN 2008D. The $UBVRI$ photometry was made by GL.*

interesting feature is a W-shaped profile at ∼4000 Å that has been also seen in other very early spectra of CC SNe but its nature is not yet clear (Quimby et al., 2007; Modjaz et al., 2009; Silverman et al., 2009). The expansion velocities and their evolution are clearly slower than the ones of broad-lined SNe.

3.4.2 THE HOST GALAXY NGC 2770

NGC 2770 has been the host of two more SNe, that were also of Type Ib: SN 2007uy and SN 1999eh. While there have been many galaxies with multiple observed SNe, NGC 2770 was the only one (at least at that time) with more than two stripped-envelope CC SNe. Our study was triggered by the following questions, among others: is there anything special about NGC 2770 that makes it produce SNe Ib, compared e.g. to NGC 6946, the top SN producer (9 SNe) that has only produced SNe II? And what are the local properties at the explosion sites?

We first studied the global properties of NGC 2770 by constructing its multi-wavelength SED (e.g. Michałowski et al., 2008). The result was revealing, since the template SED that best matched the one of NGC 2770 was the average of a Sb and Sc galaxy based on exactly NGC 6946! This is in line with the result of van den Bergh et al. (2005), i.e. that the galaxies of SNe II are no different than those of SNe Ib/c, and highlights once again that the *differences need to be sought in the local environments*.

For this reason, we obtained spectra at the locations of all 3 SNe explosions (2 of them still containing light from the SNe) and across the galaxy major axis to determine the local properties. Based on the N2 diagnostic (Pettini & Pagel, 2004), we found all metallicities at the SN sites to be subsolar ($12 + \log(\mathrm{O/H})$ ∼8.4–8.5 dex). Interestingly, these values are on the lower side of the (broad-lined) SNe Ic but higher than GRB-SNe environments (Modjaz et al., 2008b). We determine the extinction, based on the Balmer decrement (Osterbrock, 1989), to be significant, A_V ∼0.9 mag for SN 2008D, consistent with the estimates

of Malesani et al. (2009). Finally, the H_α EW was determined to be less than 80 Å in neighboring regions of the SN explosions, indicating a not particularly young stellar population. Comparatively, the existence of massive stars $> 30 - 40\ M_\odot$, with lifetimes $< 6 - 7$ Myr would correspond to H_α EW > 100 Å. This could be an indication in favor of the binary progenitor channel for these 3 explosions.

Finally, we wanted to investigate whether the occurrence of 3 SNe Ib in one galaxy in such a short time interval was peculiar. By using the rates for SNe Ib/c given by Cappellaro et al. (1999) and Mannucci et al. (2005) and comparing with the B and K luminosities of NGC 2770 and the number of monitored galaxies, we calculate that the chance of having 3 stripped-envelope CC SNe in one galaxy within a decade, is $\sim$0.6%. This is barely a 3σ statistical fluctuation and we thus conclude that it was probably just a coincidence (one more related to this event).

3.4.3 SHOCK BREAKOUT OR A GRB JET?

There has been some debate on the nature of the X-ray emission related to the explosion of SN 2008D. Soderberg et al. (2008) were the first to attribute it to the shock breakout, while this is also the view of Chevalier & Fransson (2008) and Modjaz et al. (2009). Following this interpretation, SN 2008D was a more or less ordinary stripped-envelope CC explosion, with the exception that it was caught very early due to a lucky coincidence.

An alternative suggestion, namely that SN 2008D is an object intermediate to ordinary SNe and GRB-SNe, was first proposed by Xu et al. (2008). Such an interpretation is also given by Li (2008) and Mazzali et al. (2008), based on arguments such as that the X-ray light curve follows a similar (but scaled-down evolution) as of SN 2006aj, that it follows the Amati relation (Amati et al., 2002) but at much smaller energies, and that it is more energetic than other typical SNe Ib/c. Within such an interpretation, the X-ray emission was probably due to some kind of relativistic (GRB-like) jet. The different authors do not agree on how to fit the early X-ray emission, while the determination of the progenitor size is clearly model dependent.

Tanaka et al. (2009a) indeed showed that SN 2008D produced ejecta with $E_K \sim 6 \times 10^{51}$ erg, which is higher than what is usually observed. Another established fact is that the explosion was aspherical as can be demonstrated by spectropolarimetric observations (see Maund et al., 2009, who offer two alternative jet-torus scenarios). The asphericity is also supported by observations of the nebular spectrum (Modjaz et al., 2009; Tanaka et al., 2009b). But these observations are not unusual for SNe Ib/c (Sect. 3.1) and are not inconsistent with a shock breakout.

I personally think that the arguments in favor of SN 2008D being related to a GRB are weak, although this possibility cannot be ruled out. The way of discovery, combined with the small field of the XRT, and the theoretical argumentations in favor of a shock-breakout, which was definitely observed at longer wavelengths (Malesani et al., 2009), point towards SN 2008D being an ordinary SN. As also pointed out by Soderberg et al. (2008), if this is the case, wide field X-ray instruments would be able to detect many such SNe at their moments of birth.

Published as: Leloudas, G.; Stritzinger, M. D.; Sollerman, J.; Burns, C. R.; Kozma, C.; Krisciunas, K.; Maund, J. R.; Milne, P.; Filippenko, A. V.; Fransson, C.; Ganeshalingam, M.; Hamuy, M.; Li, W.; Phillips, M. M.; Schmidt, B. P.; Skottfelt, J.; Taubenberger, S.; Boldt, L.; Fynbo, J. P. U.; Gonzalez, L.; Salvo, M.; Thomas-Osip, J. – *The normal Type Ia SN 2003hv out to very late phases* Astronomy & Astrophysics, vol. 505, pp. 265–279, October 2009.
Except from Sect. 4.7 that is based on: Maeda, K.; Taubenberger, S.; Sollerman, J.; Mazzali, P. A.; Leloudas, G.; Nomoto, K.; Motohara, K. – *Nebular Spectra and Explosion Asymmetry of Type Ia Supernovae*. Astrophysical Journal, vol. 708, pp. 1703–1715, January 2010; as well as on Maeda, K.; Leloudas, G.; Taubenberger, S.; Stritzinger, M. D.; Sollerman, J.; Elias-Rosa N.; Benetti S.; Hamuy M. – *Explosion Asymmetry and Viewing Angle as the Second Parameter in the Type Ia Supernova Luminosity Calibration?* Submitted to MNRAS.

4

THE NORMAL TYPE IA SN 2003HV OUT TO VERY LATE PHASES

We study a thermonuclear supernova, emphasizing very late phases. An extensive dataset for SN 2003hv that covers the flux evolution from maximum light to day +786 is presented. This includes 82 epochs of optical imaging, 24 epochs of near-infrared imaging, and 10 epochs of optical spectroscopy. These data are combined with published nebular-phase infrared spectra, and the observations are compared to model light curves and synthetic nebular spectra. SN 2003hv is a normal Type Ia supernova (SN Ia) with photometric and spectroscopic properties consistent with its rarely observed B-band decline-rate parameter, $\Delta m_{15}(B) = 1.61 \pm 0.02$. The blueshift of the most isolated [Fe II] lines in the nebular-phase optical spectrum appears consistent with those observed in the infrared at similar epochs. At late times there is a prevalent color evolution from the optical toward the near-infrared bands. We present the latest-ever detection of a SN Ia in the near-infrared in *Hubble Space Telescope* images. The study of the ultraviolet/optical/infrared (UVOIR) light curve reveals that a substantial fraction of the flux is 'missing' at late times. Between 300–700 days past maximum brightness, the UVOIR light curve declines linearly following the decay of radioactive ^{56}Co, assuming full and instantaneous positron trapping. At 700 days we detect a possible slowdown of the decline in optical bands, mainly in the V band. The data are incompatible with a dramatic infrared catastrophe. However, the idea that an infrared catastrophe occurred in the densest regions before 350 days can explain the missing flux from the UVOIR wavelengths and the flat-topped profiles in the near-infrared. We argue that such a scenario is possible if the ejecta are clumpy. The observations suggest that positrons are most likely trapped in the ejecta. In the last section, a brief presentation of some follow-up work in the field of SN Ia asymmetries that was triggered by SN 2003hv, is given.

4.1 INTRODUCTION

Studying the late-phase emission of Type Ia supernovae (hereafter SNe Ia) provides an excellent opportunity to elucidate the physical nature of these thermonuclear explosions. With late-time observations it is in principle possible to constrain the nucleosynthetic yields and the distribution of elements (Kozma et al., 2005; Motohara et al., 2006; Stritzinger et al., 2006b; Mazzali et al., 2007), the magnetic field configuration of the ejecta and hence of the progenitor (Colgate et al., 1980; Ruiz-Lapuente & Spruit, 1998; Milne et al., 1999), and potentially their contribution to the diffuse Galactic 511 keV line (Milne et al., 1999; Prantzos, 2008).

Previous studies of the late-time emission of SNe Ia have demonstrated the increased importance of the near-infrared (NIR) emission. This investigation builds upon earlier studies of SN 2000cx (Sollerman et al., 2004, hereafter S04) and SN 2001el (Stritzinger & Sollerman, 2007, hereafter SS07) but extends to even later phases. We present observations of SN 2003hv that cover 786 days past B-band maximum ($B_{\max}$).

One of the main motivations of this study was to investigate whether an infrared catastrophe (IRC) occurs in the ejecta at these very late phases. The IRC is a thermal instability, predicted by Axelrod (1980), which shifts the bulk of the emission from the optical and NIR regime to the mid- and far-infrared fine-structure lines once the temperature in the ejecta falls below a critical limit. While the IRC has been proposed to explain the line evolution of SN 1987A (Spyromilio & Graham, 1992; Kozma & Fransson, 1998a), it has never been observed for a thermonuclear SN (see, however, Maeda et al., 2009, on the peculiar SN 2006gz). Models suggest that the IRC should commence, depending on the structure and composition of the ejecta, sometime between 500–700 days past maximum brightness and become apparent with a dramatic drop in the optical and NIR luminosity. This corresponds to shortly after the end of our previous multi-band observations of other SNe Ia (S04; SS07).

SN 2003hv was discovered by LOTOSS (Beutler & Li, 2003) on 9.5 September 2003 (UT dates are used throughout this paper). It was located 17″ east and 57″ south of the nucleus of the S0 galaxy NGC 1201. Dressler et al. (2003) classified it as a SN Ia the day after discovery. SN 2003hv reached an apparent B-band magnitude of 12.45 mag, thus being the brightest supernova discovered in 2003, and one of the brightest SNe Ia observed over the past decade. NGC 1201 has a direct distance measurement that is based on the surface brightness fluctuations method (SBF; Tonry et al., 2001). By applying a correction of -0.16 mag (Jensen et al., 2003), the distance modulus of NGC 1201 is $\mu_{\rm SBF} = 31.37 \pm 0.30$ mag, corresponding to a distance of 18.79 ± 2.60 Mpc. The Galactic extinction in the direction of NGC 1201 is low, $E(B-V) = 0.016$ mag (Schlegel et al., 1998), and we show below that there is no evidence of any host-galaxy extinction. As SN 2003hv suffered little extinction, was located in the outskirts of its host, and was bright, it made an excellent target for our late-time photometric ($UBVRIJHK$) and spectroscopic (optical) observational campaign.

SN 2003hv has already attracted some attention in the literature. Motohara et al. (2006) published a NIR spectrum taken 394 days past maximum brightness. They found that the [Fe II] 1.644 μm emission line exhibited a flat-topped profile and was blueshifted by $\sim$2600 km s^{-1}. Gerardy et al. (2007) showed a mid-infrared (MIR) spectrum (5.2$-$15.2 μm) of SN 2003hv taken on day $+358$ with the InfraRed Spectrograph onboard the *Spitzer Space Telescope*. From the observed [Co III] emission they estimated that $\sim$0.5 M$_\odot$ of ^{56}Ni was synthesized in the explosion. In this paper, we present a comprehensive study of SN 2003hv that covers the flux evolution from early to very late phases. Some preliminary results of our study were presented by Leloudas et al. (2009a). Here, we have used more optical and NIR early-time data, have re-analysed all data in a consistent manner, and have supplemented our late-time analysis with data from the *Hubble Space Telescope (HST)* and spectral-synthesis modeling; we have also included the spectra published by Motohara et al. (2006) and Gerardy et al. (2007).

The organization of this paper is as follows. Section 4.2 presents the observations that were collected using ground-based facilities and *HST*, and Sect. 4.3 describes the corresponding data reduction. The results are described in Sect. 4.4. Section 4.5 provides a discussion, and the main conclusions are summarized in Sect. 4.6.

4.2 OBSERVATIONS

The observations presented in this paper were conducted at optical and NIR wavelengths with a variety of facilities. A brief description of the observations is given below. Observing logs for our data are found in Table 4.1 and in Tables A.1 – A.3 of the Appendix.

4.2.1 CERRO TOLOLO OBSERVATIONS

Optical photometry of SN 2003hv was obtained with the Cassegrain Direct Imager attached to the 0.9-m telescope located at the Cerro Tololo Inter-American Observatory (CTIO). Ten epochs of $UBVRI$ imaging were obtained from 1 to 74 days past $B_{\rm max}$. In addition, the CTIO 1.3-m telescope equipped

Table 4.1: *Log of spectroscopy.*

Date (UT)	MJD (days)	Phase[a] (days)	Telescope	Instrument	Resolution (Å)	Exposure time (s)
2003 09 10	52892.35	1.2	LCO Baade	IMACS	23.0	2×300
2003 09 15	52897.34	6.1	LCO Clay	LDSS2	13.5	1×60
2003 09 18	52900.39	9.2	LCO duPont	ModSpec	6.0	2×300
2003 09 26	52908.31	17.1	LCO duPont	WFCCD	6.0	2×300
2003 10 30	52942.6	51.4	SSO 2.3 m	DBS	4.8	2×900^b
2003 11 21	52964.25	73.1	VLT Antu	FORS1	11.5	2×300^c
2003 11 28	52971.69	80.5	SSO 2.3 m	DBS	4.8	2×1200^b
2003 12 28	53001.53	110.3	SSO 2.3 m	DBS	4.8	2×1200^b
2004 01 30	53034.45	143.2	SSO 2.3 m	DBS	4.8	2×1200^b
2004 07 25	53211.37	320.2	VLT Kueyen	FORS1	11.5	4×1200^c

[a] In all tables, "phase" refers to days past $B_{\max}$, which occurred at MJD = 52891.20 ± 0.30.
[b] One exposure in the blue arm and one in the red arm.
[c] Exposures shared between the 300V and the 300I grisms.

with ANDICAM was used to collect 15 epochs of early-phase $YJHK_s$ photometry that covers the flux evolution from 1 to 62 days past $B_{\max}$.

4.2.2 KAIT OBSERVATIONS

The 0.76-m Katzman Automatic Imaging Telescope (KAIT; Filippenko et al., 2001) observed SN 2003hv in $BVRI$ over the course of 42 epochs. These observations were obtained beginning 1 day after $B_{\max}$ and extend to $+135$ days.

4.2.3 LAS CAMPANAS OBSERVATIONS

Thirteen epochs of optical photometry covering 10 to 109 days past B maximum were obtained with the Swope 1-m telescope at Las Campanas Observatory (LCO) during the course of the Carnegie Type II Supernova (CATS) program (Hamuy et al., 2009). These images were obtained with a set of $UBVRI$ filters and a SITe3 detector. Four optical spectra were obtained at LCO from 1 day to 17 days past maximum. A journal of the spectroscopic observations is provided in Table 4.1.

4.2.4 SIDING SPRING OBSERVATIONS

The European Supernova Collaboration (ESC; see, e.g., Benetti et al., 2004), as part of a European Research Training Network on the study of SNe Ia,[1] obtained four optical spectra and five epochs of photometry at the Siding Spring Observatory (SSO). These data were collected with the Imager and the Double Beam Spectrograph (DBS) on the 2.3-m telescope. They cover the intermediate phases from 52 to 202 days past maximum.

4.2.5 VLT OBSERVATIONS

The Very Large Telescope (VLT) was primarily used to obtain late-epoch observations in the optical and NIR. With the exception of one epoch of optical imaging and spectroscopy obtained on day $+73$, the VLT observations were conducted from day $+320$ to $+767$. This portion of the study complements and

[1] `www.mpa-garching.mpg.de/~rtn`

extends our previous studies of SN 2000cx (S04) and SN 2001el (SS07) by over 200 days. U- and K_s-band observations, however, were only carried out to day $\sim$540.

Optical imaging was performed with the FOcal Reducer and low dispersion Spectrographs (FORS1 and FORS2) mounted on the Antu (VLT – UT1) and Kueyen (VLT – UT2) telescopes. These observations were obtained in service mode under favorable conditions. Details can be found in Table A.1. The optical data can be divided into three main epochs: approximately 340, 520, and 700 days past maximum light. No B-band imaging was conducted during the middle epoch.

Near-infrared imaging (J_sHK_s) was performed with ISAAC (Infrared Spectrometer And Array Camera) mounted on the Antu telescope. Imaging was obtained in the short-wavelength mode using a jitter-offset technique. To facilitate a multi-wavelength study, the NIR images were taken at epochs similar to those of the optical images. A log is presented in Table A.2.

On day $+320$ a nebular spectrum was taken with FORS1. Exposures were obtained with the 300V and 300I grisms, and an order-separation filter (OG590) was used with the latter grism. The nebular spectrum of SN 2003hv was obtained using a $1\farcs3$ slit and 2×20 min exposures per grism. The final wavelength range is 3600–9750 Å.

4.2.6 HST OBSERVATIONS

Late-phase observations in the optical were acquired with *HST* during two main epochs, at 307 and 433 days past maximum brightness. These data were collected as part of a Snapshot Survey of the sites of Nearby Supernovae.[2] The observations were taken with the Advanced Camera for Surveys (ACS) using the HRC detector and the F435W, F555W, F625W, and F814W filters.

A dedicated *HST* programme was approved to probe the very late phases of SN 2003hv.[3] Unfortunately, the optical-band observations, scheduled on day $+816$, were never executed due to a technical problem with acquiring a guide star. Deep NIR observations with filter F160W (similar to the H-band filter) were obtained with the Near Infrared Camera and Multi-Object Spectrometer (NICMOS) on day $+786$. The *HST* observations are summarized in Table A.3.

4.3 DATA REDUCTIONS

4.3.1 OPTICAL PHOTOMETRY

All images were reduced in a standard manner including bias and flatfield corrections using IRAF scripts.[4] The ground-based photometry of SN 2003hv was measured differentially with respect to a calibrated sequence of local stars in the field of NGC 1201. Given the wide range in the SN brightness over the different epochs ($>$12 mag), it was necessary to calibrate both relatively bright and faint local sequence stars. The former were used to measure differential photometry of the SN on the CTIO, KAIT, LCO, and SSO images, while the latter were used with the late-epoch VLT observations. The comparison stars were calibrated with the use of standard-star observations; they are indicated in Fig. 4.1, and their magnitudes are listed in Table 4.2. The brightest stars used for the early epochs (i.e., stars 1–7) were calibrated with the help of five sets of observations on three different photometric nights. To calibrate the faint local sequence, the standard-star field PG0231+051 (Landolt, 1992) was observed under photometric conditions on 12 August 2004 with the VLT. Instrumental magnitudes of the local stars were measured with a $1\farcs6$ aperture radius (8 pixels) and then an aperture correction was applied. The associated uncertainties were computed by adding in quadrature the errors associated with the nightly zero-point, the photometry error as computed by the IRAF task `phot`, and the error associated with the aperture correction.

[2] Program GO-10272, PI Filippenko.
[3] Program GO-10513, PI Milne.
[4] IRAF is distributed by the National Optical Astronomy Observatory (NOAO): `http://iraf.noao.edu/iraf/web/`

Table 4.2: *Calibrated magnitudes for the local comparison stars in Fig. 4.1.*[a]

Star	U	B	V	R	I
1	18.228(0.002)	18.000(0.013)	17.261(0.014)	16.849(0.013)	16.431(0.022)
2	19.712(0.329)	19.254(0.024)	18.071(0.019)	17.323(0.008)	16.644(0.019)
3	17.308(0.009)	16.195(0.009)	14.919(0.010)	14.123(0.010)	13.431(0.008)
4	17.879(0.006)	16.738(0.013)	15.502(0.009)	14.731(0.010)	14.062(0.008)
5	···	16.978(0.012)	16.428(0.016)	16.093(0.016)	15.766(0.005)
6	···	18.612(0.014)	17.779(0.008)	17.253(0.008)	16.797(0.012)
7	···	16.228(0.003)	15.754(0.002)	15.432(0.002)	15.123(0.003)
8	22.179(0.059)	22.029(0.015)	21.290(0.017)	20.847(0.025)	20.470(0.045)
9	21.801(0.058)	21.665(0.011)	20.925(0.016)	20.459(0.023)	20.043(0.042)
10	19.522(0.057)	20.123(0.010)	19.933(0.015)	19.586(0.023)	19.064(0.042)
11	23.595(0.080)	22.479(0.026)	21.008(0.019)	20.069(0.024)	19.069(0.043)
12	23.606(0.071)	22.399(0.014)	20.894(0.016)	19.930(0.023)	19.018(0.042)
13	22.393(0.060)	22.206(0.018)	21.352(0.019)	20.822(0.025)	20.410(0.045)
14	22.384(0.060)	21.850(0.013)	20.885(0.016)	20.302(0.023)	19.834(0.042)

[a]Numbers in parentheses are uncertainties.

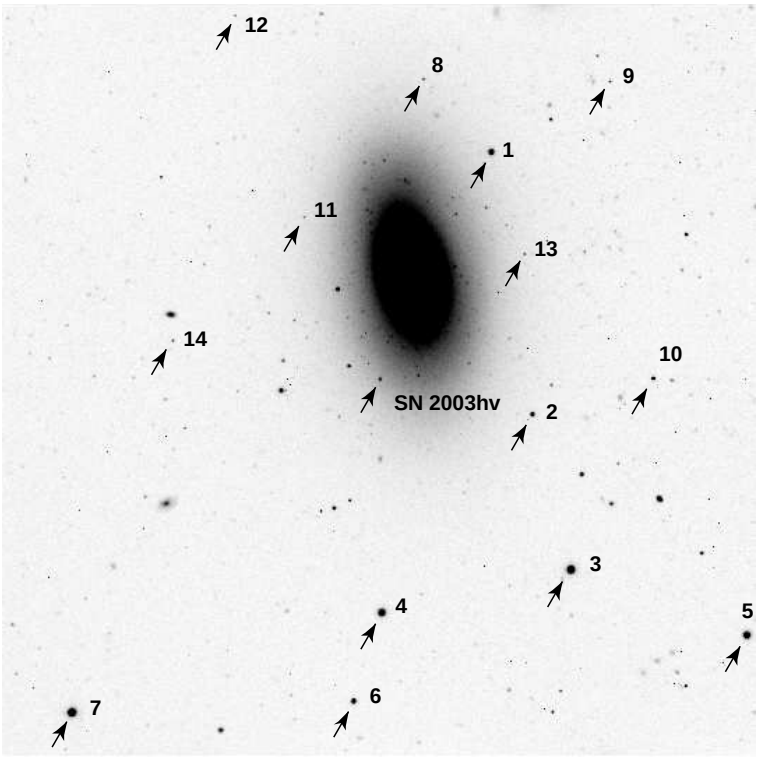

Figure 4.1: *The galaxy NGC 1201 including SN 2003hv. The field of view is north is up and east to the left. This B-band image was obtained on 12 August 2004 with VLT/FORS1, when the SN was almost 340 days past maximum. The local comparison stars are indicated with arrows. Their calibrated magnitudes are listed in Table 4.2. Stars 1–7 are brighter and were used for differential photometry in images obtained with smaller telescopes, when the SN was bright. Stars 8–14 were used mainly at later times.*

The host galaxy at the location of the supernova was subtracted from all early-epoch science images

(i.e., CTIO, LCO, SSO, KAIT) with the aid of host-galaxy templates. The template images were obtained with KAIT and the LCO duPont (+Tek5) 2.5-m telescope at times which were sufficiently late that the supernova was no longer detectable. Next, point-spread function (PSF) photometry of the local sequence and the supernova was computed from the template-subtracted images in the manner described by Hamuy et al. (2006). Galaxy subtraction was not performed on the late-time images because the templates were not deep enough. At late times (i.e., VLT), when the SN was faint, aperture photometry with small apertures ($\approx 0\farcs8$) was used to extract the light from the supernova and the comparison stars. This was done to minimize background contamination from the host galaxy. PSF photometry was also performed (with tasks in the `daophot` package) and good agreement was found with the aperture-photometry results.

Photometry of the *HST* images was done following the procedures described in the ACS Data Handbook (Pavlovsky et al., 2006) and in Sirianni et al. (2005). The flux of the supernova was measured directly in the drizzled images with a 7-pixel aperture ($0\farcs175$) and converted to the Vega magnitude system using the zero-points provided by the STScI webpage.[5] Aperture corrections as described by Sirianni et al. (2005) and a small charge transfer efficiency (CTE) correction were also applied.

4.3.2 S-CORRECTIONS

It is well known that combining data obtained with different telescopes can lead to systematic differences in the light curves of SNe. This was the case for SN 2003hv as well, with differences that were most pronounced in the R and I light curves around the time of the secondary I-band maximum. To remedy this problem we computed and applied S-corrections to our photometry (Stritzinger et al., 2002). This practice has become a standard procedure in recent years and several authors have obtained encouraging results (see, e.g., Stanishev et al., 2007; Pastorello et al., 2007; Pignata et al., 2008; Wang et al., 2009b). In the case of SN 2003hv the number of optical spectra available, especially at phases up to $+50$ days, does not offer the desired temporal and wavelength coverage necessary to compute accurate S-corrections. For this reason a different approach was chosen and our S-corrections were computed up to day $+70$ based on the spectral template sequence of Hsiao et al. (2007). At each epoch, the spectral template was multiplied by a smooth spline such that synthetic photometry constructed with this "warped" spectrum matched the observed photometry of SN 2003hv. This is a common practice when using SN spectral templates to compute K-corrections (Nugent et al., 2002; Hsiao et al., 2007).

Armed with the modified template spectra, standard procedures to compute S-corrections were followed; as a reference we adopted the $BVRI$ filter transmission functions from Bessell (1990), modified to account for the photon-counting nature of CCD detectors. The response functions used for KAIT and the CTIO 0.9-m telescope have been published by Wang et al. (2009b) and the ones for SSO 2.3-m telescope by Pastorello et al. (2007). We constructed the corresponding response functions for the LCO Swope telescope by multiplying the filter transmission functions with the detector quantum efficiency, the mirror reflectivity, and the atmospheric transmission, as functions of wavelength. To test the accuracy of the modeled passbands, they were used to derive synthetic magnitudes of a set of spectrophotometric standards (Stritzinger et al., 2005). These magnitudes were then used to derive color terms, which were compared to the color terms derived from the broad-band photometry. From this exercise we confirmed that our modeled passbands, in general, reflected a reliable model of the true global response function of each telescope. Finally, in order to compute the S-corrections we convolved the instrumental bandpasses with the spectral template sequence by Hsiao et al. (2007) modified, as described above, to match the SN 2003hv photometry. No corrections were attempted either for the U band, or for epochs past day $+70$, since this is where the spectral template sequence of Hsiao et al. (2007) ends.

The resulting values are listed in Table 4.3. Due to the fact that these S-corrections were not computed in the optimal way (i.e., based on a well-sampled series of real SN 2003hv spectra), we have chosen to provide the *uncorrected* photometry of SN 2003hv in Table 4.4. It is left to any future user of these data

[5] `www.stsci.edu/hst/acs/analysis/zeropoints`

Table 4.3: *S-corrections (mag) computed for phases up to +70 days.*[a]

MJD	B	V	R	I
52892.40	0.010	0.022	0.014	−0.034
52892.47	−0.003	0.002	0.036	−0.017
52893.39	0.010	0.021	0.015	−0.033
52893.41	−0.004	0.003	0.036	−0.018
52894.37	0.010	0.020	0.016	−0.032
52895.37	0.011	0.017	0.017	−0.031
52896.38	0.013	0.013	0.018	−0.035
52896.52	−0.005	0.007	0.037	−0.018
52897.37	0.015	0.009	0.019	−0.038
52897.51	−0.005	0.008	0.036	−0.018
52898.52	−0.006	0.009	0.034	−0.018
52899.52	−0.006	0.010	0.032	−0.018
52901.40	0.000	0.013	0.014	0.029
52901.44	−0.010	0.010	0.027	−0.019
52902.30	−0.004	0.014	0.014	0.036
52902.48	−0.016	0.010	0.025	−0.021
52903.46	−0.020	0.009	0.024	−0.022
52904.49	−0.022	0.009	0.021	−0.023
52905.26	0.034	−0.009	0.007	−0.054
52905.30	−0.012	0.015	0.010	0.057
52906.40	−0.011	0.016	0.009	0.066
52906.48	−0.018	0.008	0.018	−0.025
52907.30	−0.011	0.016	0.008	0.072
52908.30	−0.012	0.016	0.008	0.078
52910.47	−0.020	0.006	0.012	−0.026
52912.47	−0.023	0.007	0.013	−0.024
52914.40	−0.015	0.015	0.004	0.084
52914.46	−0.028	0.009	0.015	−0.020
52916.46	−0.024	0.011	0.017	−0.018
52919.42	−0.014	0.015	0.018	−0.014
52921.40	−0.012	0.017	0.019	−0.010
52925.43	−0.011	0.019	0.020	−0.007
52928.42	−0.015	0.019	0.024	−0.007
52929.40	−0.004	0.022	0.005	0.096
52930.42	−0.020	0.018	0.028	−0.007
52932.37	−0.021	0.018	0.030	−0.006
52934.41	−0.019	0.018	0.031	−0.005
52936.40	−0.015	0.018	0.030	−0.005
52939.36	−0.011	0.018	0.029	−0.004
52942.36	−0.007	0.017	0.026	−0.002
52942.66	−0.000	−0.007	−0.004	0.046
52945.38	−0.005	0.017	0.024	−0.000
52948.32	−0.004	0.016	0.023	−0.002
52951.30	0.004	0.016	0.004	0.084
52954.36	−0.003	0.016	0.022	−0.004
52959.33	0.004	0.016	0.019	−0.004
52961.28	0.022	0.003	0.004	0.010

[a] We have used these corrections everywhere in this paper by adding them to the corresponding values of Table 4.4.

to decide whether to make use of these S-corrections. An estimate of their accuracy can be based on the dispersion of the difference between the corrections derived from the templates of Hsiao et al. (2007) and real spectra. In most cases, this error was estimated to be small ($<$0.01 mag), but in a few cases the uncertainty in the correction was of the same order as the correction itself. This illustrates the limitations of the adopted method. Our experience, however, showed that the S-corrections did reduce the scatter in the light curves, and we have therefore chosen to use them everywhere throughout this paper and recommend their use. Nevertheless, some inconsistencies between the various data sets still remain, especially at times of $+$100–140 days. Resolving these remaining discrepancies is beyond the scope of this paper.

Table 4.4: Optical photometry of SN 2003hv.[a]

Date (UT)	MJD (days)	Phase (days)	Telescope	U (mag)	B (mag)	V (mag)	R (mag)	I (mag)
2003 09 10	52892.40	1.2	CTIO 0.9 m	11.940(0.152)	12.452(0.019)	12.483(0.015)	12.459(0.015)	12.759(0.015)
2003 09 10	52892.47	1.3	KAIT	···	12.523(0.015)	12.565(0.015)	12.489(0.015)	12.827(0.026)
2003 09 11	52893.39	2.2	CTIO 0.9 m	12.125(0.102)	12.505(0.020)	12.510(0.015)	12.477(0.015)	12.779(0.015)
2003 09 11	52893.41	2.2	KAIT	···	12.619(0.015)	12.616(0.015)	12.509(0.015)	12.870(0.019)
2003 09 12	52894.37	3.2	CTIO 0.9 m	12.176(0.058)	12.534(0.018)	12.546(0.015)	12.514(0.015)	12.844(0.015)
2003 09 13	52895.37	4.2	CTIO 0.9 m	12.131(0.063)	12.631(0.015)	12.573(0.015)	12.586(0.015)	12.949(0.015)
2003 09 14	52896.38	5.2	CTIO 0.9 m	12.371(0.055)	12.702(0.016)	12.594(0.015)	12.626(0.015)	12.971(0.015)
2003 09 14	52896.52	5.3	KAIT	···	12.750(0.015)	12.676(0.015)	12.693(0.015)	13.040(0.020)
2003 09 15	52897.37	6.2	CTIO 0.9 m	12.422(0.052)	12.805(0.015)	12.681(0.015)	12.742(0.015)	13.079(0.015)
2003 09 15	52897.51	6.3	KAIT	···	12.887(0.015)	12.748(0.015)	12.814(0.015)	13.180(0.020)
2003 09 16	52898.52	7.3	KAIT	···	12.985(0.015)	12.804(0.015)	12.911(0.015)	13.263(0.023)
2003 09 17	52899.52	8.3	KAIT	···	13.094(0.015)	12.858(0.015)	13.010(0.015)	13.288(0.024)
2003 09 19	52901.40	10.2	LCO Swope	13.113(0.089)	13.319(0.021)	13.004(0.018)	···	···
2003 09 19	52901.44	10.2	KAIT	···	13.406(0.015)	13.044(0.015)	13.120(0.015)	13.330(0.019)
2003 09 20	52902.30	11.1	LCO Swope	13.358(0.018)	13.410(0.015)	13.010(0.015)	13.083(0.015)	13.201(0.015)
2003 09 20	52902.48	11.3	KAIT	···	13.520(0.015)	13.055(0.015)	13.175(0.015)	13.327(0.017)
2003 09 21	52903.46	12.3	KAIT	···	13.664(0.015)	13.134(0.015)	13.193(0.015)	13.317(0.019)
2003 09 22	52904.49	13.3	KAIT	···	13.789(0.015)	13.247(0.015)	13.233(0.015)	13.277(0.019)
2003 09 23	52905.26	14.1	CTIO 0.9 m	13.788(0.039)	13.825(0.015)	13.245(0.015)	13.178(0.015)	13.207(0.015)
2003 09 23	52905.30	14.1	LCO Swope	13.838(0.040)	13.851(0.015)	13.215(0.015)	13.118(0.015)	13.128(0.015)
2003 09 24	52906.40	15.2	LCO Swope	14.034(0.035)	14.007(0.015)	13.328(0.015)	13.163(0.015)	13.180(0.015)
2003 09 24	52906.48	15.3	KAIT	···	14.106(0.015)	13.333(0.015)	13.225(0.015)	13.218(0.017)
2003 09 25	52907.30	16.1	LCO Swope	14.162(0.089)	14.157(0.016)	13.352(0.023)	13.180(0.015)	13.043(0.029)
2003 09 26	52908.30	17.1	LCO Swope	14.249(0.038)	14.298(0.015)	13.320(0.021)	13.163(0.015)	13.040(0.029)
2003 09 28	52910.47	19.3	KAIT	···	14.621(0.015)	13.610(0.015)	13.360(0.015)	13.137(0.021)
2003 09 30	52912.47	21.3	KAIT	···	14.808(0.015)	13.798(0.015)	13.478(0.015)	13.189(0.019)
2003 10 02	52914.40	23.2	LCO Swope	15.020(0.102)	14.992(0.022)	13.925(0.015)	13.561(0.020)	13.212(0.015)
2003 10 02	52914.46	23.3	KAIT	···	15.022(0.015)	13.988(0.015)	13.644(0.015)	13.308(0.022)
2003 10 04	52916.46	25.3	KAIT	···	15.158(0.015)	14.141(0.015)	13.844(0.015)	13.512(0.022)
2003 10 07	52919.42	28.2	KAIT	···	15.340(0.015)	14.393(0.015)	14.071(0.015)	13.734(0.024)
2003 10 09	52921.40	30.2	KAIT	···	15.448(0.015)	14.480(0.015)	14.189(0.015)	13.913(0.025)
2003 10 13	52925.43	34.2	KAIT	···	15.640(0.021)	14.658(0.022)	14.392(0.020)	14.143(0.030)
2003 10 16	52928.42	37.2	KAIT	···	15.646(0.015)	14.746(0.015)	14.518(0.015)	14.315(0.032)
2003 10 17	52929.40	38.2	LCO Swope	15.511(0.045)	15.624(0.015)	14.781(0.015)	14.523(0.015)	14.325(0.015)
2003 10 18	52930.42	39.2	KAIT	···	15.716(0.015)	14.806(0.015)	14.593(0.015)	14.428(0.025)
2003 10 20	52932.37	41.2	KAIT	···	15.735(0.015)	14.871(0.015)	14.671(0.015)	14.566(0.022)
2003 10 22	52934.41	43.2	KAIT	···	15.806(0.015)	14.916(0.015)	14.752(0.015)	14.629(0.018)
2003 10 24	52936.40	45.2	KAIT	···	15.843(0.015)	15.018(0.015)	14.840(0.015)	14.735(0.025)
2003 10 27	52939.36	48.2	KAIT	···	15.929(0.015)	15.094(0.015)	14.926(0.015)	14.879(0.025)
2003 10 30	52942.36	51.2	KAIT	···	15.965(0.015)	15.199(0.015)	15.049(0.015)	15.043(0.031)
2003 10 30	52942.66	51.5	SSO 2.3 m	15.792(0.039)	15.952(0.016)	15.234(0.015)	15.099(0.015)	14.877(0.017)
2003 11 02	52945.38	54.2	KAIT	···	16.053(0.015)	15.269(0.015)	15.144(0.015)	15.204(0.024)
2003 11 05	52948.32	57.1	KAIT	···	16.142(0.059)	15.385(0.015)	15.241(0.015)	15.323(0.035)
2003 11 08	52951.30	60.1	LCO Swope	16.110(0.035)	16.086(0.015)	15.408(0.015)	15.310(0.015)	15.379(0.015)
2003 11 11	52954.36	63.2	KAIT	···	16.168(0.026)	15.552(0.017)	15.593(0.026)	···
2003 11 16	52959.33	68.1	KAIT	···	16.246(0.017)	15.665(0.015)	15.651(0.015)	15.864(0.035)

Continued on the next page

Date (UT)	MJD (days)	Phase (days)	Telescope	U (mag)	B (mag)	V (mag)	R (mag)	I (mag)
2003 11 18	52961.28	70.1	CTIO 0.9 m	···	16.260(0.015)	15.667(0.015)	15.644(0.015)	15.855(0.015)
2003 11 19	52962.34	71.1	KAIT	···	16.323(0.015)	15.776(0.015)	15.744(0.015)	15.928(0.032)
2003 11 20	52964.24	73.0	VLT Antu	···	16.277(0.042)	15.793(0.015)	15.582(0.024)	16.015(0.015)
2003 11 21	52964.32	73.1	CTIO 0.9 m	···	16.298(0.015)	15.815(0.015)	15.764(0.015)	15.991(0.015)
2003 11 22	52965.29	74.1	CTIO 0.9 m	···	16.347(0.015)	15.819(0.015)	15.797(0.015)	16.036(0.015)
2003 11 22	52965.31	74.1	KAIT	···	16.338(0.015)	15.855(0.018)	15.846(0.015)	···
2003 11 27	52970.30	79.1	KAIT	···	16.465(0.015)	15.982(0.016)	16.047(0.015)	16.285(0.047)
2003 11 28	52971.67	80.5	SSO 2.3 m	16.812(0.029)	16.372(0.015)	15.935(0.015)	15.921(0.017)	15.981(0.024)
2003 12 03	52976.28	85.1	KAIT	···	16.576(0.033)	16.186(0.039)	16.244(0.030)	16.519(0.065)
2003 12 15	52988.30	97.1	LCO Swope	17.116(0.041)	16.694(0.015)	16.424(0.015)	16.512(0.015)	16.654(0.015)
2003 12 17	52990.26	99.1	KAIT	···	16.836(0.024)	16.615(0.035)	16.706(0.048)	16.854(0.087)
2003 12 22	52995.10	103.9	LCO Swope	17.349(0.036)	···	16.569(0.015)	16.736(0.015)	16.840(0.016)
2003 12 22	52995.24	104.0	KAIT	···	16.869(0.019)	16.686(0.040)	16.771(0.054)	17.052(0.091)
2003 12 23	52996.10	104.9	LCO Swope	···	16.890(0.015)	···	···	···
2003 12 27	53000.10	108.9	LCO Swope	17.549(0.032)	16.918(0.015)	16.718(0.015)	16.889(0.021)	17.012(0.017)
2003 12 28	53001.21	110.0	KAIT	···	17.010(0.023)	16.817(0.033)	17.085(0.027)	17.414(0.085)
2003 12 28	53001.57	110.4	SSO 2.3 m	17.588(0.015)	16.859(0.018)	16.786(0.015)	16.936(0.015)	17.119(0.016)
2004 01 06	53010.20	119.0	KAIT	···	17.120(0.052)	17.107(0.047)	17.336(0.048)	17.316(0.100)
2004 01 09	53013.19	122.0	KAIT	···	17.254(0.128)	17.208(0.090)	17.329(0.108)	···
2004 01 13	53017.18	126.0	KAIT	···	17.241(0.019)	17.233(0.024)	17.476(0.037)	17.576(0.081)
2004 01 16	53020.16	129.0	KAIT	···	17.299(0.026)	17.242(0.026)	17.567(0.020)	17.694(0.111)
2004 01 19	53023.13	131.9	KAIT	···	17.349(0.028)	17.347(0.026)	17.625(0.041)	17.706(0.072)
2004 01 22	53026.15	135.0	KAIT	···	17.456(0.025)	17.379(0.033)	17.638(0.037)	17.769(0.092)
2004 01 29	53033.49	142.3	SSO 2.3 m	18.440(0.057)	17.518(0.043)	17.373(0.024)	17.581(0.032)	17.686(0.101)
2004 03 29	53093.38	202.2	SSO 2.3 m	19.843(0.330)	18.634(0.055)	18.383(0.050)	18.691(0.100)	18.276(0.147)
2004 07 10	53196.55	305.4	*HST* ACS[b]	···	···	19.896(0.021)	···	20.052(0.017)
2004 07 12	53198.82	307.6	*HST* ACS	···	20.058(0.017)	···	21.210(0.029)	···
2004 07 16	53202.75	311.6	*HST* ACS	···	20.079(0.016)	···	21.219(0.024)	···
2004 08 12	53229.30	338.1	VLT Kueyen	21.648(0.039)	20.508(0.028)	20.543(0.033)	21.224(0.042)	20.587(0.032)
2004 08 13	53230.39	339.2	VLT Kueyen	···	···	···	21.263(0.034)	20.592(0.032)
2004 11 15	53324.71	433.5	*HST* ACS	···	···	21.712(0.029)	···	21.417(0.031)
2005 02 07	53408.10	516.9	VLT Antu	···	···	23.326(0.100)	23.111(0.102)	22.554(0.122)
2005 03 04	53433.02	541.8	VLT Antu	$>$22.95	···	···	···	···
2005 08 08	53590.34	699.1	VLT Kueyen	···	25.198(0.137)	···	···	24.366(0.287)[c]
2005 08 09	53591.36	700.2	VLT Kueyen	···	···	···	25.192(0.388)	···
2005 08 10	53592.39	701.2	VLT Kueyen	···	···	24.423(0.138)	···	···

[a] The quoted values do not include S-corrections. Numbers in parentheses are uncertainties. All formal errors below 0.015 have been rounded up to this value.

[b] Vega magnitudes in the *HST* filter system ($F435W$, $F555W$, $F625W$, and $F814W$).

[c] In the last VLT epoch, two R images and two I images obtained at epochs differing by 5 and 1 days (respectively) have been combined to increase the signal-to-noise ratio.

4.3.3 NEAR-IR PHOTOMETRY

The NIR standards P9106 and P9172 (Persson et al., 1998), were observed with the CTIO 1.3-m telescope on six photometric nights, in order to calibrate field stars in the vicinity of SN 2003hv. Y-band magnitudes of the Persson stars were calculated using the following relationship (Krisciunas et al., 2004b), derived from synthetic photometry of Vega, Sirius, and the Sun: $(Y - K_s) = -0.013 + 1.614(J_s - K_s)$. Stars 2 and 3 (Fig. 4.1) were calibrated in this manner; their magnitudes are listed in Table 4.5. These stars also have JHK values in the Two Micron All Sky Survey (2MASS) and good agreement was found between our values and 2MASS. The NIR photometry of the SN was then calculated differentially with respect to star 3 (the brightest) for all CTIO 1.3-m epochs. Table 4.6 contains the derived photometry.

Reductions of the VLT NIR images were done with the `Eclipse` software package (Devillard, 1999). The task `jitter` was used to estimate and remove the sky background from each individual image before creating a stacked image. Photometry of the supernova was determined on the reduced images relative to

Table 4.5: *Calibrated NIR magnitudes for local comparison stars in Fig. 4.1.*

Star	Y^a	J	H	K_s
2	16.103 (0.017)	15.792 (0.011)	15.295 (0.011)	14.927 (0.031)
3	12.842 (0.013)	12.501 (0.009)	11.868 (0.013)	11.732 (0.017)

[a] There can be an associated systematic uncertainty of 0.03 mag in the Y-band calibration (Krisciunas et al., 2004b).

Table 4.6: *Near-infrared photometry of SN 2003hv.*

Date (UT)	MJD[a] (days)	Phase (days)	Telescope	Y (mag)	J^b (mag)	H (mag)	K_s (mag)
2003 09 10	52892.37	1.2	CTIO 1.3 m	13.252(0.015)	13.081(0.015)	13.286(0.015)	13.100(0.018)
2003 09 14	52896.28	5.1	CTIO 1.3 m	13.591(0.015)	13.792(0.015)	13.423(0.015)	13.378(0.021)
2003 09 17	52899.28	8.1	CTIO 1.3 m	13.716(0.015)	14.435(0.015)	13.502(0.015)	13.529(0.026)
2003 09 24	52906.31	15.1	CTIO 1.3 m	13.403(0.015)	14.491(0.015)	13.202(0.015)	13.211(0.018)
2003 09 28	52910.26	19.1	CTIO 1.3 m	13.031(0.015)	14.179(0.015)	13.112(0.015)	13.189(0.022)
2003 10 02	52914.20	23.0	CTIO 1.3 m	12.845(0.016)	14.000(0.018)	13.283(0.020)	13.216(0.073)
2003 10 05	52917.25	26.1	CTIO 1.3 m	13.025(0.015)	14.306(0.015)	13.546(0.015)	13.524(0.020)
2003 10 08	52920.24	29.0	CTIO 1.3 m	13.255(0.015)	14.657(0.015)	13.799(0.015)	13.796(0.026)
2003 10 11	52923.22	32.0	CTIO 1.3 m	13.439(0.015)	14.980(0.015)	13.958(0.015)	13.936(0.022)
2003 10 14	52926.25	35.1	CTIO 1.3 m	13.650(0.015)	15.236(0.016)	14.145(0.016)	···
2003 10 17	52929.22	38.0	CTIO 1.3 m	13.844(0.015)	15.519(0.015)	14.273(0.015)	14.116(0.026)
2003 10 20	52932.17	41.0	CTIO 1.3 m	14.037(0.015)	15.725(0.017)	14.431(0.016)	14.306(0.024)
2003 10 24	52936.21	45.0	CTIO 1.3 m	14.468(0.015)	16.310(0.023)	14.770(0.018)	···
2003 11 03	52946.21	55.0	CTIO 1.3 m	14.912(0.015)	16.790(0.036)	15.041(0.020)	15.060(0.048)
2003 11 10	52953.22	62.0	CTIO 1.3 m	15.207(0.017)	17.088(0.065)	15.420(0.037)	···
2004 08 18	53235.37	344.2	VLT Antu	···	20.394(0.140)	···	···
2004 08 29	53246.31	355.1	VLT Antu	···	···	19.977(0.106)	20.221(0.216)
2004 08 30	53247.28	356.1	VLT Antu	···	20.078(0.122)	···	20.303(0.224)
2005 01 24	53394.06	502.9	VLT Antu	···	···	20.163(0.138)	$>$ 20.700
2005 02 24	53425.99	534.8	VLT Antu	···	···	···	$>$ 20.700
2005 02 27	53428.99	537.8	VLT Antu	···	···	20.495(0.146)	···
2005 02 28	53429.99	538.8	VLT Antu	···	21.087(0.144)	···	···
2005 10 14[c]	53657.07	765.9	VLT Antu	···	$>$ 22.310	$>$ 22.000	···
2005 11 03	53677.31	786.1	*HST* NICMOS[d]	···	···	22.691(0.051)	···

[a] All images obtained the same night are referred to a mean MJD
[b] A J filter was used at the CTIO 1.3 m telescope, while J_s was used at the VLT.
[c] All images obtained on October 13–15 are averaged here.
[d] Vega magnitudes in the *HST* filter system ($F160W$).

the two field stars mentioned above and a third 2MASS star in the field of view of ISAAC. Instrumental magnitudes were computed with `phot` using an aperture with a radius of $0\farcs5$. The quoted uncertainties in Table 4.6 account for the `phot` error, the scatter around the zero-point, and the minimum error of the 2MASS sequence. In the cases when two observations were obtained during the same night, they were combined to increase the signal-to-noise ratio. For the final epoch, images from different nights were also combined. However, since there was no detection of the supernova during the final epoch, a 3σ upper limit was computed.

For the *HST* NICMOS data, we used the *Mosaic Files* (see McLaughlin & Wiklind, 2007) generated by the STScI pipeline. The 16 dithered frames were combined in IRAF. Unfortunately, the SN was located only 5 pixels away from the erratic NICMOS middle column[6], which proved difficult to correct. For this reason, and the fact that the SN was faint, photometry of the SN was performed with a small 2.5-pixel ($0\farcs1875$) aperture. For photometry performed on half of the frames (the ones where due to the dithering pattern the SN was located farther from the bad column), a larger aperture was used and these magnitudes

[6] `www.stsci.edu/hst/nicmos/performance/anomalies`

were found to be consistent with the results obtained with the small aperture. The encircled flux was computed using the zero-points provided on the STScI webpage.[7] Appropriate aperture corrections were applied (Barker et al., 2007, Fig. 4.10), and the flux was converted to the Vega-based magnitude system.

4.3.4 SPECTROSCOPY

All spectra were reduced following standard procedures. The two-dimensional frames were bias subtracted and divided by a master flatfield image, and then the cosmic rays were removed. One-dimensional spectra were extracted, wavelength calibrated with comparison-lamp spectra, and then flux-calibrated relative to spectrophotometric standard star observations. The wavelength calibration was checked against the night-sky lines, and when appropriate the blue and red spectra were combined to create a final spectrum. Spectra obtained at SSO had telluric features removed with the aid of a telluric standard star.

4.4 RESULTS

We now present the results of our observations, first for the early phases and then for the later epochs. The complete light curves and spectral sequence for SN 2003hv are shown in Figs. 4.2 and 4.3, respectively.

4.4.1 EARLY-PHASE PHOTOMETRY

Using the method described by Prieto et al. (2006), we fit template light curves to the early-time S-corrected $BVRI$ photometry. This allowed us to determine basic parameters of the light curves and to estimate the level of host-galaxy reddening. Our slightly modified fitting method is described by Burns et al. (2010). The fits can be seen in the inset of Fig. 4.2.

The light-curve fit indicates that $B_{\rm max}$ occurred on MJD $= 52891.2\pm0.3$ (or 9.15 September 2003) with an apparent peak magnitude of 12.45 ± 0.03. Peak brightness in the VRI bands occurred at $+0.9$, $+0.1$, and -2.2 days relative to $B_{\rm max}$. We note here that the reported uncertainties are the statistical errors of the fit. Since our photometry does not cover the peak, however, a larger systematic uncertainty might be anticipated.

The computed host-galaxy reddening is $E(B-V)_{\rm host} = -0.04 \pm 0.01$ mag. Formally, one must also add a systematic uncertainty of ±0.06 mag, related to the observed color spread of SNe Ia. We note that zero reddening is consistent with the position of the supernova in the outskirts of an S0 galaxy.

The light-curve fit of SN 2003hv yields a B-band decline rate $\Delta m_{15}(B) = 1.61\pm0.02$ mag. SN 2003hv therefore lies near the faint end of the normal luminosity vs. decline-rate distribution, close to the highly subluminous SN 1991bg-like SNe Ia (e.g., Filippenko et al., 1992a), which are observed to have $\Delta m_{15}(B) > 1.7$ mag. To date there is a lack of well-studied SNe Ia with $\Delta m_{15}(B)$ values in the range between 1.5 and 1.7 (see, e.g., Prieto et al., 2006; Mazzali et al., 2007). Currently it is not clear to what extent the properties of normal and subluminous SNe Ia compare. In this sense, SN 2003hv, with its extensive data coverage, may help us understand the similarities or differences between these different types of SNe Ia.

The distance modulus of SN 2003hv is estimated to be $\mu_{\rm SN} = 31.58 \pm 0.05$ mag from these light-curve fits. The quoted error is the statistical error of the fit and we have assumed a Hubble constant of $H_0 = 72$ km s^{-1} Mpc^{-1} (Freedman et al., 2001). There is an additional systematic error (amounting up to $\sim$0.15 mag) related to the intrinsic dispersion in the luminosity of SNe Ia. This distance is consistent with the SBF distance of NGC 1201 $\mu_{\rm SBF} = 31.37\pm0.30$ mag (Tonry et al., 2001; Jensen et al., 2003). We conclude that SN 2003hv was a normal-luminosity SN Ia that obeys the Phillips relation (Phillips, 1993; Phillips et al., 1999) within its inherent scatter, since this is an underlying assumption for deriving a distance modulus with the aid of the light curves. Throughout the rest of the paper, in order to avoid any circular reasoning, we adopt the $\mu_{\rm SBF}$ distance to NGC 1201. The conclusion that SN 2003hv is a normal SN Ia is also

[7] www.stsci.edu/hst/nicmos/performance/photometry

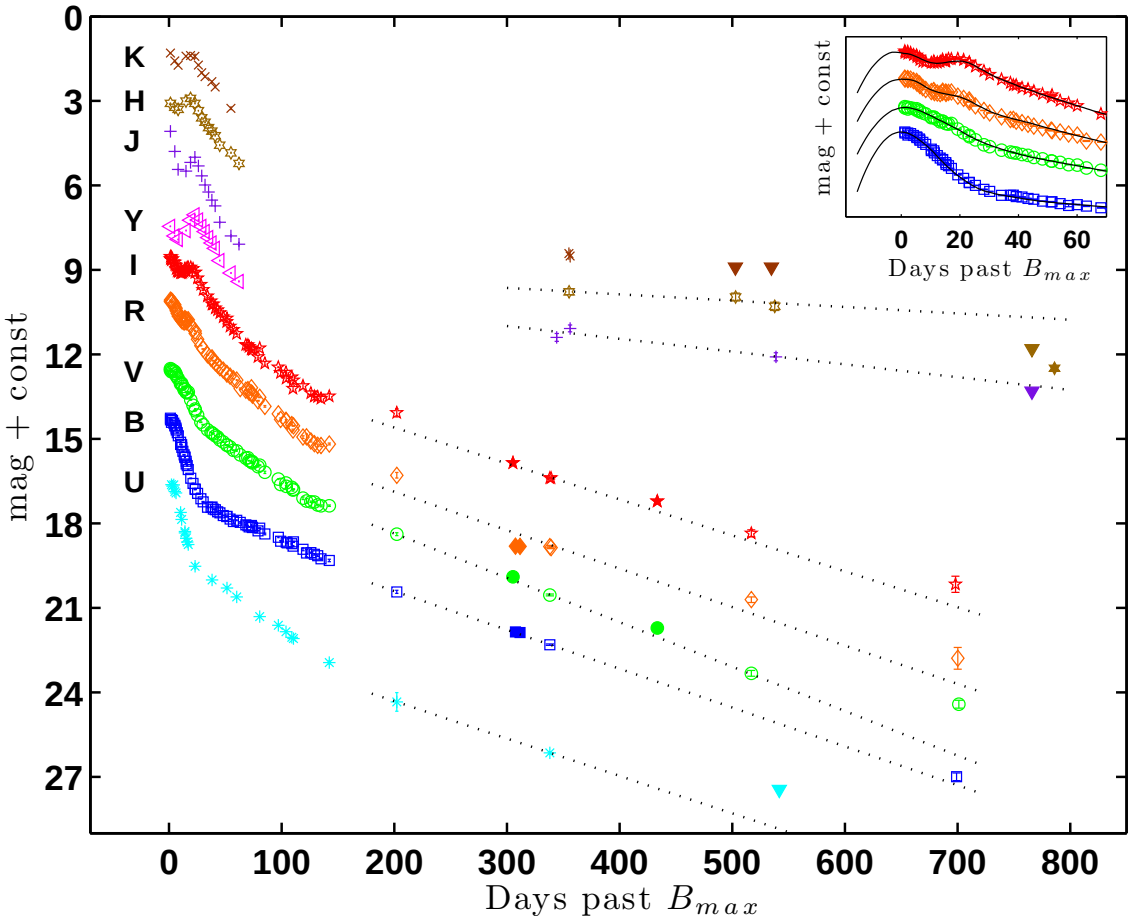

Figure 4.2: *The $UBVRIYJHK$ light curves of SN 2003hv. They have been shifted for clarity by the following constants: +4.5, +1.8, 0.0, −2.4, −4.2, −5.8, −9, −10.2, and −11.8, respectively. Filled triangles represent 3σ upper limits. The HST points (in the HST filter system) are indicated with filled symbols. Linear fits to the data in the range +200–540 days are shown with dotted lines to guide the eye. The inset contains light-curve fits to the early $BVRI$ photometry (Burns et al., 2010); the data have been shifted vertically by different constants than in the main graph.*

supported in part by the existence of a secondary maximum in the I band, whereas very rapidly declining SN 1991bg-like events lack this feature (Filippenko et al., 1992a).

By fitting only the KAIT data, which is a sufficiently large homogeneous dataset, no significant differences were obtained for the derived light-curve parameters. However, the scatter around the fit was reduced ($\chi^2_{\rm dof}$ of 3.9 versus 9.3), since this avoids systematic uncertainties introduced by combining data from different telescopes. The $\chi^2_{\rm dof}$ for the combined dataset without S-corrections was 15.6.

In Fig. 4.4, the early observed colors of SN 2003hv are compared with those of the normal SN 1992A (Suntzeff, 1996), SN 2001el (Krisciunas et al., 2003), and SN 2003du (Stanishev et al., 2007). These SNe Ia have $\Delta m_{15}(B)$ values of 1.47, 1.15, and 1.06, respectively. The $V-R$ and $V-I$ colors of SN 2003hv are similar to those of SN 1992A (the one with the most similar decline rate), while the $B-V$ color starts slightly bluer around maximum (similar to SN 2003du) and then three weeks later matches that of SN 1992A. The $B-V$ color evolution between 30 and 90 days past maximum follows the Phillips/Lira relation (Phillips et al., 1999). Note that in Fig. 4.4, the colors were only corrected for Galactic extinction to illustrate that SN 2003hv is similar to SNe having little or no host-galaxy reddening (SNe 1992A and 2003du). This is additional evidence that SN 2003hv was a normal SN Ia that suffered negligible host-

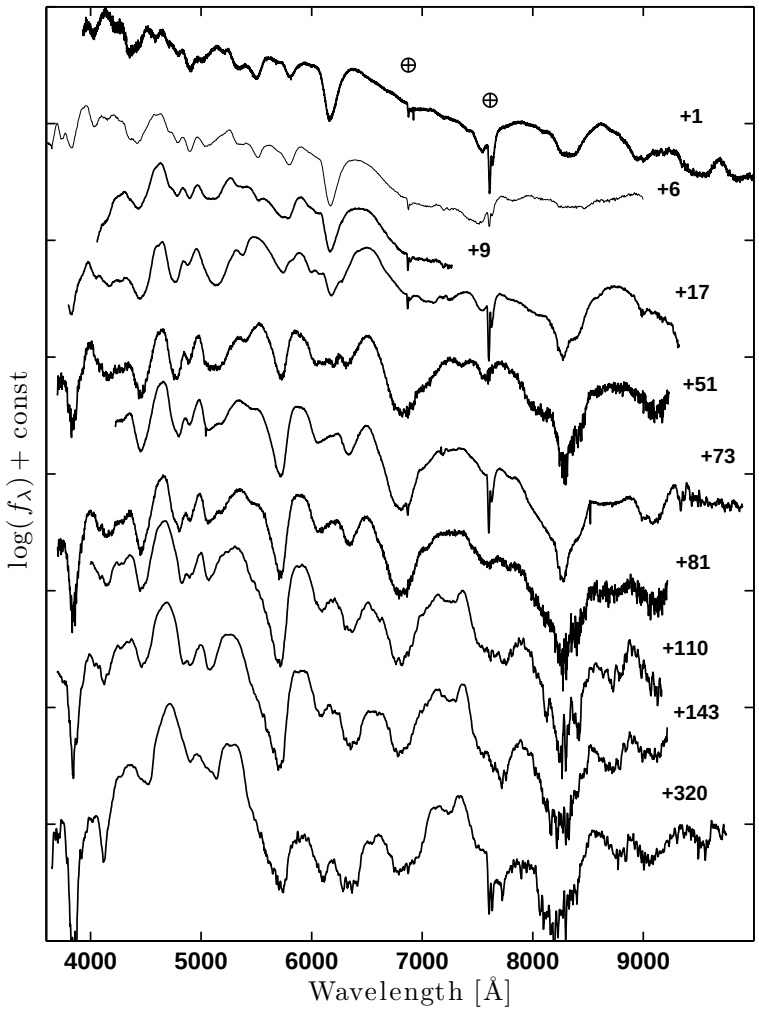

Figure 4.3: *Spectral evolution of SN 2003hv from maximum light to the nebular phase. Numbers indicate days past maximum brightness. For clarity, the spectra have been offset in flux scale with respect to each other. The Earth symbols mark telluric features. Note that the SSO spectra have had their telluric lines removed. The bottom three spectra have been smoothed (by a moving average of 5 pixels) for presentation purposes.*

galaxy extinction.

4.4.2 EARLY-PHASE SPECTROSCOPY

Figure 4.3 displays the spectroscopic sequence from 1 to 320 days past maximum. The sequence consists of four early-phase, five "mid-epoch," and one late-phase spectra.

The earliest spectra display intermediate-mass elements characteristic of a normal SN Ia near maximum brightness. The evolution of these spectra confirms that this was a normal event. We have used the "Supernova Identification" code (SNID; Blondin & Tonry, 2007) to compare the early-time spectra of SN 2003hv with a library of supernova templates. SNID indicates a good agreement (rlap quality parameter values $>$ 10) with several normal SNe Ia (e.g., SNe 1992A, 1994D, and 1996X) at epochs similar to those deduced from our light-curve fits, to within a few days.

At maximum light, the ratio of the depth of the Si II λ5972 and λ6355 absorption features was 0.40 $\pm$ 0.05. This value is somewhat larger than what is measured in other normal SNe Ia (SN 1992A being the

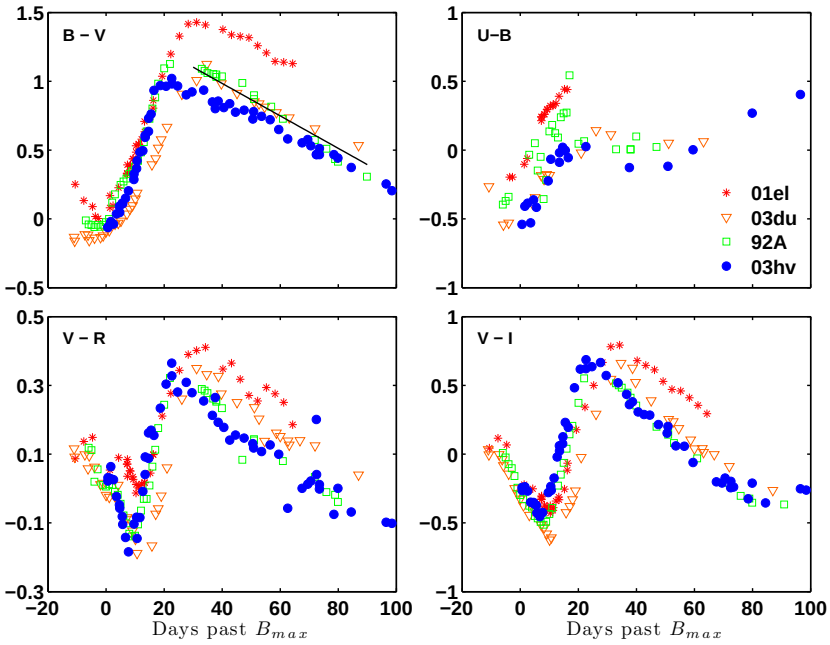

Figure 4.4: *Color evolution of SN 2003hv from maximum light to 100 days past maximum. For comparison, we have plotted the colors of SN 1992A (Suntzeff, 1996), SN 2001el (Krisciunas et al., 2003), and SN 2003du (Stanishev et al., 2007). The Phillips/Lira relation (Phillips et al., 1999) is also indicated in the $B-V$ panel (solid line). The four SNe have only been corrected for Galactic reddening ($E(B-V) = 0.016$, 0.017, 0.014, and 0.010 mag, respectively, Schlegel et al., 1998). This illustrates that SN 2003hv, as in the cases of SNe 1992A and 2003du, suffers little to no extinction from its host. SN 2001el, on the other hand, was substantially reddened and clearly does not follow the Phillips/Lira relation.*

runner-up with 0.38), but smaller than values found for subluminous SN 1991bg-like events (Nugent et al., 1995; Garnavich et al., 2004; Benetti et al., 2005).

From the four early-epoch spectra, the rate of decrease in the expansion velocity of the Si II λ6355 feature was measured to be $\dot{v} = 41 \pm 6$ km s^{-1} day^{-1}. By comparing with a large sample of events, we find that SN 2003hv lies in the low-velocity gradient (LVG) group as defined by Benetti et al. (2005).

4.4.3 LATE-PHASE PHOTOMETRY

The measured decay rates of the late-time light curves are listed in Table 4.7. To facilitate comparison with results of previous studies (Lair et al., 2006, S04; SS07), these decline rates were computed as linear slopes at time intervals out to $\sim$540 days. The measured late-phase BVR-band decline rate of $\sim$1.4 mag per 100 days in SN 2003hv is similar to values reported for other well-studied SNe Ia. A possible exception is the I band, which is found to decline slower than BVR, but not as slowly as found in other SNe Ia (i.e., $\sim$1.0 mag per 100 days). In addition, as discussed by SS07, the U band has a late-time decline rate comparable to that of BVR for at least up to 340 days.

However, in the case of SN 2003hv, the evolution of the late-epoch light curve is, for the first time, followed in multiple bands out to 700 days past maximum light. At these very late stages, an apparent slowdown of the optical light curves is observed; the drop in luminosity appears to be decelerating. This behavior is most pronounced in the V band, where it has also been observed in several other SNe Ia. We discuss this further in Sect. 4.5.3.

In the NIR bands, SN 2003hv displays a different behavior than the constant brightness observed during

Table 4.7: *Light curve decline rates.*[a]

U	B	V	R	I	J_s	H	K_s
1.33(0.24)[b]	1.38(0.05)	1.58(0.03)	1.37(0.05)	1.28(0.06)	0.45(0.09)	0.23(0.09)	$>$0.30

[a] Given in mag/100 days for the period 200–540 days. In the U band, however, only out to 340 days.
[b] Numbers in brackets are the formal errors of the weighted least-squares linear fits to the photometric data.

late-phase observations of SNe 2000cx and 2001el (S04 and SS07, respectively). SN 2003hv slowly fades in brightness between days $+350$ and $+540$. Furthermore, the SN is not detected in the VLT images at $+766$ days, indicating a further drop during this period. However, we do detect a point-like source in the *HST*/NICMOS/F160W image obtained at $+786$ days (see Fig. 4.5). From astrometry relative to nearby stars with the help of the deep VLT H-band images, we establish that this object's position is consistent with the position of the supernova to within $0\farcs061 \pm 0\farcs085$ (where the quoted error is the transformation error). With a magnitude of 22.69 ± 0.05, this is to our knowledge the latest detection ever achieved of a SN Ia in the NIR.

Notice that the *HST* ACS observations were not included in the linear fits in Table 4.7. This is because the *HST* and ground-based filter systems are significantly different. These differences can produce systematic effects in the photometry, especially when one considers the nonstellar nature of the spectral energy distribution of SNe Ia. Synthetic photometry computed with the nebular spectrum and the VLT and *HST* filter transmission functions indicates that on day $+320$ the SN would appear brighter by 0.20, 0.25, and 0.28 mag in BVI and fainter by 0.37 mag in R in the *HST* filter system.[8] However, the farther we move from the epoch of the nebular spectrum, the less accurate these corrections become; hence, they were not applied. Nevertheless, the ACS points lie fairly close to the calculated linear slopes.

The R-band $+516$ day observation was obtained using the FORS2 'special' R-band filter, which differs from the Bessell R filter. Synthetic photometry computed with the nebular spectrum reveals that SN 2003hv would appear $\sim$0.08 mag brighter in the $R_{\rm special}$ filter at $+320$ days. Assuming that the shape of the spectrum does not change out to $+516$ days, this induces a change to the respective R-band decline rates by no more than half a standard deviation, and it has no consequence to the following discussion.

4.4.4 LATE-PHASE SPECTROSCOPY

The nebular spectra (bottom Fig. 4.3) of SN 2003hv are, generally speaking, similar to those of other normal SNe Ia, and display several broad iron-group emission features. In particular, the latest spectrum is dominated by strong Fe emission features at ~ 4700 Å and 5250 Å. These are produced from the blending of forbidden transitions associated with Fe II and Fe III.

Motohara et al. (2006) and Gerardy et al. (2007) found in the NIR and MIR nebular spectra of SN 2003hv that the [Fe II] 1.644 μm and [Co III] 11.89 μm emission lines were blueshifted by $\sim$2600 km s^{-1}. These shifts were interpreted as the result of an asymmetric, off-centre explosion. In addition, the [Fe II] 1.644 μm line had a flat-topped profile. It was therefore argued (Motohara et al., 2006) that regions below $\sim$3000 km s^{-1} are filled with neutron-rich non-radioactive isotopes (see also Höflich et al., 2004).

We examined our optical nebular spectrum to investigate whether any signatures of blueshifted lines or flat-topped profiles were present. It should be stressed that the optical spectrum is produced from the blend of many overlapping transitions, and it is therefore problematic to make strong claims from the appearance of optical lines. However, a fairly isolated [Fe II] feature is present at 8621 Å. This line, which often falls outside the wavelength coverage of optical spectra, contributes according to our modeling (see Sect. 4.5.2) $\sim$90% of the flux in this wavelength region. This is comparable to the "cleanness" of the [Fe II] 1.644 μm line in the NIR and higher than the 65% contribution that our model suggests for the [Fe II] λ7155 line in its

[8] The F625W is actually an r, not an R, filter.

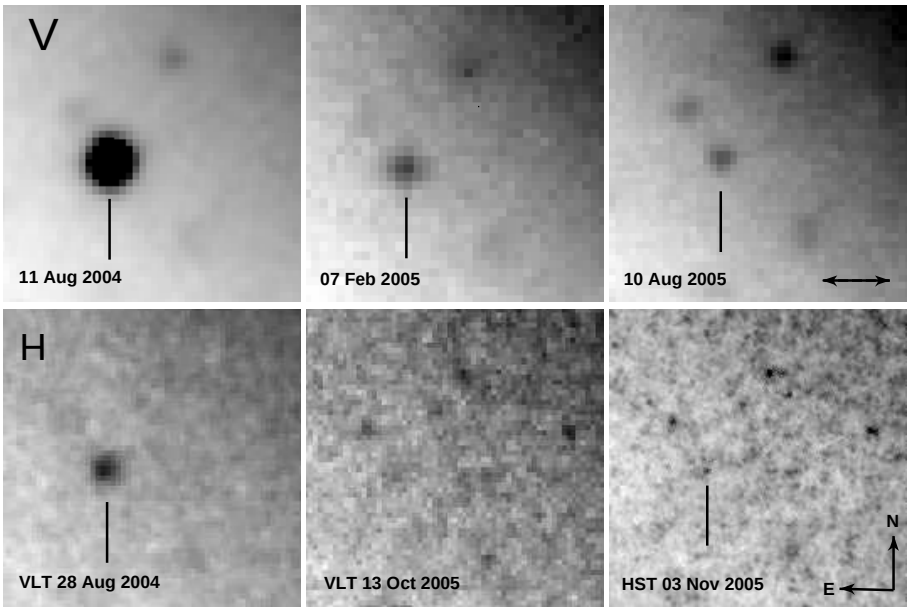

Figure 4.5: *The fading of SN 2003hv between days +340 and +786 as observed in the V band (upper sequence) and the H band (lower sequence). The double arrow in the last V-band frame is 2″ across. SN 2003hv is clearly detected in all V-band images. It is not significantly detected in the VLT/ISAAC H-band image from 13 October 2005, at an upper limit of 22 mag. However, SN 2003hv is detected in a deeper image obtained 3 weeks later with HST/NICMOS on 786 days past maximum with a magnitude of 22.69 ± 0.05. This is the latest-ever detection of a SN Ia in the NIR. The last image is constructed from the drizzled combination of 16 frames.*

corresponding region. The latter line, which is contaminated mainly by [Ca II], was inspected by Höflich et al. (2004) in the case of SN 2003du, and was found to have a peak "seemingly in contradiction" with the boxy NIR profiles. In Fig. 4.6 the 8621 Å and 1.644 μm (Motohara et al., 2006) lines are compared in velocity space. We see that these two features have somewhat similar profiles and both are apparently blueshifted by $\sim$2600 km s^{-1}. The same could be argued for the 7155 Å line. Other iron lines are more heavily blended and definitely unsuitable for such diagnostics (notice, however, that the 5250 Å feature is also flat-topped). This could be considered as supporting the findings presented by Motohara et al. (2006) and Gerardy et al. (2007). However, in addition to the concerns raised above, these lines do show some evolution (Fig. 4.3), which could be additional evidence pointing toward blending.

4.5 DISCUSSION

4.5.1 SN 2003HV IN THE CONTEXT OF ITS $\Delta m_{15}(B)$ VALUE

In this subsection, the properties of SN 2003hv are reviewed in the light of its rather uncommon light-curve decline-rate parameter. There is a general division between normal and subluminous SNe Ia, where the latter are typically observed to have $\Delta m_{15}(B) > 1.7$ mag. The subluminous SNe Ia do not seem to follow the linear luminosity vs. decline-rate relation of normal SNe Ia (Phillips, 1993; Prieto et al., 2006), although an exponential fit might be able to include them (e.g., Garnavich et al., 2004). It is not clear whether subluminous SNe Ia can be related to a different class of progenitors or explosion mechanisms (see, e.g., Hillebrandt & Niemeyer, 2000, and references therein).

As very few SNe Ia with $1.5 < \Delta m_{15}(B) < 1.7$ have been observed (and none in as much detail as SN 2003hv), we feel it is warranted to discuss SN 2003hv in this context, even if it is just a single example,

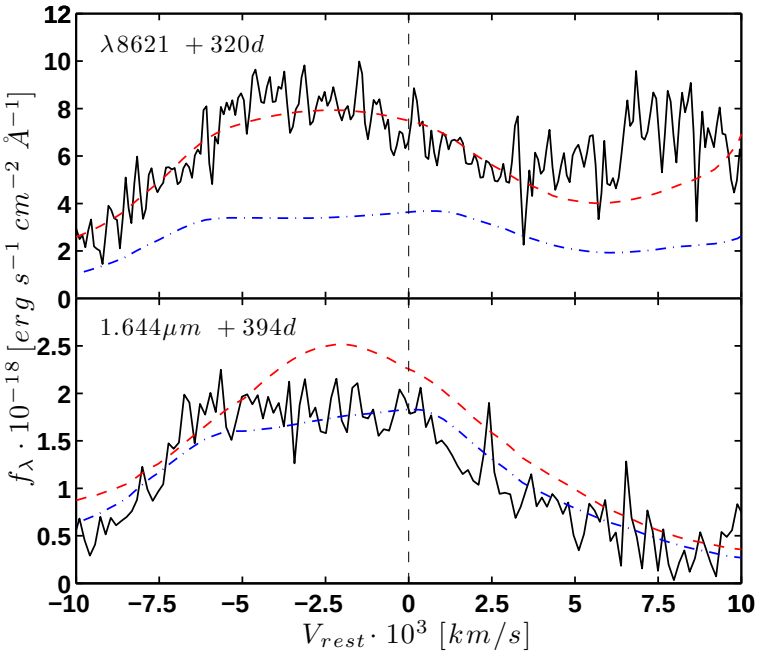

Figure 4.6: *Comparison of the [*Fe II*] line profiles at 8621 Å (our spectrum) and 1.644 μm (Motohara et al., 2006) in velocity space. These are relatively clean, isolated [*Fe II*] lines according to our model. The two lines appear equally blueshifted, and their blueshift is equal to the blueshift of [*Co III*] 11.89 μm (see Motohara et al., 2006; Gerardy et al., 2007). The 1.644 μm line exhibits a flat-topped profile while the 8621 Å line is not clearly "peaked" (assuming it is not a result of blending by neighboring lines). Also shown are the model spectra (without photoionization) at +300 days (red dashed line) and at +400 days (blue dashed-dotted line) blueshifted by 2600 km s^{-1}. In the top panel, their flux has been scaled down by a factor of 7.5 so that the +300-day model matches approximately the observed flux. The same has been done in the bottom panel, matching the +400-day model by scaling it down by a factor of 10. Notice that the 8621 Å line is also expected to develop a clear flat-topped profile at later phases.*

and confirm that it is a "normal" member of the SN Ia family. In particular, with respect to several relations proposed for SNe Ia, we make the following remarks.

∗ Adopting the independent SBF distance measurement, an absolute magnitude of $B_{\max} = -18.99 \pm 0.35$ is deduced for SN 2003hv, which is fully consistent with the expected luminosity from its decline rate (linear fits, by Prieto et al., 2006, give -19.0).

∗ Adding the SN 2003hv R(Si II) value (0.40 ± 0.05) to the R(Si II) vs. $\Delta m_{15}(B)$ correlation (Garnavich et al., 2004; Benetti et al., 2005), we find that this data point nicely connects the normal SNe Ia to the subluminous group in a previously unexplored area of this relation.

∗ Mazzali et al. (1998) showed that the full width at half-maximum intensity (FWHM) of the line at 4700 Å in nebular spectra of SNe Ia correlates well with $\Delta m_{15}(B)$. Although SN 2003hv has a FWHM value slightly larger than the one expected by the correlation in Mazzali et al. (1998), it is consistent with the existence of such a correlation.

∗ Milne et al. (2001) suggested the cut between the normal and subluminous SNe Ia to occur at $\Delta m_{15} = 1.6$ mag as far as the late light-curve shape is concerned. However, this was based on very few SNe in the appropriate range and the study was later updated with the inclusion of SN 1999by (Milne & Williams, 2005). We note here that in this sense the late-time light curve evolution of SN 2003hv is intermediate between SN 1992A and the transitional (with respect to late-time light curve behavior) SN 1986G.

∗ The peak luminosity of SN 2003hv in the NIR bands is comparable to those of normal SNe Ia. As

pointed out by Krisciunas et al. (2009b), this is also the case for a sub-sample of SNe Ia with $\Delta m_{15}(B) > 1.6$, that peak in the J band before the B band. Although our observations do not seem to cover the JHK peaks, this is almost certainly the case for SN 2003hv and estimates based on the templates by Krisciunas et al. (2004b) give -18.52, -18.17 and -18.33 ($\pm$ 0.31) for M_J, M_H and M_K, respectively. The assertion of normal peak brightness does not change even if the observed maxima are used as lower limits, instead of extrapolating back in time.

$*$ We would not expect to see a SN with such a $\Delta m_{15}(B)$ in a late-type galaxy (Hamuy et al., 2000; Jha et al., 2007). Indeed, its presence in an S0 galaxy is not surprising.

The main conclusion is that SN 2003hv appears to obey many of the known correlations with respect to the B-band decline-rate relation and is an object that is similar to the other normal SNe Ia used to derive these correlations. Seen from another perspective, we show that these particular correlations also hold for this previously underexplored value of $\Delta m_{15}(B)$.

4.5.2 NEBULAR SPECTRUM SYNTHESIS

A unique aspect of SN 2003hv is our broad wavelength coverage at nebular phases, when including the infrared spectra from Motohara et al. (2006) and Gerardy et al. (2007). This facilitates comparison with model spectra in an unprecedented manner. We have used our detailed spectral synthesis code (described in detail by Kozma & Fransson, 1998a,b; Kozma et al., 2005, S04) to generate a nebular spectrum of SN 2003hv and compare it with the observational data. The spectral synthesis code includes a self-consistent ionization and level population model to calculate the emission from each radial zone of the ejecta. Nonthermal excitation and ionization by gamma rays and positrons are included, as well as time-dependent effects. Nonlocal scattering of the emission, however, is not included. The present calculations use the W7 hydrodynamical model (Nomoto et al., 1984) as input.

Since the nebular spectra of SN 2003hv were all obtained at slightly different epochs, the optical and NIR spectra were scaled in flux with the aid of our photometry to match the date of the MIR spectrum. The V and H magnitudes were interpolated to day $+358$, assuming the linear slopes from Table 4.7. The final combined spectrum is shown in Fig. 4.7 together with our model spectrum at day $+400$.

The synthetic spectrum does a reasonable job in reproducing the general features of the observed spectrum. The dominant Fe peaks in the range 4000–5500 Å are reproduced accurately, as is the shape of the spectrum at 7000–9000 Å. In the NIR, the relative fluxes of the [Fe II] lines agree with the observations, but the absolute fluxes are overpredicted. In the MIR, our model instead underpredicts the flux levels. The model also predicts a strong stable (non-radioactive) [Ni II] line at 6.64 μm, which is also seen in the observed spectrum. [Ar ii] and [Co ii] lines are identified, as mentioned by Gerardy et al. (2007). Note that our modeling includes two different ways to treat the effect of the scattering of UV photons and their subsequent consequences for the photoionization of the metals (representing two limiting cases): *with* and *without* photoionization (see, e.g., S04). Here only the model without photoionization (i.e., assuming that all UV photons are redistributed to longer wavelengths in the scattering process) has been plotted because it is a better fit to the observed spectrum. The model with photoionization is not able to reproduce the bluest peak around the 4000 Å bumps, since the relevant [Fe I] emission is suppressed in this case.

An interesting feature, as mentioned above, is the flat-topped profiles observed in the NIR lines. It has been suggested that a detailed study of the [Fe II] 1.644 μm NIR feature could be the cleanest probe of the ejecta kinematics (e.g., Höflich et al., 2004, and references therein). Motohara et al. (2006) discussed that the NIR nebular spectra of two out of four SNe Ia exhibit a flat-topped profile in this line, with SN 2003hv being the strongest case and the one that has been observed farthest from maximum brightness. Our model was first used to investigate how "clean" this line is. It was confirmed that even though the nebular spectrum consists of a large number of overlapping lines, within our model Fe II appears to dominate the 1.7 μm region. There are a number of different Fe II transitions that contribute to the feature, but since predominantly recombination radiation is seen at this phase, uncertainties in the ionization are less

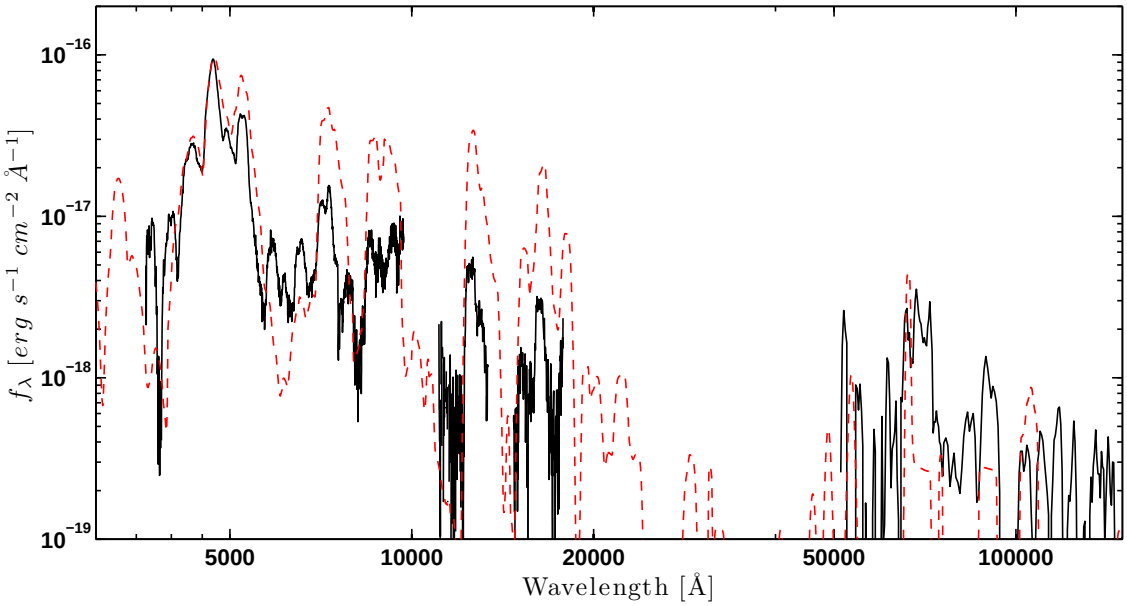

Figure 4.7: *The multi-wavelength nebular spectrum of SN 2003hv (solid line). This spectrum is a compilation of our optical spectrum at +320 days, the NIR spectrum of Motohara et al. (2006) at +394 days, and the* Spitzer *MIR spectrum of Gerardy et al. (2007) at +358 days. The optical and NIR spectra have had their flux scaled to match the age of the MIR spectrum with the aid of the V-band and H-band photometry (see text). For presentation purposes each spectrum was smoothed by a moving average of 3 pixels. Note also that the MIR spectrum has large associated error bars that are not shown here. The dashed red line shows our model spectrum (without photoionization) at +400 days.*

important in modeling the feature. As pointed out above, we also propose that the [Fe II] λ8621 line is relatively clean and isolated from other contributing lines.

The scenario favoured by Motohara et al. (2006) and Gerardy et al. (2007) to explain the flat-topped line profiles is an inner "hole" of unmixed, neutron rich, nonradioactive, iron-group elements in the core. These are the products of electron capture, which takes place in the highest density burning regions. Such a configuration of chemical elements is observed in one dimensional (1-D) deflagration explosion models (such as W7), or even 1-D delayed detonation (DDT) models, but is incompatible with current 3-D deflagration models, which predict much mixing (e.g., Röpke, 2005; Röpke et al., 2007). Motohara et al. (2006) modeled the line and found a slight asymmetry due to overlapping Fe II 1.664 and 1.667 μm lines, but argued that the overall flatness nevertheless suggested no efficient mixing between the highest density burned region and its surroundings.

Our modeling of the optical-IR spectrum at +320 days, contemporaneous with the optical spectrum, did not show any evidence for flat-topped line profiles. However, allowing the model to run to even later phases, the flat-topped line profiles start to develop. By 400 days past maximum, the line becomes flat-topped (Fig. 4.6), as also noted by Motohara et al. (2006). Note that our model assumes complete and *in situ* deposition of the energy carried by the positrons. The core of the ejecta is the densest region where both gamma rays and positrons are most efficiently deposited. The evolution from peaked to flat-topped can thus be explained by the fact that even at +300 days, there is still a fair fraction of energy deposited by gamma rays, and we can follow these as they are deposited in the central region. At even later epochs, however, the energy is provided solely by the positrons. Since these are not able to penetrate to the central regions, the absence of radioactive material in the center will give rise to a flat-topped line profile. In this sense, the flat-topped line is consistent with complete and local positron trapping, providing a diagnostic complementary to the late-time light curves (see Sect. 4.5.5).

Our optical spectrum is useful for constraining some of the alternative explanations that have been proposed for the flat-topped line profile. The alternative idea that the profile is due to a dusty core (Motohara et al., 2006) can be ruled out because no such evidence is seen at optical wavelengths. Furthermore, the possibility mentioned by Gerardy et al. (2007), that the hole may be filled with a large fraction of unburned material at low velocities as suggested by some 3-D deflagration models (e.g. Röpke, 2005), is also very unlikely: the absence of the [O I] emission at 6300 Å is clearly inconsistent with such a scenario, as discussed by Kozma et al. (2005). Gerardy et al. (2007) further mention, but do not favor, the interaction of the companion star as a possible cause of the hole. This may indeed be interesting to investigate in light of the new models by Pakmor et al. (2008), suggesting the presence of a hole in the wake of the explosion, but the observable signatures of such a hole filled by the companion star are still rather unclear.

Finally, an alternative explanation, proposed here, for the lack of emission below 2500 km s^{-1}, could be that an IRC has taken place in the highest density regions. This scenario is further discussed in Sect. 4.5.6.

4.5.3 SLOWDOWN OF OPTICAL DECAY

At very late times, the optical decline rates of SN 2003hv appear to be slowing down, especially in the V band. We first examine whether our photometry could be contaminated by a light echo or a background (or foreground) source. Light echoes have been observed in the past for a handful of SNe Ia (Schmidt et al., 1994; Cappellaro et al., 2001; Wang et al., 2008; Crotts & Yourdon, 2008). However, no evidence of extended structure was observed in our PSF subtractions, neither in the final epoch nor in the high-resolution *HST* images at $+430$ days. On the other hand, not all possible echo geometries can be resolved at this distance. In the single-scattering approximation (Patat, 2005), it is estimated that only echos in intervening clouds at distances greater than $\sim$75 pc from the SN would be resolved by ACS. But in addition, our nebular spectrum shows no evidence of blue continuum and the final colors are not particularly blue. SN 2003hv did not explode in a star-forming region, but in the outskirts of an S0 galaxy where no dust is expected and there are no signs of host extinction. Finally, if the latest-epoch photometry were dominated by a coincident background source, the corrected slope at 200–500 days would become steeper than those previously observed for SNe Ia at these phases, indicating that this is probably not the case.

We therefore believe that the final photometry indeed measures the supernova light. Actually, such a slowdown has been previously seen in several other SNe Ia observed beyond 600 days past maximum in single (usually V-band) observations: SN 1992A (Cappellaro et al., 1997), SN 2000E (Lair et al., 2006), and SN 2000cx (S04, their Sect. 6.5). Many of the same considerations apply in the case of SN 2003hv. However, our multi-color observations suggest that this slowdown may not be characteristic of only the V band. This questions the speculations in S04 about [Fe I] predominantly emitting in the V band being the explanation for this behavior.

The main consequence of this observation is that the dramatic IRC predicted by some models did not occur at these phases.

4.5.4 BOLOMETRIC LIGHT CURVE AND ^{56}Ni MASS

To construct an UV-optical-NIR (UVOIR) light curve of SN 2003hv, we used the $UBVRIJHK$ photometry from Tables 4.4 and 4.6, including the S-corrections from Table 4.3. For missing epochs, the photometry was interpolated by fitting suitable functions to the data. At early times, spline interpolation was used, while at the late nebular phases, linear fits were initially assumed. However, in some bands, due to deviations from the linear decay, quadratic or cubic polynomials gave better fits to the data and were adopted.

In the case of the U band, it was assumed that the light curve continued the linear decay obtained out to $+340$ days. For the K band we made the limiting assumption that it was *barely* not detected at $+534$ days, while the further assumption was made that the $J-H$ and $H-K$ colors do not change between

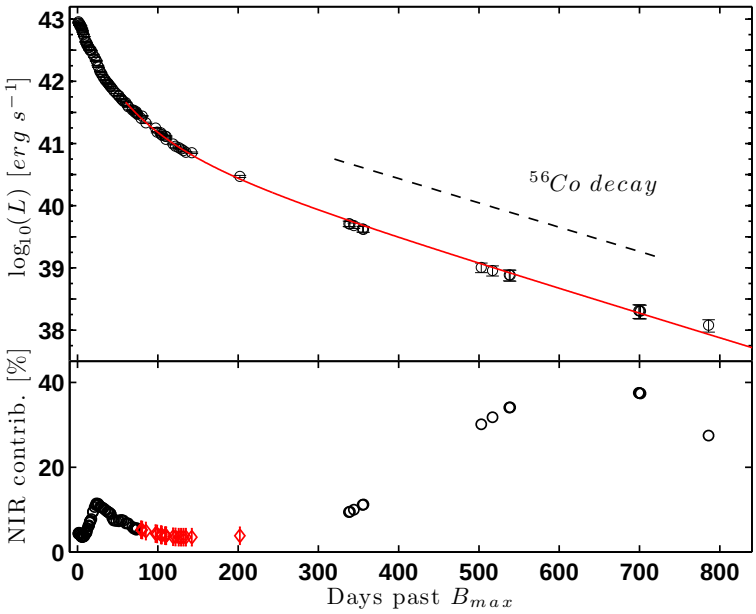

Figure 4.8: *Upper panel: the UVOIR light curve of SN 2003hv constructed as described in Sect. 4.5.4. The last point is based mostly on extrapolations, and should be regarded as rather uncertain. The red solid line is the best fit of a radioactive decay energy deposition function of* ^{56}Co *between +60 and 700 days. The estimated* ^{56}Ni *mass from the energy deposition function fit is 0.22 ± 0.02* $M_{\odot}$*, which is less than what was obtained at maximum light (0.40 ± 0.07* $M_{\odot}$*), indicating that at these late phases a substantial fraction of the flux is emitted outside the UVOIR bands. At 300–700 days past maximum the decline rate is linear and follows the expected decay time of* ^{56}Co *(dashed line) assuming full and instantaneous positron energy deposition. The displayed error bars do not include the error in the distance to NGC 1201. Lower panel: The evolution of the NIR contribution to the UVOIR light curve, computed as integrated flux from* J *to* K *over the integrated UVOIR flux. Since no NIR data were available at +60–200 days, we assumed a contribution (red diamonds in the graph) that maintains the smoothness of the curve and is compatible with the corresponding temporal evolution observed by S04.*

+530 and +786 days, in order to estimate J and K magnitudes at the final epoch. None of the upper limits in $UJHK$ bands was violated by any of these assumptions or fits. The photometry was subsequently corrected for Galactic extinction assuming $R_V = 3.1$ and following the prescription of Schlegel et al. (1998). Magnitudes were converted to fluxes within the individual filters and the UVOIR flux (and its associated error) was obtained by integrating the filter fluxes over wavelength. The UVOIR luminosity was calculated assuming a distance of 18.79 ± 2.60 Mpc. No corrections were applied for the flux lost blueward of U or redward of K. The UVOIR light curve is displayed in Fig. 4.8.

The UVOIR light curve can be used to estimate the amount of ^{56}Ni synthesized during the explosion. Using the estimate of the peak brightness and application of Arnett's rule (Arnett, 1982) suggests that 0.40–0.42 $M_{\odot}$ of ^{56}Ni was synthesized in the explosion, depending on whether we choose to correct by an additional 5% or 10% for the flux not observed blueward of the U band (Stritzinger et al., 2006a, and references therein). The associated error amounts to 0.07 $M_{\odot}$, accounting for the errors in the measured flux and the uncertainty in the rise time. The error increases to 0.11 $M_{\odot}$ if the uncertainty in the distance to NGC 1201 is included.

The ^{56}Ni mass can also be estimated by fitting an energy deposition function for the radioactive decay of ^{56}Co in the tail of the bolometric light curve. A simple model, also used by S04 and SS07, is $L = 1.3 \times 10^{43} M_{\rm Ni} e^{-t/111.3}(1 - 0.966e^{-\tau})$, where L is the bolometric luminosity, $M_{\rm Ni}$ is the ^{56}Ni mass, t is the time past maximum, and τ is the optical depth which is taken to evolve as $(t_1/t)^2$, where t_1 is the time

where the optical depth to the gamma rays becomes unity (Sollerman et al., 1998). This model assumes complete and instantaneous energy deposition from the positrons. By fitting this simple equation to our UVOIR light curve in the range +60–700 days, we obtain $M_{\rm Ni} = 0.22 \pm 0.02$ M$_\odot$ and $t_1 = 32.7 \pm 1.8$ days. The quoted errors here are merely the formal errors from the least-square fits. Since no JHK observations were available at +60–200 days, we made an assumption for the NIR contribution[9] at these phases (Fig. 4.8, lower panel). The adopted assumption ensures that the evolution of the NIR contribution is smooth and similar to that of the well-observed SN 2000cx (S04); that is, we have assumed that the NIR contribution continues its smooth decline until it reaches a minimum at around +130 days, after which there is an upturn that slowly leads to the observed high NIR contribution at late times. An associated uncertainty of ±2% was assumed for these calculations. In addition, it was checked that other reasonable assumptions do not change the derived ^{56}Ni mass by more than ± 0.02 M$_\odot$.

We point out that there is a substantial difference between the ^{56}Ni mass estimated from the energy emitted in the UVOIR bands around maximum light compared to that estimated at late phases. There could be a number of reasons for this "missing flux," including color evolution outside the UVOIR bands, positron escape, or an IRC.

Previous studies have shown that color evolution is very important at these stages within the UVOIR limits: S04 demonstrated that the contribution of the NIR bands to the UVOIR luminosity increased from about 3% to 28% between +150 and +500 days. A similar result was obtained by SS07. We find that this fraction for SN 2003hv evolves from about 9% to 30% between +330 and +500 days and increases to $\sim$ 37% by +700 days (Fig. 4.8, lower panel).

S04 and SS07 also estimated that the UVOIR light curve might probe only $\sim$ 60% of the true bolometric luminosity at these late phases. Our modeling suggests that at +350 days the UVOIR misses 27% of the total luminosity, while at +500 days this ratio increases to 44%. It is most likely that the difference in derived nickel mass is due to a significant fraction of flux at late phases being emitted in the far-infrared.

By integrating the flux contained within the nebular spectra in Fig. 4.7, we find that the flux emitted in the MIR region probed by *Spitzer* is a significant portion of the total flux probed at day +358: $L_{\rm MIR}/L_{\rm tot_{probed}} = (34 \pm 17)$%. The large error bar is due to the poor signal-to-noise ratio of the MIR spectrum, and there is an additional uncertainty in the *Spitzer* absolute-flux calibration. For comparison, our model, for which the onset of the IRC occurs later (i.e., $\sim$ 500–700 days), predicts only a value of 8% for this ratio. Note also that the probed MIR range is still blueward of most fine-structure lines in the far-infrared, to which most of the flux would shift in the event of an IRC.

4.5.5 TRAPPING OF POSITRONS

There is an ongoing debate concerning the extent to which the positrons created in the radioactive decays are trapped in the ejecta. This discussion has implications for our understanding of the magnetic field configuration of the ejecta (Ruiz-Lapuente & Spruit, 1998). It is of interest for understanding the Galactic 511 keV emission where SNe Ia have been suspected to contribute if the positrons escape (Milne et al., 1999; Prantzos, 2008), and it is also important in order to properly model the late-time emission of SNe Ia. Our spectral synthesis model assumes that all positrons are trapped and that they deposit their energy *in situ*, but more elaborate positron transfer mechanisms could be envisioned (Milne et al., 1999).

The most straightforward observational test is to measure the decline rate of the late-time bolometric light curve, since positrons are the main energy contributors during late phases when the gamma rays escape the ejecta freely. In the simplest scenario, complete positron trapping will result in a late-phase bolometric light curve that follows the decay rate of radioactive ^{56}Co (0.98 mag per 100 days), whereas positron escape would produce a faster decay rate. In particular, one would expect positron escape to become increasingly important at later phases, and therefore a bolometric light curve that deviates progressively more from the

[9] By NIR contribution to UVOIR, we define here the ratio of the integrated flux from J through K to the integrated flux from U through K.

radioactive input rate (e.g., Milne et al., 2001, their Fig. 1).

The late-time UVOIR decline rate of SN 2003hv between +300 and +700 days is 0.99 ± 0.04 mag per 100 days, exactly what is expected for complete and instantaneous positron trapping (Fig. 4.8). In addition, during these epochs, the UVOIR light curve does not show large deviations from a linear decay. Only observations past day +300 were included to minimize contamination from energy deposited by gamma rays, and the data point at +786 days was ignored because it is based mainly on extrapolations (except in the H band).

This gives little room for energy being lost in the form of positrons, at least between +300 and 700 days. There can, in principle, be alternative explanations that give a shallower light curve while allowing for positrons to escape, such as freeze-out (Fransson & Kozma, 1993). However, this would require multiple effects to "conspire" to give an extended linear decay with a slope that perfectly mimics that of radioactive decay. We therefore believe that there is no evidence for substantial leakage; it is adequate to model SNe Ia at late times assuming that positrons do not escape.

Turning to the contribution of positrons to the Galactic 511 keV line, Prantzos (2008) mentions that a constant escape fraction as small as 3% would be enough to make them an important source. It is difficult to exclude such a small contribution. We merely note that as our light curves show little evidence for positron escape at late phases, it is hard to imagine that positron escape is important at earlier epochs when the density of the ejecta is considerably higher and the magnetic field strength is greater. Of course, SNe Ia do show some diversity at late times (e.g., the peculiar SN 2006gz; Maeda et al., 2009), but our conclusions seem to hold for SN 2000cx (S04), SN 2001el (SS07), and SN 2003hv.

We already noted that within the electron capture scenario favored by Motohara et al. (2006) to explain the flat-topped line profiles, there is additional evidence for *in situ* positron trapping. If the positrons from the radioactive isotopes were able to travel inside the ejecta, they would also excite the central material and not give rise to a flat-topped profile.

4.5.6 INFRARED CATASTROPHE

Having discussed the positron trapping and the missing flux at late times in the UVOIR light curve, we now proceed to the question of whether an IRC could have occurred in the ejecta of SN 2003hv.

Figure 4.9 shows the late $UBVRIJHK$ light curves of SN 2003hv together with our detailed model light curves based on the W7 model (see also S04). The very sharp drop in the modeled light curves between +550 and 700 days is a consequence of the IRC.

From the modeling point of view, the IRC is expected to occur once the temperature of the ejecta drops below a critical threshold. In the case of SN 2003hv, the observed light curves appear to show little evidence of such a dramatic scenario. Not only do the optical bands seem to demonstrate an opposite trend, as discussed above, but the +786 day H-band detection places strong constraints on the drop of the NIR luminosity. While this has been hinted by single optical passband observations in the past, this is the first multi-wavelength study extending to such late phases.

The lack of a sudden and dramatic drop in the late-phase flux suggests that at least a portion of the ejecta is kept above the critical temperature limit which marks the onset of the IRC. One possible solution that we propose here is clumping of the ejecta. In this case, lower density regions cool more slowly and remain hot enough to avoid reaching the IRC temperature limit. The emission from these regions may dominate the optical and NIR range, thus causing the flux of the SN not to decrease as fast as predicted by a model with a more homogeneous density distribution. This is illustrated in Fig. 4.9 by the dashed curve, which represents a model with clumpy ejecta. In this simplistic model, clumping is achieved by artificially compressing and decompressing subsequent layers of the W7 ejecta. We stress that no effort has been made to "fit" the data or to simulate a realistic 3-D situation. The purpose of this experiment is to show that clumping can postpone the main observational signatures of an IRC. However, even in this model the high-density regions cool and indeed undergo the IRC. The lower density regions, on the other hand, stay

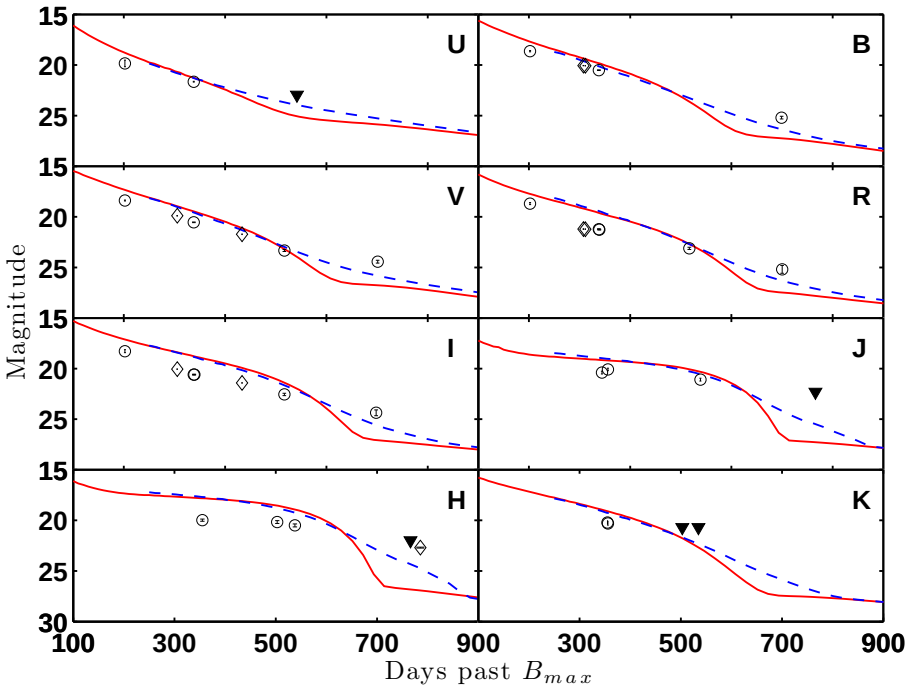

Figure 4.9: *Photometric data of SN 2003hv after 200 days past maximum compared with the model light curves of W7 and our spectral synthesis code (solid red line). Circles are ground-based data, diamonds are data from HST, and filled triangles denote upper limits. The sharp drops in the model light curves between +550 and +700 days are due to the predicted IRC. The observed data do not show such a dramatic evolution. The dashed blue line is a simplified "clumped" model illustrating how clumping can reduce or postpone the effects of the IRC: the high-density regions undergo an IRC first, but the low-density regions remain hot and continue emitting at the UVOIR wavelengths.*

hot enough for this not to occur and therefore continue to emit sufficient flux in the optical and NIR.

Support for the inhomogeneous nature of the cooling comes from the calculations by Kozma et al. (2005), based on the 3-D model by Röpke (2005): at +500 days, a large range of temperatures (and ionizations) is present, from a few hundred K to $\gtrsim$6000 K (their Fig. 7). Whether the IRC occurs in a specific region depends both on the density and composition. The dependence on composition comes mainly from the difference in ^{56}Ni content, which affects the local heating by the positrons.

One way to interpret our observations could thus be to propose that an IRC *has* taken place in the highest density regions of the ejecta. With the innermost regions having higher densities, this scenario can explain the lack of emission in these regions, resulting in the observed flat-topped line profiles. This idea can also explain the missing flux in the tail of the UVOIR light curve as estimated from the difference of the derived ^{56}Ni masses at maximum and at late phases. It is, however, required that the highest density regions must have already suffered this IRC before $\sim$ 350–700 days, since during these epochs the UVOIR light curve shows little deviation from the ^{56}Co radioactive decay rate of 0.98 mag per 100 days. The less-dense parts still continue emitting in the optical and NIR wavelengths. This scenario is also supported by the excess flux measured in the MIR at +358 days.

Further pursuit of the idea of clumpiness is beyond the scope of this paper, but we suggest this to be an interesting topic of investigation for future 3-D modeling efforts. Here we restrict ourselves to pointing out that an IRC might have occurred in the innermost, highest density regions of SN 2003hv, and that this idea is compatible with the multi-wavelength observations of the ejecta.

4.5.7 GEOMETRY OF THE EXPLOSION

As also pointed out by Motohara et al. (2006), the blueshifted lines observed in some of the emission features of the nebular spectrum may suggest an asymmetry in the distribution of ^{56}Ni that was formed during the explosion. This is also the conclusion of Maeda et al. (2010b), who model the nebular spectra of SN 2003hv with the aid of a simplified kinematical model and propose that we are viewing the explosion toward an offset high-density region. Hillebrandt et al. (2007) and Sim et al. (2007) showed that the viewing angle of off-centre explosions can have a significant effect on the light-curve properties of SNe Ia. An enhancement in brightness is expected in their models when the bulk of ^{56}Ni is moving toward the observer. However, this is not observed in SN 2003hv, which has a normal luminosity.

A different diagnostic of (another kind of) asymmetry comes from the analysis of spectropolarimetry of SN 2003hv at +6 days (unpublished data). While the lack of continuum polarization suggests that the photosphere was spherical at these times, non-negligible line polarization (0.19%) associated with Fe II and Si II features implies an asymmetric or clumpy line-forming region for these two species. Note that the polarization of the Si II feature at these times is at odds with the suggested evolutionary trend of Si II polarization in normal SNe Ia, for which zero polarization is expected at $+6$ days after maximum (e.g., SNe 2001el, 2002bo, see Wang et al., 2003, 2007). Despite the fact that these two observations probe completely different parts of the ejecta, and it is very difficult to link them in a common conclusion, they might hint that a simple spherically symmetric explosion cannot accurately describe SN 2003hv. This is not incompatible with our idea of clumping. A complete treatment and analysis of the spectropolarimetry will be given by Maund et al. (2009, in prep.).

4.6 SUMMARY AND CONCLUSIONS

We have presented observations of SN 2003hv that were obtained with a multitude of instruments. This study includes systematic multi-band observations from early to very late phases, and the latest-ever detection of a SN Ia in the NIR. It also features a comparison of our nebular spectrum synthesis model with the widest (in wavelength coverage) nebular spectrum of a SN Ia.

SN 2003hv is a SN Ia with the unusual value of $\Delta m_{15}(B) = 1.61 \pm 0.02$ mag, and it exhibits photometric and spectroscopic properties that are consistent with its decline-rate parameter.

The main conclusions of the late-phase study are as follows.

$*$ The individual light curves have decline rates similar to what has been observed for other SNe Ia in the past, confirming that there is an evolution of the flux from the optical to the NIR wavelengths.

$*$ At $+700$ days, a deceleration in the fading of the SN emission is observed in the individual optical bands, particularly in the V band. Such tendencies have been seen in other SNe Ia observed past 600 days.

$*$ By comparing the radioactive energy input to the ejecta, as expressed from the ^{56}Ni masses derived from the UVOIR light curve at maximum light and in the tail, we find that the amount of energy probed within the UVOIR wavelengths is substantially less at late times than at maximum brightness.

$*$ A possible explanation for this could be that positrons escape the ejecta, thus stealing energy away from it. The UVOIR light curve, however, follows very accurately the radioactive decay of ^{56}Co in the range $+300$–700 days, assuming complete and instantaneous positron trapping. This slope is difficult to reconcile with positron escape. Alternatively, the UVOIR light curve is not a good probe of the real bolometric light curve at late times, because the energy is still within the ejecta but a significant part of it is emitted at even longer wavelengths.

$*$ A hypothesis proposed here to explain the SN 2003hv data is that an IRC has occurred in the densest (i.e., innermost) part of the ejecta. This idea can explain (i) the missing flux in the tail of the UVOIR curve, (ii) the flat-topped NIR profiles, and (iii) the excess flux observed in the MIR spectrum. However, such an IRC must have taken place before $\sim$300–350 days, since this is when the slope settles down, the flat-topped profiles start to emerge, and the *Spitzer* observation took place.

∗ The notion of an IRC occurring locally (and not simultaneously all over the SN ejecta) is consistent with models that feature a clumped (or inhomogeneous) distribution of the ejecta. The high-density regions undergo the IRC first, since it is these that experience the most efficient cooling.

∗ Deviations from spherical symmetry are suggested for SN 2003hv by the blueshifts of the iron-family element lines from the optical to the MIR and, independently, from early spectropolarimetric observations.

4.7 IMPACT AND FOLLOW-UP WORK

The previous sections of the present chapter were published in Leloudas et al. (2009b). In this section I briefly comment on some related follow-up work in the field of SN Ia asymmetries (Maeda et al., 2010b,a).

In Sect. 4.5.7 it was mentioned that there were strong hints for SN 2003hv being an asymmetric off-centre explosion. This was both motivated from nebular IR observations (Motohara et al., 2006; Gerardy et al., 2007) and from shifts in individual isolated lines in the optical, similar to the ones observed in the IR (Fig. 4.6). Since, however, the 'trademark' lines of SN Ia nebular spectra ([Fe III] λ4700) did not demonstrate such a shift (although a blend of many lines), we did not investigate this idea further in Leloudas et al. (2009b).

Maeda et al. (2010b), however, showed that it is possible to construct a simple, theoretically motivated, off-centre deflagration-to-detonation explosion model (Fig. 4.10) that *can simultaneously explain a velocity shift in some lines* (e.g. [Fe II] λ7150, [Ni II] λ7378, [Fe II] λ8621, [Fe II] λ16440) *but no shift in other lines* (most notably [Fe III] λ4700). By fitting the model predictions to the unique multi-wavelength dataset of SN 2003hv, it is possible to determine the parameter values, such as the off-set and outer velocities and the mass distribution within the different zones.

This success motivated Maeda et al. (2010b) to look for signs of asymmetry in nebular spectra of other SNe, available in the SUSPECT database.[10] Indeed, a variation in the observed wavelength of the [Fe II] λ7150 & [Ni II] λ7378 lines was found (in contrast with [Fe III] λ4700), which can be explained by the combination of the off-centre explosion model and a variation in the observer viewing angle (Fig. 4.11). In addition, the observed shift distribution agrees well with the statistical predictions for a random distribution of viewing angles, in a picture where SN 2003hv was an explosion seen directly in the off-set direction and demonstrates the highest observed velocity shift. We thus believe that we have found observational evidence for asymmetries in SN Ia explosions by probing the inner part of the ejecta.

This idea can be further explored to investigate effects of the discovered asymmetry in other observed properties of SNe Ia as e.g. luminosity. It has been theoretically shown (Sim et al., 2007; Kasen et al., 2009) that the combination of an asymmetric explosion and the viewing angle can contribute to the dispersion of the observed luminosities of SNe Ia (see also Fig. 2.4). This should be observed as a dispersion in the SN Ia Hubble diagram, even after correcting for the Phillips relation (1993). It widely accepted that the Phillips relation is governed by the mass of synthesized ^{56}Ni that controls the luminosity of a SN Ia to a first order. A 'second parameter' in the calibration of the SN Ia luminosity has long been sought for and different parameters have been proposed, including metallicity, progenitor age, host galaxy mass or spectroscopic diversity (e.g. Gallagher et al., 2005; Kelly et al., 2009; Neill et al., 2009; Wang et al., 2009a). In Maeda et al. (2010a) we, for the first time, examined observationally the possibility that the viewing angle in an off-centre explosion, as determined by line shifts in nebular spectra, can manifest itself as a residual in the Hubble diagram, after correcting for the Phillips relation. Indeed, we observed that such a correlation might exist (Fig. 4.12). Although the significance of this correlation is low (2.1σ), it is encouraging: SNe that demonstrate a blueshift are brighter, while those demonstrating a redshift are fainter than expected by the Phillips relation. These results were supported by modeling, which gives the same trends as the observed one (Maeda et al., 2010a). It should be stressed that the main uncertainties in these calculations lie in the accurate distance determination (and reddening) of these events and that a larger sample, preferably in the

[10] The Supernova Spectrum Archive: `http://bruford.nhn.ou.edu/~suspect/`

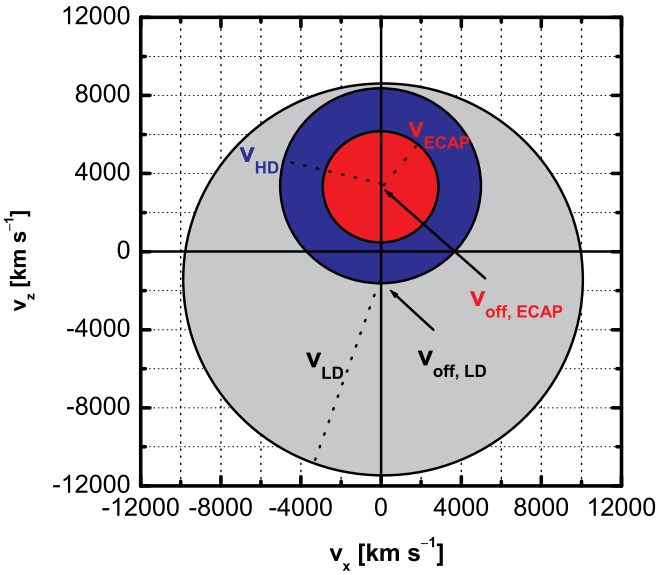

Figure 4.10: *From Maeda et al. (2010b): The simple explosion model that can explain the multi-wavelength nebular spectrum of SN 2003hv. The red area contains the electron-capture (ECAP) products of the initial deflagration that was ignited off-centre by ∼3500 km s^{-1}. It is surrounded by a high density (HD) area of radioactive ^{56}Ni with a similar off-set. The detonation wave washes away the asymmetries (e.g. Röpke, 2007) and produces a zone where the density is lower (LD). All zones are shown to have different electron densities and temperatures and are at different ionization states: the lines presenting a velocity shift originate in the ECAP and HD zones, while the ones that don't, form in the LD zone.*

Hubble flow, is needed to confirm these results.

Exploring observationally the asymmetries of SNe Ia is an exciting field, behind a physically motivated idea, with important implications for better understanding the physics of these explosions and for cosmology.

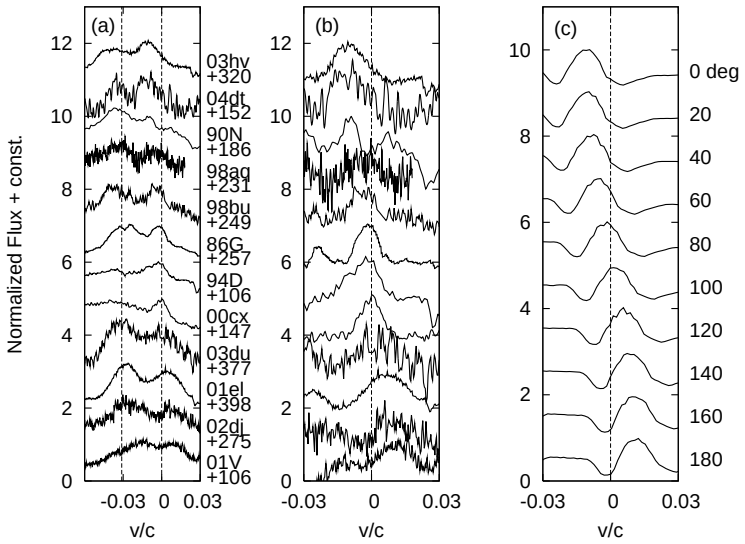

Figure 4.11: *From Maeda et al. (2010b): Observed line profiles for 12 nebular SNe Ia spectra focusing on the region around [*Fe II*] λ7155 and [*Ni II*] λ7378 (dotted lines mark the rest wavelengths). (b) [*Ni II*] λ7378, after removing the underlying continuum (or possible other lines) as much as possible (see discussion in Maeda et al., 2010b). (c) Synthetic line profiles of the [*Ni II*], depending on the viewing orientation. It is demonstrated that shifts are both observed in the real data and predicted by the off-center explosion model.*

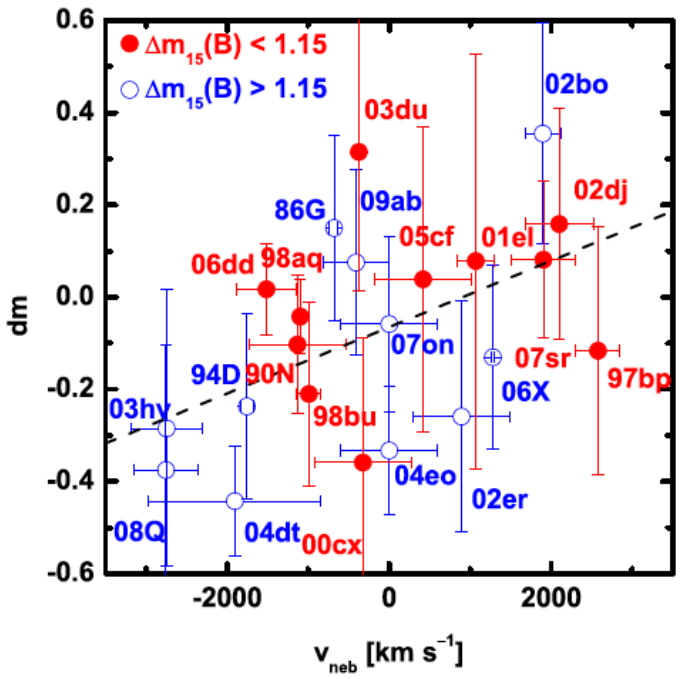

Figure 4.12: *From Maeda et al. (2010a): A plot of the residual in the Hubble diagram after correcting for the Phillips relation (Folatelli et al., 2010), versus the nebular velocity shift. A tentative correlation is observed (at the 2.1σ level) indicating that (on average) SNe that demonstrate a blueshift are brighter, while those demonstrating a redshift are fainter than expected by the Phillips relation. This behavior is consistent with the trend observed in the model of Maeda et al. (2010a), but also of Sim et al. (2007).*

Published as: Leloudas, G.; Sollerman, J.; Levan, A. J.; Malesani, D.; Fynbo, J. P. U.; Maund, J. R. – *Do Wolf-Rayet stars have similar locations in hosts as type Ib/c supernovae and long gamma-ray bursts?* Accepted for publication in Astronomy & Astrophysics, arXiv: 1002.3164.

5

DO WOLF-RAYET STARS HAVE SIMILAR LOCATIONS IN HOSTS AS TYPE IB/C SUPERNOVAE AND LONG GAMMA-RAY BURSTS?

We study the distribution of Wolf-Rayet (WR) stars and their subtypes with respect to their host galaxy light distribution. We thus want to investigate whether WR stars are potential progenitors of stripped-envelope core-collapse supernovae (SNe) and/or long-duration gamma-ray bursts (LGRBs). We used the method applied by Fruchter et al. (2006) and Kelly et al. (2008) for the hosts of LGRBs and SNe and compare with their respective results. We examined two nearby galaxies, M 83 and NGC 1313, for which a comprehensive study of the WR population exists. These two galaxies contain a sufficiently large number of WR stars and sample different metallicities. To enable the comparison, the images of the galaxies were processed to make them appear as they would look at a higher redshift. The robustness of our results against several sources of uncertainty was investigated with the aid of Monte Carlo simulations. We find that the WC star distribution favours brighter pixels than the WN star population. WC stars are more likely drawn from the same distribution as SNe Ic than from other SN distributions, while WN stars show a higher degree of association with SNe Ib. It can also not be excluded that WR (especially WC) stars are related to LGRBs. Some differences between the two galaxies do exist, especially in the subtype distributions, and may stem from differences in metallicity. Although a conclusive answer is not possible, the expectation that WR stars are the progenitors of SNe Ib/c and LGRBs survives this test. The trend observed between the distributions of WN and WC stars, as compared to those of SNe Ib and Ic, is consistent with the theoretical picture that SNe Ic result from progenitors that have been stripped of a larger part of their envelope.

5.1 INTRODUCTION

To understand the origin of cosmic explosions like supernovae (SNe) and gamma-ray bursts (GRBs), it is important to study and constrain their environments. Fruchter et al. (2006; hereafter F06) presents a sample of 32 long-duration GRB (LGRB) host galaxies and has developed a new technique to show that LGRBs have a tendency to occur in the brightest pixels of their host galaxies. This contrasts to a comparison sample of core-collapse (CC) SNe where the SN locations instead follow the light distribution of their hosts. Kelly et al. (2008; hereafter K08) further shows that not all CC SNe follow the same host galaxy light distribution, with SNe Ic strongly skewed towards the brightest regions of their hosts. The SN Ic population is thus broadly consistent with that of LGRBs. Indeed, SNe Ic, and in particular broad-lined SNe Ic, are so far the only type that have been been firmly observationally connected to LGRBs (Galama

et al., 1998; Hjorth et al., 2003; Stanek et al., 2003; Malesani et al., 2004) or their lower energy siblings, X-ray flashes (Pian et al., 2006; Campana et al., 2006; Sollerman et al., 2006).

Using a similar method, Anderson & James (2008) mapped the association of nearby SNe with Hα regions. They find that SNe Ic trace the Hα emission, and recent star formation, to a higher degree than other CC SN types. This was attributed to SNe Ic having more massive progenitors than SNe Ib, which are in turn more massive than SNe II. Larsson et al. (2007) modeled the F06 results and derived minimum masses for CC SNe and LGRBs of 8 and 20 $M_{\odot}$, respectively. A theoretical-modeling approach was also taken by Raskin et al. (2008), who uses the F06 method and a simulated solar-metallicity spiral galaxy to predict the (increasing) minimum cut-off masses of the progenitors of SNe II and Ic.

The next step is to expand this type of study to the potential progenitors of these cosmic explosions. The most plausible candidates are Wolf-Rayet (WR) stars (Woosley & Bloom, 2006; Crowther, 2007). In single-star evolutionary models, WR stars are the final phases in the life of very massive stars (minimum initial mass $> 22 - 37\ M_{\odot}$, depending on the metallicity and rotation; Meynet & Maeder, 2005), which have shed their hydrogen envelope. WR stars can also result from close binary star interaction, through Roche-lobe overflow, in which case the minimum mass can be decreased down to $\sim 15\ M_{\odot}$ (Eldridge et al., 2008). A comprehensive review of WR stars is given by Crowther (2007). Here we restrict ourselves to giving the background information that is essential for the purposes of this study: WR stars are further divided into nitrogen-rich (WN) and carbon-rich (WC) stars. WN and WC stars are believed to give rise to supernova explosions of Type Ib and Ic, respectively (Crowther, 2007; Georgy et al., 2009). Depending on their emission line properties, width, and appearance, they can be further divided into 'early' or 'late' types (WNE, WNL, WCE, and WCL, respectively). The WR star populations strongly depends on metallicity, with both the total number of WR stars and the relative ratio of WC/WN stars increasing dramatically with metallicity (Crowther, 2007; Meynet & Maeder, 2005). This is attributed to the dependence of winds on metallicity, which leads to much more effective mass loss in the presence of metals (Vink & de Koter, 2005).

Our purpose here is to study the distribution of WR stars and their subtypes within their hosts, using the method applied by F06 and K08. The main motivation is the following: if WR stars are the immediate progenitors of SNe Ib/c and LGRBs, then we would also expect their distributions with respect to the host galaxy light to be similar. Since the progenitors of SNe Ib/c still evade direct detection (see e.g. Maund et al., 2005; Crockett et al., 2008b; Smartt, 2009), this method can give us hints to their nature. The same is true for LGRBs, for which a direct progenitor detection seems impossible, at least in the near future. It is noteworthy that WR features have been clearly identified in the host of the most nearby LGRB (GRB 980425/SN 1998bw), albeit with a considerable offset to the explosion position (Hammer et al., 2006; Christensen et al., 2008) and more recently in four more LGRB hosts (Han et al., 2010).

This chapter is structured as follows. In Sect. 5.2 we discuss the galaxies chosen for studying the WR distribution. In Sect. 5.3 we outline the methods used throughout the study, and in Sect. 5.4 we present our results. Section 5.5 contains a discussion of the results and several uncertainty factors, and Sect. 5.6 summarizes our conclusions.

5.2 GALAXY SELECTION

It is essential for our purposes to use galaxies where the WR star population has been mapped accurately and systematically in an unbiased way, as much as that is possible. For this reason we used the results of P. Crowther and collaborators, who have recently identified and spectroscopically classified the WR stars in a number of galaxies beyond the Local Group, in an essentially complete way (Schild et al., 2003; Hadfield et al., 2005; Hadfield & Crowther, 2007). The method used is explained in detail in, e.g., Hadfield & Crowther (2007) and includes the following steps: first imaging of the galaxy is obtained and then regions with candidate WR stars are identified by their excess in a narrow-band He II λ4684 filter over the continuum. Subsequently, the regions containing WR stars are confirmed with spectroscopy of the

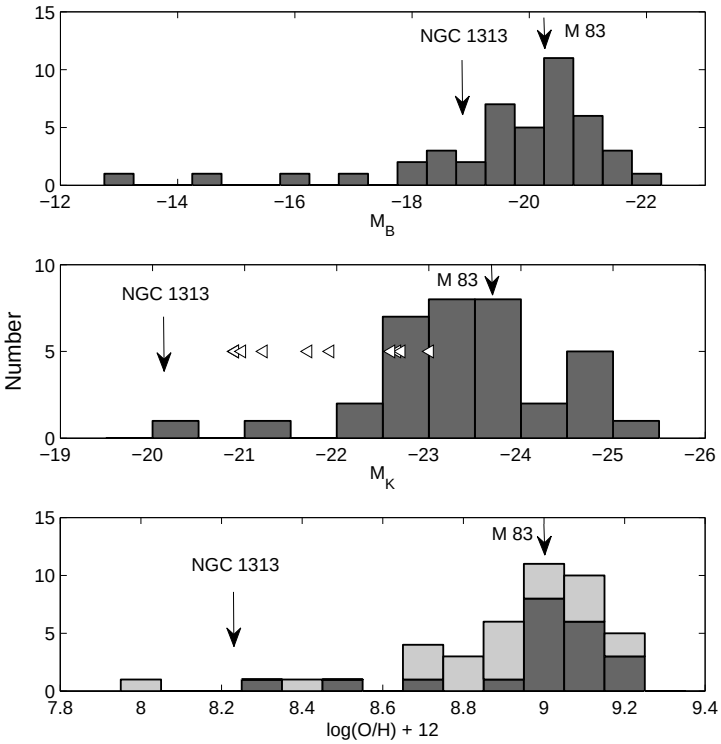

Figure 5.1: *Global properties of M 83 and NGC 1313 compared to those of the K08 SNe Ib/c hosts. Histograms of the absolute magnitudes M_B, M_K (a better tracer of the total stellar mass), and metallicity are presented. The information presented here was collected from NED, SDSS, and from Prieto et al. (2008), for the metallicities. These are global metallicities on the scale used by Tremonti et al. (2004). The M_K histogram is incomplete towards the faintest galaxies and upper limits, compatible with the 2MASS survey upper limit, are provided (white arrows). To get an indicative value for the galaxies with no metallicity reported in Prieto et al. (2008), i.e. the ones not included in SDSS DR4, we used an approximate luminosity-metallicity relation (see Sect. 5.3.4). These galaxies are represented by the light-grey shaded histogram. The corresponding values for M 83 are marked, indicating that this galaxy is very typical of the K08 sample, just closer. NGC 1313, on the other hand, is a galaxy that is fainter and more metal-poor, hence more reminiscent of LGRB hosts.*

candidates. Their spectral type (WN, WC, early, late) is determined, and the number of WR stars is estimated by fitting template spectra to the flux-calibrated, integrated spectrum of the WR-star region. By excluding galaxies where the survey did not cover the entire galaxy (Schild et al., 2003; Hadfield & Crowther, 2006), we decided to rely on the following two galaxies: M 83 (Hadfield et al., 2005) and NGC 1313 (Hadfield & Crowther, 2007).

We did not use the existing catalogues for other (very nearby) galaxies, such as the LMC (Breysacher et al., 1999), the SMC (Massey et al., 2003), or other Local Group galaxies (Massey & Johnson, 1998), because they suffer from several incompleteness-related issues (chance discoveries, Malmquist bias) and have complicated revision histories (see e.g. Massey & Johnson, 1998). Another practical disadvantage with these galaxies is their large angular size. The WR galaxy catalogue in Schaerer et al. (1999) is also unsuitable for our purposes, because it is a list of diverse objects that have been defined from the appearance of a broad He II feature in their integrated spectra.

Table 5.1: *Key properties of M 83 and NGC 1313.*[a]

Property	M 83	NGC 1313
log(O/H)+12	9.00	8.23
D (Mpc)	4.5	4.1
Pix. scale[b]	5.3[2]	4.0[2]
M_B (mag)	-20.2	-18.9
M_K (mag)	-23.7	-20.1
Morph.	SAB(s)c	SB(s)d
Confirmed regions[c]	132	70
WNE[d]	232	29
WNL	250	22
WCE	28	34
WCL	526	...
Candidate regions[e]	89	12[f]

[a] Compiled from Hadfield et al. (2005); Hadfield & Crowther (2007) and NED.
[b] In pc^2 pix^{-1} in the images from ESO/MPI 2.2m (+WFI) and VLT/FORS used in the analysis. A galaxy at $z = 0.01$ in the SDSS 2.5m images used by K08 would have $\sim$80^2 pc^2 pix^{-1}.
[c] Confirmed regions containing one or more WR stars.
[d] These numbers may differ slightly from those reported in the literature, for the following reasons: WN5-6 stars have been included in the WNE distribution; WO in WCE; transitional WN/WC have been included in both WN and WC.
[e] Candidate regions for which spectroscopy has not been conducted.
[f] 11 of these are photometrically consistent with WN stars.

The number of WR stars contained in the two selected galaxies ($\sim$1000 and 100, respectively) exceeds the number of 32 LGRB used by F06 and 44 SNe Ib/c used by K08 (out of 504 SNe of all types). While F06 and K08 constructed their distributions by looking at one explosion site per galaxy for many galaxies, discovered in searches that are not unbiased themselves, we look at many (potential) explosion sites in a few galaxies. Such a comparison should be valid, as long as the galaxies we choose are not different from the typical galaxies studied by K08 and F06. While this statement is obviously more problematic for the high-redshift F06 hosts (see also discussion in K08), we can compare the global properties of M 83 and NGC 1313 (see Sects. 5.2.1 and 5.2.2) to those of the K08 SNe Ib/c host sample. M 83 turns out to be a galaxy very typical of the K08 sample in terms of absolute magnitude, metallicity (Fig. 5.1), and morphological type - with its only difference that it is closer to us. NGC 1313 is somewhat different, although such galaxies are present in the K08 sample: fainter, metal-poor, and more irregular, it is more reminiscent of the LGRB hosts of F06. It is important for our study, as we will see, that the two galaxies probe two different metallicity limits.

Below, a more detailed description of the individual galaxies used in this study is given, containing only those details necessary for our discussion. Some of their key properties are also summarized in Table 5.1.

5.2.1 M 83

M83 is a nearby (4.5 $\pm$ 0.3 Mpc), Milky-Way type SAB(s)c spiral galaxy with a super-solar metallicity[1] of 9.0 (Hadfield et al., 2005, and references therein). In total, 132 WR regions containing $\sim$1000 $\pm$ 300 WR stars were spectroscopically confirmed by Hadfield et al. (2005), while 89 more regions are labeled as candidates, still awaiting spectroscopic follow-up. As part of the same study, Crowther et al. (2004) points

[1] Metallicities are expressed here as oxygen abundances $\log(\mathrm{O/H}) + 12$.

out the large number of WCL stars found in M 83, directly related to its high metallicity.

Hadfield et al. (2005) were not able to look for WR stars in the nucleus of M 83 (owing to saturation in the images). However, K08 also provide results after the removal of the bulge, for galaxies with a significant bulge contribution, so comparison is still possible. For our analysis we used a wide field image obtained using the ESO/MPI 2.2m (+WFI).

While very different from the LGRB host galaxies (F06), M 83 is a prodigious SN producer, with 6 observed SNe in the 20th century. Although most of them remain unclassified, one of them is a prototypical SN Ib (SN 1983N; Uomoto & Kirshner, 1985; Elias et al., 1985). The host site of SN 1983N is not associated with a confirmed WR site and is $\sim 7''$ away from the nearest candidate region. If an isolated WR star (such as several others identified in M 83) had been responsible for the 1983 explosion, it would of course have disappeared (e.g. Maund & Smartt, 2009) from the frames obtained later by Hadfield et al. (2005).

5.2.2 NGC 1313

NGC 1313 is a SB(s)d spiral at a distance of 4.1 ± 0.1 Mpc and has a metallicity of 8.23, i.e., intermediate between the SMC and the LMC (Hadfield & Crowther, 2007, and references therein). This galaxy is more reminiscent of the LGRB hosts than M 83, both regarding the more irregular shapes of the LGRB hosts (F06) and their, usually, low metallicity (Sollerman et al., 2005; Modjaz et al., 2008b; Savaglio et al., 2009). Two Type II SNe have been recorded in this galaxy, SNe 1962M and 1978K. Hadfield & Crowther (2007) report on the spectroscopic confirmation of 70 WR regions (success rate of 85% over the candidates followed with spectroscopy), while 12 more regions remain candidates and are photometrically consistent with WN stars. Unlike M 83, few of the identified regions contain more than one WR star, with their total number estimated to be between 84 and 115.

Our analysis was performed on the VLT/FORS images obtained by Hadfield & Crowther (2007). We included the single WO star (star #31)[2] in the WC stars, while the transitional WN/C star #11 was included in both the WN and WC distributions. For the WN5-6 stars we adopted a WNE classification, although this choice is not unique (Crowther, 2007). The results presented here do not change, however, if we include them in the WNL distribution instead.

5.3 METHODS

5.3.1 FRACTIONAL FLUX

As fractional flux of a pixel belonging to a galaxy, we define the sum of all counts in pixels less bright than the pixel in question, over the sum of all counts in all the pixels belonging to the galaxy. This is the same definition as the one used by F06 and K08.

5.3.2 PIXEL DETECTION

As in F06 and K08, the SExtractor software (Bertin & Arnouts, 1996) was used to identify the pixels that belong to the galaxies. The parameters used were similar to the ones in these references to make the comparison as close as possible. We used B-band images, which correspond to the same (rest-frame) wavelength window examined by F06 and K08.

5.3.3 PRE-PROCESSING OF IMAGES

Identification of individual stars in other galaxies requires that the galaxies are nearby. As a consequence, the apparent dimensions of M 83 and NGC 1313 (at $z = 0.0017$ and 0.0016, respectively) are much

[2] We follow the numbering of Hadfield et al. (2005) and Hadfield & Crowther (2007).

larger than the SN hosts of K08, and their images cover thousands of pixels on the CCD. While usually an advantage, for our type of analysis this can pose problems in two different ways. First, a considerable number of foreground stars are superimposed on the image and contribute to the pixel fractional fluxes. It is desirable to remove the foreground star point-spread functions (PSF), but it is not straightforward to identify which stars are in the foreground and which belong to the host galaxy. It has been shown that it is possible to distinguish between massive stars in other galaxies and foreground dwarfs by use of colour-colour diagrams (Massey, 1998; Massey et al., 2009) or other kinematical techniques involving spectroscopy (Drout et al., 2009). However, it was not necessary to resort to such detailed techniques for our purposes, because it is sufficient to remove only the brightest stars that are clearly in the foreground and contribute with significant light. To this end, all stars brighter than ∼20 mag were removed from our images by subtracting their PSF with tasks in the package `daophot` in IRAF[3]. At the distances of our galaxies, there is no degeneracy below this limit, and all stars can safely be considered Galactic. To assess the effect of stars fainter than 20 mag, we performed a Monte Carlo (MC) simulation: the expected number of foreground stars in the field (Bahcall & Soneira, 1981) and their corresponding counts, per magnitude bin, were removed randomly and repetitively from our images. This experiment showed that our results are not sensitive to their presence.

Second, each of our pixels contains light from a much smaller physical area than the ones studied by K08: the pixel scale in our images is ∼4 and 5 pc (along a pixel side) for NGC 1313 and M 83, respectively. On the other hand, the SN Ib/c hosts of K08 have a median redshift of $z \gtrsim 0.01$, which corresponds to a distance of $\sim$ 42 Mpc for $H_0 = 72$ km s^{-1} Mpc^{-1}. At this distance, one pixel on the SDSS 2.5m telescope, used by K08, corresponds to an area of $\sim 80 \times 80$ pc^2. Consequently the pixel fractional fluxes they quote refer to these large areas. To enable the comparison we thus binned our images by factors of 15-19 in order to 'bring our galaxies' to a redshift of $z = 0.01$. Subsequently, the images were convolved with a Gaussian in order to simulate the typical seeing of 3.2 pixels measured on the K08 SDSS plates. The final images are shown in Fig. 5.2.

5.3.4 THE METALLICITY DEPENDENCE

As mentioned above, both the total number of WR stars and the WC/WN ratio increase drastically with metallicity. This trend is also observed for M 83 and NGC 1313 (Hadfield et al., 2005; Hadfield & Crowther, 2007). If WR stars are the progenitors of SNe Ib/c, we therefore expect to observe relatively more SNe Ib/c in galaxies with high than low metallicity. This has, in fact, been shown by Prantzos & Boissier (2003), Prieto et al. (2008) and Boissier & Prantzos (2009). Anderson & James (2009) even claim that they can disentangle the metallicity dependence from the mass dependence and that SNe Ic come from higher metallicity environments than SNe Ib. On the other hand, LGRBs are often found in low-metallicity environments (Sollerman et al., 2005; Stanek et al., 2006; Savaglio et al., 2009; Levesque et al., 2010a), especially in comparison to broad-lined SNe Ic that are not associated with known LGRBs (Modjaz et al., 2008b). However, it has not been completely settled whether all LGRB hosts are metal poor or if we are simply missing more metal-rich hosts owing to a dust-obscuration bias (e.g. Fynbo et al., 2009; Levesque et al., 2010b; Svensson et al., 2010). Because of these strong metallicity dependencies, in the following section, our results will be presented separately for the metal-rich M 83 and the metal-poor NGC 1313.

We have also attempted to look for possible metallicity signatures in the K08 sample. To do so, the K08 SN Type Ib and Ic fractional flux distributions were divided into two equal number bins of 'high' and 'low' metallicity. For the host galaxies for which Prieto et al. (2008) do not report metallicities, we followed Prantzos & Boissier (2003) in using the galaxy global luminosity as a proxy for metallicity. Although it has been shown that the local metallicities at the explosion sites can differ from the global metallicity or its proxies (e.g. Modjaz et al., 2008b; Thöne et al., 2009), this should not pose any problems for the rough separation of the sample in two bins. It was thus assumed that the galaxies without reported metallicities

[3]IRAF is distributed by the National Optical Astronomy Observatory: `http://iraf.noao.edu/iraf/web/`.

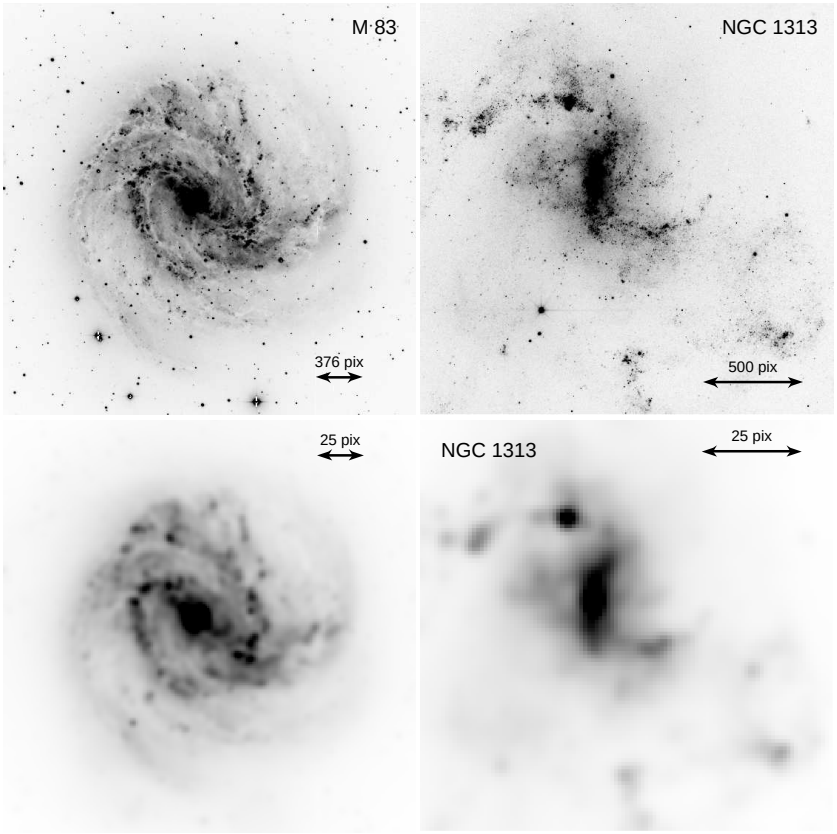

Figure 5.2: **Top left:** *ESO/MPI 2.2m (+WFI) B-band image of M 83 ($z = 0.0017$, $D = 4.5$ Mpc). The displayed part is 3300×3300 pixels.* **Top right:** *VLT/FORS B-band image of NGC 1313 ($z = 0.0016$, $D = 4.1$ Mpc). The image is 2048×2048 pixels.* **Bottom:** *Processed images, which simulate how the galaxies above would look at $z = 0.01$ at the SDSS 2.5m telescope. Bright foreground stars have been removed and the images have been binned such that one pixel side is ∼80 pc along. A Gaussian filter has been used to smooth the resulting images to an FWHM of ∼3.2 pixels, typical of the SDSS frames. The pixel dimensions of the resulting images are 220×220 and 108×108, respectively. In each panel, a double arrow spanning 2 kpc across has been drawn and the corresponding pixel scale is noted.*

have metallicities consistent with the best fit luminosity-metallicity relation, as derived from the galaxies with reported metallicities (light-grey histogram in Fig. 5.1, lower panel). We see no convincing evidence that the high and low metallicity SNe are different in terms of their fractional flux distributions. This investigation is, however, clearly limited by the small number of SNe in the sample and by the absence of very low (i.e. subsolar) metallicities.

5.4 RESULTS

To compare with the fractional flux distributions of LGRBs (F06) and various types of SNe (K08), it is necessary to consider the number of WR stars contained within each WR confirmed region, because each one of them is a potential progenitor of a SN and/or LGRB explosion. Hadfield et al. (2005) and Hadfield & Crowther (2007) give estimates for the numbers or WR stars contained in each region, as well as for the corresponding errors. The number of stars per region is simply taken into account by, e.g., including the fractional flux value of the pixel that hosts 5 WR stars 5 times in the corresponding distribution.

The pixel fractional fluxes measured at the locations of the WR stars, together with their number and subtype, are listed for the two galaxies in Table 5.2. In Figs. 5.3 and 5.4 (left panels), we have plotted the

Table 5.2: *Fractional fluxes at the locations of the WR stars.*[a]

	ID[b]	Subtype[c]	Number	FF[d]
	1	WNL	3	0.29
	2	WCL	2	0.34
	3	WCL	2	0.26
M 83	4	WNE	16	0.48
	5	WCL	8	0.48
	6	WCE	3	0.06
	...	...	...	...
	133	cand.	...	0.25
	134	cand.	...	0.54
	1	WNE	1	0.37
	2	WCE	1	0.30
NGC 1313	3	WNL	1	0.06
	...	...	...	...
	28	cand.	...	0.38

[a] An indicative portion of this table is shown. The full table is given in Appendix B.
[b] We follow the exact numbering of Hadfield et al. (2005) and Hadfield & Crowther (2007). Additional info (e.g. fluxes, errors in star numbers) can be found in these references.
[c] 'cand.' stands for candidate region.
[d] These fractional fluxes refer to a binning of 15 and 19 for the images of M 83 and NGC 1313 we have used, respectively. Although we have shown that the results do not change significantly with the choice of binning, individual fractional fluxes can vary.

WN and WC fractional flux distributions for the two galaxies, together with the data from F06 and K08. Table 5.3 contains the corresponding Kolmogorov-Smirnov (KS) test p-values that two distributions are drawn from the same parent distribution. To keep the graph as uncrowded as possible, we focused on the most relevant WR and SN types. The table, however, contains more information including the division of WR stars into their subtypes.

The null hypothesis of the KS test is that two samples are drawn from the same distribution and the purpose of the test is to reject (or not) this null hypothesis. The KS test should not be used to deduce new physics, but rather for the opposite purpose, namely to test whether an idea with strong theoretical background, such as that WR stars and some CC SNe are associated, can be rejected. In that respect, a definite rejection of the null hypothesis requires a p-value $< 0.3\%$. Doubts can exist for p-values $< 5\%$, but these are certainly not enough to disprove a well-justified hypothesis. Inspired by the Gaussian distribution, from now on we call these significance levels (or rather the very similar 0.3% and 4.6%) the 3σ and 2σ levels at which the hypothesis can be rejected, although this is purely a naming convention. For higher p-values, including the (Gaussian) 1σ, or 31.7% limit, there is very weak evidence against the null hypothesis.

To better illustrate this, in Figs. 5.3 and 5.4 (right panels) we have colour-mapped the KS p-values from Table 5.3 reflecting their significance levels. The only conclusive result ($> 3\sigma$ exclusion) is coloured in red. Orange, yellow, and green show the progressive decreasing significance at which the hypothesis of common parent distribution can be rejected. In that context, yellow is more probable than orange, but even orange cannot be excluded by the present data. From now on, when we refer to our 'results', we are mostly refering to these significance levels and their relative order.

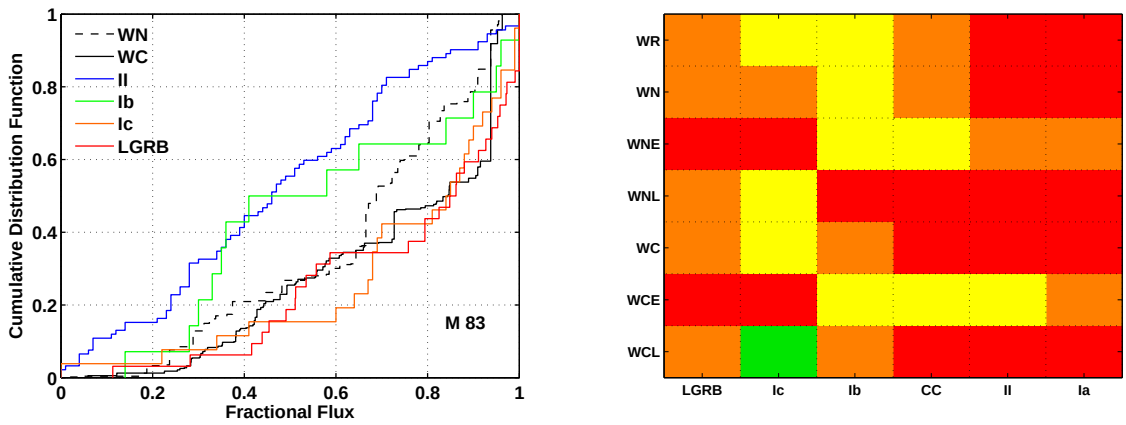

Figure 5.3: **Left panel:** *The distribution of WN and WC stars in M 83, a galaxy with properties typical of the K08 SN Ib/c sample, with respect to their location on their host light, plotted with the distributions of LGRBs and SNe II, Ib, and Ic (F06, K08).* **Right panel:** *This colour map indicates at what significance level we can exclude that a SN or LGRB explosion is associated to a certain (sub)type of a progenitor WR star. Red shows p-values* $< 0.3\%$*, orange* $0.3 < p < 4.6\%$*, yellow* $4.6 < p < 31.7\%$*, and green* $p > 31.7\%$ *(Table 5.3). The comparison has been done after the removal of the bulge, because no detailed information about the nuclear WR population exists and a bulge can be visually identified and removed (K08). The WC distribution is more skewed towards brighter pixels than the WN distribution. It is more probable that WC stars are drawn from the same population as SNe Ic than SNe Ib (or any other type of SN), and it is more probable that WN stars are associated to SNe Ib than with SNe Ic (or any other type of SN). This is consistent with theoretical predictions (Crowther, 2007; Georgy et al., 2009).*

Table 5.3: *KS test p-values (%).*

		LGRB	Ic	Ib	CC	II	Ia
	WR	1.2	20.7	8.3	2.1	0.0	0.0
	WN	0.7	2.4	16.6	1.8	0.0	0.0
M 83	WNE	0.0	0.0	5.2	29.4	1.5	1.5
(High *Z*)	WNL	3.5	29.8	0.2	0.0	0.0	0.0
	WC	2.0	31.1	4.6	0.2	0.0	0.0
	WCE	0.0	0.0	8.3	11.5	5.0	3.7
	WCL	2.2	33.0	2.6	0.1	0.0	0.0
	WR	0.3	0.2	77.2	53.0	7.5	9.4
	WN	0.1	0.0	81.3	96.4	68.1	89.7
NGC 1313	WNE	5.9	8.1	47.6	64.4	6.5	10.3
(Low *Z*)	WNL	0.0	0.0	22.9	25.1	20.0	15.3
	WC	17.9	14.5	22.8	6.1	1.0	0.8
	WCE	17.9	14.5	22.8	6.1	1.0	0.8
	WCL	...	...	...	...	...	...

5.4.1 HIGH METALLICITY – M 83

For the metal-rich galaxy M 83, which is typical of the K08 SNe Ib/c sample, we make the following observations.

∗ The distribution of WR stars as a whole is consistent with those of SNe Ib/c (yellow in Fig. 5.3) or even LGRBs (orange). It is however inconsistent with SNe II (red).

∗ The distribution of WC stars is more consistent with SNe Ic ($p = 31.5\%$, almost green) than with

any other type of SN ($p < 4.6\%$, which occurs for SNe Ib). From the WC subtypes, it is mostly the WCL stars that are responsible for this association. The less abundant WCE stars, on the other hand, seem to better follow the host galaxy light and are more consistent with SNe that behave in a similar way.

∗ WN stars are more consistent with SNe Ib (yellow) than with other kinds of supernovae (orange or red). We caution, however, that the early and late WN distributions behave quite differently. By excluding WNL stars, which might not be direct SN progenitors (see Sect. 5.5), WNE stars alone show a clearer preference to SNe Ib and their association to SNe Ic can be ruled out with a certainty of over 3σ.

∗ SNe II and Ia, which follow their host galaxy light distribution well (K08), show no association (null hypothesis excluded at over 3σ) with most WR stars, with the possible exception of early subtypes that seem to occupy fainter locations than their late counterparts. The same claim, but not as strict, could be made for the high-redshift CC SN sample of F06 (which most likely consists of SNe II).

To study how the errors in the number of WR stars can affect the results above, we have followed an MC approach. Multiple realizations of the distributions were generated where the numbers of WR stars per region were drawn randomly from Gaussian distributions with the mean and standard deviation specified by the number of WR stars and the associated errors provided by Hadfield et al. (2005). While this causes the p-values to fluctuate around their central values in Table 5.3, none of the qualitative conclusions above are affected. By this, we mean that p-values rarely jump to another σ significance level (i.e. their colour in Fig. 5.3 does not change) and that their relative ordering remains the same. The standard deviations on the p-values scale with the p-values themselves: typical fluctuations are of the order of $\pm$6% for a p-value of 26% or $\pm$1% for a p-value of 3.4%. Of course, if the number estimates of Hadfield et al. (2005) are biased in a systematic way, significant changes might be expected. The match may also be susceptible to changes in the limited number of SNe and LGRBs in the comparison samples.

The above results were obtained after removing the bulge contribution of M 83 and comparing with the corresponding results of K08. This is because we have no detailed information about the nuclear WR population of this galaxy, and a bulge can be visually identified and removed. The bulge light removal was done, similar to K08, by placing a circular ring around the bulge and by replacing all bulge pixels with the mean pixel value inside the ring.

5.4.2 Low metallicity – NGC 1313

In the case of the metal-poor NGC 1313, we observe the following:

∗ The global WR population is this time mostly consistent with SNe Ib (at a highly significant p-value), while at the same time an association with H-rich SNe is probable as well.

∗ This is especially obvious in the case of WN stars that trace well the light of the host galaxy. WN stars are again mostly consistent with SNe Ib, while a relation to SNe Ic can be excluded this time at high significance. On the other hand, their association to SNe II cannot be excluded any more, but instead shows a high probability. Again, differences are seen between the WNE and WNL distributions.

∗ WC stars, on the other hand, show significant association probabilities with SNe Ic and even LGRBs. We recall here that the WC population at the metallicity of NGC 1313 consists entirely of WCE stars.

Again, we checked on how the total WR content in the range discussed by Hadfield & Crowther (2007) affects the distributions and we did not find any qualitative difference with the results above. In the case of NGC 1313, the numbers of WR stars per region are considerably lower than in M 83. If region #64 contains 6 rather than 3 WC stars, as suspected by Hadfield & Crowther (2007), the WC distribution is pushed even closer to the SNe Ic and further from the SNe II (which turn red).

5.5 Discussion

From the results presented in the previous section, a qualitative pattern seems to emerge: WC stars are on average found in brighter pixels than WN stars. As a consequence, WC stars show higher probabilities

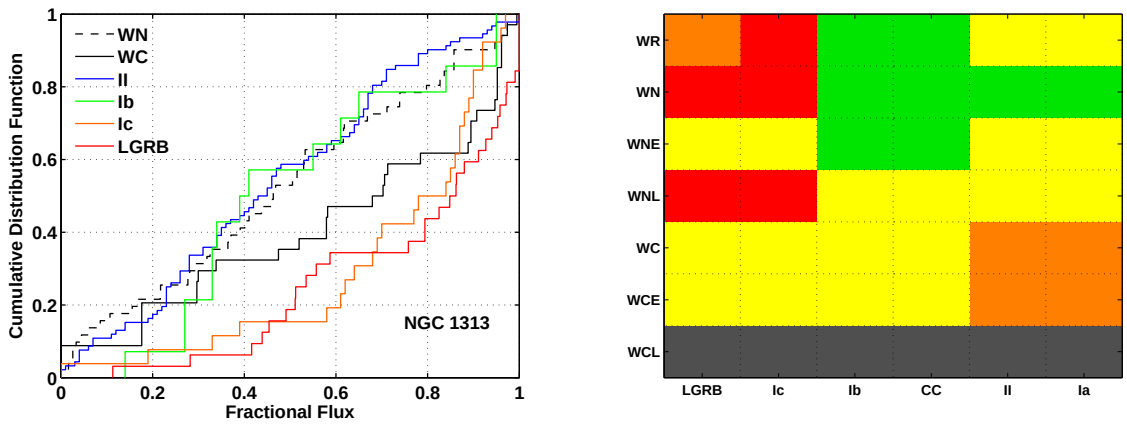

Figure 5.4: *The same as in Fig. 5.3 but for NGC 1313, a more metal-poor and irregular galaxy, probably similar to a low-redshift counterpart of the high-redshift F06 hosts. The colour-coding in the right panel is the same as in Fig. 5.3, but grey has been used for WCL stars that are not present in this galaxy.*

of association with SNe Ic. On the other hand, WN stars are most consistent with the locations of SN Ib explosions. This is the main result of this study and is in broad agreement with the theoretical expectations, i.e., that SNe Ic result from progenitors that have been stripped of a larger part of their outer envelope (Crowther, 2007). Also from a statistical point of view the WN and WC distributions are almost (geographically) incompatible (at significance $> 3\sigma$ for M 83, while $p = 5.9\%$ for NGC 1313), which highlights the need to consider these two subtypes separately when discussing SN progenitors, despite their strong physical connection. Other studies, however, caution that there is no strict one-to-one correlation between progenitor and supernova type, but that leaks might exist, e.g., less massive WC stars exploding as SNe Ib (Georgy et al., 2009).

Concerning LGRBs, they are not inconsistent with being drawn from the WR population, although typically at lower significance than SNe Ic. This is not a surprise since not all SNe Ic produce LGRBs (e.g. Soderberg et al., 2006). It is, however, tempting to point out that the highest p-value obtained for LGRBs (yellow) is the one for WC stars at low metallicity, in agreement with the proposed low-metallicity requirement (Yoon & Langer, 2005; Woosley & Heger, 2006).

Besides the general trend that is common for the two galaxies, differences do exist between the individual WN and WC fractional flux distributions. The difference is more pronounced in the case of the WN distributions that are almost mutually inconsistent ($p = 0.6\%$). The WN distribution in NGC 1313 tracks the host galaxy light better and is more consistent with SNe II. To some degree, this difference can be attributed to the important metallicity difference between the two galaxies: Georgy et al. (2009) predict that at low metallicity (similar to NGC 1313) the highest fraction of WN stars are actually expected to explode as SNe II and not SNe Ib. Due to lower mass-loss, the less massive stars are still expected to leave enough hydrogen to be detectable in the explosion spectra.

Other differences, however, especially at the subtype level, are more difficult to explain. The most striking is related to the WNL populations of the two galaxies. In M 83 they are found on the brightest pixels, while in NGC 1313 they lie on the faintest ones. Indeed, the two WNL distributions are inconsistent with each other, at a significance $> 3\sigma$. The reason for this is unclear, but it should be mentioned that WNL stars are not always stripped-envelope massive stars. In many cases, they are very luminous H-rich WN stars that are still burning H in their core. They are therefore in a phase preceding the LBV phase and *not* direct progenitors of SNe Ib/c (Crowther, 2007; Smith & Conti, 2008). According to Crowther (2007), a possible way to distinguish between H-rich WNL stars and stripped WNL stars is that the former usually lie in young massive clusters. One could argue that this is mostly the case for the WNL stars in M 83, while the

ones in NGC 1313 are mostly isolated. If this is true, caution should be applied when comparing the WNL distribution of M 83 to those of SNe or LGRBs. (WNE stars alone share most of the qualitative properties discussed for WN stars in this galaxy.) On the other hand, their positions in NGC 1313 are consistent with the predictions of Georgy et al. (2009): that WNL stars are expected to give SNe II, especially at low metallicity. We may thus be probing different WNL populations in the two galaxies.

Below we assess the robustness of our results, with respect to several uncertainty factors. We call a result robust as long as the significance levels in the KS test between two distributions (in the form of colours in Figs. 5.3 and 5.4) remain unchanged and retain their relative values with respect to other p-values. Indeed, with small exceptions, this is the case for most p-values. We conclude therefore that our main results are not sensitive to these uncertainties.

5.5.1 THE REMAINING CANDIDATES LOCATIONS AND THEIR IMPLICATIONS.

The number and nature of the remaining candidate regions in our galaxies has until now been ignored. To determine how important that is, we have followed an MC approach. By comparing the fractional flux distribution of the candidate pixels of M 83 to the corresponding distribution of the WN and WC pixel positions (i.e. without taking the number of stars per region into account this time, since we lack this kind of information for the candidate regions) we find that the candidate locations are more likely drawn from the WN ($p = 60\%$) than the WC ($p = 0.5\%$) pool. A possible reason could be that WC stars have stronger narrow-band excess over the continuum and might have been preferentially selected for follow-up spectroscopy. Indeed, WN stars, especially weak-lined WNE and very late WNL types, might suffer from some incompleteness (P. Crowther, priv. comm.). For NGC 1313, Hadfield & Crowther (2007) state that the (few) remaining candidate regions are photometrically consistent with WN stars.

In our MC simulation for M 83, we attempted many realizations where we allowed 66% of the candidates (a percentage equal to the success rate of the actual spectroscopic survey) to be genuine WR regions containing a number of stars equal to the median number of stars per confirmed WR region (plus their median error). We made simulations for the two limiting cases that the candidate regions included in the actual WR distributions were all included in the WN distribution or were divided between WN and WC stars according to the observed WC/WN ratio. The latter simulation is displayed as an example in Fig. 5.5. In both simulations we see only small differences in the results reported in Table 5.3, which do not change any of our conclusions. Similarly, we found no significant differences in our main results for NGC 1313.

5.5.2 THE EFFECT OF TEMPORAL EVOLUTION

A possible objection concerning the significance between the apparent difference between the WN and WC distributions is that sometimes a WN star is just on an evolutionary path towards a WC final stage, while all WC stars have already been through the WN phase once (Meynet & Maeder, 2005; Crowther, 2007). Whether this evolution will occur at all, and the related timescale, is strongly dependent on mass and metallicity (Meynet & Maeder, 2005). The mass range for which stars actually die as WN stars is quite narrow (Georgy et al., 2009) but if convolved with the IMF their number can become important. By using the mass limits from Georgy et al. (2009; their table 4), we estimate that, at the metallicity of NGC 1313, only $\sim 1/6$ of the observed WN stars (the most massive) will evolve to WC stars. In M 83, however, we expect this ratio to increase to almost $2/3$.

In an MC simulation for each galaxy, we allowed the above-mentioned ratios of WN stars to be removed from the WN and be included in the WC distributions. The expected result is that the WC distribution will be pushed towards fainter pixels, since it will be contaminated by WN stars. This simulation ignores that, while some WN stars evolve to WC, some new WN stars will be born, and many stars will explode. It also ignores the related timescales (all of a few Myr), and the brightness evolution of the stars themselves and has deliberately not made any assumptions about masses based on the positional information of the stars

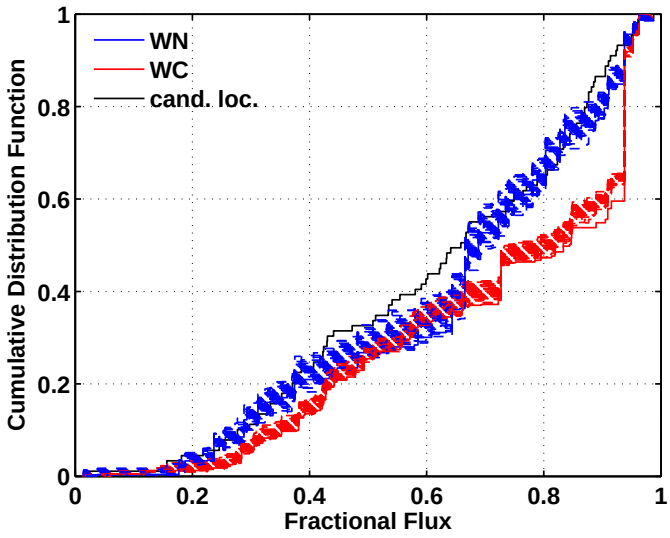

Figure 5.5: *Example MC simulation for the inclusion of the candidate regions in the WR distributions in M 83. Each realization results in a different WN and WC distribution (dashed lines), while the solid lines denote the original distributions (Fig. 5.3). For visual purposes, only the first 50 realizations have been plotted although the simulation contains 1000 runs. In the displayed simulation, the candidates were divided to WC and WN stars according to the observed WC/WN ratio. Our main conclusions remain unchanged, as do the colours in Fig. 5.3, right panel. Only the p-value between WC stars to SNe Ib changed colour, becoming yellow ($p = 6.6 \pm 1.3\%$) from being (marginally) orange ($p = 4.6\%$). Similar MC simulations were used for both galaxies in order to assess the importance of effects like the presence of foreground stars fainter than 20 mag, that the number of stars per region have an associated error estimate, and the evolution of WN to WC stars.*

on the galaxy. A hidden (reasonable) assumption is therefore that we do not observe these galaxies at a very special time in their existence and that, in this context, these simulations represent a limiting worst case. For both galaxies, we note that the probability of associating WC to SNe Ib jumps up one significance level, while their association to SNe Ic and LGRBs is reduced, although the significance remains the same. The WN central association p-values remain unchanged, as expected, while all WN and WC p-values get assigned error bars that can occasionally cross different significance levels. However, even in this limiting worst case, the relative scaling between the p-values remains unchanged and the WC distribution is always skewed towards brighter pixels than WN.

5.5.3 How much does binning affect the results?

To compare with results obtained for galaxies at higher redshift, our images were subject to the degradation process (binning) described in Sect. 5.3.3. We examine here the implications of this process.

If the fractional fluxes are measured in the original images, considerably higher values are obtained and the WR distributions become skewed towards brighter pixels, even brighter than for distant SNe Ic and LGRBs, especially in the case of WC stars. The effect of binning is that a bright isolated star (that has a high pixel fractional flux value in our original image) will be smoothed out and have a low fractional flux in the processed image. A bright association of many pixels, however, such as a cluster, will be less affected and therefore have a high fractional flux also in the processed image. This mimics the effect of distance, where isolated stars cannot be detected at higher redshift but clusters can. Although not binning would result in an apparently stronger result with regard to the probable association of WR stars to SNe Ib/c and

LGRBs, this degradation is needed to make a fair comparison. In that context, if WR stars are indeed the progenitors of these explosions, the fractional flux values at the low brightness tails of the F06 and K08 distributions, are probably caused by isolated WR stars, while the ones with high fractional fluxes are those that are found in bright clusters. That these explosions tend to occur in pixels brighter than average (F06, K08) can then be explained by the preference of WR stars to be found in large associations.

We have also tested various degrees of binning to confirm that our results are not tuned to the chosen values (simulated redshift $\sim$0.01). Although some small changes occur, we checked that our conclusions are robust to lower and higher values of binning as long as the PSF in the original image is not subsampled.

5.6 CONCLUSIONS

We performed a F06 type analysis on the WR populations of two nearby galaxies and compared our results to the distributions of different types of SNe (K08), focusing on SNe Ib/c, and LGRBs (F06). M 83 is a metal-rich galaxy, typical of the K08 SNe Ib/c host sample, while NGC 1313 is more metal poor, irregular, and similar to high-redshift LGRB host galaxies. To enable the comparison we resampled our images to simulate a higher redshift.

WR stars are consistent with being the progenitors of SNe Ib/c or even LGRBs. Furthermore, the WC stars are distributed in brighter locations of their hosts than WN stars. It is therefore more likely that WC stars are the progenitors of SNe Ic and WN stars of SNe Ib, as also expected by theoretical arguments. This result is robust to a number of systematic checks that we carried out.

Although encouraging, these results are based on the only two galaxies for which such an analysis is possible at present. Even though they contain enough of WR stars and we have shown that they are, most probably, not special in any way, it would of course be desirable to validate our results on a larger galaxy sample, once such a sample becomes available. Ideally, such a sample should span a wide range of metallicities.

Based on observations collected at the European Southern Observatory during ESO Program 081.D-0757(A), PI: G. Leloudas

6

A PROGRAM TO STUDY THE EXPLOSION SITES OF NORMAL SNE IB/C

We study spectroscopically the properties of galaxies that have hosted stripped-envelope core-collapse supernovae. Our sample is selected from hosts of normal Type Ib/c events that have been closely monitored by either the Carnegie Supernova Project (CSP) or the SDSS-II Supernova Survey. We proposed and obtained telescope time at the ESO NTT, from where we observed a total of 22 galaxies. Three additional galaxies were observed with the NOT. The motivation behind this project is to obtain local metallicities, star formation rates and stellar populations ages at the SN explosion sites. Ultimately this could lead to a study relating the local environment properties to the properties of the SNe. Here I present the data collected at the NTT, the extracted spectra, measured line fluxes and estimates of the explosion site metallicities. The preliminary results, based on the present sample, do not yield any statistically significant difference between the environment metallicities of normal SNe Ib and SNe Ic, or even those of broad-lined SNe Ic.

6.1 CONTEXT - MOTIVATION

As long as the progenitors of stripped-envelope CC SNe evade direct detection, valuable insight to their nature can be gained through observations of their environments. As explained in Chapter 3, there exist at least two hot topics in relation to these explosions: (i) what fraction comes from single massive progenitors and what fraction is a product of binary evolution and (ii) which explosions give a GRB and what differentiates them from ordinary explosions?

In relation to the second question it has been suggested that the crucial parameter may be metallicity (Yoon & Langer, 2005; Woosley & Heger, 2006). Indeed, Modjaz et al. (2008b) obtained spectra for the environments of 11 broad-lined SNe Ic, without an observed GRB, and showed that their metallicities were higher than the ones of broad-lined SNe Ic with an observed GRB (a sample of 5 GRB-SNe, including XRF 020903).

However, to date no direct spectroscopic study has been made for normal events.. While there exist direct (Prieto et al., 2008) or indirect (Prantzos & Boissier, 2003) *global* host galaxy metallicity measurements, all studies focusing on the local environments have until now been based on proxies of metallicity (Anderson & James, 2009; Boissier & Prantzos, 2009). Direct local measurements are necessary not only because they are more accurate than their proxies, which contain considerable dispersion, but also for allowing a meaningful comparison with the peculiar events. In addition, the directly derived local properties can be used for a number of tests related to the origin of SNe Ib/c. In particular, in the single massive star evolutionary scenario, normal SNe Ic are expected to arise in higher metallicity environments than SNe Ib due to the increased mass loss. If however the mass loss is due to binary evolution, it should be independent of metallicity. Determining the age of the local stellar population is another probe of the explosion mechanism, since single massive stars can only be found in young actively star-forming regions. While

limited data exist (e.g. Thöne et al., 2009), a larger sample is necessary for a statistical approach.

Finally, unlike for SNe Ia, no study has been made relating the properties of SNe Ib/c to those of their environments. Such studies can yield important hints for the nature of the explosions, as in the case of SNe Ia where increasing evidence is showing that the brighter events are preferentially found in young stellar environments while the dimmer explode in older environments (e.g. Hamuy et al., 2000; Neill et al., 2009; Brandt et al., 2010; Kelly et al., 2009).

6.2 THE PROPOSAL

To address these questions and observe a large sample of stripped-envelope CC SN galaxies, we applied in September 2007 for telescope time at ESO. Our proposal was approved and we were granted time (3 nights) in period P81 at the NTT.

6.2.1 SAMPLE SELECTION

In the history of SN discoveries, there have been many reported stripped-envelope CC SNe. However, a large fraction of these SNe are objects that have been classified based on a single optical spectrum but have little further useful observations (e.g. SN 2007rb; Sollerman & Leloudas, 2007).

We wanted to select SNe that were well-observed. This decision was partly motivated by the fact that there has not yet been a study relating properties of SNe Ib/c as determined by the observables (light curves and spectra) to their host galaxy properties. The SN properties include e.g. peak luminosity, M_{Ni}, M_{ej}, ejecta velocities while the environment properties can contain metallicity, SFR, stellar age population and can be used to attack the problem of the explosion nature from two different angles. We thus wanted to increase the value of our study by targeting a sample for which good SN data exists.

We therefore decided to target normal stripped-envelope CC SNe that at the time of proposal submission had been closely followed by the Carnegie Supernova Project (CSP) or the SDSS-II Supernova Survey. To these we added a few objects that were discovered between proposal submission and the actual observing run. We excluded previously studied objects such as SNe related to GRBs or the broad-lined SNe Ic studied by Modjaz et al. (2008b).

The CSP obtained unprecedented photometry and spectra for $\sim$200 SNe of all varieties. These SNe were discovered by different surveys that typically monitor bright ($m_B \sim 11 - 16$) galaxies, which, of course, introduces an unavoidable selection bias. On the other hand, these galaxies have the advantage that they are relatively extended sources and it is possible to perform spectroscopy at the *exact* explosion site.

The SDSS-II Supernova Survey (Frieman et al., 2008) scanned an equatorial stripe of the sky (Stripe 82) for 3 months per year for 3 consecutive years searching mainly for SNe Ia to be used for cosmology. Other SN types were also discovered: during the first two years of the survey 14 SNe Ib/c were spectroscopically confirmed, while the number increased during the last year, i.e. after the submission of our NTT proposal. The SDSS detected SNe irrespective of their host galaxy magnitude. As a result, the SN host galaxies are fainter ($m_g \sim 17 - 22$) and less resolved than the ones followed by the CSP. Spectra for some of these galaxies (the brightest ones) exist in the SDSS database (e.g. Prieto et al., 2008) but they are centered at the galaxy nucleus and not at the SN location. The SDSS sample is a relatively unbiased sample (concerning discovery), although we stress that SDSS was targeting mainly SNe Ia and a fraction of these CC SNe events were initially misidentified as such.

Our sample therefore consisted of two sub-samples, each one with different advantages: the brighter and more extended hosts (CSP) allow a more detailed study, while the SDSS sample offers a more objective view and is in addition suitable to compare to the overall SDSS galaxy sample.

6.3 THE OBSERVING RUN

The data were obtained during 3 consecutive nights at the NTT (+EFOSC2): August 21, 22 and 23 UT 2008. Unfortunately, these dates were a result of re-scheduling from the original allocated nights (August 24-26). This meant that, despite having applied for grey moon, the moon was relatively bright during our run (illumination 69% decreasing to 48%). In addition, many of our targets (the ones with early RAs) were close to the moon with angular distances reaching down to 27-35 degrees, or even 20 degrees the 21st of August. This has significantly affected the quality of our data in the blue part of the spectra.

During this run, we observed almost all CSP and SDSS selected targets that were visible from La Silla at this time of the year. A list of the observed galaxies is provided in Table 6.1. The table contains basic information on the host galaxy, such as coordinates, redshift and absolute magnitude, as well as the hosted SN, its Type, offset with respect to the galaxy centre and its selection sub-sample (CSP or SDSS). In addition, the table contains details concerning our observations (grism, exposure time and airmass). Since no SN IIb hosts were observed, we will from now on use the terms SNe Ib/c and stripped-envelope CC SNe interchangeably without distinction. To give a better idea of the real SN offsets, which are important for metallicity gradients, instead of angular offsets, we provide projected distances in kpc based on the redshift of the host galaxies. For the two galaxies that are not in the Hubble flow (i.e. NGC 1187 and NGC 4981), we have used the distances reported by Tully et al. (2009). The absolute magnitudes have been retrieved from the HyperLEDA database[1] that contains a consistent derivation (parameter *mabs*). For the SDSS galaxies without HyperLEDA entries we used their SDSS Petrosian g and r magnitudes and the transformations by Jester et al. (2005) to obtain B-band magnitudes. Correcting for Galactic extinction (Schlegel et al., 1998) and for the redshift derived distance modulus, we arrive at the displayed M_B. No k-corrections have been applied, but these represent only a minor second order correction that is irrelevant for the purposes of this study. Figure 6.1 shows a mosaic of the galaxies together with arrows designating the SN locations. One can immediately observe that there is a big variation in apparent sizes, with the SDSS selected galaxies (the ones with names starting with J) being smaller on average.

Our observing strategy involved positioning the slit to contain both the explosion site and the galaxy centre. This was done at the expense of not observing at parallactic angle in order to (i) be able to deduce metallicity gradients towards the explosion site and (ii) at least use the nuclear properties in case the SN location site contained too little flux. Most objects were observed at low airmasses so the differential slit losses should be minimal. The slit position angle was calculated with the aid of images containing the SN for the CSP sample. For the SDSS SNe, we calculated the position angle using the SN astrometry reported by SDSS, which is tied to the astrometry of the 'SDSS explore' tool.[2] We were careful not to apply any offset between the last acquisition image and the science frame (spectrum). This was done in order to use the acquisition image to astrometrically determine the exact position (column) of the explosion site trace in the science frame. At the NTT, the acquisition images are typically obtained in a faster read-out mode than science frames to accelerate the procedure. This was not a problem for us since we did not wish to perform e.g. photometry on these frames but only use them for identifying the position of the SN.

For the spectra we used different grisms, trying to optimize the resolution, depending on the galaxy redshift. In general, we tried to cover the whole (restframe) wavelength region 3700- 6800 Å where the strong lines we were interested in lie. In most cases we used grism 11, but other grisms were also used (in some cases complementarily). The grisms used and their specifications are listed in Table 6.2. A $1''$wide slit was used throughout the observing run. We did not use any second order blocking filter.

[1] `http://leda.univ-lyon1.fr/`
[2] `http://cas.sdss.org/astro/en/tools/explore/`

Table 6.1: *Host galaxies: properties and observing log*

Galaxy	SN	RA (J2000) (° ′ ″)	DEC (J2000) (° ′ ″)	offset[a] (kpc)	M_B	z	Type	sample	grism[b]	Exp. time (sec)	night[c]	Airmass
2MASXJ21024677−0405233	2007hn	21 02 46.85	−04 05 25.2	1.06		0.0273[d]	Ibc	CSP	g4	4×1800	1,3	1.14
ESO 153−G17	2004ew	02 05 06.17	−55 06 31.6	5.40	-20.98	0.0218	Ib	CSP	g11	1800	1	1.13
ESO 552−G40	2004ff	04 58 46.19	−21 34 12.0	5.47	-21.05	0.0226	Ic	CSP	g11	1800	1	1.11
IC 4837A	2005aw	19 15 17.44	−54 08 24.9	6.11	-21.60	0.0094	Ic	CSP	g11	2×1200	1,3	1.13
									g18	2×1800	1,3	1.11
J000109.19+010409.5	2007nc	00 01 09.30	+01 04 06.5	9.16	-19.83	0.0860[d]	Ib	SDSS	g11	2×1800	2	1.44
J001039.34−000310.4	2007sj	00 10 39.63	−00 03 10.2	3.54	-20.86	0.0390	Ic	SDSS	g11	2×1800	3	1.25
J002741.89+011356.6	2007qx	00 27 41.78	+01 13 59.6	5.63	-19.93	0.0800	Ib	SDSS	g11	2×1800	2	1.18
J012314.96−001948.8	2006jo	01 23 14.71	−00 19 46.7	6.79	-20.51	0.0770	Ib	SDSS	g11	2×1800	2	1.16
J023239.17+003700.1	2006fo	02 32 38.89	+00 37 03.0	2.49	-19.87	0.0210	Ic	both	g11	2×1800	3	1.16
J034918.33−004129.4	2005mn	03 49 18.44	−00 41 31.4	2.31	-19.08	0.0470	Ib	SDSS	g11	1800	2	1.14
J205121.43+002357.8	2007jy	20 51 21.43	+00 23 57.8	0.00	-18.61	0.1819[d]	Ib	SDSS	g6	2100,	1	1.45
									g17	2×1200	2	1.21
J205519.76+003234.4	2005hl	20 55 19.79	+00 32 34.8	5.37	-19.77	0.0230	Ib	SDSS	g18	3×1500	1	1.18
J213900.63−010138.6	2005hm	21 39 0.64	−01 01 38.6	0.00	-14.57	0.034[d]	Ib	SDSS	g11	2100	1	1.30
J223529.00+002856.1	2007qw	22 35 29.01	+00 28 56.2	0.00	-18.85	0.1494[d]	Ic	SDSS	g6	1800	2	1.30
									g11	1800	2	1.30
KUG 2302+073	2006ir	23 04 35.68	+07 36 21.5	1.79	-16.95	0.0200	Ibc	CSP	g11	695	3	1.41
MGC+03−43−5	2005bj	16 49 44.74	+17 51 48.7	5.83	-20.02	0.0222	Ic	CSP	g11	2×1800	1	1.50
NGC 1187	2007Y	03 02 35.92	−22 53 50.1	9.83	-20.17	0.0046	Ib	CSP	g11	2×1800	1	1.07
NGC 214	2006ep	00 41 24.88	+25 29 46.7	13.44	-21.62	0.0151	Ib	CSP	g11	2×1800	2	1.74
NGC 4981	2007C	13 08 48.80	−06 46 45.0	2.79	-20.25	0.0056	Ib	CSP	g11	2×1800	3	2.06
NGC 7364	2006lc	22 44 24.48	−00 09 53.5	3.14	-21.21	0.0162	Ic	both	g11	1800	1	1.25
NGC 7803	2007kj	00 01 19.58	+13 06 30.6	4.15	-20.88	0.0178	Ibc	CSP	g11	1200	2	1.42
									g18	1800	2	1.42

[a] projected distance based on the angular offset and the galaxy distances (see text).

[b] See Table 6.2 for details concerning the individual grisms.

[c] 1, 2 and 3 stand for the nights of 2008 August 21, 22 and 23 UT respectively.

[d] Redshift based on own spectroscopic observations.

Table 6.2: *EFOSC2 Grisms used during the run*

Grism	Wavelength range (Å)	Dispersion (Å/pixel)	Resolution FWHM (Å/1″)
g4	4085−7520	1.68	13.65
g6	3860−8070	2.06	16.77
g11	3380−7520	2.04	17.16
g17	6895−8765	0.86	7.02
g18	4700−6770	1.00	8.19

For calibrations we obtained bias frames, spectroscopic flats (5 frames per grism) and HeAr arcs at the beginning of each night and also during day-time after the last night. The spectrophotometric standard stars LTT 7379, HR 7596 and HR 7950 were observed with identical settings as the science spectra for purposes of flux calibration. Finally, we also obtained suitable calibration frames (bias and flats) in the fast read-out mode to reduce the acquisition images.

Except the tabulated spectroscopic observations, in one case (SN 2006oz) we obtained gri imaging to locate the host of an object that was classified as a probable SN Ib (Stritzinger et al., 2006c) but initially reported as a 'strange hostless transient' within SDSS. Although a small number of hostless SNe have recently been discovered in surveys that target the field, this is quite unusual. Unfortunately, the seeing deteriorated (1.8″) during our observations and did not permit us to reach limits significantly deeper than the SDSS. We do not detect any host for this event down to a limit of $r > 24.5$ (Fig. 6.2). The spectrum has been re-reduced (Östman et al., in prep.) but it is noisy and it does not offer a unambiguous classification. A tentative identification of a narrow line (Hβ?) at $z \sim 0.286$, permits a consistent identification of the bumps at ∼5500, 6300 and 8600 Å, as Hα, Hβ and Hγ, i.e. a Type II explosion. Also SNID (Blondin & Tonry, 2007) gives good matches with some SNe II at this redshift. This would imply however an unusually bright event with $M_r = -20.4$. For the host we obtain $M_r > -16$, i.e. a galaxy of very low luminosity and, likely, low metallicity.

6.3.1 COMPLEMENTARY NOT OBSERVATIONS

We have also obtained similar spectroscopic observations at the NOT for 5 galaxies: 2 that were also observed at the NTT (KUG 2302+073 and ESO 552−G40) and 3 additional ones (NGC 1832, NGC 856 and UGC 5392). These observations are not discussed here.

6.4 DATA REDUCTIONS

The data were reduced in the following way: all science and standard star frames were bias subtracted and flat-fielded with standard tasks in IRAF. The spectroscopic flats were first normalized with the task `response` to correct for the non-uniform illumination along the dispersion axis due to the wavelength dependence of the quartz lamp used to create them. Since the illumination along the spatial axis was rather uniform, it was not deemed necessary to normalize across this direction. The last 16 rows of the CCD were trimmed because they only contain bad pixels and cosmic rays were removed from the science spectra with the help of the task `LACosmic` (van Dokkum, 2001). The tasks `identify`, `reidentify` and `fitcoords` were used on the HeAr arcs in order to create a 2D dispersion map, per night and per grism. Subsequently, all 2D spectra were wavelength calibrated with the help of the task `transform`. By checking against the skyline wavelengths, we found that the wavelength calibration was not perfect but could differ by 1-2 pixels during the same night for the same grism. This can be due to instrument flexures, although these values are larger than the ones reported in the EFOSC2 manual (0.5 pix.).

We extracted the 1D spectra of the spectrophotometric standard stars in the custom way and used them

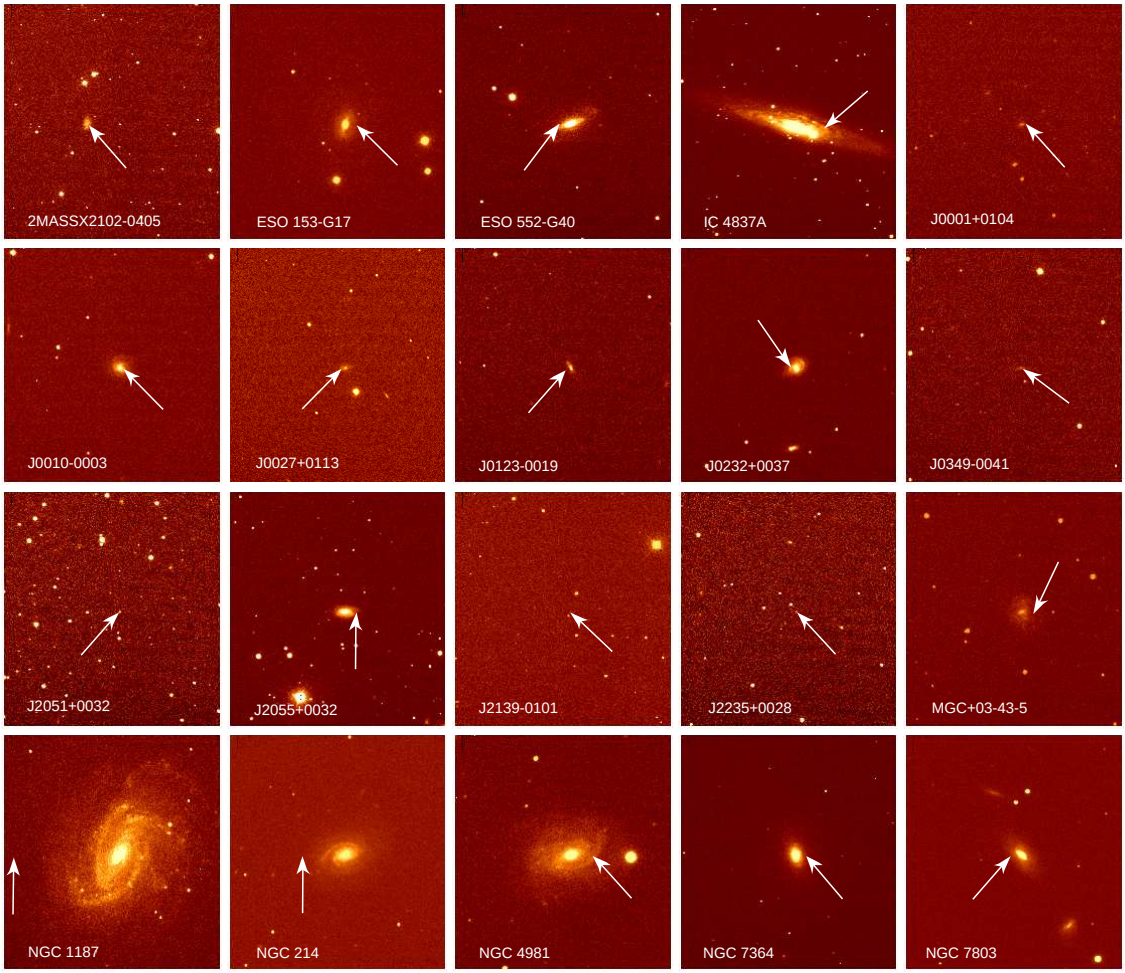

Figure 6.1: *A mosaic of 20 SN Ib/c host galaxies observed at the NTT, constructed from the last acquisition images (R-band) before introducing the slit. KUG 2302+073 has been omitted, while the host of SN 2006oz, for which we obtained imaging instead of spectroscopy, is presented in Fig. 6.2. The white arrows indicate the location of the SN explosions. The SDSS galaxies have had their names abbreviated (e.g. J0123-0019 instead of J012314.96−001948.8). All the images are* $4.1' \times 4.1'$ *and have different orientations (not indicated). This is because the fields have been rotated by different angles to get both the SN location and the galaxy nucleus in the slit (which is horizontal).*

to produce sensitivity functions (per night and per grism) to be used for absolute flux calibration of the science spectra. We compared the sensitivity functions obtained during different nights and found them to be fairly similar. For grisms g4 and g6, we observed signs of second order contamination above 7200 Å as also noted in the EFOSC2 manual, which could have been avoided by the use of second order blocking filters and by obtaining internal flats at the SN position. Caution should be used in interpreting data above this wavelength. Nevertheless, our study is not affected.

The acquisition frames were calibrated with the aid of corresponding bias frames and sky flats obtained in the fast read-out mode. The only useful sky-flats proved to be the ones from the second night and this led to an imperfect flat-fielding for the other nights. As these images are used purely for positional information, this did not pose any problems.

We extracted spectra with the task `apall` both at the SN location and at the galaxy nucleus. For the SN location we tried to use as small apertures as possible (e.g. 7-10 pixel columns) to minimize contamination from neighboring regions. In some cases this still corresponds to integrated light from areas of the order of

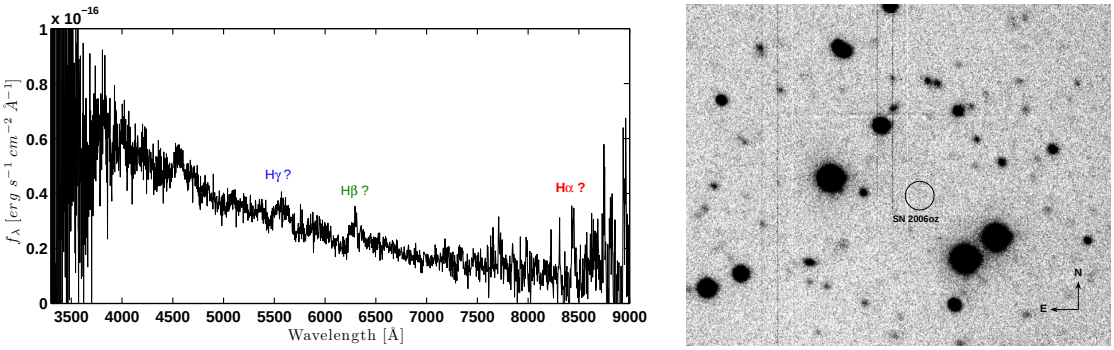

Figure 6.2: *SN 2006oz that was classified as a probable SN Ib by SDSS. What is remarkable is that this SN does not have an obvious host galaxy. The spectrum of this object, obtained at the NOT by Max Stritzinger and GL, is displayed to the left. This is a new reduction (Östman et al., in prep.) but it remains difficult to give a conclusive answer on the nature of this object. The locations of Hα, Hβ and Hγ have been marked at a common redshift of $z = 0.286$, tentatively suggesting a Type II classification. The NTT image is displayed to the right. No host galaxy is detected at $r > 24.5$ anywhere near the position of SN 2006oz (noted by a circle).*

1 kpc^2, especially if the effect of seeing is included. Clearly this illustrates the limitations of this method, i.e. that the 'local' SN environment probed is still a very large region, although this method remains much better than using the nuclear galaxy spectrum. In some cases we also extracted spectra of other interesting regions, usually those containing sufficient signal and being relatively nearby to the SN location. In all cases we used the trace of the nuclear galaxy spectrum for all other apertures, including the SN locations.

When extracting the science spectra, special care was taken in determining the background. This was done for the following reason: since the purpose is to measure line fluxes at different regions within the galaxy, the choice of background is not obvious, but it should definitely not be local, i.e. include light from the galaxy. So the background was taken in regions clearly outside the galaxy, which in the case of very extended galaxies, meant in the outer columns of the CCD.

The most serious difficulty, however, was encountered by the presence of the bright moon close to many of our targets. This was manifested as a halo in the blue part of the CCD. This pattern was complicated and proved difficult to correct for, causing problems in the background removal, especially below row 150 or 4000 Å in g11. Combined with the reduced sensitivity of the CCD in the blue, data below this wavelength has large associated uncertainties. We also tried an alternative approach, by removing the background in the 2D images with the task `background`, before extracting the spectra. However, we found this 2D-surface fitting approach even more sensitive to the halo pattern, and preferred to use the spectra extracted in the previous way.

6.5 Analysis

The spectra extracted in the manner described above are displayed in Figs. 6.3, 6.4, 6.5 and 6.6. We display both the nuclear spectra and the SN location spectra or, in the cases where this was not possible, spectra of regions as nearby as possible to these. The local spectra have often been cut in the blue since the low S/N combined with the increased background contamination led to an extraction that cannot be trusted at these wavelengths. In some cases we have over-plotted spectra taken with two different grisms applying a small offset for visual reasons. The spectrum of J034918.33−004129.4 yielded a very low S/N and it is not displayed.

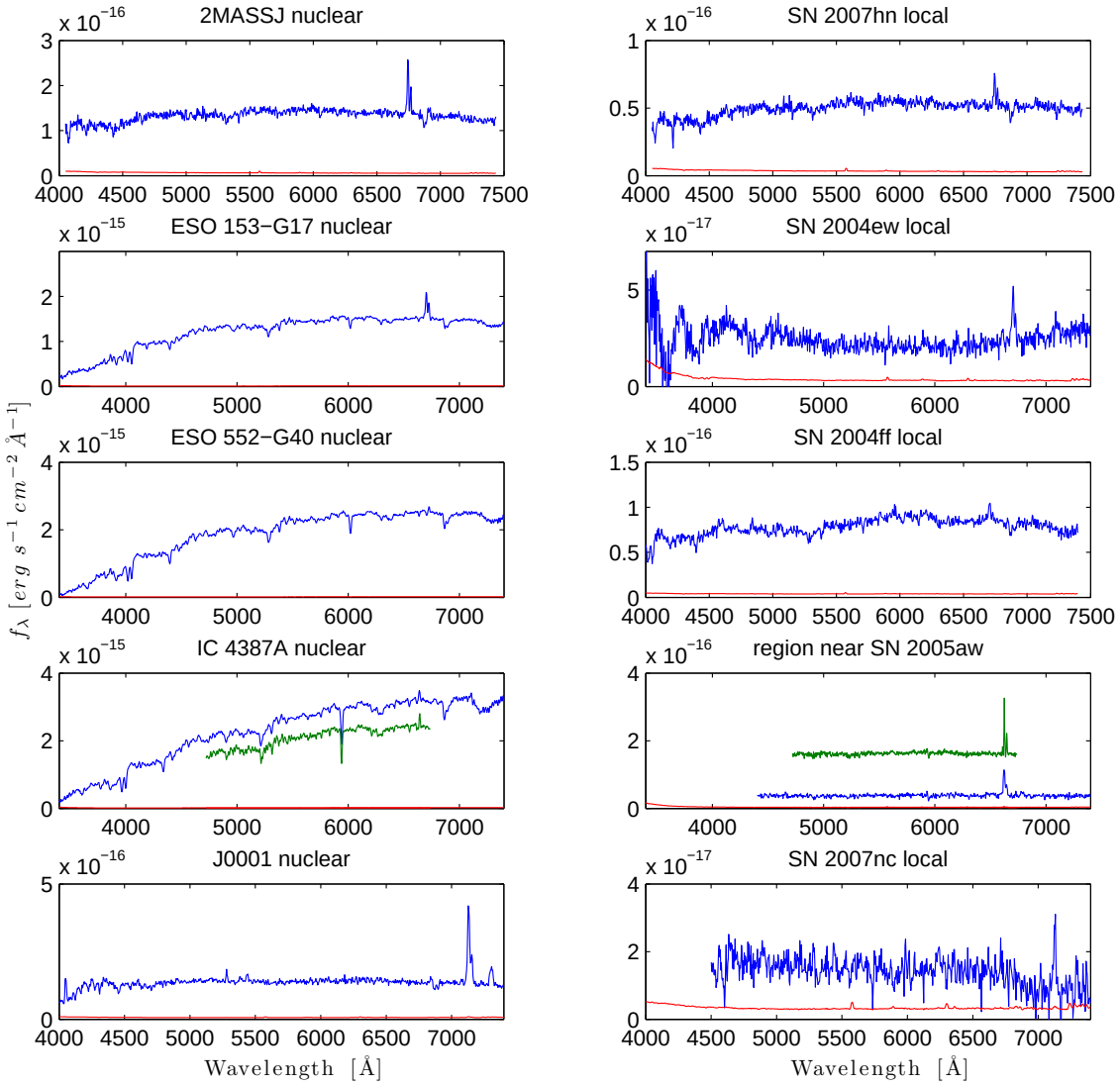

Figure 6.3: *Spectra for 5 SN Ib/c host galaxies observed at the NTT. The left column shows spectra extracted at the galaxy nucleus, while the right column shows extractions at the location of the SN explosions. When no flux could be extracted at the SN location, the most nearby region with flux is displayed (this is the case here for IC 4387A). The corresponding error spectra are colored in red. In the case of galaxies observed with 2 different grisms, as IC 4387A in this figure, the second spectrum is plotted with a different color (dark green) and a small offset is applied for reasons of visual presentation. Due to the increased background contribution in the blue, combined with the low S/N, many local spectra are of poor quality below 4000 Å. This is clearly illustrated here by the spectrum at the location of SN 2004ew (host galaxy ESO 153−G17). Since we do not trust this region, it has been cut from the remaining local spectra and is not displayed. The names of some galaxies have been abbreviated in an non-ambiguous manner. The spectra are displayed in the observer (not rest-frame) wavelength.*

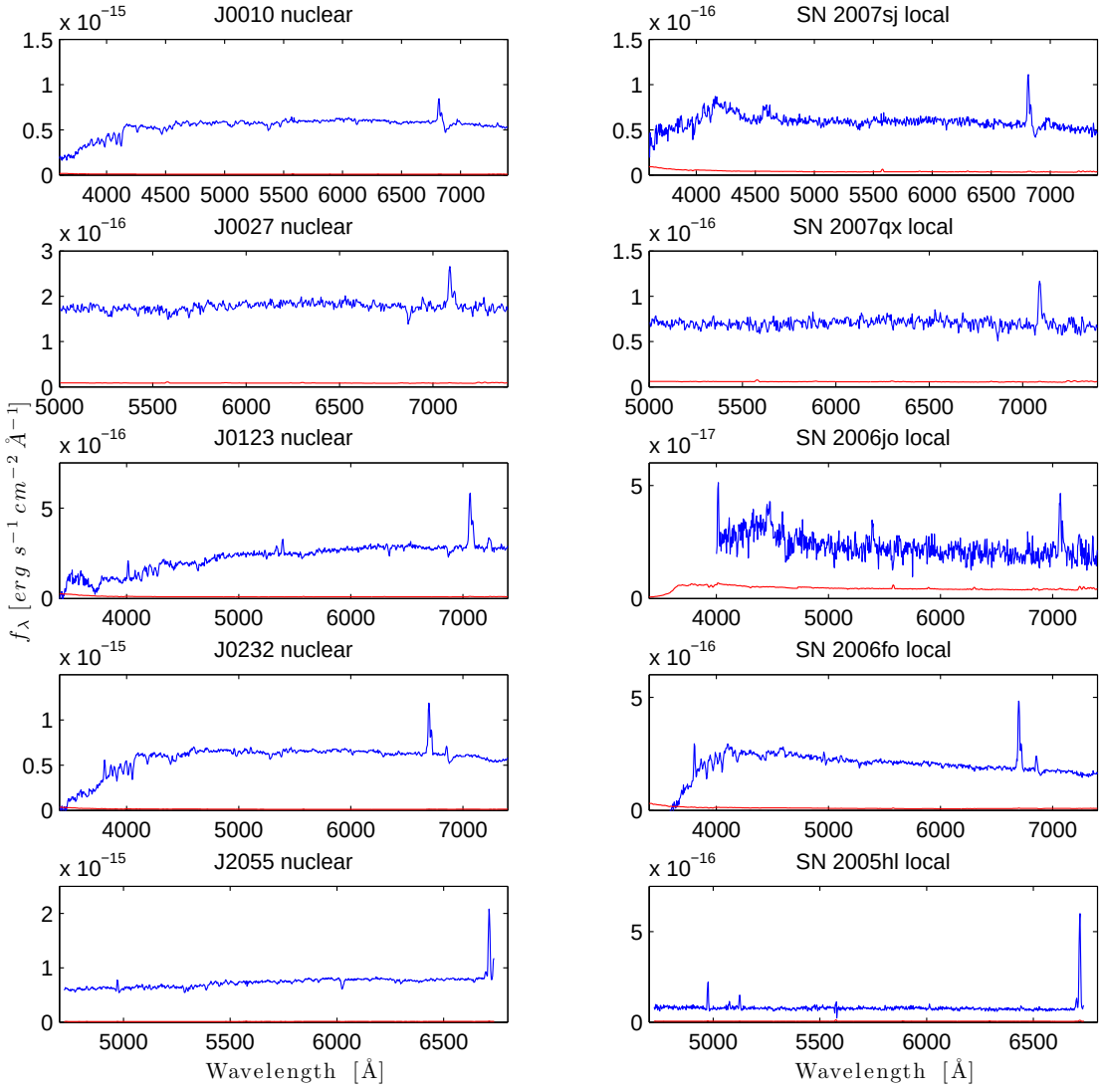

Figure 6.4: *Spectra for 5 more SN Ib/c host galaxies. See caption Fig. 6.3.*

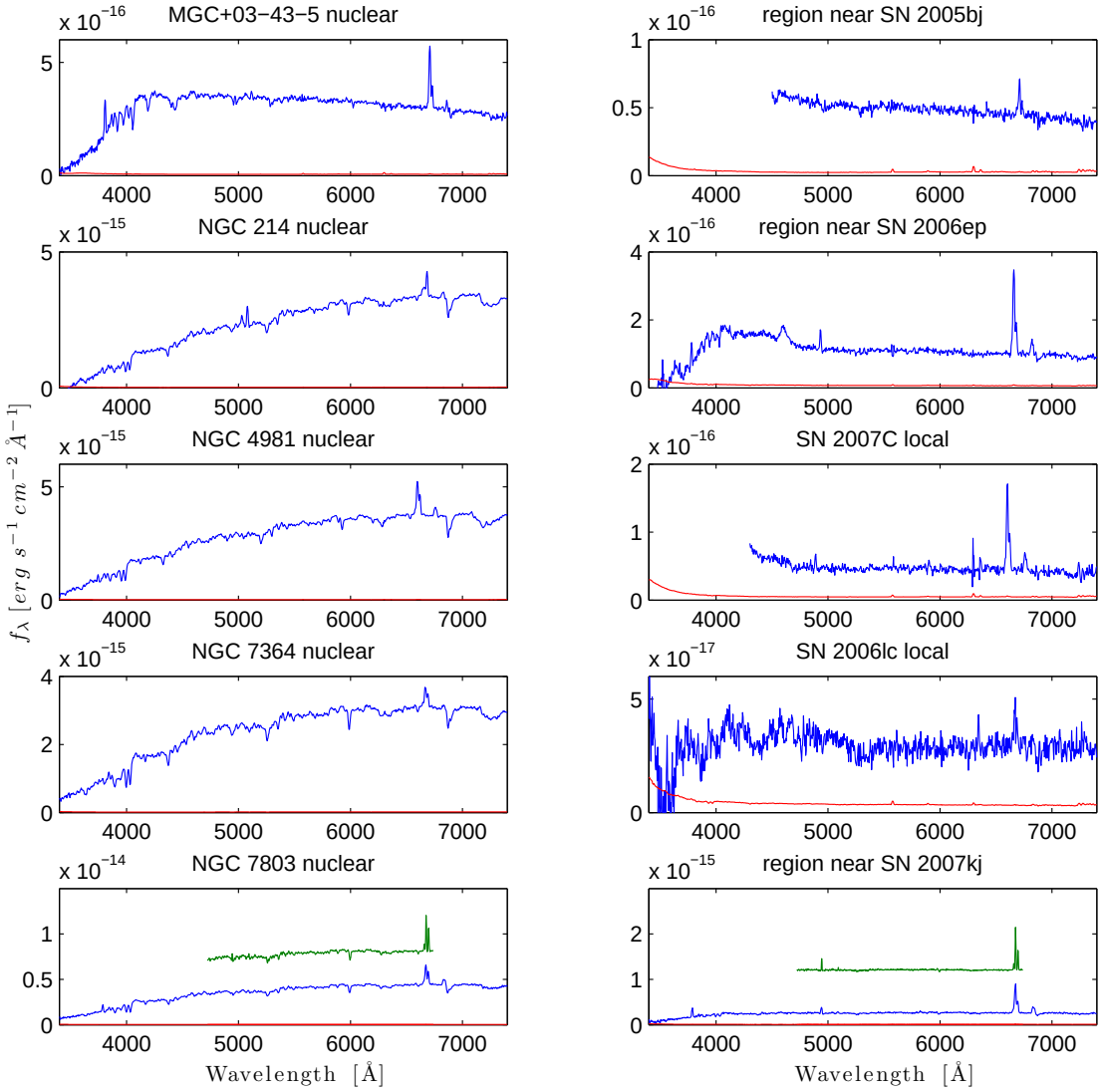

Figure 6.5: *Spectra for 5 more SN Ib/c host galaxies. See caption Fig. 6.3. Notice that for 3 of the galaxies presented in this figure, it was not possible to recover any flux at the exact SN location and we resort to the most nearby region that a spectrum could be extracted.*

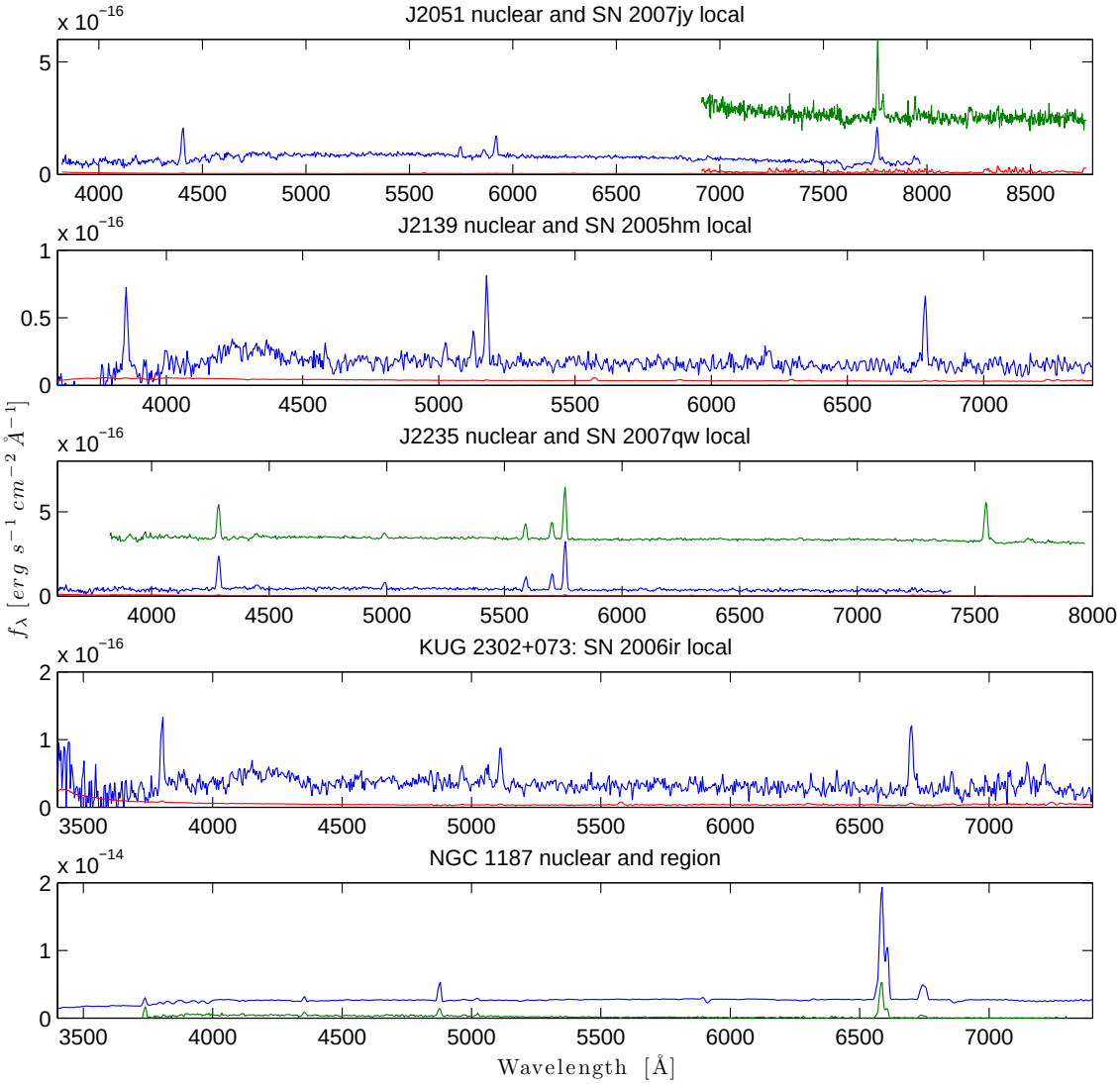

Figure 6.6: *Spectra for 5 more SN Ib/c host galaxies. Compared to Fig. 6.3 there are some differences: the top 3 galaxies are unresolved and the SNe occurred at the galaxy centre. For these 3 galaxies we make no distinction between the SN local environment and the galaxy as a whole. In the case of KUG 2302+073 we were only able to extract some flux at the SN location (in a spiral arm region) but not at the galaxy nucleus that is faint. The spectrum displayed is the local one. Finally in NGC 1187, we have plotted in the same panel the central spectrum and the spectrum of a region where flux could be measured (green). For visual purposes the latter has been multiplied by a factor of 40.*

Table 6.3: *Line fluxes and metallicities*

Galaxy	Hβ		[O III] λ5009		Hα		[N II] λ6584		12+log(O/H)	12+log(O/H)
	central	local	central	local	central	local	central	local	O3N2	N2
2MASXJ21024677−0405233	... [d]	... [d]	11.68	...	150.80	27.53	63.19	13.85	...	8.73
ESO 153−G17	... [d]	...	...	...	865.80	49.69	504.40	23.44	...	8.71
ESO 552−G40	... [d]	...	...	...	... [d]	34.99	195.90	13.34	...	8.66
IC 4837A [a]	... [d]	50.16	...	15.68	... [d]	276.10	500.50	114.30	8.77	8.68
J000109.19+010409.5	50.93	...	47.15	...	528.00	37.06	187.20	6.43	...	8.47
J001039.34−000310.4	... [d]	...	...	...	456.50	99.30	180.10	37.89	...	8.66
J002741.89+011356.6	... [d]	...	...	...	150.00	90.09	57.25	23.06	...	8.56
J012314.96−001948.8	22.86[e]	...	128.40	22.04	622.30	53.35	296.80	22.07	...	8.68
J023239.17+003700.1	50.21[e]	44.67[e]	88.56	...	979.30	525.20	432.30	179.80	...	8.63
J034918.33−004129.4	...	...	...	...	...	...	...	...	...	...
J205121.43+002357.8 [b]	61.34	61.34	138.10	138.10	237.10	237.10	46.03	46.03	8.39	8.49
J205519.76+003234.4	98.19[e]	93.88	...	51.45	1188.00	428.30	698.60[f]	...	...	8.77[f]
J213900.63−010138.6 [b]	21.08	21.08	84.30	84.30	77.64	77.64	4.73	4.73	8.15	8.21
J223529.00+002856.1 [b]	115.40	115.40	439.40	439.40	399.80	399.80	33.96	33.96	8.20	8.29
KUG 2302+073	...	36.18	...	75.09	...	162.90	...	25.89	8.37	8.44
MGC+03−43−5 [c]	... [d]	...	52.76	...	455.00	39.98	147.50	12.65	...	8.62
NGC 1187 [c]	3652.00	38.97	470.00	11.97	26560.00	184.70	12120.00	52.31	8.72	8.59
NGC 214 [c]	... [d]	84.14	1148.00	...	823.50[e]	458.00	1800.00	155.60	...	8.63
NGC 4981	... [d]	29.44	...	...	2700.00	226.20	1551.00	94.56	...	8.68
NGC 7364	... [d]	...	...	...	1076.00	26.09	656.90	16.90	...	8.79
NGC 7803 [c]	... [d]	176.10	...	37.29	3451.00	786.80	2257.00	365.20	8.84	8.71

The fluxes are given in units of 10^{-17} erg s^{-1} cm^{-2} for the galaxy centre and for the local SN environment. The O3N2 and N2 scales are computed according to Pettini & Pagel (2004) and are only given for the local environments.

[a] For this galaxy the SN location fell out of the slit and fluxes in a nearby region are provided.

[b] These galaxies are either point sources or the SN location coincides with the galaxy nucleus.

[c] For these galaxies no flux was recovered at the SN location. The local fluxes correspond to the most nearby non-nuclear region with flux.

[d] These Balmer lines (most often Hβ in the nuclear spectra) are present in absorption.

[e] Similarly as above, these lines are clearly affected by an absorption component although a measurement is possible.

[f] This line was at the edge of the CCD frame. The total flux has been assumed by extrapolation. The central N2 is given.

Even before proceeding to more detailed measurements, it becomes immediately apparent that differences exist between the nuclear and the local spectra. In particular, the galaxy nuclei are often dominated by an older stellar population as can be seen both by the red SED shape and the multiple absorption lines. The SN locations, however, have spectra more characteristic of star forming regions with flatter SED and more pronounced emission lines. Representative examples are, e.g., IC 4387A or NGC 214. This justifies our choice of obtaining spectra at the exact SN location, as very different properties could have been deduced by studying the global galaxy spectra. On the other hand, it can also be seen that the local spectra are not of particularly high S/N and that in some cases only the Hα region contains some useful information. This was dictated by the fact that we had to achieve a balance between the total number of observed galaxies and the exposure time per individual galaxy.

We have used the spectra to measure line fluxes, both centrally and locally, and we tabulate their values in Table 6.3. The fluxes were measured by fitting Gaussians with the task `splot`. Especially in the case of [N II] λ6548, Hα and [N II] λ6584 that appear blended in the resolution of many grisms, we performed de-blending by fitting simultaneously 3 Gaussians with a single FWHM. We have only listed the fluxes for Hβ, [O III] λ5009, Hα and [N II] λ6584, although the spectra vary a lot in the number of detected lines. In particular, some galaxies display many more lines, including [O II] λ3728, [O III] λ4959 and [S II] $\lambda\lambda$6717, 31, especially when measured in the higher S/N central regions. However, the lines listed are the ones that are more consistently detected and, at the same time, the ones that are useful for our metallicity determinations. We observe that in many cases, especially near the galaxy bulge, the Balmer lines are affected by absorption components from the underlying stellar population. This is most notable in the case of Hβ that is often present only in absorption, as noted in Table 6.3.

To derive metallicities we have used the empirical O3N2 and N2 calibrations described by Pettini & Pagel (2004). These methods present a number of advantages over other strong line diagnostics (such as R23, e.g. Kewley & Dopita, 2002), namely that they are based on ratios of neighboring lines and are therefore independent of extinction and uncertainties in flux calibration. In any case, due to the reasons described above, and the limited number of the [O II] λ3728 detections combined with the large uncertainties in the blue, it was impossible to resort on R23-based methods that rely on this line.

The N2 calibrator presents a (2σ) dispersion of 0.4 dex, which is comparable to the one of R23-based methods (Pettini & Pagel, 2004). Even smaller dispersion (0.18 dex) can be achieved by using the O3N2 method. However, in our case this was possible for only a few cases. We have tabulated the resulting metallicities in Table 6.3 as well, but *only for the local SN environments*. We note that these metallicities are lower than the ones measured at the galaxy centre by up to 0.4 dex in a few cases (although only 0.1 dex on average). We caution that in the case of 5 galaxies (indicated in Table 6.3) we have not used the exact SN location, since no flux could be recovered there, but instead the emission at another (non-nuclear) region, as nearby as possible to the SN.

In Fig. 6.7 we have plotted metallicities at the SN locations versus host galaxy luminosity. To our data, we have also added the GRB-SNe and broad-lined SNe Ic studied by Modjaz et al. (2008b) and the 3 SNe Ib in NGC 2770 (Thöne et al., 2009). To maximize our sample we use the N2 derived metallicity and we have converted the additional data to this scale based on the reported fluxes (Modjaz et al., 2008b; Sollerman et al., 2005; Hammer et al., 2006; Margutti et al., 2007; Wiersema et al., 2007).

We do not observe any difference between the environmental metallicities of SNe Ib and Ic. This is apparent both by visual inspection of the graph but also by a KS test (p-value 12% for a null hypothesis of a common parent metallicity distribution). The same is true, i.e. no differences are seen, if we restrict ourselves to using the less biased SDSS sample (5 SNe Ib and 3 SNe Ic). We point out that with the exception of a single SN Ic (the SDSS-discovered SN 2007qw), all other SNe Ic are clustered however at solar metallicity (or above) while SN Ib environments present a larger dispersion and extend to lower values. But even if we, arbitrarily, remove this SN from the sample, there is still no strong evidence supporting a different underlying metallicity distribution (p-value 3%). Furthermore, this KS test ignores the errors associated with the metallicity measurements. The difference between the average metallicities

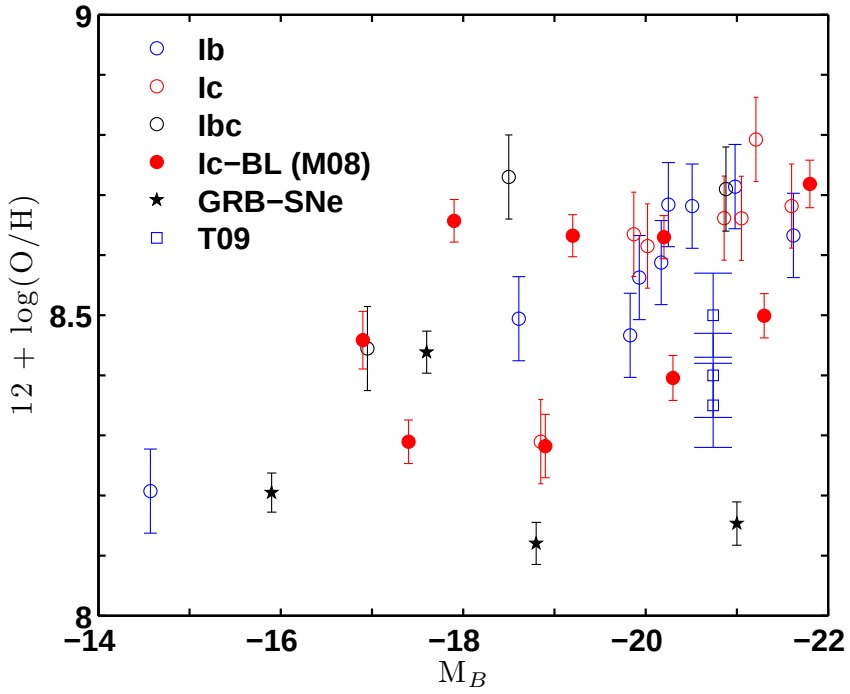

Figure 6.7: *Metallicities at the locations of stripped-envelope CC SNe versus their host galaxies magnitudes. The metallicities are given in the N2 scale of Pettini & Pagel (2004). Data from this work (Table 6.3; open circles) is complemented by measurements at 3 more SN Ib locations (squares; Thöne et al., 2009) as well as by the sample of broad-lined SNe Ic (filled circles) and GRB-SNe (stars) used by Modjaz et al. (2008b). In the last case the line fluxes have been obtained directly from Sollerman et al. (2005); Hammer et al. (2006); Margutti et al. (2007) and Wiersema et al. (2007). Blue color is used for SNe Ib and red for SNe Ic (including broad-lined). However 3 SNe with mixed classification (i.e. SNe Ib/c), as well as the SNe associated with GRBs, are colored in black. For the present analysis we have assumed a conservative 20% error in the fluxes reported in Table 6.3 resulting in the displayed error bars. We do not observe any significant difference between the metallicities of SNe Ib and Ic or even broad-lined Ic.*

of the two groups, ignoring SN 2007qw, is 0.15 ± 0.16 dex, i.e. a not significant value.

We do not observe any statistically significant difference between the metallicities of normal SNe Ib/c and broad-lined SNe Ic either. Interestingly, the metallicities of broad-lined SNe Ic are more likely drawn from the SN Ib than the SN Ic distribution (p-values 97% and 20% respectively). This is probably due to the fact that, within the present sample, broad-lined SN Ic metallicities are on average lower by 0.1 dex from those of SNe Ic. We stress, however, that this is just a weak observed trend and not a significant result.

We finally note that although the GRB-SNe are found at lower metallicity, in this scale there is no 'dividing line', as found by Modjaz et al. (2008b), between the metallicities of GRB-SNe and broad-lined SNe Ic (or other SNe Ib/c) but this dividing line is broken by SN 1998bw. That SN 1998bw was located in a non-particularly low metallicity was also noted by Sollerman et al. (2005). However this galaxy was not included by Modjaz et al. (2008b) in their O3N2 plot, where it would also break their dividing line.

6.6 Conclusions and future prospects

With the present sample and the given data quality, it seems that, at least to a first order, there is no strong evidence showing that normal SNe Ic occur at higher metallicities than SNe Ib. Such a qualitative trend

would be expected in the single massive star progenitor scenario due to the strong dependence of mass loss on metallicity. However, it would be very premature to promote the binary channel scenario based on these results because: (i) it needs to be better investigated how strong a difference we would expect to see, (ii) it is possible that SNe Ib/c are a mix of explosions resulting from both channels and (iii) the metallicity determinations suffer from an additional uncertainty related to the dispersion in the N2 index calibration.

The results presented in this chapter are preliminary. In particular, a proper determination of the error in the line fluxes presented in Table 6.3 has been postponed. For the purposes of calculating the metallicity, a conservative error of 20% in all line fluxes has been assumed. This results in the 1σ error-bars of $\sim$0.07 dex associated with the N2 abundances plotted in Fig. 6.7. It is pointed out, however, that 20% is a rather exaggerated value, except perhaps in the lowest S/N cases, and should be considered as an upper limit. In addition, this shows that the errors in the line fluxes contribute much less than the intrinsic dispersion of the N2 index itself (0.18 dex in 1σ; Pettini & Pagel, 2004) to the metallicity uncertainty, so it is unlikely that a more sophisticated treatment is going to significantly improve the accuracy of our results. Nevertheless, the error analysis is pending.

Another very interesting analysis that remains to be conducted with the present dataset is an effort to constrain the stellar population age of the SN environments. We intend to use the spectral synthesis code STARLIGHT (Cid Fernandes et al., 2005), which is based on Bruzual & Charlot (2003) evolutionary population synthesis models, to model the continuum and stellar absorption lines of our spectra. Despite the fact that there exist many SFH-related degeneracies and that many of our local spectra are of low S/N, we hope like this to place constraints on the ages of at least some of the SN progenitors in our sample. This will be very valuable in comparing with the predictions of single and binary star progenitor models. In addition, modeling the spectra will enable us to get more reliable fluxes for the Hβ emission line and thus better estimates of the reddening and star formation.

Finally, as mentioned above, all the SN explosion sites studied in this chapter are associated with SNe with good available data. The ultimate goal would therefore be a study relating the explosion and the environmental properties of SNe Ib/c.

7

ULTRAVISTA AS A SUPERNOVA SURVEY?

This chapter is based on a study I made (mostly during the end of 2009) on the prospect of using a deep NIR galaxy survey, UltraVISTA, as a SN survey as well. To set the context, a short description of how SN surveys operate is given, followed by some relevant details concerning UltraVISTA. Numerical estimates for the SNe expected to be discovered by UltraVISTA are provided and the science case for these SNe is deployed. It turns out that UltraVISTA has a great potential in SN science, in areas including cosmology, SN rates and SN host galaxy studies. However, some small modifications, that will not affect the galaxy survey, mainly concerning filter rotation, might be warranted.

7.1 DISCOVERING SNE: TRADITIONAL METHODS AND LARGER SURVEYS

There exist several types of transient surveys. Since the pioneering efforts of Zwicky, the large majority have traditionally been those that repeatedly target nearby bright galaxies looking for new stars. This is the method used both by amateur astronomers but also by more systematic surveys (e.g. LOSS; Filippenko et al., 2001). Newer approaches, such as the searches conducted with ROTSE III (Akerlof et al., 2003) or the CRTS survey (Drake et al., 2009), involve targeting blank fields to avoid the biases related with the galaxy selection. It is noteworthy that this different method has opened the window to different SN types, not noticed before, like over-luminous SNe (e.g. Quimby et al., 2007). Other synoptic surveys are coming into operation now (e.g. PTF, PanSTARRS, SkyMapper), or in the near-future (LSST), and their strategy will involve observing with different cadences, from minutes to years, in order to increase the variety of the detected transient phenomena.

Here, however, we focus on the surveys that have gone deeper to find distant SNe (primarily SNe Ia for cosmology) as their set-up is the most similar to the one of UltraVISTA. The two most relevant examples are the SNLS (Astier et al., 2006) and ESSENCE (Miknaitis et al., 2007) surveys, while SDSS-II (Frieman et al., 2008) covered a much larger field of view, but at a shallower depth. The SNLS was conducted with MegaCam on CFHT targeting four different 1 deg^2 fields. The typical cadence was $\sim$4 days, breaking for bright time, for a period of $\sim$6 months per field in a total period of 5 years. The filters used for the imaging survey were $griz$. ESSENCE run over a period of 3 months per year, for 6 consecutive years, on the Blanco 4m telescope at CTIO, targeting 32 different fields of 0.36 deg^2 in RI with a typical cadence of 4 days per field (Miknaitis et al., 2007).

The methods used in this type of surveys after data collection are similar: first, image subtraction techniques are used to identify transients and then SN candidates are selected based on their light curves and colors. SNLS and ESSENCE used 8-10 m class telescopes to spectroscopically follow-up their best candidates, while SDSS mostly relied on 3-4 m telescopes for their more nearby sample.

All the above-mentioned surveys have detected their SNe at the optical wavelengths.

7.2 THE ULTRAVISTA SURVEY: SOME KEY FEATURES

The UltraVISTA survey is one of the ESO public surveys[1] with the 4m VISTA telescope[2] at Paranal. The main scientific purposes of the survey are to find high-redshift (z>6) galaxies, to elucidate the reionization epoch and to study the growth of stellar mass.

The survey will repeatedly observe the COSMOS field,[3] whenever it is visible (i.e. between November and June). The survey will cover a total field of view of 1.5 deg^2. However, more than 85% of the total exposure time ($\sim$1800 hrs) will be spent on the *ultra-deep* survey, as opposed to the *wide* survey, which covers approximately half (0.73 deg^2) of the total area. The expected duration of the survey is 4–5 years and the wide survey is expected to be completed during the first year of operation. Observations will be done through the $YJHK$ and a narrow-band (NB) filter. UltraVISTA is expected to use the best 75% of the time (constraint on seeing $< 0.8''$) of the VISTA telescope, when the COSMOS field is above airmass 2.

The total observation time will be divided in units of 1 hr that constitute the fundamental Observing Block (OB). Since the effective field of view of the telescope, known as the 'pawprint', is 0.6 deg^2, with gaps between the detectors, three 1 hr OBs are going to be executed consecutively in order to cover the whole 0.73 deg^2 field in one filter. In this sequence, each part of the sky will fall on a detector area 2/3 times, hence a total exposure time of 2 hrs. It is one of the purposes of the UltraVISTA survey to build up the required S/N simultaneously in all filters. There are, however, some filter-time dependencies: observations through Y and J (and NB) will be done during dark time and far from astronomical twilight to avoid the bright sky background, while these constraints apply less to H and especially K, for which observations during brighter times and closer to twilight are scheduled. The limiting magnitudes that will be achieved in 1hr observations will be 23.6, 23.5, 23.0 and 22.5 in $YJHK$ respectively (AB magnitudes).

The data reduction will be done at several stages and at different intitutions. Basic reductions are going to be performed in CASU, Cambridge, while Terapix, in France, will deliver the final reduced 1 hr images.

7.3 COMPARISON, ADVANTAGES AND DISADVANTAGES: WHERE SURVEYS OF DIFFERENT NATURE MEET

Although its scientific purpose is different, the UltraVISTA survey shares many of the characteristics of high-redshift SN surveys, namely a wide field of view, frequent observations of the same field and it reaches faint magnitude limits. So although it is neither designed nor optimized for a SN search, it could also be used as such without compromising the primary scientific goals, as this study aims to demonstrate. In this context, we point out below some key differences that UltraVISTA would have compared with traditional SN searches, emphasizing the main advantages and disadvantages coming from their different nature.

- The undisputed advantage will be the large science output that will come *for free* as a by-product of the UltraVISTA survey. Implementing a SN search in UltraVISTA will be at a relatively low cost (effectively only manpower) compared to the budget of dedicated SN surveys. It is shown below that the scientific outcome is considerable. Science has always profited by such interactions: we recall here the similar example of the HST GOODS survey that was also used to detect SNe (e.g. Riess et al., 2004b, 2007).

- The fact that the search will be conducted in the NIR is a novelty (at least at these large scales), which will permit to select transients with criteria that are less biased against dust extinction. Despite the motivation, systematic NIR searches have not been possible until today (mostly for reasons related with the size and effectivity of the detectors) but synoptic surveys in the infrared are being planned for

[1] `http://www.eso.org/sci/observing/policies/PublicSurveys/sciencePublicSurveys.html` or e.g. Arnaboldi et al. (2007).
[2] `http://www.vista.ac.uk/`
[3] `http://cosmos.astro.caltech.edu/index.html`

the future (SASIR[4]), while SN searches will also be conducted with the JWST. UltraVISTA, together with VIDEO[5] but at a different depth, has the opportunity of being the first significant producer of NIR selected SNe, thus gaining considerable know-how and advantage in view of future facilities.

- An important benefit will be the fact that the UltraVISTA discovered SNe will be in the COSMOS field. This is one of the best observed fields on the sky and data is available at all wavelengths from X-rays to radio from a variety of facilities (including XMM, GALEX, HST/ACS, Subaru, CFHT, Spitzer, VLA and forthcoming SCUBA2 and Herschel). This data could enable the most complete studies of SN host galaxies ever attempted. There are good photometric redshifts for the galaxies in the COSMOS field. In addition, the zCOSMOS-bright project (Lilly et al., 2007, 2009) has so-far obtained more than 10000 spectra of galaxies brighter than I <22.5, mostly at $z < 0.8$, i.e the area the SN search is going to target. It is therefore conceivable that discovered SNe will already have a redshift from their host galaxy.

- The biggest question-mark remains the final cadence per filter, which is essential for obtaining good light curves of the SNe. It is later shown that (by considering the total number of hours awarded to the project) light curves with an *average* cadence of 3 days per filter can be obtained. This means that, in some cases, the cadence will even reach down to 1 day, which is unprecedented for traditional SN searches that, in hunt for a larger number of SNe, cannot afford re-visiting the same field so often (a cadence of 4-5 days is more common). This extra-information is very welcome and will enable a better study of the light curves, resulting in smaller uncertainties in e.g. rise times, age of maximum as well as in more secure photometric typing. However, as shown later, it constitutes an important topic of study how to optimize the filter rotation, with respect to the SN output, without affecting the goals of the main survey.

- The largest disadvantage is the difficulty to implement a fast-response follow-up campaign in the form of a ToO, either providing spectroscopy or extra optical photometry. The difficulty arises from the fact that the data reduction procedure (Paranal → Cambridge → Paris) has not been optimized for such a fast reaction but rather for final (excellent) quality. A fast follow-up campaign is not necessary (spectroscopic redshifts can be obtained a posteriori by MOS of host galaxies) but some science applications (most notably cosmology) would benefit from the existence of additional data. In that case, it would be mandatory to set-up a secondary, quick-and-dirty, on-mountain, reduction pipeline allowing for the timely identification of transients. On the other hand, for the final analysis and photometry, a SN survey will definitely profit and make use of the reduction process and the high quality final images delivered by the UltraVISTA consortium.

7.4 ESTIMATES FOR SNE DETECTED BY ULTRAVISTA

In all the estimates below, we have assumed the following:

- An *ultra deep* survey, with FOV of 0.73 deg^2, that will run for three consecutive seasons (2010-2011, 2011-2012 and 2012-2013) and will built its S/N simultaneously in all $YJHK$ and NB filters. A crucial point is that *simultaneously* is interpreted here by an assumption that filters with equal constraints, such as Y and J (and NB), will be changed (rotated) after 3 hrs of observations.

- We have therefore ignored in these calculations the *wide* survey, with FOV 1.5 deg^2 and the start season 2010, which is shorter and might be erratic due to the newly delivered telescope and unforeseen problems. Nevertheless, we have supposed that the *wide* survey (a total of 212 hours) will be completed during this season together with ~ 80 hours of the *ultra deep* survey. It should therefore

[4] Synoptic All-Sky Infrared Survey, PI: J. Bloom; `http://sasir.org/`
[5] VISTA Deep Extragalactic Observations Survey, PI: M. Jarvis; `http://star-www.herts.ac.uk/~mjarvis/video/`

be understood that many more SNe will be detected during the first year in addition to the ones estimated below. At this point however, we have chosen to just treat this data as a potential test sample for the verification of our calculations.

- For the ~ 24 week period that the field is visible in each season, we have assumed that the Y and J observations (and NB) will only be distributed during the 3 darkest weeks of the moon cycle.
- We have assumed that the default observation time per filter will be 3 hours (i.e. $3\times$1hr OBs), at least when the night length allows it, *and that the filter will be changed after this*.
- This results in an *average* cadence of 3 days per filter, excluding bright time, by dividing the total number of hours per filter awarded to the project to the total amount of available time (taking bad weather and seeing constraint into account).
- Although probably less accurate, we have temporarily assumed the same observing strategy and final cadence pattern for the H filter.
- The K filter is of lower interest for a SN search and it is expected to follow a completely different strategy, which will make it even less useful. Nevertheless, in order to demonstrate this, we quote our predictions for the K band based on the same pattern.
- The resulting limiting magnitudes (5σ) per pointing are therefore 24.0, 23.9, 23.4, and 22.8 (AB) or 23.5, 22.9, 22.0 and 20.9 (Vega) for $YJHK$ respectively (assuming a 2hr, out of 3, effective exposure time per point in the field).
- We adopt the traditional approach that we want the SNe at maximum light to be *1 mag brighter* than these limiting magnitudes and this is what goes into the calculations below. This approach can however be conservative, especially for some types of SNe, and different strategies involving multi-epoch stacking can be investigated that would boost the number of detections at higher depths.

Based on the assumptions above, we have used especially developed tools, similar to SNOC (Goobar et al., 2002) and other routines, to make predictions on the number of detected SNe per type and redshift bin during the course of the UltraVISTA survey. The algorithms of these tools are described in, e.g., Goobar et al. (2002). They basically rely on redshifting SED templates for different types of SNe (modified versions of Nugent templates were used) and convolving with filter response functions (HAWK-I responses were used) to obtain the corresponding light curves at different distances. The spread of absolute luminosities per class as well as statistical noise and host extinction ($R_V = 2$ assumed) is also taken into account.

We reach the following conclusions, illustrated also in Fig. 7.1:

1. UltraVISTA is expected to discover $\sim$260 SNe Ia with useful Y-band light curves and $\sim$160 with both Y and J observations (i.e. with one color).
2. The bulk of these SNe will be at medium (z$\sim$0.3-0.5) redshift, while very few detections are expected at z$>$0.6.
3. The sensitivity goes down, the redder the filter: the H filter is only expected to detect $\sim$8 SNe Ia per year out to z=0.3.
4. The K-band is not going to contribute with any useful information, especially given the different observing strategy.
5. UltraVISTA is also going to discover an equal number of SNe IIP ($\sim$270). This time the most productive filter is going to be J.

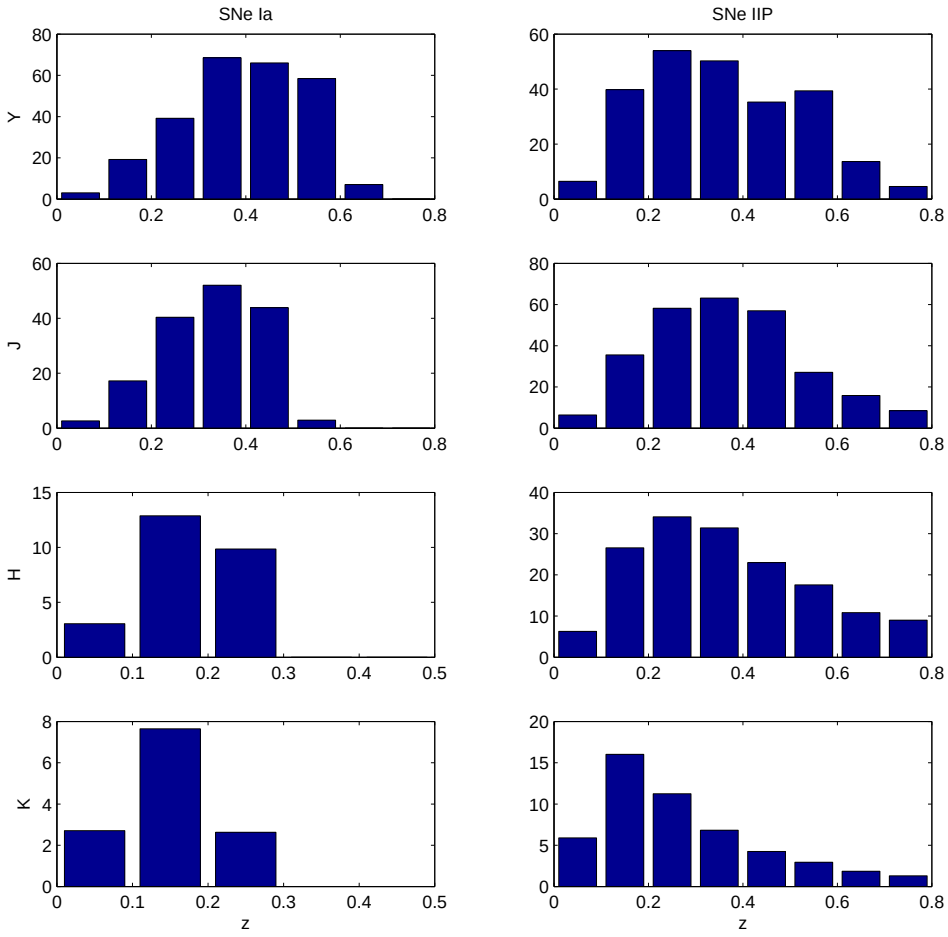

Figure 7.1: *Estimates on the numbers of detected SNe Ia and IIP per filter and redshift bin, based on the assumptions in the main text (Ariel Goobar, priv. comm.). These calculations are based on the SN Ia rates in Neill et al. (2006), partly based on the COSMOS field, and the SN IIP rates in Dahlen et al. (2004). For an explanation why SNe IIP seem to extend to longer redshift than SNe Ia, see text.*

6. Y-band observations will be possible for $\sim$240 SNe IIP, while the H-band will also be competitive with $\sim$150 light curves. The relative differences with SNe Ia are due to the fact that SNe IIP are redder objects.

7. In these calculations we have included a dispersion of $\pm$1.1 mag in the intrinsic maximum luminosities of SNe IIP. For this reason, the distribution of the detected events seem to extend further in redshift than for SNe Ia (which have more uniform luminosities), but in reality only the highest brightness tail of these explosions is probed at high z. Normal events will be detected to redshifts of $\leq$0.4.

8. A smaller number of other SN types is also going to be detected.

We see that the number of SNe that will be detected by UltraVISTA (as a simple by-product) is considerable. It will also be unique in its wavelength range, for these redshifts, and will allow original studies in the fields of cosmology, cosmic explosion rate and host galaxies.

These predictions are of course indicative, as there exist several related uncertainties. Most of them have to do with the poorly known rest-frame NIR properties of SNe, especially core-collapse, but also with the exact observing strategy of UltraVISTA (final cadence per filter). We do not expect however these numbers to be severely affected as long as the cadence remains below or equal to 5-6 days.

7.5 SCIENCE CASE FOR THE ULTRAVISTA DISCOVERED SNE

7.5.1 SN IA SCIENCE

It is well known that the use of SNe Ia as standardizable candles (Phillips, 1993; Phillips et al., 1999) has revolutionized cosmology by discovering the acceleration of the universe and Dark Energy (Riess et al., 1998; Perlmutter et al., 1999). It is also well known that (i) extinction is the main source of systematic errors in estimating the luminosity of a SN, with different teams having different approaches to the subject (Astier et al., 2006; Wood-Vasey et al., 2007; Kessler et al., 2009) and (ii) SNe Ia are better standard candles in the NIR than in the optical bands (Meikle, 2000; Krisciunas et al., 2004a; Wood-Vasey et al., 2008). As a matter of fact, Wood-Vasey et al. (2008) demonstrate that SNe Ia, are *not just standardizable* but real *standard* candles (i.e. no light-curve correction is needed) in the rest-frame H-band, where they present very luminosity small scatter. This is also supported by theoretical models (Kasen, 2006).

Although measuring rest-frame NIR magnitudes (especially H-band) of SNe Ia at higher redshift is an interesting possibility for the future, it still remains impossible with present facilities. Nevertheless, even the efforts of using observer-frame NIR data (corresponding roughly to rest-frame I) have until now been sparse: Nobili et al. (2005) constructed a rest-frame I-band Hubble diagram by supplementing local data with 2 SNe at z$\sim$0.5. The sample was doubled with the inclusion of 2 out of 5 SNe observed with HST and NICMOS (Nobili et al., 2009). Note that all these SNe were observed in the days before 2000 and have only on average $\sim$3 photometric points in one band. Although SNe Ia are still not standard candles in the I-band, the motivation is still strong in using observations at this wavelength. This has to do with extinction being $\sim$3 times less than in the B-band. Disentangling host-galaxy extinction from intrinsic SN Ia color remains the largest systematic uncertainty in SN cosmology and better results can be obtained by trying to minimize it.

An important progress was made in this field with the release of the CSP high-z results (Freedman et al., 2009). Here 35 SNe, selected in the optical by other high-z SN surveys (SNLS, ESSENCE, SDSS) were followed in the Y and J bands in order to construct a rest-frame I-band Hubble diagram, out to z$\sim$0.7 and to place constraints on cosmological parameters. Their results also seem to point in the direction that dust in SN Ia host galaxies behaves differently ($R_V = 1.8$) than in our Galaxy, as is also supported by increasing amount of evidence (e.g. Nobili & Goobar, 2008; Hicken et al., 2009b; Folatelli et al., 2010).

The comparison to this study is interesting because it has very similar data as it is expected from UltraVISTA, both in the number of SNe (order of magnitude), redshift range and useful bands (YJ). UltraVISTA will at least be able to conduct a similar study and more than double the sample of high-z SNe with NIR observations. However, two important differences need to be stressed: (i) the CSP followed SNe discovered by other surveys. As a result, there exists no pre-maximum data in their YJ light curves and the number of observations per SN, that go in their light-curve fits, varies between 2–5. The UltraVISTA SNe are expected to have a significantly better sampling, including pre-maximum data, allowing for a better study and minimization of the uncertainties. In addition (ii) the UltraVISTA SNe will be *NIR-selected*. Except from being the first of its kind, this dataset will allow a better assessment of the biases related to SNe discoveries, especially regarding extinction.

Spectroscopy of the SNe is not mandatory. The redshift can be estimated from a galaxy photometric redshift or spectroscopically *a posteriori* (if it does not already exist in z-COSMOS). Concerning typing of the SNe, it should not be a problem with a well-sampled LC in two colors. For the study of extinction and reddening as a systematic effect however, the existence of additional (optical) colors would be an

advantage.

7.5.2 CORE-COLLAPSE SN SCIENCE

Core-collapse SNe are the explosions of stars more massive than $\sim$8 $M_{\odot}$. As such, they are closely linked, and accurately probe, the young stellar population and star formation rate. The CC SN rate is therefore directly linked to the star formation history, through the IMF.

Recently there has also been an increased interest for the use of SNe IIP as cosmological probes (see corresponding Astro2010 white paper; Poznanski et al., 2009a). Except from the need for new methods of getting independent measurements across the distance ladder, SNe IIP present the following advantage: unlike SNe Ia, their progenitors *are* known (they are red supergiants; Smartt et al., 2009). We thus have a better understanding of the physical processes taking place and, therefore, a better handle on systematic effects.

Two kinds of methods exist to date to determine distances to SNe IIP. The first involves the calculation of the angular distance, through detailed spectral fitting and modeling of the expanding photosphere (e.g. Kirshner & Kwan, 1974; Baron et al., 2004; Dessart & Hillier, 2005). These methods are, however, very demanding and require a series of spectra with high S/N. So they are not expected to be applicable at higher redshift until the next generation of instruments and telescopes (ELTs). Another promising tool is the *standardizable candle method* (Hamuy & Pinto, 2002; Nugent et al., 2006; Poznanski et al., 2009b), where the luminosity of the plateau is correlated to the ejecta expansion velocity, as measured by the Fe II λ5169 line in a single spectrum obtained around the middle of the plateau phase. Although these methods still do not provide Hubble diagrams as tight as SNe Ia (D'Andrea et al., 2009), they are under development and a very promising tool for the future. Again the use of NIR data is beneficial for SNe IIP, because it allows a better separation of the extinction from the intrinsic color (Krisciunas et al., 2009a). Recently, Maguire et al. (2010) presented the first local NIR Hubble diagram for SNe IIP (based on 12 events) and demonstrated that the scatter is reduced with the use of NIR data. They argue that a sample of 10-15 well observed events between redshift 0.3-0.5 will be competitive to SNe Ia and will independently confirm the acceleration of the universe. UltraVISTA, together with a ToO component, would be able to deliver this result ahead of any other experiment.

The plateau phase of a SN IIP, where the luminosity remains constant, has a duration of around 100 days (rest frame). So the detection limits can be significantly enhanced by stacking frames of 1 or 2 months, or even a whole observing season, in order to go deeper. Different strategies can be envisioned and optimized depending on the desired outcome and should be studied in detail.

An excellent example of such alternative strategies was demonstrated by Cooke (2008), who showed that SNe IIn should be detectable at very high redshift and used this method on CFHTLS archival data to discover the highest redshift SNe to date ($z = 2.35$; Cooke et al., 2009). Preliminary calculations (based on the FOV ratios), however, show that not many ($\sim$1) similar events are expected in the UltraVISTA data.

Finally, it should be noted that the predictions mentioned above for CC SNe, are hampered exactly from the poor knowledge of their NIR properties (spectra and light curves). As a matter of fact, the existing templates are of poor quality, although data already obtained at low-z (e.g. CSP) should improve the situation in the near future. At z$>$0.3, however, NIR data is absolutely absent. UltraVISTA will thus cover a gap that nobody else is expected to cover, except VIDEO but at more moderate redshifts.

In contrast to SN Ia cosmology, this project relies on obtaining spectra of the SNe. It is therefore dependent on a follow-up campaign.

7.5.3 SN RATES IN THE NIR

Studying the rates of SN explosions is a topic of research in itself. It is closely linked to the study of their progenitors, the IMF and the star formation history (SFH) of the universe. Many studies have been

conducted in the past, targeting different types of SNe (Ia vs. CC), different selection methods (bright galaxies, clusters or the field) and different redshift ranges (e.g. Cappellaro et al., 1999; Dahlen et al., 2004, 2008; Maoz & Gal-Yam, 2004; Neill et al., 2006; Dilday et al., 2008; Botticella et al., 2008; Smartt et al., 2009), not always yielding consistent results.

Without exception, however, *all* the studies above (including ongoing experiments as PanSTARRS) were made based on SNe *discovered at the optical wavelengths*. Selecting SNe in the NIR is very interesting because it is less dependent on dust extinction and less biased against heavily reddened SNe. By comparing the NIR with the optically deduced SN rate, we can make estimates of how many SNe we are missing (Mannucci et al., 2007) and thereby draw conclusions on the nature and evolution of dust in the nearby universe.

A similar NIR study, with the same motivations, will be conducted by VIDEO at the same telescope, albeit at shallower depths. UltraVISTA will nicely complement this study, extending the NIR SN rate (and thereby SFH) to redshifts of z$\sim$0.5.

We finally note that due to the very good knowledge of the control (revisit) time of the single field observed by UltraVISTA, it will be relatively easy to calculate the SN rate.

7.5.4 A COMPLETE HOST GALAXY STUDY OF SNE

Studying the host galaxies of SNe can give valuable information on their progenitors through knowledge of the environment age, metallicity, stellar mass, star formation rate and dust content. Furthermore, in the case of SNe Ia, the study of host galaxies is a method to better assess systematic errors affecting their use as standard candles like the 'two-component' model (e.g. Sullivan et al., 2006b).

The local SN hosts have traditionally been related to the SN properties by means of their morphology, colors, luminosity, spectroscopic properties and in some cases multi-wavelength data (e.g. Hamuy et al., 2000; van den Bergh et al., 2002; Sullivan et al., 2006b; Prieto et al., 2008; Boissier & Prantzos, 2009; Hicken et al., 2009b). The higher redshift SN hosts have been studied through their optical colors (Cooper et al., 2009) or through SEDs built based on $ugriz$ data (Sullivan et al., 2006b). Recently, Neill et al. (2009) presented a study of local hosts of SNe Ia, including UV data from GALEX. Interesting results relating the SN peak luminosity with the host age and (probably) metallicity were extracted, but it is reminded that the selection of local SNe is exactly biased by targeting their (usually bright) hosts.

The plethora of multi-wavelength data available in the COSMOS field (including the data obtained by UltraVISTA) will permit *the most complete and bias-free* study of distant SN host galaxies to date. This could be done in many different ways, including multi-wavelength SED fitting, a method that has been applied in studies of other galaxy groups, e.g. GRB host galaxies or sub-milimetre galaxies (Michałowski et al., 2008, 2009).

7.5.5 OPENING A NEW WAVELENGTH WINDOW AND FUTURE PROSPECTS

Worth mentioning is also the potential for new transient discoveries in the NIR. While pioneer searches have been attempted (e.g. Mattila et al., 2004; Goobar et al., 2009), these were all with considerably smaller FOVs and typical cadences of > 1 month, yielding only a couple of SNe and with data of insufficient quality to draw any firm conclusions.[6]

UltraVISTA is the *first* survey that is expected to yield a considerable number of transients at medium redshift, accompanied with data of sufficient quality to do science with. This will be many years in advance of SASIR, a 170 M$ project which will use a 6.5m telescope and a wide-field camera to map the infrared transient sky, starting in 2017. One of the science cases, as pointed out by Bloom et al. (2009), is that, except the well studied phenomena, there exist classes of transients that have been predicted, but never discovered, and that are expected to have NIR signatures. Indeed, experience has shown that every-time a

[6] see also the ongoing Padova HAWK-I SN Search `http://graspa.oapd.inaf.it/`

search method changes (whether this involves target selection, cadence or wavelength), a different view of the universe has been revealed. Although the total area covered by UltraVISTA is rather small to expect surprises, this prospect should not be excluded. In addition, with its unprecedented cadence in the NIR, UltraVISTA has better chances of correctly identifying peculiar phenomena, should these occur.

Furthermore, such an effort will create valuable know-how to be used in future experiments, such as the JWST.

7.6 IMPLEMENTATION REQUIREMENTS AND OTHER ASPECTS

In this section, I examine, mostly in the form of a constructive brainstorm, some additional aspects of a potential SN search with UltraVISTA, mostly concerning its feasibility and its potential synergy with other projects. This section does not claim to be complete.

The feasibility is examined through the required steps for implementation. Ignoring temporarily a ToO component, i.e. concentrating on the science that can be performed when the final 1hr images are delivered from the UltraVISTA pipeline, these steps include:

1. The identification of transients. This can be done by the established method of image subtraction (e.g. Alard, 2000). It is noted that due to the nature of the UltraVISTA survey, these images will be constructed to be co-added easily, and therefore subtraction is not expected to be complicated either.

2. Photometry and the construction of the transient light curves. Again standard techniques (e.g. PSF photometry) can be applied for this step. It is pointed out that absolute photometry will be facilitated by the fact that the UltraVISTA field will become a standard field itself.

3. The most important part will be to photometrically type the different SN types (i.e. Ia, Ib/c, II) and separate them from other transient contaminants (e.g. AGN, variable stars, asteroids, etc). Since this is the major problem that future transients surveys will face (i.e. spectroscopic time will only suffice for a small fraction of the detected transients), this is currently an active topic of research (e.g. Poznanski et al., 2007). Developing such a method will be mandatory. However, this should be feasible, especially with the help of the existing tools, developed for optical wavelengths, as a starting point. It is usually not a problem distinguishing between a Type Ia and a CC SN, based on their LC shape and colors, especially if the LC is well sampled. The photometric redshifts of the SN host galaxies are also sufficient for the purposes of typing.

4. Once the SNe have been classified, the studies of rates and host galaxies are independent of the SN data itself and can be accomplished based on well established methods. For the SN Ia cosmology analysis it will be necessary, in addition, to develop or, more realistically modify for use in the NIR, one of the existing tools for standardizing the SNe Ia based on their light curves. Spectroscopic redshifts for the SN host galaxies can be obtained at a later stage.

It is therefore concluded that such a project is feasible. Adding a ToO component, will be more demanding for the following reason: a fast response is required and one cannot wait for the data to be shipped to Europe and take its usual UltraVISTA pipeline path. It will therefore be necessary to set-up a quicker (even if that means less sophisticated) path for the reduction of the raw data to 1 hr frames. This possibility is one of the big question marks of such an initiative. In addition, the method for the photometric selection of candidate SNe will also need to be more advanced than the one described above because it will not afford to be based on the complete light curve, but only on a few epochs, probably during rise-time. Such methods have been developed for optical surveys (e.g. Sullivan et al., 2006a; Miknaitis et al., 2007) and they have proved efficient. But they will need to be tailored to the (NIR) specialities of the UltraVISTA data. Last but not least, telescope time in ToO mode is required. For spectroscopy, the VLT is the obvious choice and X-shooter would be the ideal instrument to deliver (also) the NIR spectrum of these NIR-discovered

SNe. For additional optical photometry, however, it will be sufficient to resort to 2-3m class telescopes. While the complexity of the project is increased, there is still nothing making it unfeasible, e.g. lack of technology.

Finally, a SN search with UltraVISTA does not lack potential for synergistic collaborations. The most closely related project is the VIDEO survey, which will use the same telescope to make a shallower survey over a wider area. Since the data products will be very similar, a collaboration with VIDEO on the field of common data pipelines (e.g. image subtraction and detection techniques) could be very fruitful. Scientifically very interesting will also be the comparison and link with similar results obtained at lower redshifts (e.g. rates). In the field of cosmology, near-future surveys, such as DES[7] are expected to obtain multi-color optical light curves of thousands of SNe. DES is not expected to have a large time overlap with UltraVISTA. If however DES, during season 2012-2013, selected the COSMOS field as one of their survey fields, this would yield a common dataset of $\sim$20-30 SNe Ia at medium redshift, without any changes being required by UltraVISTA. Although small numerically, this sample will have unprecedented wavelength coverage and a large scientific impact.

7.7 SUMMARY

UltraVISTA is expected to discover around $\sim$250 SNe Ia and an equal number of core-collapse SNe, as a by-product of its main scientific outcome. These SNe will be mostly at intermediate redshifts (z$\sim$0.4-0.5).

Once obtained, these SNe will constitute a unique dataset, selected in the NIR wavelengths, that will enable (i) cosmological studies with a better handle on host galaxy extinction, (ii) a less biased determination of the SN rate, and thereby star formation history, at intermediate redshifts, (iii) the most complete study of SN host galaxies making use of the COSMOS field data, complemented by UltraVISTA. Table 7.1 summarizes the relevant studies that will be possible within UltraVISTA, with or without an additional ToO component.

In addition, it is elaborated that taking advantage of the large SN potential within UltraVISTA contains some reasonable challenges, especially if one envisions to include a ToO component, but it is feasible. The case becomes more appealing by the relatively low cost, negligible compared to dedicated SN surveys, in conjunction with the large scientific output. There is still time to initiate such a project: in this context, the first season data (2010) could be used for science verification.

This investigation is hampered by some limiting parameters: these conclusions were based on a number of assumptions, mainly concerning the filter rotation during the UltraVISTA survey. However, it was found that the real observing strategy during the first two trial months of operations, did not follow these assumptions (Fig. 7.2) but that Y and J observations were clustered in time. It is, however, believed that this was not done due to a specific reason and that a better rotation between the filters with equal observing constraints (i.e. Y, J and NB) is possible. A proper optimization study, based on SN light curve simulations, is necessary in order to determine the best observational strategy with respect to filter rotation, without affecting other UltraVISTA science.

[7] https://www.darkenergysurvey.org/

Table 7.1: *SN science possibilities within UltraVISTA*[a]

Science case	UltraVISTA	with ToO
A better view of SNe in the NIR	y	y
A study of the effect of dust in SNe	y	y
Unextincted SN rates to z∼0.4	y	y
SN Ia cosmology	y	y
SN IIP cosmology	n	y
A most complete SN host galaxy study	y	y
Detection of SNe IIP at z∼0.8	y	y
Detection of SNe IIn at high-z	?	?
Spectroscopic studies	n	y
Synergy with other projects	y	y
A new wavelength window: surprises?	?	?

[a] Two cases are examined: using the UltraVISTA data *alone* or *together with a ToO component*. It is observed that most science is possible already within the first scenario, although some science cases (e.g. SN Ia cosmology) would definitely profit from additional data.

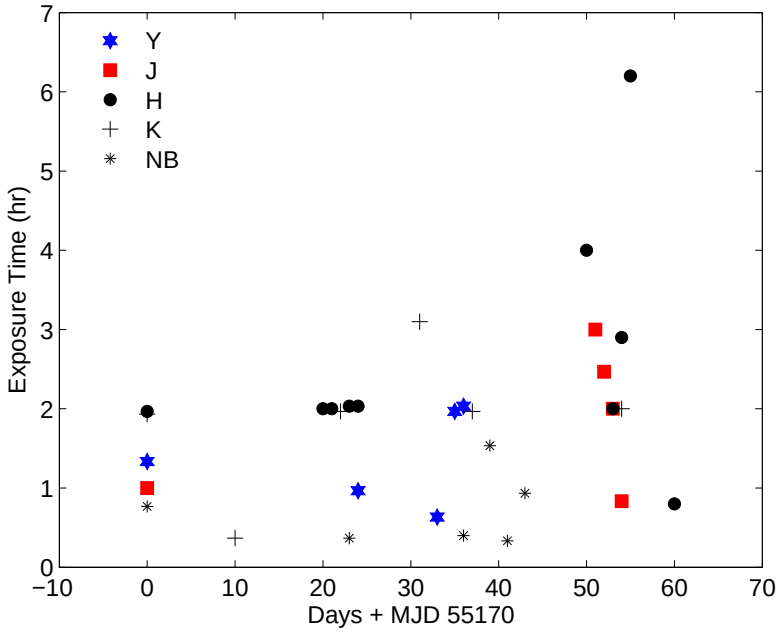

Figure 7.2: *The distribution of the UltraVISTA observing time per filter during the first two months of operations (December – January 2010). It is noted, however, that this corresponds to a trial period both for the VISTA telescope and for UltraVISTA. It is observed that, at present, the observing strategy does not favor the construction of good light curves for SNe: observations in Y and J are clustered together rather than evenly distributed between them, even though the observing constraints for the two filters are identical. But, in principle, this means that changes can be accommodated without affecting UltraVISTA. For visual purposes, this figure does not include observations during days with exposure times $<$10 mins (typically aborted after a few seconds).*

8

CONCLUSIONS

This thesis has presented work that aimed in the better understanding of supernovae, their physics and their birthplaces.

In the field of thermonuclear explosions, this was achieved through observations of SN 2003hv that extended to very late phases. SN 2003hv was shown to be a normal SN Ia with properties consistent with its rarely observed decline rate of $\Delta m_{15}(B) = 1.61$. The study of the late time photometry and spectra allowed us to conclude that the positrons produced during the radioactive decays remain probably trapped within the ejecta and that a dramatic infrared catastrophe does not occur. It is proposed, however, that the ejecta might be clumpy and that a mild infrared catastrophe might have occurred in the densest regions. A discussion on SN Ia explosion asymmetry based on optical nebular spectroscopy was initiated.

Stripped-envelope core-collapse SNe have been studied through their environments. Their locations within their host galaxies were found to be compatible with those of WR stars. In addition, the WC stars were shown to be distributed in brighter locations than WN stars. These results are in accordance with theoretical expectations. The host galaxies of 22 SNe Ib/c have been studied by means of spectroscopy probing the exact explosion sites. Preliminary results suggest that the environmental metallicities of SNe Ib and SNe Ic are not significantly different.

Finally, the potential of using the UltraVISTA survey to discover SNe in NIR wavelengths has been examined and it has been found to be very promising.

In the next decade we are likely going to witness important progress in the fields of research described above: the use of new-generation instruments, such as X-shooter on the VLT that can capture the entire SED from the UV to NIR in medium resolution, will open new dimensions in the late time studies of SNe. An exciting field that has just been born is probing observationally the inner explosion asymmetries of SNe Ia.

At the same time, it seems that we are closing down of the progenitors of SNe Ib/c from many different directions: as more and better data becomes available, it will be possible to better constrain the explosion properties. It is also conceivable that in the near future we might experience a direct detection of a SN Ib/c progenitor in pre-explosion images. Studying the explosions indirectly through their environment is a third alternative method, with important statistical power, that is also expected to yield valuable results.

One thing that will be very satisfying will be seeing the SN capabilities within UltraVISTA materialize. In times where the budgets of astronomical surveys become larger and larger, it is our duty to fully exploit every last science opportunity that is possible with the resulting data. UltraVISTA can pave the way to a better understanding of dust extinction in SNe and to a better estimation of the cosmic SN rate.

A

VLT AND HST OBSERVATION LOGS FOR SN 2003HV

Table A.1: *VLT late-time optical observations of SN 2003hv.*

Date (UT)	MJD (days)	Phase (days)	Filter	Exposure (s)	Airmass	Seeing ($''$)	Instrument
2004 08 12	53229.33	338.1	U	3×1000	1.17	1.02	FORS1
2004 08 12	53229.37	338.2	B	3×420	1.06	0.85	FORS1
2004 08 12	53229.39	338.2	V	3×300	1.03	0.74	FORS1
2004 08 12	53229.40	338.2	R	2×420	1.01	0.75	FORS1
2004 08 12	53229.41	338.2	I	1×500	1.01	0.70	FORS1
2004 08 13	53230.36	339.2	I	4×500	1.08	0.78	FORS1
2004 08 13	53230.39	339.2	R	2×420	1.03	0.76	FORS1
2005 02 07	53408.03	516.8	I	12×240	1.13	1.13	FORS2
2005 02 07	53408.08	516.9	R^a	3×600	1.37	0.93	FORS2
2005 02 07	53408.09	516.9	V	3×400	1.49	0.98	FORS2
2005 03 04	53433.02	541.8	U^a	3×1140	1.48	1.24	FORS2
2005 08 04	53586.40	695.2	R	2×900	1.04	0.70	FORS1
2005 08 07	53589.41	698.2	I	2×900	1.02	0.75	FORS1
2005 08 08	53590.31	699.1	I	4×900	1.39	0.82	FORS1
2005 08 08	53590.34	699.1	B	5×540	1.19	0.82	FORS1
2005 08 09	53591.36	700.2	R	3×900	1.12	0.62	FORS1
2005 08 10	53592.39	701.2	V	3×480	1.03	0.71	FORS1

[a]The U and R filters on FORS2 are slightly different than the ones on FORS1.

Table A.2: *VLT late-time NIR observations of SN 2003hv.*

Date (UT)	MJD (days)	Phase (days)	Filter	Exposure[a] (s)	Airmass	Seeing ($''$)
2004 08 18	53235.37	344.2	J_s	30×4×24	1.04	0.55
2004 08 29	53246.25	355.1	K_s	10×6×30	1.37	0.47
2004 08 29	53246.29	355.1	H	10×6×59	1.17	0.75
2004 08 29	53246.32	355.1	K_s	10×6×30	1.07	0.57
2004 08 29	53246.39	355.2	H	10×6×30	1.00	0.75
2004 08 30	53247.26	356.1	J_s	30×4×23	1.29	0.77
2004 08 30	53247.30	356.1	K_s	10×6×30	1.13	0.50
2005 01 24	53394.02	502.8	K_s	10×6×60	1.03	0.47
2005 01 24	53394.09	502.9	H	10×6×30	1.24	0.74
2005 02 24	53425.99	534.8	K_s	10×6×30	1.18	0.62
2005 02 25[b]	53426.99	535.8	J_s	30×4×46	1.19	0.83
2005 02 27	53428.99	537.8	H	10×6×30	1.22	0.55
2005 02 28	53429.99	538.8	J_s	30×4×23	1.22	0.56
2005 10 13	53656.18	765.0	J_s	30×4×46	1.11	0.70
2005 10 13	53656.35	765.2	J_s	30×4×23	1.14	0.56
2005 10 14	53657.21	766.0	J_s	30×4×46	1.04	0.54
2005 10 14	53657.32	766.1	H	10×6×60	1.05	0.72
2005 10 15	53658.31	767.1	H	10×6×30	1.04	0.40

[a] Detector integration time (DIT) × number of DITs per exposure × number of exposures.
[b] Image not included in the final photometry as it is a poor image and gives bad results.

Table A.3: *HST observations of SN 2003hv.*[a]

Date (UT)	MJD (days)	Phase (days)	Instrument	Filter	Exposure (s)
2004 07 10	53196.55	305.4	ACS	$F555W$	480
2004 07 10	53196.56	305.4	ACS	$F814W$	720
2004 07 12	53198.82	307.6	ACS	$F435W$	840
2004 07 12	53198.83	307.6	ACS	$F625W$	360
2004 07 16	53202.75	311.6	ACS	$F435W$	840
2004 07 16	53202.76	311.6	ACS	$F625W$	360
2004 11 15	53324.71	433.5	ACS	$F555W$	480
2004 11 15	53324.72	433.5	ACS	$F814W$	720
2005 11 03	53677.31	786.1	NICMOS	$F160W$	16×640

[a] Observations not conducted due to guide-star failure are not included.

B

FULL VERSION OF TABLE 5.2

Table B.1: Fractional fluxes at the WR star locations. Full version of Table 5.2.

galaxy	ID	Subtype	Number	FF	galaxy	ID	Subtype	Number	FF
M 83	1	WNL	3	0.29	**M 83**	32	WCL	12	0.43
	2	WCL	2	0.34		33	WNL	1	0.71
	3	WCL	2	0.26		34	WCL	3	0.51
	4	WNE	16	0.48		35	WNE	14	0.72
	5	WCL	8	0.48		36	WCL	5	0.72
	6	WCE	3	0.06		37	WCL	4	0.91
	7	WNL	5	0.61		38	WNL	7	0.95
	8	WCL	1	0.40		38	WCL	21	0.95
	9	WCE	1	0.58		39	WCE	2	0.81
	10	WCL	2	0.54		40	WCL	6	0.89
	11	WNE	4	0.26		41	WNL	14	0.91
	12	WNE	2	0.36		41	WCL	13	0.91
	13	WCE	3	0.56		42	WNL	5	0.95
	14	WCL	4	0.12		43	WNL	3	0.86
	15	WCE	1	0.38		44	WNL	5	0.74
	16	WCE	2	0.44		45	WNL	1	0.63
	17	WCL	6	0.42		46	WCL	3	0.82
	18	WCL	6	0.38		47	WCE	1	0.69
	19	WCL	1	0.38		48	WNE	44	0.67
	20	WCL	2	0.35		49	WCL	13	0.49
	21	WCL	1	0.30		50	WNL	8	0.69
	22	WNE	4	0.34		51	WNL	1	0.23
	23	WCE	1	0.29		52	WNE	18	0.29
	24	WCL	4	0.28		53	WCL	2	0.23
	25	WNL	4	0.32		54	WCL	6	0.56
	26	WNL	2	0.72		55	WNE	20	0.24
	27	WCL	6	0.85		56	WNE	15	0.69
	28	WCL	8	0.85		57	WNL	9	0.73
	29	WCL	1	0.55		58	WCL	5	0.42
	30	WCL	1	0.23		59	WNL	14	0.83
	31	WCL	42	0.73		60	WNE	6	0.75

Continued.

galaxy	ID	Subtype	Number	FF	galaxy	ID	Subtype	Number	FF
M 83	61	WCL	2	0.84	**M 83**	104	WCL	3	0.73
	62	WCL	4	0.44		105	WNL	8	0.89
	63	WCL	5	0.28		106	WCL	6	0.85
	64	WNL	10	0.31		107	WNE	15	0.78
	65	WCL	4	0.52		108	WNL	2	0.58
	66	WNL	8	0.59		109	WCL	7	0.83
	66	WCL	4	0.59		110	WCL	3	0.64
	67	WCL	5	0.57		111	WCL	3	0.32
	68	WCL	3	0.44		112	WCL	2	0.78
	69	WCL	2	0.28		113	WCL	5	0.38
	70	WCL	2	0.25		114	WNE	4	0.18
	71	WCL	3	0.62		115	WCL	4	0.58
	72	WCL	1	0.75		116	WNL	12	0.67
	73	WNL	2	0.74		117	WNE	1	0.33
	74	WNL	52	0.94		118	WCL	6	0.66
	74	WCL	179	0.94		119	WCL	2	0.51
	75	WCL	1	0.39		120	WNE	6	0.53
	76	WNL	1	0.66		121	WNE	17	0.37
	77	WCL	2	0.61		122	WCE	3	0.27
	78	WNL	11	0.91		123	WCL	2	0.42
	79	WCL	5	0.66		124	WCL	3	0.31
	80	WNL	1	0.33		125	WCL	3	0.31
	81	WCL	3	0.46		126	WCE	1	0.49
	82	WCL	4	0.61		127	WCE	3	0.30
	83	WCL	2	0.56		128	WCL	2	0.39
	84	WCL	9	0.92		129	WCE	4	0.35
	85	WCL	4	0.58		130	WNE	1	0.04
	86	WNL	9	0.96		131	WCL	1	0.27
	86	WCL	24	0.96		132	WNE	1	0.02
	87	WCE	3	0.41		133	cand.	···	0.25
	88	WCL	1	0.39		134	cand.	···	0.54
	89	WCL	3	0.79		135	cand.	···	0.38
	90	WCL	2	0.82		136	cand.	···	0.41
	91	WCL	3	0.45		137	cand.	···	0.37
	92	WCL	3	0.31		138	cand.	···	0.43
	93	WNE	10	0.19		139	cand.	···	0.60
	94	WNE	23	0.64		140	cand.	···	0.62
	95	WNL	1	0.43		141	cand.	···	0.18
	96	WNL	2	0.79		142	cand.	···	0.31
	97	WNL	5	0.90		143	cand.	···	0.27
	98	WCL	4	0.38		144	cand.	···	0.82
	99	WNL	1	0.71		145	cand.	···	0.73
	100	WNL	5	0.89		146	cand.	···	0.75
	101	WNE	11	0.45		147	cand.	···	0.51
	102	WNL	9	0.84		148	cand.	···	0.95
	103	WNL	29	0.80		149	cand.	···	0.91

Continued.

galaxy	ID	Subtype	Number	FF	galaxy	ID	Subtype	Number	FF
M 83	150	cand.	···	0.95	**M 83**	196	cand.	···	0.88
	151	cand.	···	0.95		197	cand.	···	0.67
	152	cand.	···	0.87		198	cand.	···	0.85
	153	cand.	···	0.86		199	cand.	···	0.67
	154	cand.	···	0.79		200	cand.	···	0.84
	155	cand.	···	0.31		201	cand.	···	0.55
	156	cand.	···	0.89		202	cand.	···	0.33
	157	cand.	···	0.76		203	cand.	···	0.64
	158	cand.	···	0.42		204	cand.	···	0.67
	159	cand.	···	0.91		205	cand.	···	0.84
	160	cand.	···	0.96		206	cand.	···	0.89
	161	cand.	···	0.30		207	cand.	···	0.88
	162	cand.	···	0.53		208	cand.	···	0.87
	163	cand.	···	0.82		209	cand.	···	0.79
	164	cand.	···	0.25		210	cand.	···	0.44
	165	cand.	···	0.59		211	cand.	···	0.66
	166	cand.	···	0.28		212	cand.	···	0.88
	167	cand.	···	0.16		213	cand.	···	0.54
	168	cand.	···	0.86		214	cand.	···	0.82
	169	cand.	···	0.33		215	cand.	···	0.70
	170	cand.	···	0.87		216	cand.	···	0.47
	171	cand.	···	0.82		217	cand.	···	0.22
	172	cand.	···	0.35		218	cand.	···	0.51
	173	cand.	···	0.81		219	cand.	···	0.42
	174	cand.	···	0.37		220	cand.	···	0.39
	175	cand.	···	0.83		221	cand.	···	0.01
	176	cand.	···	0.58	**NGC 1313**	1	WNE	1	0.37
	177	cand.	···	0.74		2	WCE	1	0.30
	178	cand.	···	0.74		3	WNL	1	0.06
	179	cand.	···	0.99		7	WNL	1	0.03
	180	cand.	···	0.43		8	WNL	1	0.16
	181	cand.	···	0.15		9	WNE	1	0.28
	182	cand.	···	0.42		10	WCE	2	0.30
	183	cand.	···	0.63		11	WNE[a]	1	0.00
	184	cand.	···	0.63		11	WCE	1	0.00
	185	cand.	···	0.91		12	WCE	1	0.47
	186	cand.	···	0.62		13	WNL	1	0.11
	187	cand.	···	0.60		14	WNE[a]	1	0.67
	188	cand.	···	0.37		15	WCE	1	0.34
	189	cand.	···	0.93		16	WCE	1	0.71
	190	cand.	···	0.92		17	WNE	1	0.71
	191	cand.	···	0.77		18	WNL	1	0.22
	192	cand.	···	0.67		19	WNE	1	0.02
	193	cand.	···	0.34		20	WCE	1	0.70
	194	cand.	···	0.91		21	WNL	1	0.74
	195	cand.	···	0.96		22	WNL	1	0.74

Continued.

galaxy	ID	Subtype	Number	FF	galaxy	ID	Subtype	Number	FF
NGC 1313	23	WNE	1	0.46	**NGC 1313**	59	WCE	1	0.95
	24	WNL	1	0.62		60	WCE	1	0.97
	25	WNL	1	0.46		61	WCE	3	0.18
	28	cand.	···	0.38		62	WCE	1	0.18
	29	WNE	1	0.39		63	cand.	···	0.56
	30	WNL	1	0.03		64	WCE	3	0.95
	31	WCE	1	0.78		65	cand.	···	0.98
	32	WNL	1	0.03		66	WCE	2	0.96
	33	WNE	3	0.86		67	WNE[a]	1	0.96
	34	cand.	···	0.91		67	WCE	1	0.96
	35	WCE	1	0.89		68	cand.	···	0.45
	37	WCE	1	0.99		70	WNE	1	0.28
	39	WNL	1	0.52		71	WNE	1	0.47
	40	WNE	1	0.84		72	WNL	1	0.40
	41	WCE	1	0.71		73	WNL	1	0.44
	42	WCE	1	0.68		75	cand.	···	0.00
	44	WNE	1	0.53		76	WNE	1	0.22
	45	WNE	1	0.41		77	WNL	1	0.36
	46	WNE	1	0.62		78	WNE	1	0.30
	47	WNL	1	0.62		79	WNE	1	0.04
	48	WCE	2	0.58		80	cand.	···	0.54
	49	WCE	1	0.58		81	WCE	1	0.52
	50	WCE	1	0.89		82	cand.	···	0.64
	51	WNE	1	0.83		83	WNL	1	0.53
	52	WNE	1	0.60		85	WNL	1	0.53
	53	WNE	1	0.80		86	cand.	···	0.15
	54	cand.	···	0.60		87	cand.	···	0.20
	55	WNE	1	0.51		88	WCE	2	0.00
	56	WCE	1	0.89		90	WNL	1	0.33
	57	WCE	1	0.91		91	WNL	1	0.17
	58	WNE[a]	3	0.97		92	WNL	1	0.32
	59	WNE[a]	1	0.95		94	WNL	1	0.09

[a] These are stars classified as WN5-6 and we have included them in the WNE distribution.

ACRONYMS

This is an almost complete list of the most important (or most encountered) abbreviations in this thesis:

2MASS	Two Micron All Sky Survey
ACS	Advanced Camera for Surveys (onboard HST)
AGN	Active Galactic Nucleus
BAO	Baryonic Acoustic Oscillations
CC	Core-collapse (supernova)
CCD	Charge-Coupled Device
CFHT	Canada–France–Hawai Telescope
CFHTLS	Canada–France–Hawai Telescope Legacy Survey
CGRO	Compton Gamma-Ray Observatory
CMB	Cosmic Microwave Background
CSP	Carnegie Supernova Project
CTIO	Cerro Tololo Inter–american Observatory
dof	degrees of freedom (in χ_{dof})
DDT	Delayed Detonation (explosion model)
EFOSC2	ESO Faint Object Spectrograph and Camera 2
ELT	Extremely Large Telescope
ESO	European Southern Observatory
ESSENCE	Equation of State: SupErNovae trace Cosmic Expansion
EW	Equivalent Width
FORS	FOcal Reducer and low dispersion Spectrograph (at the VLT)
FOV	Field of View
FWHM	Full Width Half Maximum
GRB	Gamma-Ray Burst
HAWK-I	High Acuity Wide field K-band Imager (at the VLT)
HST	Hubble Space Telescope
IAU	International Astronomical Union
IME	Intermediate Mass Element
IMF	Initial Mass Function
IR	Infrared
IRAF	Image Reduction and Analysis (Facility)
IRC	Infrared Catastrophe
ISAAC	Infrared Spectrometer and Array Camera (at the VLT)
JWST	James Webb Space Telescope
KAIT	Katzman Automatic Imaging Telescope
KS	Kolmogorov–Smirnov (test)
LBV	Luminous Blue Variable (star)

LC	Light Curve
LCO	Las Campanas Observatory
LGRB	Long (duration) Gamma-Ray Burst
LMC	Large Magelanic Cloud
LOSS	Lick Observatory Supernova Search
MC	Monte Carlo (simulation)
MIR	Mid-Infrared
MJD	Modified Julian Date
MOS	Multi-Object Spectroscopy
NB	Narrow Band (filter)
NED	NASA/IPAC Extragalactic Database
NICMOS	Near Infrared Camera and Multi-Object Spectrometer
NIR	Near-Infrared
NOT	Nordic Optical Telescope
NTT	New Technology Telescope
PI	Principal Investigator
PSF	Point Spread Function
SASIR	Synoptic All-Sky Infrared Survey
SBF	Surface Brightness Fluctuation
SDSS	Sloan Digital Sky Survey
SED	Spectral Energy Distribution
SFH	Star formation History
SFR	Star formation Rate
SMC	Small Magelanic Cloud
S/N	Signal-to-Noise (ratio)
SN	Supernova
SNID	SuperNova IDentification (code)
SNLS	Supernova Legacy Survey
SNOC	Supernova Observation Calculator
SSO	Siding Spring Observatory
ToO	Target-of-Opportunity (observations)
UVOIR	UltraViolet Optical Infrared (light curve)
VIDEO	VISTA Deep Extragalactic Observations Survey
VISTA	Visible and Infrared Survey Telescope for Astronomy
VLT	Very Large Telescope (Paranal/Chile)
WD	White Dwarf
WFI	Wide Field Imager (at ESO/MPI 2.2 m telescope)
WR	Wolf-Rayet (star)
XRF	X-Ray Flash
XRT	X-ray telescope (onboard *Swift*)

PUBLICATIONS

This is a list with all the publications I have participated in during my PhD studies:

Peer - reviewed

- Maeda, K.; **Leloudas, G.**; Taubenberger, S.; Stritzinger, M. D.; Sollerman, J.; Elias-Rosa N.; Benetti S.; Hamuy M.; (2010): *Explosion Asymmetry and Viewing Angle as the Second Parameter in the Type Ia Supernova Luminosity Calibration?* Submitted to MNRAS.

- Maeda, K.; Benetti, S.; Stritzinger, M; Roepke, F. K.; Folatelli, G.; Sollerman, J.; Taubenberger, S; Nomoto, K.; **Leloudas, G.**; Hamuy, M.; Tanaka, M; Mazzali, P. A.; Elias-Rosa, N.; (2010): *Unifying the Spectral Evolution Diversity of Type Ia Supernovae by Asymmetric Explosions.* Accepted for publication in Nature.

- **Leloudas, G.**; Sollerman, J.; Levan, A. J.; Malesani, D.; Fynbo, J. P. U.; Maund, J. R. (2010): *Do Wolf-Rayet stars share the same environments in hosts as Type Ib/c Supernovae and long gamma-ray bursts?* Accepted for publication in A&A, arXiv: 1002.3164

- Maeda, K.; Taubenberger, S.; Sollerman, J.; Mazzali, P. A.; **Leloudas, G.**; Nomoto, K.; Motohara, K. (2010): *Nebular Spectra and Explosion Asymmetry of Type Ia Supernovae.* ApJ, 708, 1703-1715

- **Leloudas, G.**; Stritzinger, M. D.; Sollerman, J.; Burns, C. R.; Kozma, C.; Krisciunas, K.; Maund, J. R.; Milne, P.; Filippenko, A. V.; Fransson, C.; Ganeshalingam, M.; Hamuy, M.; Li, W.; Phillips, M. M.; Schmidt, B. P.; Skottfelt, J.; Taubenberger, S.; Boldt, L.; Fynbo, J. P. U.; Gonzalez, L.; Salvo, M.; Thomas-Osip, J.(2009): *The normal Type Ia SN 2003hv out to very late phases.* A&A, 505, 265-279

- Thöne, C. C.; Michałowski, M. J.; **Leloudas, G.**; Cox, N. L. J.; Fynbo, J. P. U.; Sollerman, J.; Hjorth, J.; Vreeswijk, P. M. (2009): *NGC 2770: A Supernova Ib Factory?* ApJ, 698, 1307-1320

- Malesani, D.; Fynbo, J. P. U.; Hjorth, J.; **Leloudas, G.**; Sollerman, J.; Stritzinger, M. D.; Vreeswijk, P. M.; Watson, D. J.; Gorosabel, J.; Michałowski, M. J.; Thöne, C. C.; Augusteijn, T.; Bersier, D.; Jakobsson, P.; Jaunsen, A. O.; Ledoux, C.; Levan, A. J.; Milvang-Jensen, B.; Rol, E.; Tanvir, N. R.; Wiersema, K.; Xu, D.; Albert, L.; Bayliss, M.; Gall, C.; Grove, L. F.; Koester, B. P.; Leitet, E.; Pursimo, T.; Skillen, I. (2009): *Early Spectroscopic Identification of SN 2008D.* ApJL, 692, 84-87

- Zheng, C.; Romani, R. W.; Sako, M.; Marriner, J.; Bassett, B.; Becker, A.; Choi, C.; Cinabro, D.; DeJongh, F.; Depoy, D. L.; Dilday, B.; Doi, M.; Frieman, J. A.; Garnavich, P. M.; Hogan, C. J.; Holtzman, J.; Im, M.; Jha, S.; Kessler, R.; Konishi, K.; Lampeitl, H.; Marshall, J. L.; McGinnis, D.; Miknaitis, G.; Nichol, R. C.; Prieto, J. L.; Riess, A. G.; Richmond, M. W.; Schneider, D. P.; Smith, M.; Takanashi, N.; Tokita, K.; van der Heyden, K.; Yasuda, N.; Assef, R. J.; Barentine, J.; Bender, R.; Blandford, R. D.; Bremer, M.; Brewington, H.; Collins, C. A.; Crotts, A.; Dembicky, J.; Eastman, J.; Edge, A.; Elson, E.; Eyler, M. E.; Filippenko, A. V.; Foley, R. J.; Frank, S.; Goobar,

A.; Harvanek, M.; Hopp, U.; Ihara, Y.; Kahn, S.; Ketzeback, W.; Kleinman, S. J.; Kollatschny, W.; Krzesinski, J.; **Leloudas, G.**; Long, D. C.; Lucey, J.; Malanushenko, E.; Malanushenko, V.; McMillan, R. J.; Morgan, C. W.; Morokuma, T.; Nitta, A.; Ostman, L.; Pan, K.; Romer, A. K.; Saurage, G.; Schlesinger, K.; Snedden, S. A.; Sollerman, J.; Stritzinger, M.; Watson, L. C.; Watters, S.; Wheeler, J. C.; York, D. (2008): *First-Year Spectroscopy for the Sloan Digital Sky Survey-II Supernova Survey.* AJ, 135, 1766-1784.

- Frieman, J. A.; Bassett, B.; Becker, A.; Choi, C.; Cinabro, D.; DeJongh, F.; Depoy, D. L.; Dilday, B.; Doi, M.; Garnavich, P. M.; Hogan, C. J.; Holtzman, J.; Im, M.; Jha, S.; Kessler, R.; Konishi, K.; Lampeitl, H.; Marriner, J.; Marshall, J. L.; McGinnis, D.; Miknaitis, G.; Nichol, R. C.; Prieto, J. L.; Riess, A. G.; Richmond, M. W.; Romani, R.; Sako, M.; Schneider, D. P.; Smith, M.; Takanashi, N.; Tokita, K.; van der Heyden, K.; Yasuda, N.; Zheng, C.; Adelman-McCarthy, J.; Annis, J.; Assef, R. J.; Barentine, J.; Bender, R.; Blandford, R. D.; Boroski, W. N.; Bremer, M.; Brewington, H.; Collins, C. A.; Crotts, A.; Dembicky, J.; Eastman, J.; Edge, A.; Edmondson, E.; Elson, E.; Eyler, M. E.; Filippenko, A. V.; Foley, R. J.; Frank, S.; Goobar, A.; Gueth, T.; Gunn, J. E.; Harvanek, M.; Hopp, U.; Ihara, Y.; Ivezic, Z.; Kahn, S.; Kaplan, J.; Kent, S.; Ketzeback, W.; Kleinman, S. J.; Kollatschny, W.; Kron, R. G.; Krzesinski, J.; Lamenti, D.; **Leloudas, G.**; Lin, H.; Long, D. C.; Lucey, J.; Lupton, R. H.; Malanushenko, E.; Malanushenko, V.; McMillan, R. J.; Mendez, J.; Morgan, C. W.; Morokuma, T.; Nitta, A.; Ostman, L.; Pan, K.; Rockosi, C. M.; Romer, A. K.; Ruiz-Lapuente, P.; Saurage, G.; Schlesinger, K.; Snedden, S. A.; Sollerman, J.; Stoughton, C.; Stritzinger, M.; Subba Rao, M.; Tucker, D.; Vaisanen, P.; Watson, L. C.; Watters, S.; Wheeler, J. C.; Yanny, B.; York, D. (2008): *The Sloan Digital Sky Survey-II Supernova Survey: Technical Summary.* AJ, 135, 338-347.

Conference proceedings

- **Leloudas, G.**; Stritzinger, M.; Sollerman, J.; Hamuy, M.; Suntzeff, N. (2009): *The Type Ia SN 2003hv: Focus on Late Times.* AIP Conference Proceedings, Volume 1111, pp. 456-459
- Malesani, D.; Fynbo, J. P. U.; Hjorth, J.; **Leloudas, G.**; Sollerman, J.; Stritzinger, M. D.; Vreeswijk, P. M.; Watson, D. J.; Gorosabel, J.; Michałowski, M. J.; Thöne, C. C. (2009): *Early and late spectroscopy of SN 2008D.* AIP Conference Proceedings, 1111, 627-628.
- Thöne, C. C.; Michałowski, M. J.; **Leloudas, G.**; Cox, N. L. J.; Fynbo, J. P. U.; Hjorth, J.; Sollerman, J. (2009): *NGC 2770-a SN Ib factory?* AIP Conference Proceedings, 1111, 532-535.

Astronomical telegrams and circulars

- Malesani, D.; Tanvir, N. R.; Xu, D.; **Leloudas, G.**; Jakobsson, P.; Somero, A.; Katajainen, S. (2010): *GRB100213B: NOT Optical Observations* (GCN 10413)
- Malesani, D.; **Leloudas, G.**; Fynbo, J. P. U.; Xu, D.; Jakobsson, P.; Somero, A.; Katajainen, S.; Pursimo, T. (2010): *GRB100212A: Candidate Optical Afterglow* (GCN 10402)
- **Leloudas, G.**; Xu, D.; Malesani, D.; Levan A. J.; Jakobsson, P.; & Djupvik, A. A. (2010): *GRB100206A: NOT NIR Observations* (GCN 10387)
- Levan A. J.; Tanvir, N. R.; Wiersema K.; Niederste-Ostholt M.; Malesani, D.; **Leloudas, G.**; & Xu, D. (2010): *GRB100206A: WHT Candidate Afterglow* (GCN 10386)
- Xu, D.; Malesani, D.; **Leloudas, G.**; Fynbo, J. P. U.; Djupvik, A. A.; Karjalainen, R.; Tanvir N. R.; & Jakobsson, P. (2010): *GRB100117A: Possible Afterglow from NOT Observation* (GCN 10337)

- Xu, D.; **Leloudas, G.**; Malesani, D.; Jakobsson, P.; Lindberg, J.; Andersen, J. (2009): *GRB091208B: NOT Optical Observations* (GCN 10269)
- Xu, D.; Fynbo, J. P. U.; Tanvir, N. R.; Hjorth, J.; **Leloudas, G.**; Malesani, D.; Jakobsson, P.; Wilson P. A.; Andersen, J. (2009): *GRB091020: NOT Spectroscopic Redshift* (GCN 10053)
- Xu, D.; **Leloudas, G.**; Fynbo, J. P. U.; Malesani, D.; Jakobsson, P.; Furesz, G. (2009): *GRB 090809: further NOT optical observations* (GCN 9766)
- Xu, D.; **Leloudas, G.**; Malesani, D.; Fynbo, J. P. U.; Jakobsson, P.; Furesz, G. (2009): *GRB 090809: afterglow confirmation at the NOT.* (GCN 9755)
- Malesani, D.; Telting, J.; Wilson, P.; Jakobsson, P.; Fynbo, J. P. U.; **Leloudas, G.**; Levan, A. J.; Wiersema, K. (2009): *GRB 090709A: NOT optical observations.* (GCN 9644)
- Xu, D.; **Leloudas, G.**; Malesani, D.; Fynbo, J. P. U.; Hjorth, J.; Jakobsson, P.; Liimets, T. (2009): *GRB 090530: further NOT optical observations.* (GCN 9488)
- Xu, D.; **Leloudas, G.**; Malesani, D.; Fynbo, J. P. U.; Maund, J.; Jakobsson, P.; Liimets, T. (2009): *GRB090529: further NOT optical observations.* (GCN 9482)
- **Leloudas, G.**; Malesani, D.; Xu, D.; Fynbo, J. P. U.; Jakobsson, P.; Brown, M. E.; Schaller, E. L.; Liimets, T. (2009): *GRB 090529: NOT optical observations.* (GCN 9453)
- Malesani, D.; Xu, D.; **Leloudas, G.**; Fynbo, J. P. U.; Jakobsson, P.; Brown, M. E.; Schaller, E. L.; Liimets, T. (2009): *GRB 090530: NOT optical observations.* (GCN 9452)
- **Leloudas, G.**; Fynbo, J.; Sollerman, J. (2008): *Supernovae 2008et and 2008eu* (CBET 1476)
- Malesani, D.; Fynbo, J. P. U.; **Leloudas, G.**; Pedersen, H.; Jakobsson, P.; Niemi, S.-M.; Uthas, H.; Villforth, C. (2008): *GRB 081128: afterglow observations.* (GCN 8639)
- Malesani, D.; Sollerman, J.; Fynbo, J. P. U.; Thöne, C. C.; Xu, D.; Hjorth, J.; **Leloudas, G.**; Vreeswijk, P. M.; Watson, D. J.; Jakobsson, P.; Augusteijn, T.; Villforth, C.; Niemi, S.-M. (2008): *XRF 080109 / SN 2008D: spectroscopic evolution.* (GCN 7184)
- Bassett, B. et al. (61 co-authors) (2007): *Supernovae 2007rg and 2007sb-2007sn* (CBET 1167)
- Bassett, B. et al. (57 co-authors) (2007): *Supernovae 2007qz and 2007rc-2007rs* (CBET 1146)
- Sollerman, J.; **Leloudas, G.** (2007): *Supernova 2007rb in NGC 2889* (CBET 1141)
- Bassett, B. et al. (72 co-authors) (2007): *Supernovae 2007qf-2007ra* (CBET 1139)
- Bassett, B. et al. (55 co-authors) (2007): *Supernova 2007qd* (CBET 1137)
- Bassett, B. et al. (60 co-authors) (2007): *Supernovae 2007pn-2007qb* (CBET 1135)
- Bassett, B. et al. (71 co-authors) (2007): *Supernovae 2007oq-2007pj* (CBET 1128)
- Bassett, B. et al. (59 co-authors) (2007): *Supernovae 2007oe-2007om* (CBET 1117)
- Bassett, B. et al. (59 co-authors) (2007): *Supernovae 2007lx and 2007nr-2007oa* (CBET 1109)
- Bassett, B. et al. (71 co-authors) (2007): *Supernovae 2007md and 2007mr-2007nl* (CBET 1104)
- Bassett, B. et al. (70 co-authors) (2007): *Supernovae 2007lf-2007mp* (CBET 1102)

- Sollerman, J.; **Leloudas, G.**; Jakobsson, P.; Fynbo, J. P. U.; Malesani, D.; Vreeswijk, P. (2007): *GRB071112C: NOT observations.* (GCN 7070)
- Stritzinger, M.; Sollerman, J.; Goobar, A.; Nichol, R.; Smith, M.; **Leloudas, G.** (2006): *Supernovae 2006oy-2006qm* (CBET 762)
- Bassett, B. et al. (59 co-authors) (2006): *Supernovae 2006ns-2006ob* (CBET 743)

BIBLIOGRAPHY

Akerlof, C. W., Kehoe, R. L., McKay, T. A., Rykoff, E. S., Smith, D. A., Casperson, D. E., McGowan, K. E., Vestrand, W. T., Wozniak, P. R., Wren, J. A., Ashley, M. C. B., Phillips, M. A., Marshall, S. L., Epps, H. W., & Schier, J. A. 2003, PASP, 115, 132

Alard, C. 2000, A&AS, 144, 363

Aldering, G., Antilogus, P., Bailey, S., Baltay, C., Bauer, A., Blanc, N., Bongard, S., Copin, Y., Gangler, E., Gilles, S., Kessler, R., Kocevski, D., Lee, B. C., Loken, S., Nugent, P., Pain, R., Pécontal, E., Pereira, R., Perlmutter, S., Rabinowitz, D., Rigaudier, G., Scalzo, R., Smadja, G., Thomas, R. C., Wang, L., & Weaver, B. A. 2006, ApJ, 650, 510

Amati, L., Frontera, F., Tavani, M., in't Zand, J. J. M., Antonelli, A., Costa, E., Feroci, M., Guidorzi, C., Heise, J., Masetti, N., Montanari, E., Nicastro, L., Palazzi, E., Pian, E., Piro, L., & Soffitta, P. 2002, A&A, 390, 81

Anderson, J. P. & James, P. A. 2008, MNRAS, 390, 1527

—. 2009, MNRAS, 399, 559

Arnaboldi, M., Neeser, M. J., Parker, L. C., Rosati, P., Lombardi, M., Dietrich, J. P., & Hummel, W. 2007, The Messenger, 127, 28

Arnett, W. D. 1982, ApJ, 253, 785

Arnett, W. D., Bahcall, J. N., Kirshner, R. P., & Woosley, S. E. 1989, ARA&A, 27, 629

Astier, P., Guy, J., Regnault, N., Pain, R., Aubourg, E., Balam, D., Basa, S., Carlberg, R. G., Fabbro, S., Fouchez, D., Hook, I. M., Howell, D. A., Lafoux, H., Neill, J. D., Palanque-Delabrouille, N., Perrett, K., Pritchet, C. J., Rich, J., Sullivan, M., Taillet, R., Aldering, G., Antilogus, P., Arsenijevic, V., Balland, C., Baumont, S., Bronder, J., Courtois, H., Ellis, R. S., Filiol, M., Gonçalves, A. C., Goobar, A., Guide, D., Hardin, D., Lusset, V., Lidman, C., McMahon, R., Mouchet, M., Mourao, A., Perlmutter, S., Ripoche, P., Tao, C., & Walton, N. 2006, A&A, 447, 31

Axelrod, T. S. 1980, PhD thesis, California Univ., Santa Cruz.

Baade, W. & Zwicky, F. 1934a, Proceedings of the National Academy of Science, 20, 259

—. 1934b, Proceedings of the National Academy of Science, 20, 254

Bahcall, J. N. & Soneira, R. M. 1981, ApJS, 47, 357

Barbon, R., Cappellaro, E., & Turatto, M. 1989, A&AS, 81, 421

Barker, E., Dahlen, T., Koekemoer, A., L. Bergeron, R. de Jong, McLaughlin, H., Pirzkal, N., Shaw, B., & Wiklind, T. 2007, NICMOS Instrument Handbook, Version 10.0, Baltimore: STScI

Baron, E., Nugent, P. E., Branch, D., & Hauschildt, P. H. 2004, ApJ, 616, L91

Bassett, B., Becker, A., Bizyaev, D., Brewington, H., Choi, C., Cinabro, D., D'Andrea, C., Dembicky, J., Depoy, D. L., Dilday, B., Doi, M., Eastman, J., Frieman, J., Garnavich, P., Goobar, A., Hogan, C., Holtzman, J., Im, M., Jha, S., Kessler, R., Ketzeback, B., Konishi, K., Krzesinski, J., Lampeitl, H., Leloudas, G., Long, D., Malanushenko, O., Marriner, J., McMillan, R., Miknaitis, G., Morokuma, T., Mosher, J., Nichol, R., Oravetz, D., Pan, K., Ostman, L., Prieto, J. L., Richmond, M., Riess, A., Romani, R., Sako, M., Schneider, D., Simmons, A., Smith, M., Snedden, S., Sollerman, J., Stritzinger, M., Takanashi, N., Tokita, K., Taylor, M. F., van der Heyden, K., Watters, S., Yasuda, N., Wheeler, C., Zheng, C., Filippenko, A. V., Silverman, J. M., Foley, R. J., Modjaz, M., Bremer, M., Turatto, M., Ruiz-Lapuente, P., Castander, F., Romer, A. K., Collins, C., Lucey, J., Edge, A., Bender, R., Hopp, U., Kollatschny, W., & McGinnis, D. 2007, Central Bureau Electronic Telegrams, 1104, 1

Benetti, S., Cappellaro, E., Mazzali, P. A., Turatto, M., Altavilla, G., Bufano, F., Elias-Rosa, N., Kotak, R., Pignata, G., Salvo, M., & Stanishev, V. 2005, ApJ, 623, 1011

Benetti, S., Cappellaro, E., Turatto, M., Taubenberger, S., Harutyunyan, A., & Valenti, S. 2006, ApJ, 653, L129

Benetti, S., Meikle, P., Stehle, M., Altavilla, G., Desidera, S., Folatelli, G., Goobar, A., Mattila, S., Mendez, J., Navasardyan, H., Pastorello, A., Patat, F., Riello, M., Ruiz-Lapuente, P., Tsvetkov, D., Turatto, M., Mazzali, P., & Hillebrandt, W. 2004, MNRAS, 348, 261

Berger, E. 2009, ApJ, 690, 231

Berger, E. & Soderberg, A. M. 2008, GRB Coordinates Network, 7159, 1

Bertin, E. & Arnouts, S. 1996, A&AS, 117, 393

Bessell, M. S. 1990, PASP, 102, 1181

Beutler, B. & Li, W. 2003, IAU Circ., 8197, 1

Blondin, S., Matheson, T., & Modjaz, M. 2008, GRB Coordinates Network, 7173, 1

Blondin, S. & Tonry, J. L. 2007, ApJ, 666, 1024

Bloom, J. S., Kulkarni, S. R., & Djorgovski, S. G. 2002, AJ, 123, 1111

Bloom, J. S., Prochaska, J. X., Lee, W., Jesús González, J., Ramírez-Ruiz, E., Bolte, M., Franco, J., Guichard, J., Carramiñana, A., Strittmatter, P., Avila-Reese, V., Bernstein, R., Bigelow, B., Brodwin, M., Burgasser, A., Butler, N., Chávez, M., Cobb, B., Cook, K., Cruz-González, I., de Diego, J. A., Farah, A., Georgiev, L., Girard, J., Hernández-Toledo, H., Jiménez-Bailón, E., Krongold, Y., Mayya, D., Meza, J., Miyaji, T., Mújica, R., Nugent, P., Porras, A., Poznanski, D., Raga, A., Richer, M., Rodríguez, L., Rosa, D., Stanford, A., Szentgyorgyi, A., Tenorio-Tagle, G., Thomas, R., Valenzuela, O., Watson, A. M., & Wehinger, P. 2009, ArXiv e-prints

Boissier, S. & Prantzos, N. 2009, A&A, 503, 137

Botticella, M. T., Riello, M., Cappellaro, E., Benetti, S., Altavilla, G., Pastorello, A., Turatto, M., Greggio, L., Patat, F., Valenti, S., Zampieri, L., Harutyunyan, A., Pignata, G., & Taubenberger, S. 2008, A&A, 479, 49

Branch, D., Dang, L. C., & Baron, E. 2009, PASP, 121, 238

Brandt, T. D., Tojeiro, R., Aubourg, É., Heavens, A., Jimenez, R., & Strauss, M. A. 2010, ArXiv e-prints

Breysacher, J., Azzopardi, M., & Testor, G. 1999, A&AS, 137, 117

Bromm, V. & Loeb, A. 2006, ApJ, 642, 382

Brown, P. J., Holland, S. T., Immler, S., Milne, P., Roming, P. W. A., Gehrels, N., Nousek, J., Panagia, N., Still, M., & Vanden Berk, D. 2009, AJ, 137, 4517

Bruzual, G. & Charlot, S. 2003, MNRAS, 344, 1000

Bufano, F., Benetti, S., Cappellaro, E., Covino, S., Vergani, S., Goldoni, P., Della Valle, M., Pian, E., Campana, S., Tagliaferri, G., Malesani, D., Fynbo, J., Turatto, M., Patat, F., & Mazzali, P. 2010, Central Bureau Electronic Telegrams, 2227, 1

Bufano, F., Immler, S., Turatto, M., Landsman, W., Brown, P., Benetti, S., Cappellaro, E., Holland, S. T., Mazzali, P., Milne, P., Panagia, N., Pian, E., Roming, P., Zampieri, L., Breeveld, A. A., & Gehrels, N. 2009, ApJ, 700, 1456

Burns et al. 2010, in preparation

Campana, S., Mangano, V., Blustin, A. J., Brown, P., Burrows, D. N., Chincarini, G., Cummings, J. R., Cusumano, G., Della Valle, M., Malesani, D., Mészáros, P., Nousek, J. A., Page, M., Sakamoto, T., Waxman, E., Zhang, B., Dai, Z. G., Gehrels, N., Immler, S., Marshall, F. E., Mason, K. O., Moretti, A., O'Brien, P. T., Osborne, J. P., Page, K. L., Romano, P., Roming, P. W. A., Tagliaferri, G., Cominsky, L. R., Giommi, P., Godet, O., Kennea, J. A., Krimm, H., Angelini, L., Barthelmy, S. D., Boyd, P. T., Palmer, D. M., Wells, A. A., & White, N. E. 2006, Nature, 442, 1008

Cappellaro, E., Evans, R., & Turatto, M. 1999, A&A, 351, 459

Cappellaro, E., Mazzali, P. A., Benetti, S., Danziger, I. J., Turatto, M., della Valle, M., & Patat, F. 1997, A&A, 328, 203

Cappellaro, E., Patat, F., Mazzali, P. A., Benetti, S., Danziger, J. I., Pastorello, A., Rizzi, L., Salvo, M., & Turatto, M. 2001, ApJ, 549, L215

Castro Cerón, J. M., Michałowski, M. J., Hjorth, J., Malesani, D., Gorosabel, J., Watson, D., & Fynbo, J. P. U. 2008, ArXiv e-prints

Chan, K. & Lingenfelter, R. E. 1993, ApJ, 405, 614

Chevalier, R. A. & Fransson, C. 2006, ApJ, 651, 381

—. 2008, ApJ, 683, L135

Chornock, R., Soderberg, A. M., Foley, R. J., Berger, E., Frebel, A., Challis, P., Simon, J. D., & Sheppard, S. 2010, Central Bureau Electronic Telegrams, 2228, 1

Christensen, L., Vreeswijk, P. M., Sollerman, J., Thöne, C. C., Le Floc'h, E., & Wiersema, K. 2008, A&A, 490, 45

Chugai, N. N. 2008, Astronomy Letters, 34, 389

Cid Fernandes, R., Mateus, A., Sodré, L., Stasińska, G., & Gomes, J. M. 2005, MNRAS, 358, 363

Clark, D. H. & Stephenson, F. R. 1977, The historical supernovae, ed. Clark, D. H. & Stephenson, F. R.

Colgate, S. A., Petschek, A. G., & Kriese, J. T. 1980, ApJ, 237, L81

Contreras, C., Hamuy, M., Phillips, M. M., Folatelli, G., Suntzeff, N. B., Persson, S. E., Stritzinger, M., Boldt, L., González, S., Krzeminski, W., Morrell, N., Roth, M., Salgado, F., José Maureira, M., Burns, C. R., Freedman, W. L., Madore, B. F., Murphy, D., Wyatt, P., Li, W., & Filippenko, A. V. 2010, AJ, 139, 519

Cooke, J. 2008, ApJ, 677, 137

Cooke, J., Sullivan, M., Barton, E. J., Bullock, J. S., Carlberg, R. G., Gal-Yam, A., & Tollerud, E. 2009, Nature, 460, 237

Cooper, M. C., Newman, J. A., & Yan, R. 2009, ApJ, 704, 687

Costa, E., Frontera, F., Heise, J., Feroci, M., in't Zand, J., Fiore, F., Cinti, M. N., Dal Fiume, D., Nicastro, L., Orlandini, M., Palazzi, E., Rapisarda#, M., Zavattini, G., Jager, R., Parmar, A., Owens, A., Molendi, S., Cusumano, G., Maccarone, M. C., Giarrusso, S., Coletta, A., Antonelli, L. A., Giommi, P., Muller, J. M., Piro, L., & Butler, R. C. 1997, Nature, 387, 783

Crockett, R. M., Eldridge, J. J., Smartt, S. J., Pastorello, A., Gal-Yam, A., Fox, D. B., Leonard, D. C., Kasliwal, M. M., Mattila, S., Maund, J. R., Stephens, A. W., & Danziger, I. J. 2008a, MNRAS, 391, L5

Crockett, R. M., Maund, J. R., Smartt, S. J., Mattila, S., Pastorello, A., Smoker, J., Stephens, A. W., Fynbo, J., Eldridge, J. J., Danziger, I. J., & Benn, C. R. 2008b, ApJ, 672, L99

Crockett, R. M., Smartt, S. J., Eldridge, J. J., Mattila, S., Young, D. R., Pastorello, A., Maund, J. R., Benn, C. R., & Skillen, I. 2007, MNRAS, 381, 835

Crotts, A. P. S. & Yourdon, D. 2008, ApJ, 689, 1186

Crowther, P. A. 2007, ARA&A, 45, 177

Crowther, P. A., Hadfield, L. J., Schild, H., & Schmutz, W. 2004, A&A, 419, L17

Dahlen, T., Strolger, L., & Riess, A. G. 2008, ApJ, 681, 462

Dahlen, T., Strolger, L., Riess, A. G., Mobasher, B., Chary, R., Conselice, C. J., Ferguson, H. C., Fruchter, A. S., Giavalisco, M., Livio, M., Madau, P., Panagia, N., & Tonry, J. L. 2004, ApJ, 613, 189

D'Andrea, C. B., Sako, M., Dilday, B., Frieman, J. A., Holtzman, J., Kessler, R., Konishi, K., Schneider, D. P., Sollerman, J., Wheeler, J. C., Yasuda, N., Cinabro, D., Jha, S., Nichol, R. C., Lampeitl, H., Smith, M., Atlee, D. W., Basset, B., Castander, F. J., Goobar, A., Miquel, R., Nordin, J., Östman, L., Prieto, J. L., Quimby, R., Riess, A. G., & Stritzinger, M. 2009, ArXiv e-prints

Della Valle, M., Chincarini, G., Panagia, N., Tagliaferri, G., Malesani, D., Testa, V., Fugazza, D., Campana, S., Covino, S., Mangano, V., Antonelli, L. A., D'Avanzo, P., Hurley, K., Mirabel, I. F., Pellizza, L. J., Piranomonte, S., & Stella, L. 2006, Nature, 444, 1050

Della Valle, M., Malesani, D., Benetti, S., Testa, V., Hamuy, M., Antonelli, L. A., Chincarini, G., Cocozza, G., Covino, S., D'Avanzo, P., Fugazza, D., Ghisellini, G., Gilmozzi, R., Lazzati, D., Mason, E., Mazzali, P., & Stella, L. 2003, A&A, 406, L33

Della Valle, M., Panagia, N., Padovani, P., Cappellaro, E., Mannucci, F., & Turatto, M. 2005, ApJ, 629, 750

Deng, J. & Zhu, Y. 2008, GRB Coordinates Network, 7160, 1

Dessart, L. & Hillier, D. J. 2005, A&A, 439, 671

Devillard, N. 1999, in Astronomical Society of the Pacific Conference Series, Vol. 172, Astronomical Data Analysis Software and Systems VIII, ed. D. M. Mehringer, R. L. Plante, & D. A. Roberts, 333–+

Dilday, B., Kessler, R., Frieman, J. A., Holtzman, J., Marriner, J., Miknaitis, G., Nichol, R. C., Romani, R., Sako, M., Bassett, B., Becker, A., Cinabro, D., DeJongh, F., Depoy, D. L., Doi, M., Garnavich, P. M., Hogan, C. J., Jha, S., Konishi, K., Lampeitl, H., Marshall, J. L., McGinnis, D., Prieto, J. L., Riess, A. G., Richmond, M. W., Schneider, D. P., Smith, M., Takanashi, N., Tokita, K., van der Heyden, K., Yasuda, N., Zheng, C., Barentine, J., Brewington, H., Choi, C., Crotts, A., Dembicky, J., Harvanek, M., Im, M., Ketzeback, W., Kleinman, S. J., Krzesiński, J., Long, D. C., Malanushenko, E., Malanushenko, V., McMillan, R. J., Nitta, A., Pan, K., Saurage, G., Snedden, S. A., Watters, S., Wheeler, J. C., & York, D. 2008, ApJ, 682, 262

Drake, A. J., Djorgovski, S. G., Mahabal, A., Beshore, E., Larson, S., Graham, M. J., Williams, R., Christensen, E., Catelan, M., Boattini, A., Gibbs, A., Hill, R., & Kowalski, R. 2009, ApJ, 696, 870

Dressler, A., Phillips, M., Morrell, N., & Hamuy, M. 2003, IAU Circ., 8198, 2

Drout, M. R., Massey, P., Meynet, G., Tokarz, S., & Caldwell, N. 2009, ApJ, 703, 441

Eichler, D., Livio, M., Piran, T., & Schramm, D. N. 1989, Nature, 340, 126

Eisenstein, D. J., Zehavi, I., Hogg, D. W., Scoccimarro, R., Blanton, M. R., Nichol, R. C., Scranton, R., Seo, H., Tegmark, M., Zheng, Z., Anderson, S. F., Annis, J., Bahcall, N., Brinkmann, J., Burles, S., Castander, F. J., Connolly, A., Csabai, I., Doi, M., Fukugita, M., Frieman, J. A., Glazebrook, K., Gunn, J. E., Hendry, J. S., Hennessy, G., Ivezić, Z., Kent, S., Knapp, G. R., Lin, H., Loh, Y., Lupton, R. H., Margon, B., McKay, T. A., Meiksin, A., Munn, J. A., Pope, A., Richmond, M. W., Schlegel, D., Schneider, D. P., Shimasaku, K., Stoughton, C., Strauss, M. A., SubbaRao, M., Szalay, A. S., Szapudi, I., Tucker, D. L., Yanny, B., & York, D. G. 2005, ApJ, 633, 560

Eldridge, J. J., Izzard, R. G., & Tout, C. A. 2008, MNRAS, 384, 1109

Elias, J. H., Matthews, K., Neugebauer, G., & Persson, S. E. 1985, ApJ, 296, 379

Filippenko, A. V. 1997, ARA&A, 35, 309

Filippenko, A. V., Barth, A. J., Matheson, T., Armus, L., Brown, M., Espey, B. R., Fan, X., Goodrich, R. W., Ho, L. C., Junkkarinen, V. T., Koo, D. C., Lehnert, M. D., Martel, A. R., Mazzarella, J. M., Miller, J. S., Smith, G. H., Tytler, D., & Wirth, G. D. 1995, ApJ, 450, L11+

Filippenko, A. V., Li, W. D., Treffers, R. R., & Modjaz, M. 2001, in Astronomical Society of the Pacific Conference Series, Vol. 246, IAU Colloq. 183: Small Telescope Astronomy on Global Scales, ed. B. Paczynski, W.-P. Chen, & C. Lemme, 121–+

Filippenko, A. V., Matheson, T., & Ho, L. C. 1993, ApJ, 415, L103+

Filippenko, A. V., Richmond, M. W., Branch, D., Gaskell, M., Herbst, W., Ford, C. H., Treffers, R. R., Matheson, T., Ho, L. C., Dey, A., Sargent, W. L. W., Small, T. A., & van Breugel, W. J. M. 1992a, AJ, 104, 1543

Filippenko, A. V., Richmond, M. W., Matheson, T., Shields, J. C., Burbidge, E. M., Cohen, R. D., Dickinson, M., Malkan, M. A., Nelson, B., Pietz, J., Schlegel, D., Schmeer, P., Spinrad, H., Steidel, C. C., Tran, H. D., & Wren, W. 1992b, ApJ, 384, L15

Folatelli, G., Contreras, C., Phillips, M. M., Woosley, S. E., Blinnikov, S., Morrell, N., Suntzeff, N. B., Lee, B. L., Hamuy, M., González, S., Krzeminski, W., Roth, M., Li, W., Filippenko, A. V., Foley, R. J., Freedman, W. L., Madore, B. F., Persson, S. E., Murphy, D., Boissier, S., Galaz, G., González, L., McCarthy, P. J., McWilliam, A., & Pych, W. 2006, ApJ, 641, 1039

Folatelli, G., Phillips, M. M., Burns, C. R., Contreras, C., Hamuy, M., Freedman, W. L., Persson, S. E., Stritzinger, M., Suntzeff, N. B., Krisciunas, K., Boldt, L., González, S., Krzeminski, W., Morrell, N., Roth, M., Salgado, F., Madore, B. F., Murphy, D., Wyatt, P., Li, W., Filippenko, A. V., & Miller, N. 2010, AJ, 139, 120

Foley, R. J., Chornock, R., Filippenko, A. V., Ganeshalingam, M., Kirshner, R. P., Li, W., Cenko, S. B., Challis, P. J., Friedman, A. S., Modjaz, M., Silverman, J. M., & Wood-Vasey, W. M. 2009, AJ, 138, 376

Foley, R. J., Filippenko, A. V., & Jha, S. W. 2008, ApJ, 686, 117

Fransson, C. & Kozma, C. 1993, ApJ, 408, L25

Freedman, W. L., Burns, C. R., Phillips, M. M., Wyatt, P., Persson, S. E., Madore, B. F., Contreras, C., Folatelli, G., Gonzalez, E. S., Hamuy, M., Hsiao, E., Kelson, D. D., Morrell, N., Murphy, D. C., Roth, M., Stritzinger, M., Sturch, L., Suntzeff, N. B., Astier, P., Balland, C., Bassett, B., Boldt, L., Carlberg, R. G., Conley, A. J., Frieman, J. A., Garnavich, P. M., Guy, J., Hardin, D., Howell, D. A., Kessler, R., Lampeitl, H., Marriner, J., Pain, R., Perrett, K., Regnault, N., Riess, A. G., Sako, M., Schneider, D. P., Sullivan, M., & Wood-Vasey, M. 2009, ApJ, 704, 1036

Freedman, W. L., Madore, B. F., Gibson, B. K., Ferrarese, L., Kelson, D. D., Sakai, S., Mould, J. R., Kennicutt, Jr., R. C., Ford, H. C., Graham, J. A., Huchra, J. P., Hughes, S. M. G., Illingworth, G. D., Macri, L. M., & Stetson, P. B. 2001, ApJ, 553, 47

Frieman, J. A., Bassett, B., Becker, A., Choi, C., Cinabro, D., DeJongh, F., Depoy, D. L., Dilday, B., Doi, M., Garnavich, P. M., Hogan, C. J., Holtzman, J., Im, M., Jha, S., Kessler, R., Konishi, K., Lampeitl, H., Marriner, J., Marshall, J. L., McGinnis, D., Miknaitis, G., Nichol, R. C., Prieto, J. L., Riess, A. G., Richmond, M. W., Romani, R., Sako, M., Schneider, D. P., Smith, M., Takanashi, N., Tokita, K., van der Heyden, K., Yasuda, N., Zheng, C., Adelman-McCarthy, J., Annis, J., Assef, R. J., Barentine, J., Bender, R., Blandford, R. D., Boroski, W. N., Bremer, M., Brewington, H., Collins, C. A., Crotts, A., Dembicky, J., Eastman, J., Edge, A., Edmondson, E., Elson, E., Eyler, M. E., Filippenko, A. V., Foley, R. J., Frank, S., Goobar, A., Gueth, T., Gunn, J. E., Harvanek, M., Hopp, U., Ihara, Y., Ivezić, Ž., Kahn, S., Kaplan, J., Kent, S., Ketzeback, W., Kleinman, S. J., Kollatschny, W., Kron, R. G., Krzesiński, J., Lamenti, D., Leloudas, G., Lin, H., Long, D. C., Lucey, J., Lupton, R. H., Malanushenko, E., Malanushenko, V., McMillan, R. J., Mendez, J., Morgan, C. W., Morokuma, T., Nitta, A., Ostman, L., Pan, K., Rockosi, C. M., Romer, A. K., Ruiz-Lapuente, P., Saurage, G., Schlesinger, K., Snedden, S. A., Sollerman, J., Stoughton, C., Stritzinger, M., Subba Rao, M., Tucker, D., Vaisanen, P., Watson, L. C., Watters, S., Wheeler, J. C., Yanny, B., & York, D. 2008, AJ, 135, 338

Fruchter, A. S., Levan, A. J., Strolger, L., Vreeswijk, P. M., Thorsett, S. E., Bersier, D., Burud, I., Castro Cerón, J. M., Castro-Tirado, A. J., Conselice, C., Dahlen, T., Ferguson, H. C., Fynbo, J. P. U., Garnavich, P. M., Gibbons, R. A., Gorosabel, J., Gull, T. R., Hjorth, J., Holland, S. T., Kouveliotou, C., Levay, Z., Livio, M., Metzger, M. R., Nugent, P. E., Petro, L., Pian, E., Rhoads, J. E., Riess, A. G., Sahu, K. C., Smette, A., Tanvir, N. R., Wijers, R. A. M. J., & Woosley, S. E. 2006, Nature, 441, 463

Fryer, C. L., Mazzali, P. A., Prochaska, J., Cappellaro, E., Panaitescu, A., Berger, E., van Putten, M., van den Heuvel, E. P. J., Young, P., Hungerford, A., Rockefeller, G., Yoon, S.-C., Podsiadlowski, P., Nomoto, K., Chevalier, R., Schmidt, B., & Kulkarni, S. 2007, PASP, 119, 1211

Fynbo, J. P. U., Jakobsson, P., Prochaska, J. X., Malesani, D., Ledoux, C., de Ugarte Postigo, A., Nardini, M., Vreeswijk, P. M., Wiersema, K., Hjorth, J., Sollerman, J., Chen, H., Thöne, C. C., Björnsson, G., Bloom, J. S., Castro-Tirado, A. J., Christensen, L., De Cia, A., Fruchter, A. S., Gorosabel, J., Graham, J. F., Jaunsen, A. O., Jensen, B. L., Kann, D. A., Kouveliotou, C., Levan, A. J., Maund, J., Masetti, N., Milvang-Jensen, B., Palazzi, E., Perley, D. A., Pian, E., Rol, E., Schady, P., Starling, R. L. C., Tanvir, N. R., Watson, D. J., Xu, D., Augusteijn, T., Grundahl, F., Telting, J., & Quirion, P. 2009, ApJS, 185, 526

Fynbo, J. P. U., Watson, D., Thöne, C. C., Sollerman, J., Bloom, J. S., Davis, T. M., Hjorth, J., Jakobsson, P., Jørgensen, U. G., Graham, J. F., Fruchter, A. S., Bersier, D., Kewley, L., Cassan, A., Castro Cerón, J. M., Foley, S., Gorosabel, J., Hinse, T. C., Horne, K. D., Jensen, B. L., Klose, S., Kocevski, D., Marquette, J., Perley, D., Ramirez-Ruiz, E., Stritzinger, M. D., Vreeswijk, P. M., Wijers, R. A. M., Woller, K. G., Xu, D., & Zub, M. 2006, Nature, 444, 1047

Gal-Yam, A., Fox, D. B., Price, P. A., Ofek, E. O., Davis, M. R., Leonard, D. C., Soderberg, A. M., Schmidt, B. P., Lewis, K. M., Peterson, B. A., Kulkarni, S. R., Berger, E., Cenko, S. B., Sari, R., Sharon, K., Frail, D., Moon, D., Brown, P. J., Cucchiara, A., Harrison, F., Piran, T., Persson, S. E., McCarthy, P. J., Penprase, B. E., Chevalier, R. A., & MacFadyen, A. I. 2006, Nature, 444, 1053

Galama, T. J., Vreeswijk, P. M., van Paradijs, J., Kouveliotou, C., Augusteijn, T., Böhnhardt, H., Brewer, J. P., Doublier, V., Gonzalez, J.-F., Leibundgut, B., Lidman, C., Hainaut, O. R., Patat, F., Heise, J., in't Zand, J., Hurley, K., Groot, P. J., Strom, R. G., Mazzali, P. A., Iwamoto, K., Nomoto, K., Umeda, H., Nakamura, T., Young, T. R., Suzuki, T., Shigeyama, T., Koshut, T., Kippen, M., Robinson, C., de Wildt, P., Wijers, R. A. M. J., Tanvir, N., Greiner, J., Pian, E., Palazzi, E., Frontera, F., Masetti, N., Nicastro, L., Feroci, M., Costa, E., Piro, L., Peterson, B. A., Tinney, C., Boyle, B., Cannon, R., Stathakis, R., Sadler, E., Begam, M. C., & Ianna, P. 1998, Nature, 395, 670

Gallagher, J. S., Garnavich, P. M., Berlind, P., Challis, P., Jha, S., & Kirshner, R. P. 2005, ApJ, 634, 210

Gamezo, V. N., Khokhlov, A. M., & Oran, E. S. 2005, ApJ, 623, 337

Gamezo, V. N., Khokhlov, A. M., Oran, E. S., Chtchelkanova, A. Y., & Rosenberg, R. O. 2003, Science, 299, 77

Garnavich, P. M., Bonanos, A. Z., Krisciunas, K., Jha, S., Kirshner, R. P., Schlegel, E. M., Challis, P., Macri, L. M., Hatano, K., Branch, D., Bothun, G. D., & Freedman, W. L. 2004, ApJ, 613, 1120

Gehrels, N., Norris, J. P., Barthelmy, S. D., Granot, J., Kaneko, Y., Kouveliotou, C., Markwardt, C. B., Mészáros, P., Nakar, E., Nousek, J. A., O'Brien, P. T., Page, M., Palmer, D. M., Parsons, A. M., Roming, P. W. A., Sakamoto, T., Sarazin, C. L., Schady, P., Stamatikos, M., & Woosley, S. E. 2006, Nature, 444, 1044

Gehrels, N., Ramirez-Ruiz, E., & Fox, D. B. 2009, ARA&A, 47, 567

Georgy, C., Meynet, G., Walder, R., Folini, D., & Maeder, A. 2009, A&A, 502, 611

Gerardy, C. L., Meikle, W. P. S., Kotak, R., Höflich, P., Farrah, D., Filippenko, A. V., Foley, R. J., Lundqvist, P., Mattila, S., Pozzo, M., Sollerman, J., Van Dyk, S. D., & Wheeler, J. C. 2007, ApJ, 661, 995

Goobar, A., Mörtsell, E., Amanullah, R., Goliath, M., Bergström, L., & Dahlén, T. 2002, A&A, 392, 757

Goobar, A., Paech, K., Stanishev, V., Amanullah, R., Dahlén, T., Jönsson, J., Kneib, J. P., Lidman, C., Limousin, M., Mörtsell, E., Nobili, S., Richard, J., Riehm, T., & von Strauss, M. 2009, A&A, 507, 71

Greiner, J., Krühler, T., Fynbo, J. P. U., Rossi, A., Schwarz, R., Klose, S., Savaglio, S., Tanvir, N. R., McBreen, S., Totani, T., Zhang, B. B., Wu, X. F., Watson, D., Barthelmy, S. D., Beardmore, A. P., Ferrero, P., Gehrels, N., Kann, D. A., Kawai, N., Yoldaş, A. K., Mészáros, P., Milvang-Jensen, B., Oates, S. R., Pierini, D., Schady, P., Toma, K., Vreeswijk, P. M., Yoldaş, A., Zhang, B., Afonso, P., Aoki, K., Burrows, D. N., Clemens, C., Filgas, R., Haiman, Z., Hartmann, D. H., Hasinger, G., Hjorth, J., Jehin, E., Levan, A. J., Liang, E. W., Malesani, D., Pyo, T., Schulze, S., Szokoly, G., Terada, K., & Wiersema, K. 2009, ApJ, 693, 1610

Guetta, D. & Della Valle, M. 2007, ApJ, 657, L73

Hadfield, L. J. & Crowther, P. A. 2006, MNRAS, 368, 1822

—. 2007, MNRAS, 381, 418

Hadfield, L. J., Crowther, P. A., Schild, H., & Schmutz, W. 2005, A&A, 439, 265

Hammer, F., Flores, H., Schaerer, D., Dessauges-Zavadsky, M., Le Floc'h, E., & Puech, M. 2006, A&A, 454, 103

Hamuy, M., Deng, J., Mazzali, P. A., Morrell, N. I., Phillips, M. M., Roth, M., Gonzalez, S., Thomas-Osip, J., Krzeminski, W., Contreras, C., Maza, J., González, L., Huerta, L., Folatelli, G., Chornock, R., Filippenko, A. V., Persson, S. E., Freedman, W. L., Koviak, K., Suntzeff, N. B., & Krisciunas, K. 2009, ApJ, 703, 1612

Hamuy, M., Folatelli, G., Morrell, N. I., Phillips, M. M., Suntzeff, N. B., Persson, S. E., Roth, M., Gonzalez, S., Krzeminski, W., Contreras, C., Freedman, W. L., Murphy, D. C., Madore, B. F., Wyatt, P., Maza, J., Filippenko, A. V., Li, W., & Pinto, P. A. 2006, PASP, 118, 2

Hamuy, M., Phillips, M. M., Suntzeff, N. B., Maza, J., González, L. E., Roth, M., Krisciunas, K., Morrell, N., Green, E. M., Persson, S. E., & McCarthy, P. J. 2003, Nature, 424, 651

Hamuy, M. & Pinto, P. A. 2002, ApJ, 566, L63

Hamuy, M., Trager, S. C., Pinto, P. A., Phillips, M. M., Schommer, R. A., Ivanov, V., & Suntzeff, N. B. 2000, AJ, 120, 1479

Han, X. H., Hammer, F., Liang, Y. C., Flores, H., Rodrigues, M., Hou, J. L., & Wei, J. Y. 2010, ArXiv e-prints

Hansen, L., Jorgensen, H. E., & Norgaard-Nielsen, H. U. 1987, The Messenger, 47, 46

Hashimoto, T., Ohta, K., Aoki, K., Tanaka, I., Yabe, K., Kawai, N., Aoki, W., Furusawa, H., Hattori, T., Iye, M., Kawabata, K. S., Kobayashi, N., Komiyama, Y., Kosugi, G., Minowa, Y., Mizumoto, Y., Niino, Y., Nomoto, K., Noumaru, J., Ogasawara, R., Pyo, T., Sakamoto, T., Sekiguchi, K., Shirasaki, Y., Suzuki, M., Tajitsu, A., Takata, T., Tamagawa, T., Terada, H., Totani, T., Watanabe, J., Yamada, T., & Yoshida, A. 2010, ArXiv e-prints

Hicken, M., Challis, P., Jha, S., Kirshner, R. P., Matheson, T., Modjaz, M., Rest, A., Michael Wood-Vasey, W., Bakos, G., Barton, E. J., Berlind, P., Bragg, A., Briceño, C., Brown, W. R., Caldwell, N., Calkins, M., Cho, R., Ciupik, L., Contreras, M., Dendy, K., Dosaj, A., Durham, N., Eriksen, K., Esquerdo, G., Everett, M., Falco, E., Fernandez, J., Gaba, A., Garnavich, P., Graves, G., Green, P., Groner, T., Hergenrother, C., Holman, M. J., Hradecky, V., Huchra, J., Hutchison, B., Jerius, D., Jordan, A., Kilgard, R., Krauss, M., Luhman, K., Macri, L., Marrone, D., McDowell, J., McIntosh, D., McNamara, B., Megeath, T., Mochejska, B., Munoz, D., Muzerolle, J., Naranjo, O., Narayan, G., Pahre, M., Peters, W., Peterson, D., Rines, K., Ripman, B., Roussanova, A., Schild, R., Sicilia-Aguilar, A., Sokoloski, J., Smalley, K., Smith, A., Spahr, T., Stanek, K. Z., Barmby, P., Blondin, S., Stubbs, C. W., Szentgyorgyi, A., Torres, M. A. P., Vaz, A., Vikhlinin, A., Wang, Z., Westover, M., Woods, D., & Zhao, P. 2009a, ApJ, 700, 331

Hicken, M., Garnavich, P. M., Prieto, J. L., Blondin, S., DePoy, D. L., Kirshner, R. P., & Parrent, J. 2007, ApJ, 669, L17

Hicken, M., Wood-Vasey, W. M., Blondin, S., Challis, P., Jha, S., Kelly, P. L., Rest, A., & Kirshner, R. P. 2009b, ApJ, 700, 1097

Hillebrandt, W. & Niemeyer, J. C. 2000, ARA&A, 38, 191

Hillebrandt, W., Sim, S. A., & Röpke, F. K. 2007, A&A, 465, L17

Hjorth, J., Sollerman, J., Møller, P., Fynbo, J. P. U., Woosley, S. E., Kouveliotou, C., Tanvir, N. R., Greiner, J., Andersen, M. I., Castro-Tirado, A. J., Castro Cerón, J. M., Fruchter, A. S., Gorosabel, J., Jakobsson, P., Kaper, L., Klose, S., Masetti, N., Pedersen, H., Pedersen, K., Pian, E., Palazzi, E., Rhoads, J. E., Rol, E., van den Heuvel, E. P. J., Vreeswijk, P. M., Watson, D., & Wijers, R. A. M. J. 2003, Nature, 423, 847

Hjorth, J., Watson, D., Fynbo, J. P. U., Price, P. A., Jensen, B. L., Jørgensen, U. G., Kubas, D., Gorosabel, J., Jakobsson, P., Sollerman, J., Pedersen, K., & Kouveliotou, C. 2005, Nature, 437, 859

Hoeflich, P. & Khokhlov, A. 1996, ApJ, 457, 500

Höflich, P., Gerardy, C. L., Nomoto, K., Motohara, K., Fesen, R. A., Maeda, K., Ohkubo, T., & Tominaga, N. 2004, ApJ, 617, 1258

Howell, D. A. 2001, ApJ, 554, L193

Howell, D. A., Sullivan, M., Nugent, P. E., Ellis, R. S., Conley, A. J., Le Borgne, D., Carlberg, R. G., Guy, J., Balam, D., Basa, S., Fouchez, D., Hook, I. M., Hsiao, E. Y., Neill, J. D., Pain, R., Perrett, K. M., & Pritchet, C. J. 2006, Nature, 443, 308

Hsiao, E. Y., Conley, A., Howell, D. A., Sullivan, M., Pritchet, C. J., Carlberg, R. G., Nugent, P. E., & Phillips, M. M. 2007, ApJ, 663, 1187

Iben, Jr., I. & Tutukov, A. V. 1984, ApJS, 54, 335

Immler, S., Brown, P. J., Milne, P., The, L., Petre, R., Gehrels, N., Burrows, D. N., Nousek, J. A., Williams, C. L., Pian, E., Mazzali, P. A., Nomoto, K., Chevalier, R. A., Mangano, V., Holland, S. T., Roming, P. W. A., Greiner, J., & Pooley, D. 2006, ApJ, 648, L119

Jensen, J. B., Tonry, J. L., Barris, B. J., Thompson, R. I., Liu, M. C., Rieke, M. J., Ajhar, E. A., & Blakeslee, J. P. 2003, ApJ, 583, 712

Jester, S., Schneider, D. P., Richards, G. T., Green, R. F., Schmidt, M., Hall, P. B., Strauss, M. A., Vanden Berk, D. E., Stoughton, C., Gunn, J. E., Brinkmann, J., Kent, S. M., Smith, J. A., Tucker, D. L., & Yanny, B. 2005, AJ, 130, 873

Jha, S., Riess, A. G., & Kirshner, R. P. 2007, ApJ, 659, 122

Kasen, D. 2006, ApJ, 649, 939

Kasen, D., Röpke, F. K., & Woosley, S. E. 2009, Nature, 460, 869

Kawai, N., Kosugi, G., Aoki, K., Yamada, T., Totani, T., Ohta, K., Iye, M., Hattori, T., Aoki, W., Furusawa, H., Hurley, K., Kawabata, K. S., Kobayashi, N., Komiyama, Y., Mizumoto, Y., Nomoto, K., Noumaru, J., Ogasawara, R., Sato, R., Sekiguchi, K., Shirasaki, Y., Suzuki, M., Takata, T., Tamagawa, T., Terada, H., Watanabe, J., Yatsu, Y., & Yoshida, A. 2006, Nature, 440, 184

Kelly, P. L., Hicken, M., Burke, D. L., Mandel, K. S., & Kirshner, R. P. 2009, ArXiv e-prints

Kelly, P. L., Kirshner, R. P., & Pahre, M. 2008, ApJ, 687, 1201

Kessler, R., Becker, A. C., Cinabro, D., Vanderplas, J., Frieman, J. A., Marriner, J., Davis, T. M., Dilday, B., Holtzman, J., Jha, S. W., Lampeitl, H., Sako, M., Smith, M., Zheng, C., Nichol, R. C., Bassett, B., Bender, R., Depoy, D. L., Doi, M., Elson, E., Filippenko, A. V., Foley, R. J., Garnavich, P. M., Hopp, U., Ihara, Y., Ketzeback, W., Kollatschny, W., Konishi, K., Marshall, J. L., Mc Millan, R. J., Miknaitis, G., Morokuma, T., Mörtsell, E., Pan, K., Prieto, J. L., Richmond, M. W., Riess, A. G., Romani, R., Schneider, D. P., Sollerman, J., Takanashi, N., Tokita, K., van der Heyden, K., Wheeler, J. C., Yasuda, N., & York, D. 2009, ApJS, 185, 32

Kewley, L. J. & Dopita, M. A. 2002, ApJS, 142, 35

Khokhlov, A. M. 1991, A&A, 245, 114

Kirshner, R. P. 2009, ArXiv 0910.0257

Kirshner, R. P. & Kwan, J. 1974, ApJ, 193, 27

Komatsu, E., Dunkley, J., Nolta, M. R., Bennett, C. L., Gold, B., Hinshaw, G., Jarosik, N., Larson, D., Limon, M., Page, L., Spergel, D. N., Halpern, M., Hill, R. S., Kogut, A., Meyer, S. S., Tucker, G. S., Weiland, J. L., Wollack, E., & Wright, E. L. 2009, ApJS, 180, 330

Kotak, R., Meikle, W. P. S., Adamson, A., & Leggett, S. K. 2004, MNRAS, 354, L13

Kouveliotou, C., Meegan, C. A., Fishman, G. J., Bhat, N. P., Briggs, M. S., Koshut, T. M., Paciesas, W. S., & Pendleton, G. N. 1993, ApJ, 413, L101

Kowal, C. T. 1968, AJ, 73, 1021

Kowalski, M., Rubin, D., Aldering, G., Agostinho, R. J., Amadon, A., Amanullah, R., Balland, C., Barbary, K., Blanc, G., Challis, P. J., Conley, A., Connolly, N. V., Covarrubias, R., Dawson, K. S., Deustua, S. E., Ellis, R., Fabbro, S., Fadeyev, V., Fan, X., Farris, B., Folatelli, G., Frye, B. L., Garavini, G., Gates, E. L., Germany, L., Goldhaber, G., Goldman, B., Goobar, A., Groom, D. E., Haissinski, J., Hardin, D., Hook, I., Kent, S., Kim, A. G., Knop, R. A., Lidman, C., Linder, E. V., Mendez, J., Meyers, J., Miller, G. J., Moniez, M., Mourão, A. M., Newberg, H., Nobili, S., Nugent, P. E., Pain, R., Perdereau, O., Perlmutter, S., Phillips, M. M., Prasad, V., Quimby, R., Regnault, N., Rich, J., Rubenstein, E. P., Ruiz-Lapuente, P., Santos, F. D., Schaefer, B. E., Schommer, R. A., Smith, R. C., Soderberg, A. M., Spadafora, A. L., Strolger, L., Strovink, M., Suntzeff, N. B., Suzuki, N., Thomas, R. C., Walton, N. A., Wang, L., Wood-Vasey, W. M., & Yun, J. L. 2008, ApJ, 686, 749

Kozma, C. & Fransson, C. 1998a, ApJ, 496, 946

—. 1998b, ApJ, 497, 431

Kozma, C., Fransson, C., Hillebrandt, W., Travaglio, C., Sollerman, J., Reinecke, M., Röpke, F. K., & Spyromilio, J. 2005, A&A, 437, 983

Krisciunas, K., Hamuy, M., Suntzeff, N. B., Espinoza, J., Gonzalez, D., Gonzalez, L., Gonzalez, S., Koviak, K., Krzeminski, W., Morrell, N., Phillips, M. M., Roth, M., & Thomas-Osip, J. 2009a, AJ, 137, 34

Krisciunas, K., Marion, G. H., Suntzeff, N. B., Blanc, G., Bufano, F., Candia, P., Cartier, R., Elias-Rosa, N., Espinoza, J., Gonzalez, D., Gonzalez, L., Gonzalez, S., Gooding, S. D., Hamuy, M., Knox, E. A., Milne, P. A., Morrell, N., Phillips, M. M., Stritzinger, M., & Thomas-Osip, J. 2009b, AJ, 138, 1584

Krisciunas, K., Phillips, M. M., & Suntzeff, N. B. 2004a, ApJ, 602, L81

Krisciunas, K., Phillips, M. M., Suntzeff, N. B., Persson, S. E., Hamuy, M., Antezana, R., Candia, P., Clocchiatti, A., DePoy, D. L., Germany, L. M., Gonzalez, L., Gonzalez, S., Krzeminski, W., Maza, J., Nugent, P. E., Qiu, Y., Rest, A., Roth, M., Stritzinger, M., Strolger, L.-G., Thompson, I., Williams, T. B., & Wischnjewsky, M. 2004b, AJ, 127, 1664

Krisciunas, K., Suntzeff, N. B., Candia, P., Arenas, J., Espinoza, J., Gonzalez, D., Gonzalez, S., Höflich, P. A., Landolt, A. U., Phillips, M. M., & Pizarro, S. 2003, AJ, 125, 166

Lair, J. C., Leising, M. D., Milne, P. A., & Williams, G. G. 2006, AJ, 132, 2024

Landolt, A. U. 1992, AJ, 104, 340

Larsson, J., Levan, A. J., Davies, M. B., & Fruchter, A. S. 2007, MNRAS, 376, 1285

Leibundgut, B. 2000, A&A Rev., 10, 179

—. 2001, ARA&A, 39, 67

—. 2008, General Relativity and Gravitation, 40, 221

Leloudas, G., Stritzinger, M., Sollerman, J., Hamuy, M., & Suntzeff, N. 2009a, in American Institute of Physics Conference Series, Vol. 1111, American Institute of Physics Conference Series, ed. G. Giobbi, A. Tornambe, G. Raimondo, M. Limongi, L. A. Antonelli, N. Menci, & E. Brocato, 456–459

Leloudas, G., Stritzinger, M. D., Sollerman, J., Burns, C. R., Kozma, C., Krisciunas, K., Maund, J. R., Milne, P., Filippenko, A. V., Fransson, C., Ganeshalingam, M., Hamuy, M., Li, W., Phillips, M. M., Schmidt, B. P., Skottfelt, J., Taubenberger, S., Boldt, L., Fynbo, J. P. U., Gonzalez, L., Salvo, M., & Thomas-Osip, J. 2009b, A&A, 505, 265

Levesque, E. M., Berger, E., Kewley, L. J., & Bagley, M. M. 2010a, AJ, 139, 694

Levesque, E. M., Kewley, L. J., Graham, J. F., & Fruchter, A. S. 2010b, ApJ, 712, L26

Li, L. 2008, MNRAS, 388, 603

Li, W. & Filippenko, A. V. 2008, Central Bureau Electronic Telegrams, 1202, 1

Li, W., Filippenko, A. V., Treffers, R. R., Riess, A. G., Hu, J., & Qiu, Y. 2001, ApJ, 546, 734

Lilly, S. J., Le Fèvre, O., Renzini, A., Zamorani, G., Scodeggio, M., Contini, T., Carollo, C. M., Hasinger, G., Kneib, J., Iovino, A., Le Brun, V., Maier, C., Mainieri, V., Mignoli, M., Silverman, J., Tasca, L. A. M., Bolzonella, M., Bongiorno, A., Bottini, D., Capak, P., Caputi, K., Cimatti, A., Cucciati, O., Daddi, E., Feldmann, R., Franzetti, P., Garilli, B., Guzzo, L., Ilbert, O., Kampczyk, P., Kovac, K., Lamareille, F., Leauthaud, A., Borgne, J., McCracken, H. J., Marinoni, C., Pello, R., Ricciardelli, E., Scarlata, C., Vergani, D., Sanders, D. B., Schinnerer, E., Scoville, N., Taniguchi, Y., Arnouts, S., Aussel, H., Bardelli, S., Brusa, M., Cappi, A., Ciliegi, P., Finoguenov, A., Foucaud, S., Franceschini, R., Halliday, C., Impey, C., Knobel, C., Koekemoer, A., Kurk, J., Maccagni, D., Maddox, S., Marano, B., Marconi, G., Meneux, B., Mobasher, B., Moreau, C., Peacock, J. A., Porciani, C., Pozzetti, L., Scaramella, R., Schiminovich, D., Shopbell, P., Smail, I., Thompson, D., Tresse, L., Vettolani, G., Zanichelli, A., & Zucca, E. 2007, ApJS, 172, 70

Lilly, S. J., LeBrun, V., Maier, C., Mainieri, V., Mignoli, M., Scodeggio, M., Zamorani, G., Carollo, M., Contini, T., Kneib, J., LeFèvre, O., Renzini, A., Bardelli, S., Bolzonella, M., Bongiorno, A., Caputi, K., Coppa, G., Cucciati, O., de la Torre, S., de Ravel, L., Franzetti, P., Garilli, B., Iovino, A., Kampczyk, P., Kovac, K., Knobel, C., Lamareille, F., LeBorgne, J., Pello, R., Peng, Y., Pérez-Montero, E., Ricciardelli, E., Silverman, J. D., Tanaka, M., Tasca, L., Tresse, L., Vergani, D., Zucca, E., Ilbert, O., Salvato, M., Oesch, P., Abbas, U., Bottini, D., Capak, P., Cappi, A., Cassata, P., Cimatti, A., Elvis, M., Fumana, M., Guzzo, L., Hasinger, G., Koekemoer, A., Leauthaud, A., Maccagni, D., Marinoni, C., McCracken, H., Memeo, P., Meneux, B., Porciani, C., Pozzetti, L., Sanders, D., Scaramella, R., Scarlata, C., Scoville, N., Shopbell, P., & Taniguchi, Y. 2009, ApJS, 184, 218

Livio, M. 2000, in Type Ia Supernovae, Theory and Cosmology, ed. J. C. Niemeyer & J. W. Truran, 33–+

Lundmark, K. 1925, MNRAS, 85, 865

MacFadyen, A. I. & Woosley, S. E. 1999, ApJ, 524, 262

Maeda, K., Kawabata, K., Li, W., Tanaka, M., Mazzali, P. A., Hattori, T., Nomoto, K., & Filippenko, A. V. 2009, ApJ, 690, 1745

Maeda, K., Kawabata, K., Mazzali, P. A., Tanaka, M., Valenti, S., Nomoto, K., Hattori, T., Deng, J., Pian, E., Taubenberger, S., Iye, M., Matheson, T., Filippenko, A. V., Aoki, K., Kosugi, G., Ohyama, Y., Sasaki, T., & Takata, T. 2008, Science, 319, 1220

Maeda, K., Leloudas, G., Taubenberger, S., Stritzinger, M., Sollerman, J., Elias-Rosa, N., Benetti, S., & Hamuy, M. 2010a, MNRAS submitted

Maeda, K., Taubenberger, S., Sollerman, J., Mazzali, P. A., Leloudas, G., Nomoto, K., & Motohara, K. 2010b, ApJ, 708, 1703

Maguire, K., Kotak, R., Smartt, S. J., Pastorello, A., Hamuy, M., & Bufano, F. 2010, MNRAS, 403, L11

Malesani, D., Fynbo, J. P. U., Hjorth, J., Leloudas, G., Sollerman, J., Stritzinger, M. D., Vreeswijk, P. M., Watson, D. J., Gorosabel, J., Michałowski, M. J., Thöne, C. C., Augusteijn, T., Bersier, D., Jakobsson, P., Jaunsen, A. O., Ledoux, C., Levan, A. J., Milvang-Jensen, B., Rol, E., Tanvir, N. R., Wiersema, K., Xu, D., Albert, L., Bayliss, M., Gall, C., Grove, L. F., Koester, B. P., Leitet, E., Pursimo, T., & Skillen, I. 2009, ApJ, 692, L84

Malesani, D., Hjorth, J., Jakobsson, P., Vreeswijk, P. M., Thoene, C. C., Fynbo, J. P. U., Watson, D. J., Sollerman, J., Tanvir, N. R., & Stanke, T. 2008a, GRB Coordinates Network, 7169, 1

Malesani, D., Sollerman, J., Fynbo, J. P. U., Thoene, C. C., Xu, D., Hjorth, J., Leloudas, G., Vreeswijk, P. M., Watson, D. J., Jakobsson, P., Augusteijn, T., Villforth, C., & Niemi, S. 2008b, GRB Coordinates Network, 7184, 1

Malesani, D., Tagliaferri, G., Chincarini, G., Covino, S., Della Valle, M., Fugazza, D., Mazzali, P. A., Zerbi, F. M., D'Avanzo, P., Kalogerakos, S., Simoncelli, A., Antonelli, L. A., Burderi, L., Campana, S., Cucchiara, A., Fiore, F., Ghirlanda, G., Goldoni, P., Götz, D., Mereghetti, S., Mirabel, I. F., Romano, P., Stella, L., Minezaki, T., Yoshii, Y., & Nomoto, K. 2004, ApJ, 609, L5

Mannucci, F., Della Valle, M., & Panagia, N. 2007, MNRAS, 377, 1229

Mannucci, F., Della Valle, M., Panagia, N., Cappellaro, E., Cresci, G., Maiolino, R., Petrosian, A., & Turatto, M. 2005, A&A, 433, 807

Maoz, D. & Gal-Yam, A. 2004, MNRAS, 347, 951

Margutti, R., Chincarini, G., Covino, S., Tagliaferri, G., Campana, S., Della Valle, M., Filippenko, A. V., Fiore, F., Foley, R., Fugazza, D., Giommi, P., Malesani, D., Moretti, A., & Stella, L. 2007, A&A, 474, 815

Massey, P. 1998, ApJ, 501, 153

Massey, P. & Johnson, O. 1998, ApJ, 505, 793

Massey, P., Olsen, K. A. G., & Parker, J. W. 2003, PASP, 115, 1265

Massey, P., Silva, D. R., Levesque, E. M., Plez, B., Olsen, K. A. G., Clayton, G. C., Meynet, G., & Maeder, A. 2009, ApJ, 703, 420

Mattila, S., Meikle, W. P. S., & Greimel, R. 2004, New Astronomy Review, 48, 595

Maund, J. R. & Smartt, S. J. 2009, Science, 324, 486

Maund, J. R., Smartt, S. J., Kudritzki, R. P., Podsiadlowski, P., & Gilmore, G. F. 2004, Nature, 427, 129

Maund, J. R., Smartt, S. J., & Schweizer, F. 2005, ApJ, 630, L33

Maund, J. R., Wheeler, J. C., Baade, D., Patat, F., Höflich, P., Wang, L., & Clocchiatti, A. 2009, ApJ, 705, 1139

Maund, J. R., Wheeler, J. C., Patat, F., Wang, L., Baade, D., & Höflich, P. A. 2007, ApJ, 671, 1944

Maund et al. 2009, in preparation

Mazzali, P. A., Cappellaro, E., Danziger, I. J., Turatto, M., & Benetti, S. 1998, ApJ, 499, L49+

Mazzali, P. A., Kawabata, K. S., Maeda, K., Nomoto, K., Filippenko, A. V., Ramirez-Ruiz, E., Benetti, S., Pian, E., Deng, J., Tominaga, N., Ohyama, Y., Iye, M., Foley, R. J., Matheson, T., Wang, L., & Gal-Yam, A. 2005, Science, 308, 1284

Mazzali, P. A., Röpke, F. K., Benetti, S., & Hillebrandt, W. 2007, Science, 315, 825

Mazzali, P. A., Valenti, S., Della Valle, M., Chincarini, G., Sauer, D. N., Benetti, S., Pian, E., Piran, T., D'Elia, V., Elias-Rosa, N., Margutti, R., Pasotti, F., Antonelli, L. A., Bufano, F., Campana, S., Cappellaro, E., Covino, S., D'Avanzo, P., Fiore, F., Fugazza, D., Gilmozzi, R., Hunter, D., Maguire, K., Maiorano, E., Marziani, P., Masetti, N., Mirabel, F., Navasardyan, H., Nomoto, K., Palazzi, E., Pastorello, A., Panagia, N., Pellizza, L. J., Sari, R., Smartt, S., Tagliaferri, G., Tanaka, M., Taubenberger, S., Tominaga, N., Trundle, C., & Turatto, M. 2008, Science, 321, 1185

McCray, R. 1993, ARA&A, 31, 175

McLaughlin, H. & Wiklind, T. 2007, NICMOS Data Handbook, Version 7.0, Baltimore: STScI

Meikle, W. P. S. 2000, MNRAS, 314, 782

Mészáros, P. 2002, ARA&A, 40, 137

Metzger, M. R., Djorgovski, S. G., Kulkarni, S. R., Steidel, C. C., Adelberger, K. L., Frail, D. A., Costa, E., & Frontera, F. 1997, Nature, 387, 878

Meynet, G. & Maeder, A. 2005, A&A, 429, 581

Michałowski, M. J., Hjorth, J., Castro Cerón, J. M., & Watson, D. 2008, ApJ, 672, 817

Michałowski, M. J., Hjorth, J., & Watson, D. 2009, ArXiv e-prints

Miknaitis, G., Pignata, G., Rest, A., Wood-Vasey, W. M., Blondin, S., Challis, P., Smith, R. C., Stubbs, C. W., Suntzeff, N. B., Foley, R. J., Matheson, T., Tonry, J. L., Aguilera, C., Blackman, J. W., Becker, A. C., Clocchiatti, A., Covarrubias, R., Davis, T. M., Filippenko, A. V., Garg, A., Garnavich, P. M., Hicken, M., Jha, S., Krisciunas, K., Kirshner, R. P., Leibundgut, B., Li, W., Miceli, A., Narayan, G., Prieto, J. L., Riess, A. G., Salvo, M. E., Schmidt, B. P., Sollerman, J., Spyromilio, J., & Zenteno, A. 2007, ApJ, 666, 674

Milisavljevic, D., Fesen, R. A., Gerardy, C. L., Kirshner, R. P., & Challis, P. 2010, ApJ, 709, 1343

Milne, P. A., The, L.-S., & Leising, M. D. 1999, ApJS, 124, 503

—. 2001, ApJ, 559, 1019

Milne, P. A. & Williams, G. G. 2005, in IAU Colloq. 192: Cosmic Explosions, On the 10th Anniversary of SN1993J, ed. J.-M. Marcaide & K. W. Weiler, 183–+

Minkowski, R. 1941, PASP, 53, 224

—. 1964, ARA&A, 2, 247

Modjaz, M., Chornock, R., Foley, R. J., Filippenko, A. V., Li, W., & Stringfellow, G. 2008a, Central Bureau Electronic Telegrams, 1221, 1

Modjaz, M., Kewley, L., Kirshner, R. P., Stanek, K. Z., Challis, P., Garnavich, P. M., Greene, J. E., Kelly, P. L., & Prieto, J. L. 2008b, AJ, 135, 1136

Modjaz, M., Kirshner, R. P., Blondin, S., Challis, P., & Matheson, T. 2008c, ApJ, 687, L9

Modjaz, M., Li, W., Butler, N., Chornock, R., Perley, D., Blondin, S., Bloom, J. S., Filippenko, A. V., Kirshner, R. P., Kocevski, D., Poznanski, D., Hicken, M., Foley, R. J., Stringfellow, G. S., Berlind, P., Barrado y Navascues, D., Blake, C. H., Bouy, H., Brown, W. R., Challis, P., Chen, H., de Vries, W. H., Dufour, P., Falco, E., Friedman, A., Ganeshalingam, M., Garnavich, P., Holden, B., Illingworth, G., Lee, N., Liebert, J., Marion, G. H., Olivier, S. S., Prochaska, J. X., Silverman, J. M., Smith, N., Starr, D., Steele, T. N., Stockton, A., Williams, G. G., & Wood-Vasey, W. M. 2009, ApJ, 702, 226

Motohara, K., Maeda, K., Gerardy, C. L., Nomoto, K., Tanaka, M., Tominaga, N., Ohkubo, T., Mazzali, P. A., Fesen, R. A., Höflich, P., & Wheeler, J. C. 2006, ApJ, 652, L101

Neill, J. D., Sullivan, M., Balam, D., Pritchet, C. J., Howell, D. A., Perrett, K., Astier, P., Aubourg, E., Basa, S., Carlberg, R. G., Conley, A., Fabbro, S., Fouchez, D., Guy, J., Hook, I., Pain, R., Palanque-Delabrouille, N., Regnault, N., Rich, J., Taillet, R., Aldering, G., Antilogus, P., Arsenijevic, V., Balland, C., Baumont, S., Bronder, J., Ellis, R. S., Filiol, M., Gonçalves, A. C., Hardin, D., Kowalski, M., Lidman, C., Lusset, V., Mouchet, M., Mourao, A., Perlmutter, S., Ripoche, P., Schlegel, D., & Tao, C. 2006, AJ, 132, 1126

Neill, J. D., Sullivan, M., Howell, D. A., Conley, A., Seibert, M., Martin, D. C., Barlow, T. A., Foster, K., Friedman, P. G., Morrissey, P., Neff, S. G., Schiminovich, D., Wyder, T. K., Bianchi, L., Donas, J., Heckman, T. M., Lee, Y., Madore, B. F., Milliard, B., Rich, R. M., & Szalay, A. S. 2009, ArXiv e-prints

Nobili, S., Amanullah, R., Garavini, G., Goobar, A., Lidman, C., Stanishev, V., Aldering, G., Antilogus, P., Astier, P., Burns, M. S., Conley, A., Deustua, S. E., Ellis, R., Fabbro, S., Fadeyev, V., Folatelli, G., Gibbons, R., Goldhaber, G., Groom, D. E., Hook, I., Howell, D. A., Kim, A. G., Knop, R. A., Nugent, P. E., Pain, R., Perlmutter, S., Quimby, R., Raux, J., Regnault, N., Ruiz-Lapuente, P., Sainton, G., Schahmaneche, K., Smith, E., Spadafora, A. L., Thomas, R. C., Wang, L., & The Supernova Cosmology Project. 2005, A&A, 437, 789

Nobili, S., Fadeyev, V., Aldering, G., Amanullah, R., Barbary, K., Burns, M. S., Dawson, K. S., Deustua, S. E., Faccioli, L., Fruchter, A. S., Goldhaber, G., Goobar, A., Hook, I., Howell, D. A., Kim, A. G., Knop, R. A., Lidman, C., Meyers, J., Nugent, P. E., Pain, R., Panagia, N., Perlmutter, S., Rubin, D., Spadafora, A. L., Strovink, M., Suzuki, N., & The Supernova Cosmology Project. 2009, ApJ, 700, 1415

Nobili, S. & Goobar, A. 2008, A&A, 487, 19

Nomoto, K., Suzuki, T., Shigeyama, T., Kumagai, S., Yamaoka, H., & Saio, H. 1993, Nature, 364, 507

Nomoto, K., Thielemann, F.-K., & Yokoi, K. 1984, ApJ, 286, 644

Nørgaard-Nielsen, H. U., Hansen, L., Jorgensen, H. E., Aragon Salamanca, A., & Ellis, R. S. 1989, Nature, 339, 523

Nugent, P., Kim, A., & Perlmutter, S. 2002, PASP, 114, 803

Nugent, P., Phillips, M., Baron, E., Branch, D., & Hauschildt, P. 1995, ApJ, 455, L147+

Nugent, P., Sullivan, M., Ellis, R., Gal-Yam, A., Leonard, D. C., Howell, D. A., Astier, P., Carlberg, R. G., Conley, A., Fabbro, S., Fouchez, D., Neill, J. D., Pain, R., Perrett, K., Pritchet, C. J., & Regnault, N. 2006, ApJ, 645, 841

Osterbrock, D. E. 1989, Astrophysics of gaseous nebulae and active galactic nuclei, ed. Osterbrock, D. E.

Östlin, G., Zackrisson, E., Sollerman, J., Mattila, S., & Hayes, M. 2008, MNRAS, 387, 1227

Pakmor, R., Kromer, M., Röpke, F. K., Sim, S. A., Ruiter, A. J., & Hillebrandt, W. 2010, Nature, 463, 61

Pakmor, R., Röpke, F. K., Weiss, A., & Hillebrandt, W. 2008, A&A, 489, 943

Panagia, N., Sramek, R. A., & Weiler, K. W. 1986, ApJ, 300, L55

Panagia, N., Van Dyk, S. D., Weiler, K. W., Sramek, R. A., Stockdale, C. J., & Murata, K. P. 2006, ApJ, 646, 369

Pastorello, A., Kasliwal, M. M., Crockett, R. M., Valenti, S., Arbour, R., Itagaki, K., Kaspi, S., Gal-Yam, A., Smartt, S. J., Griffith, R., Maguire, K., Ofek, E. O., Seymour, N., Stern, D., & Wiethoff, W. 2008, MNRAS, 389, 955

Pastorello, A., Taubenberger, S., Elias-Rosa, N., Mazzali, P. A., Pignata, G., Cappellaro, E., Garavini, G., Nobili, S., Anupama, G. C., Bayliss, D. D. R., Benetti, S., Bufano, F., Chakradhari, N. K., Kotak, R., Goobar, A., Navasardyan, H., Patat, F., Sahu, D. K., Salvo, M., Schmidt, B. P., Stanishev, V., Turatto, M., & Hillebrandt, W. 2007, MNRAS, 376, 1301

Patat, F. 2005, MNRAS, 357, 1161

Patat, F., Baade, D., Höflich, P., Maund, J. R., Wang, L., & Wheeler, J. C. 2009, A&A, 508, 229

Patat, F., Chandra, P., Chevalier, R., Justham, S., Podsiadlowski, P., Wolf, C., Gal-Yam, A., Pasquini, L., Crawford, I. A., Mazzali, P. A., Pauldrach, A. W. A., Nomoto, K., Benetti, S., Cappellaro, E., Elias-Rosa, N., Hillebrandt, W., Leonard, D. C., Pastorello, A., Renzini, A., Sabbadin, F., Simon, J. D., & Turatto, M. 2007, Science, 317, 924

Pavlovsky, C., Koekemoer, A., & Mack, J. 2006, ACS Data Handbook, Version 5.0, Baltimore: STScI

Perlmutter, S., Aldering, G., Goldhaber, G., Knop, R. A., Nugent, P., Castro, P. G., Deustua, S., Fabbro, S., Goobar, A., Groom, D. E., Hook, I. M., Kim, A. G., Kim, M. Y., Lee, J. C., Nunes, N. J., Pain, R., Pennypacker, C. R., Quimby, R., Lidman, C., Ellis, R. S., Irwin, M., McMahon, R. G., Ruiz-Lapuente, P., Walton, N., Schaefer, B., Boyle, B. J., Filippenko, A. V., Matheson, T., Fruchter, A. S., Panagia, N., Newberg, H. J. M., Couch, W. J., & The Supernova Cosmology Project. 1999, ApJ, 517, 565

Persson, S. E., Murphy, D. C., Krzeminski, W., Roth, M., & Rieke, M. J. 1998, AJ, 116, 2475

Pettini, M. & Pagel, B. E. J. 2004, MNRAS, 348, L59

Phillips, M. M. 1993, ApJ, 413, L105

Phillips, M. M., Li, W., Frieman, J. A., Blinnikov, S. I., DePoy, D., Prieto, J. L., Milne, P., Contreras, C., Folatelli, G., Morrell, N., Hamuy, M., Suntzeff, N. B., Roth, M., González, S., Krzeminski, W., Filippenko, A. V., Freedman, W. L., Chornock, R., Jha, S., Madore, B. F., Persson, S. E., Burns, C. R., Wyatt, P., Murphy, D., Foley, R. J., Ganeshalingam, M., Serduke, F. J. D., Krisciunas, K., Bassett, B., Becker, A., Dilday, B., Eastman, J., Garnavich, P. M., Holtzman, J., Kessler, R., Lampeitl, H., Marriner, J., Frank, S., Marshall, J. L., Miknaitis, G., Sako, M., Schneider, D. P., van der Heyden, K., & Yasuda, N. 2007, PASP, 119, 360

Phillips, M. M., Lira, P., Suntzeff, N. B., Schommer, R. A., Hamuy, M., & Maza, J. 1999, AJ, 118, 1766

Pian, E., Mazzali, P. A., Masetti, N., Ferrero, P., Klose, S., Palazzi, E., Ramirez-Ruiz, E., Woosley, S. E., Kouveliotou, C., Deng, J., Filippenko, A. V., Foley, R. J., Fynbo, J. P. U., Kann, D. A., Li, W., Hjorth, J., Nomoto, K., Patat, F., Sauer, D. N., Sollerman, J., Vreeswijk, P. M., Guenther, E. W., Levan, A., O'Brien, P., Tanvir, N. R., Wijers, R. A. M. J., Dumas, C., Hainaut, O., Wong, D. S., Baade, D., Wang, L., Amati, L., Cappellaro, E., Castro-Tirado, A. J., Ellison, S., Frontera, F., Fruchter, A. S., Greiner, J., Kawabata, K., Ledoux, C., Maeda, K., Møller, P., Nicastro, L., Rol, E., & Starling, R. 2006, Nature, 442, 1011

Pignata, G., Benetti, S., Mazzali, P. A., Kotak, R., Patat, F., Meikle, P., Stehle, M., Leibundgut, B., Suntzeff, N. B., Buson, L. M., Cappellaro, E., Clocchiatti, A., Hamuy, M., Maza, J., Mendez, J., Ruiz-Lapuente, P., Salvo, M., Schmidt, B. P., Turatto, M., & Hillebrandt, W. 2008, MNRAS, 388, 971

Plewa, T., Calder, A. C., & Lamb, D. Q. 2004, ApJ, 612, L37

Podsiadlowski, P., Hsu, J. J. L., Joss, P. C., & Ross, R. R. 1993, Nature, 364, 509

Podsiadlowski, P., Joss, P. C., & Hsu, J. J. L. 1992, ApJ, 391, 246

Poznanski, D., Baron, E., Blondin, S., Bloom, J. S., D'Andrea, C., Della Valle, M., Dessart, L., ellis, R. S., Gal-Yam, A., Goobar, A., Hamuy, M., Hicken, M., Kasen, D. N., Krisciunas, K. L., Leonard, D. C., Li, W., Livio, M., Marion, H., Matheson, T., Neill, J. D., Nomoto, K., Nugent, P. E., Quimby, R., Sako, M., Sullivan, M., Thomas, R. C., Turatto, M., Van Dyk, S. D., & Wood-Vasey, W. M. 2009a, in Astronomy, Vol. 2010, AGB Stars and Related Phenomenastro2010: The Astronomy and Astrophysics Decadal Survey, 237–+

Poznanski, D., Butler, N., Filippenko, A. V., Ganeshalingam, M., Li, W., Bloom, J. S., Chornock, R., Foley, R. J., Nugent, P. E., Silverman, J. M., Cenko, S. B., Gates, E. L., Leonard, D. C., Miller, A. A., Modjaz, M., Serduke, F. J. D., Smith, N., Swift, B. J., & Wong, D. S. 2009b, ApJ, 694, 1067

Poznanski, D., Maoz, D., & Gal-Yam, A. 2007, AJ, 134, 1285

Prantzos, N. 2008, New Astronomy Review, 52, 457

Prantzos, N. & Boissier, S. 2003, A&A, 406, 259

Prieto, J. L., Rest, A., & Suntzeff, N. B. 2006, ApJ, 647, 501

Prieto, J. L., Stanek, K. Z., & Beacom, J. F. 2008, ApJ, 673, 999

Quimby, R. M., Aldering, G., Wheeler, J. C., Höflich, P., Akerlof, C. W., & Rykoff, E. S. 2007, ApJ, 668, L99

Racusin, J. L., Karpov, S. V., Sokolowski, M., Granot, J., Wu, X. F., Pal'Shin, V., Covino, S., van der Horst, A. J., Oates, S. R., Schady, P., Smith, R. J., Cummings, J., Starling, R. L. C., Piotrowski, L. W., Zhang, B., Evans, P. A., Holland, S. T., Malek, K., Page, M. T., Vetere, L., Margutti, R., Guidorzi, C., Kamble, A. P., Curran, P. A., Beardmore, A., Kouveliotou, C., Mankiewicz, L., Melandri, A., O'Brien, P. T., Page, K. L., Piran, T., Tanvir, N. R., Wrochna, G., Aptekar, R. L., Barthelmy, S., Bartolini, C., Beskin, G. M., Bondar, S., Bremer, M., Campana, S., Castro-Tirado, A., Cucchiara, A., Cwiok, M., D'Avanzo, P., D'Elia, V., Della Valle, M., de Ugarte Postigo, A., Dominik, W., Falcone, A., Fiore, F., Fox, D. B., Frederiks, D. D., Fruchter, A. S., Fugazza, D., Garrett, M. A., Gehrels, N., Golenetskii, S., Gomboc, A., Gorosabel, J., Greco, G., Guarnieri, A., Immler, S., Jelinek, M., Kasprowicz, G., La Parola, V., Levan, A. J., Mangano, V., Mazets, E. P., Molinari, E., Moretti, A., Nawrocki, K., Oleynik, P. P., Osborne, J. P., Pagani, C., Pandey, S. B., Paragi, Z., Perri, M., Piccioni, A., Ramirez-Ruiz, E., Roming, P. W. A., Steele, I. A., Strom, R. G., Testa, V., Tosti, G., Ulanov, M. V., Wiersema, K., Wijers, R. A. M. J., Winters, J. M., Zarnecki, A. F., Zerbi, F., Mészáros, P., Chincarini, G., & Burrows, D. N. 2008, Nature, 455, 183

Raskin, C., Scannapieco, E., Rhoads, J., & Della Valle, M. 2008, ApJ, 689, 358

Richardson, D., Branch, D., & Baron, E. 2006, AJ, 131, 2233

Richmond, M. W., van Dyk, S. D., Ho, W., Peng, C. Y., Paik, Y., Treffers, R. R., Filippenko, A. V., Bustamante-Donas, J., Moeller, M., Pawellek, C., Tartara, H., & Spence, M. 1996, AJ, 111, 327

Riess, A. G., Filippenko, A. V., Challis, P., Clocchiatti, A., Diercks, A., Garnavich, P. M., Gilliland, R. L., Hogan, C. J., Jha, S., Kirshner, R. P., Leibundgut, B., Phillips, M. M., Reiss, D., Schmidt, B. P., Schommer, R. A., Smith, R. C., Spyromilio, J., Stubbs, C., Suntzeff, N. B., & Tonry, J. 1998, AJ, 116, 1009

Riess, A. G., Strolger, L., Casertano, S., Ferguson, H. C., Mobasher, B., Gold, B., Challis, P. J., Filippenko, A. V., Jha, S., Li, W., Tonry, J., Foley, R., Kirshner, R. P., Dickinson, M., MacDonald, E., Eisenstein, D., Livio, M., Younger, J., Xu, C., Dahlén, T., & Stern, D. 2007, ApJ, 659, 98

Riess, A. G., Strolger, L., Tonry, J., Casertano, S., Ferguson, H. C., Mobasher, B., Challis, P., Filippenko, A. V., Jha, S., Li, W., Chornock, R., Kirshner, R. P., Leibundgut, B., Dickinson, M., Livio, M., Giavalisco, M., Steidel, C. C., Benítez, T., & Tsvetanov, Z. 2004a, ApJ, 607, 665

Riess, A. G., Strolger, L., Tonry, J., Tsvetanov, Z., Casertano, S., Ferguson, H. C., Mobasher, B., Challis, P., Panagia, N., Filippenko, A. V., Li, W., Chornock, R., Kirshner, R. P., Leibundgut, B., Dickinson, M., Koekemoer, A., Grogin, N. A., & Giavalisco, M. 2004b, ApJ, 600, L163

Roelofs, G., Bassa, C., Voss, R., & Nelemans, G. 2008, MNRAS, 391, 290

Röpke, F. K. 2005, A&A, 432, 969

—. 2007, ApJ, 668, 1103

Röpke, F. K., Hillebrandt, W., Schmidt, W., Niemeyer, J. C., Blinnikov, S. I., & Mazzali, P. A. 2007, ApJ, 668, 1132

Röpke, F. K. & Niemeyer, J. C. 2007, A&A, 464, 683

Ruiz-Lapuente, P. & Spruit, H. C. 1998, ApJ, 500, 360

Sahu, K. C., Livio, M., Petro, L., Macchetto, F. D., van Paradijs, J., Kouveliotou, C., Fishman, G. J., Meegan, C. A., Groot, P. J., & Galama, T. 1997, Nature, 387, 476

Salvaterra, R., Della Valle, M., Campana, S., Chincarini, G., Covino, S., D'Avanzo, P., Fernández-Soto, A., Guidorzi, C., Mannucci, F., Margutti, R., Thöne, C. C., Antonelli, L. A., Barthelmy, S. D., de Pasquale, M., D'Elia, V., Fiore, F., Fugazza, D., Hunt, L. K., Maiorano, E., Marinoni, S., Marshall, F. E., Molinari, E., Nousek, J., Pian, E., Racusin, J. L., Stella, L., Amati, L., Andreuzzi, G., Cusumano, G., Fenimore, E. E., Ferrero, P., Giommi, P., Guetta, D., Holland, S. T., Hurley, K., Israel, G. L., Mao, J., Markwardt, C. B., Masetti, N., Pagani, C., Palazzi, E., Palmer, D. M., Piranomonte, S., Tagliaferri, G., & Testa, V. 2009, Nature, 461, 1258

Savaglio, S., Glazebrook, K., & LeBorgne, D. 2009, ApJ, 691, 182

Scalzo, R. A., Aldering, G., Antilogus, P., Aragon, C., Bailey, S., Baltay, C., Bongard, S., Buton, C., Childress, M., Chotard, N., Copin, Y., Fakhouri, H. K., Gal-Yam, A., Gangler, E., Hoyer, S., Kasliwal, M., Loken, S., Nugent, P., Pain, R., Pécontal, E., Pereira, R., Perlmutter, S., Rabinowitz, D., Rau, A., Rigaudier, G., Runge, K., Smadja, G., Tao, C., Thomas, R. C., Weaver, B., & Wu, C. 2010, ApJ, 713, 1073

Scannapieco, E. & Bildsten, L. 2005, ApJ, 629, L85

Schaerer, D., Contini, T., & Pindao, M. 1999, A&AS, 136, 35

Schild, H., Crowther, P. A., Abbott, J. B., & Schmutz, W. 2003, A&A, 397, 859

Schlegel, D. J., Finkbeiner, D. P., & Davis, M. 1998, ApJ, 500, 525

Schmidt, B. P., Kirshner, R. P., Leibundgut, B., Wells, L. A., Porter, A. C., Ruiz-Lapuente, P., Challis, P., & Filippenko, A. V. 1994, ApJ, 434, L19

Silverman, J. M., Mazzali, P., Chornock, R., Filippenko, A. V., Clocchiatti, A., Phillips, M. M., Ganeshalingam, M., & Foley, R. J. 2009, PASP, 121, 689

Sim, S. A., Sauer, D. N., Röpke, F. K., & Hillebrandt, W. 2007, MNRAS, 378, 2

Sirianni, M., Jee, M. J., Benítez, N., Blakeslee, J. P., Martel, A. R., Meurer, G., Clampin, M., De Marchi, G., Ford, H. C., Gilliland, R., Hartig, G. F., Illingworth, G. D., Mack, J., & McCann, W. J. 2005, PASP, 117, 1049

Smartt, S. J. 2009, ARA&A, 47, 63

Smartt, S. J., Eldridge, J. J., Crockett, R. M., & Maund, J. R. 2009, MNRAS, 395, 1409

Smith, N. & Conti, P. S. 2008, ApJ, 679, 1467

Soderberg, A. M., Berger, E., Page, K. L., Schady, P., Parrent, J., Pooley, D., Wang, X., Ofek, E. O., Cucchiara, A., Rau, A., Waxman, E., Simon, J. D., Bock, D., Milne, P. A., Page, M. J., Barentine, J. C., Barthelmy, S. D., Beardmore, A. P., Bietenholz, M. F., Brown, P., Burrows, A., Burrows, D. N., Byrngelson, G., Cenko, S. B., Chandra, P., Cummings, J. R., Fox, D. B., Gal-Yam, A., Gehrels, N., Immler, S., Kasliwal, M., Kong, A. K. H., Krimm, H. A., Kulkarni, S. R., Maccarone, T. J., Mészáros, P., Nakar, E., O'Brien, P. T., Overzier, R. A., de Pasquale, M., Racusin, J., Rea, N., & York, D. G. 2008, Nature, 453, 469

Soderberg, A. M., Chakraborti, S., Pignata, G., Chevalier, R. A., Chandra, P., Ray, A., Wieringa, M. H., Copete, A., Chaplin, V., Connaughton, V., Barthelmy, S. D., Bietenholz, M. F., Chugai, N., Stritzinger, M. D., Hamuy, M., Fransson, C., Fox, O., Levesque, E. M., Grindlay, J. E., Challis, P., Foley, R. J., Kirshner, R. P., Milne, P. A., & Torres, M. A. P. 2010, Nature, 463, 513

Soderberg, A. M., Nakar, E., Berger, E., & Kulkarni, S. R. 2006, ApJ, 638, 930

Sollerman, J., Jaunsen, A. O., Fynbo, J. P. U., Hjorth, J., Jakobsson, P., Stritzinger, M., Féron, C., Laursen, P., Ovaldsen, J.-E., Selj, J., Thöne, C. C., Xu, D., Davis, T., Gorosabel, J., Watson, D., Duro, R., Ilyin, I., Jensen, B. L., Lysfjord, N., Marquart, T., Nielsen, T. B., Näränen, J., Schwarz, H. E., Walch, S., Wold, M., & Östlin, G. 2006, A&A, 454, 503

Sollerman, J., Leibundgut, B., & Spyromilio, J. 1998, A&A, 337, 207

Sollerman, J. & Leloudas, G. 2007, Central Bureau Electronic Telegrams, 1141, 1

Sollerman, J., Lindahl, J., Kozma, C., Challis, P., Filippenko, A. V., Fransson, C., Garnavich, P. M., Leibundgut, B., Li, W., Lundqvist, P., Milne, P., Spyromilio, J., & Kirshner, R. P. 2004, A&A, 428, 555

Sollerman, J., Mörtsell, E., Davis, T. M., Blomqvist, M., Bassett, B., Becker, A. C., Cinabro, D., Filippenko, A. V., Foley, R. J., Frieman, J., Garnavich, P., Lampeitl, H., Marriner, J., Miquel, R., Nichol, R. C., Richmond, M. W., Sako, M., Schneider, D. P., Smith, M., Vanderplas, J. T., & Wheeler, J. C. 2009, ApJ, 703, 1374

Sollerman, J., Östlin, G., Fynbo, J. P. U., Hjorth, J., Fruchter, A., & Pedersen, K. 2005, New Astronomy, 11, 103

Spyromilio, J., Gilmozzi, R., Sollerman, J., Leibundgut, B., Fransson, C., & Cuby, J.-G. 2004, A&A, 426, 547

Spyromilio, J. & Graham, J. R. 1992, MNRAS, 255, 671

Stanek, K. Z., Gnedin, O. Y., Beacom, J. F., Gould, A. P., Johnson, J. A., Kollmeier, J. A., Modjaz, M., Pinsonneault, M. H., Pogge, R., & Weinberg, D. H. 2006, Acta Astronomica, 56, 333

Stanek, K. Z., Matheson, T., Garnavich, P. M., Martini, P., Berlind, P., Caldwell, N., Challis, P., Brown, W. R., Schild, R., Krisciunas, K., Calkins, M. L., Lee, J. C., Hathi, N., Jansen, R. A., Windhorst, R., Echevarria, L., Eisenstein, D. J., Pindor, B., Olszewski, E. W., Harding, P., Holland, S. T., & Bersier, D. 2003, ApJ, 591, L17

Stanishev, V., Goobar, A., Benetti, S., Kotak, R., Pignata, G., Navasardyan, H., Mazzali, P., Amanullah, R., Garavini, G., Nobili, S., Qiu, Y., Elias-Rosa, N., Ruiz-Lapuente, P., Mendez, J., Meikle, P., Patat, F., Pastorello, A., Altavilla, G., Gustafsson, M., Harutyunyan, A., Iijima, T., Jakobsson, P., Kichizhieva, M. V., Lundqvist, P., Mattila, S., Melinder, J., Pavlenko, E. P., Pavlyuk, N. N., Sollerman, J., Tsvetkov, D. Y., Turatto, M., & Hillebrandt, W. 2007, A&A, 469, 645

Stephenson, F. R. & Green, D. A. 2005, Journal for the History of Astronomy, 36, 217

Stritzinger, M., Hamuy, M., Suntzeff, N. B., Smith, R. C., Phillips, M. M., Maza, J., Strolger, L.-G., Antezana, R., González, L., Wischnjewsky, M., Candia, P., Espinoza, J., González, D., Stubbs, C., Becker, A. C., Rubenstein, E. P., & Galaz, G. 2002, AJ, 124, 2100

Stritzinger, M., Leibundgut, B., Walch, S., & Contardo, G. 2006a, A&A, 450, 241

Stritzinger, M., Mazzali, P., Phillips, M. M., Immler, S., Soderberg, A., Sollerman, J., Boldt, L., Braithwaite, J., Brown, P., Burns, C. R., Contreras, C., Covarrubias, R., Folatelli, G., Freedman, W. L., González, S., Hamuy, M., Krzeminski, W., Madore, B. F., Milne, P., Morrell, N., Persson, S. E., Roth, M., Smith, M., & Suntzeff, N. B. 2009, ApJ, 696, 713

Stritzinger, M., Mazzali, P. A., Sollerman, J., & Benetti, S. 2006b, A&A, 460, 793

Stritzinger, M. & Sollerman, J. 2007, A&A, 470, L1

Stritzinger, M., Sollerman, J., Goobar, A., Nichol, R., Smith, M., & Leloudas, G. 2006c, Central Bureau Electronic Telegrams, 762, 3

Stritzinger, M., Suntzeff, N. B., Hamuy, M., Challis, P., Demarco, R., Germany, L., & Soderberg, A. M. 2005, PASP, 117, 810

Sullivan, M., Howell, D. A., Perrett, K., Nugent, P. E., Astier, P., Aubourg, E., Balam, D., Basa, S., Carlberg, R. G., Conley, A., Fabbro, S., Fouchez, D., Guy, J., Hook, I., Lafoux, H., Neill, J. D., Pain, R., Palanque-Delabrouille, N., Pritchet, C. J., Regnault, N., Rich, J., Taillet, R., Aldering, G., Baumont, S., Bronder, J., Filiol, M., Knop, R. A., Perlmutter, S., & Tao, C. 2006a, AJ, 131, 960

Sullivan, M., Le Borgne, D., Pritchet, C. J., Hodsman, A., Neill, J. D., Howell, D. A., Carlberg, R. G., Astier, P., Aubourg, E., Balam, D., Basa, S., Conley, A., Fabbro, S., Fouchez, D., Guy, J., Hook, I., Pain, R., Palanque-Delabrouille, N., Perrett, K., Regnault, N., Rich, J., Taillet, R., Baumont, S., Bronder, J., Ellis, R. S., Filiol, M., Lusset, V., Perlmutter, S., Ripoche, P., & Tao, C. 2006b, ApJ, 648, 868

Suntzeff, N. B. 1996, in IAU Colloq. 145: Supernovae and Supernova Remnants, 41–+

Svensson, K. M., Levan, A. J., Tanvir, N. R., Fruchter, A. S., & Strolger, L. 2010, ArXiv:1001.5042

Tanaka, M., Tominaga, N., Nomoto, K., Valenti, S., Sahu, D. K., Minezaki, T., Yoshii, Y., Yoshida, M., Anupama, G. C., Benetti, S., Chincarini, G., Della Valle, M., Mazzali, P. A., & Pian, E. 2009a, ApJ, 692, 1131

Tanaka, M., Yamanaka, M., Maeda, K., Kawabata, K. S., Hattori, T., Minezaki, T., Valenti, S., Della Valle, M., Sahu, D. K., Anupama, G. C., Tominaga, N., Nomoto, K., Mazzali, P. A., & Pian, E. 2009b, ApJ, 700, 1680

Tanvir, N. R., Fox, D. B., Levan, A. J., Berger, E., Wiersema, K., Fynbo, J. P. U., Cucchiara, A., Krühler, T., Gehrels, N., Bloom, J. S., Greiner, J., Evans, P. A., Rol, E., Olivares, F., Hjorth, J., Jakobsson, P., Farihi, J., Willingale, R., Starling, R. L. C., Cenko, S. B., Perley, D., Maund, J. R., Duke, J., Wijers, R. A. M. J., Adamson, A. J., Allan, A., Bremer, M. N., Burrows, D. N., Castro-Tirado, A. J., Cavanagh, B., de Ugarte Postigo, A., Dopita, M. A., Fatkhullin, T. A., Fruchter, A. S., Foley, R. J., Gorosabel, J., Kennea, J., Kerr, T., Klose, S., Krimm, H. A., Komarova, V. N., Kulkarni, S. R., Moskvitin, A. S., Mundell, C. G., Naylor, T., Page, K., Penprase, B. E., Perri, M., Podsiadlowski, P., Roth, K., Rutledge, R. E., Sakamoto, T., Schady, P., Schmidt, B. P., Soderberg, A. M., Sollerman, J., Stephens, A. W., Stratta, G., Ukwatta, T. N., Watson, D., Westra, E., Wold, T., & Wolf, C. 2009, Nature, 461, 1254

Taubenberger, S., Valenti, S., Benetti, S., Cappellaro, E., Della Valle, M., Elias-Rosa, N., Hachinger, S., Hillebrandt, W., Maeda, K., Mazzali, P. A., Pastorello, A., Patat, F., Sim, S. A., & Turatto, M. 2009, MNRAS, 397, 677

Thöne, C. C., Fynbo, J. P. U., Östlin, G., Milvang-Jensen, B., Wiersema, K., Malesani, D., Della Monica Ferreira, D., Gorosabel, J., Kann, D. A., Watson, D., Michałowski, M. J., Fruchter, A. S., Levan, A. J., Hjorth, J., & Sollerman, J. 2008, ApJ, 676, 1151

Thöne, C. C., Michałowski, M. J., Leloudas, G., Cox, N. L. J., Fynbo, J. P. U., Sollerman, J., Hjorth, J., & Vreeswijk, P. M. 2009, ApJ, 698, 1307

Tonry, J. L., Dressler, A., Blakeslee, J. P., Ajhar, E. A., Fletcher, A. B., Luppino, G. A., Metzger, M. R., & Moore, C. B. 2001, ApJ, 546, 681

Tremonti, C. A., Heckman, T. M., Kauffmann, G., Brinchmann, J., Charlot, S., White, S. D. M., Seibert, M., Peng, E. W., Schlegel, D. J., Uomoto, A., Fukugita, M., & Brinkmann, J. 2004, ApJ, 613, 898

Tully, R. B., Rizzi, L., Shaya, E. J., Courtois, H. M., Makarov, D. I., & Jacobs, B. A. 2009, AJ, 138, 323

Uomoto, A. & Kirshner, R. P. 1985, A&A, 149, L7

Valenti, S., Elias-Rosa, N., Taubenberger, S., Stanishev, V., Agnoletto, I., Sauer, D., Cappellaro, E., Pastorello, A., Benetti, S., Riffeser, A., Hopp, U., Navasardyan, H., Tsvetkov, D., Lorenzi, V., Patat, F., Turatto, M., Barbon, R., Ciroi, S., Di Mille, F., Frandsen, S., Fynbo, J. P. U., Laursen, P., & Mazzali, P. A. 2008a, ApJ, 673, L155

Valenti, S., Fugazza, D., Maiorano, E., D'Elia, V., Antonelli, L. A., Covino, S., Magazzu', A., Pinilla-Alonso, N., Della Valle, M., Chincarini, G., Pian, E., Mazzali, P. A., Harutyunyan, A., & Benetti, S. 2008b, GRB Coordinates Network, 7171, 1

Valenti, S., Pastorello, A., Cappellaro, E., Benetti, S., Mazzali, P. A., Manteca, J., Taubenberger, S., Elias-Rosa, N., Ferrando, R., Harutyunyan, A., Hentunen, V. P., Nissinen, M., Pian, E., Turatto, M., Zampieri, L., & Smartt, S. J. 2009, Nature, 459, 674

van den Bergh, S., Li, W., & Filippenko, A. V. 2002, PASP, 114, 820

—. 2005, PASP, 117, 773

van Dokkum, P. G. 2001, PASP, 113, 1420

van Dyk, S. D., Hamuy, M., & Filippenko, A. V. 1996, AJ, 111, 2017

van Paradijs, J., Groot, P. J., Galama, T., Kouveliotou, C., Strom, R. G., Telting, J., Rutten, R. G. M., Fishman, G. J., Meegan, C. A., Pettini, M., Tanvir, N., Bloom, J., Pedersen, H., Nørdgaard-Nielsen, H. U., Linden-Vørnle, M., Melnick, J., van der Steene, G., Bremer, M., Naber, R., Heise, J., in't Zand, J., Costa, E., Feroci, M., Piro, L., Frontera, F., Zavattini, G., Nicastro, L., Palazzi, E., Bennet, K., Hanlon, L., & Parmar, A. 1997, Nature, 386, 686

van Paradijs, J., Kouveliotou, C., & Wijers, R. A. M. J. 2000, ARA&A, 38, 379

Vink, J. S. & de Koter, A. 2005, A&A, 442, 587

Voss, R. & Nelemans, G. 2008, Nature, 451, 802

Wang, L., Baade, D., Höflich, P., Khokhlov, A., Wheeler, J. C., Kasen, D., Nugent, P. E., Perlmutter, S., Fransson, C., & Lundqvist, P. 2003, ApJ, 591, 1110

Wang, L., Baade, D., & Patat, F. 2007, Science, 315, 212

Wang, L. & Wheeler, J. C. 2008, ARA&A, 46, 433

Wang, X., Filippenko, A. V., Ganeshalingam, M., Li, W., Silverman, J. M., Wang, L., Chornock, R., Foley, R. J., Gates, E. L., Macomber, B., Serduke, F. J. D., Steele, T. N., & Wong, D. S. 2009a, ApJ, 699, L139

Wang, X., Li, W., Filippenko, A. V., Foley, R. J., Kirshner, R. P., Modjaz, M., Bloom, J., Brown, P. J., Carter, D., Friedman, A. S., Gal-Yam, A., Ganeshalingam, M., Hicken, M., Krisciunas, K., Milne, P., Silverman, J. M., Suntzeff, N. B., Wood-Vasey, W. M., Cenko, S. B., Challis, P., Fox, D. B., Kirkman, D., Li, J. Z., Li, T. P., Malkan, M. A., Moore, M. R., Reitzel, D. B., Rich, R. M., Serduke, F. J. D., Shang, R. C., Steele, T. N., Swift, B. J., Tao, C., Wong, D. S., & Zhang, S. N. 2009b, ApJ, 697, 380

Wang, X., Li, W., Filippenko, A. V., Foley, R. J., Smith, N., & Wang, L. 2008, ApJ, 677, 1060

Webbink, R. F. 1984, ApJ, 277, 355

Weiler, K. W., Panagia, N., Montes, M. J., & Sramek, R. A. 2002, ARA&A, 40, 387

Wheeler, J. C. & Harkness, R. P. 1990, Reports on Progress in Physics, 53, 1467

Wheeler, J. C. & Levreault, R. 1985, ApJ, 294, L17

Whelan, J. & Iben, Jr., I. 1973, ApJ, 186, 1007

Wiersema, K., Savaglio, S., Vreeswijk, P. M., Ellison, S. L., Ledoux, C., Yoon, S., Møller, P., Sollerman, J., Fynbo, J. P. U., Pian, E., Starling, R. L. C., & Wijers, R. A. M. J. 2007, A&A, 464, 529

Wilson, O. C. 1939, ApJ, 90, 634

Wood-Vasey, W. M., Friedman, A. S., Bloom, J. S., Hicken, M., Modjaz, M., Kirshner, R. P., Starr, D. L., Blake, C. H., Falco, E. E., Szentgyorgyi, A. H., Challis, P., Blondin, S., Mandel, K. S., & Rest, A. 2008, ApJ, 689, 377

Wood-Vasey, W. M., Miknaitis, G., Stubbs, C. W., Jha, S., Riess, A. G., Garnavich, P. M., Kirshner, R. P., Aguilera, C., Becker, A. C., Blackman, J. W., Blondin, S., Challis, P., Clocchiatti, A., Conley, A., Covarrubias, R., Davis, T. M., Filippenko, A. V., Foley, R. J., Garg, A., Hicken, M., Krisciunas, K., Leibundgut, B., Li, W., Matheson, T., Miceli, A., Narayan, G., Pignata, G., Prieto, J. L., Rest, A., Salvo, M. E., Schmidt, B. P., Smith, R. C., Sollerman, J., Spyromilio, J., Tonry, J. L., Suntzeff, N. B., & Zenteno, A. 2007, ApJ, 666, 694

Woosley, S. E. 1993, ApJ, 405, 273

Woosley, S. E. & Bloom, J. S. 2006, ARA&A, 44, 507

Woosley, S. E., Eastman, R. G., Weaver, T. A., & Pinto, P. A. 1994, ApJ, 429, 300

Woosley, S. E. & Heger, A. 2006, ApJ, 637, 914

Xu, D., Watson, D., Fynbo, J., Fan, Y., Zou, Y., & Hjorth, J. 2008, in COSPAR, Plenary Meeting, Vol. 37, 37th COSPAR Scientific Assembly, 3512–+

Yamanaka, M., Kawabata, K. S., Kinugasa, K., Tanaka, M., Imada, A., Maeda, K., Nomoto, K., Arai, A., Chiyonobu, S., Fukazawa, Y., Hashimoto, O., Honda, S., Ikejiri, Y., Itoh, R., Kamata, Y., Kawai, N., Komatsu, T., Konishi, K., Kuroda, D., Miyamoto, H., Miyazaki, S., Nagae, O., Nakaya, H., Ohsugi, T., Omodaka, T., Sakai, N., Sasada, M., Suzuki, M., Taguchi, H., Takahashi, H., Tanaka, H., Uemura, M., Yamashita, T., Yanagisawa, K., & Yoshida, M. 2009, ApJ, 707, L118

Yoon, S. & Langer, N. 2005, A&A, 443, 643

Zwicky, F. 1938, ApJ, 88, 529